Entwicklungsbegleitende Untersuchungen polymerbasierter Mehrkomponentensysteme für kardiovaskuläre Implantate

kumulative Dissertation

zur

Erlangung des akademischen Grades

Doktor-Ingenieur (Dr.-Ing.)

der Fakultät für Maschinenbau und Schiffstechnik

der Universität Rostock

Rostock, Mai 2022

vorgelegt von:

Dipl.-Phys. Daniela Koper, ehem. Arbeiter

aus Rostock

geboren am 5.11.1981 in Suhl

https://doi.org/10.18453/rosdok_id00004144

Gutachter:

1. Gutachter: Prof. Dr.-Ing. habil. Niels Grabow
Universitätsmedizin Rostock,
Institut für Biomedizinische Technik

2. Gutachter: Prof. Dr.-Ing. Hermann Seitz
Universität Rostock,
Fakultät für Maschinenbau und Schiffstechnik,
Lehrstuhl für Mikrofluidik

Datum der Einreichung: 19.05.2022

Datum der Verteidigung: 07.12.2022

“On ne fait jamais attention à ce qui a été fait;

on ne voit que ce qui reste à faire.”

Marie Skłodowska Curie

Inhalt

Abkürzungsverzeichnis

1-KS	Einkomponentensystem
AFM	Rasterkraftmikroskopie (atomic force microscope)
API	aktiver pharmazeutischer Wirkstoff (active pharmaceutical ingredient)
BMS	metallische Gefäßstütze (bare metal stent)
CF	kristalliner Anteil (crystalline fraction)
$CHCl_3$	Chloroform
CoCr	Kobalt-Chrom Legierung
CoNi	Kobalt-Nickel Legierung
CYCLO	Cyclosporin A
DES	wirkstofffreisetzende Gefäßstütze (drug-eluting stent)
DEX	Dexamethason
DSC	Dynamische Differenzkalorimetrie (differential scanning calorimetry)
FEA	Finite Elemente Analyse
ICH	International Conference on Harmonization
LCST	untere kritische Lösungstemperatur (lower critical solution temperature)
L210	Poly(L-lactid), M_w = 320.000 g/mol
L214	Poly(L-lactid), M_w = 700.000 g/mol
MAF	mobiler amorpher Anteil (mobile amorphous fraction)
MeOH	Methanol
MKS	Mehrkomponentensystem
PCL	Poly(*ε*-caprolacton)
PDLA	Poly(D-D-Lactid)
PDLLA	Poly(*meso*-D-L-Lactid)
PEG	Polyethylenglycol
PEVA/PBMA	Poly(ethylen-*co*-vinylacetat)/Poly(n-butyl-methacrylat)-Blend
PLA	Polylactid
PLGA	Poly(lactid-*co*-glycolid)
PLLA	Poly(L-Lactid)
PTCA	perkutane transluminale Coronar-Angioplastie
PtCr	Platin-Chrom Legierung
PtIr	Platin-Iridium Legierung
PTX	Paclitaxel
PVDF-HFP	Poly(vinylidenfluorid-*co*-hexafluorpropylen)
RAF	starr amorpher Anteil (rigid amorphous fraction)
REM	Rasterelektronenmikroskopie

SIBS	Poly(styrol-isobutylen-styrol)
SIR	Sirolimus
UCST	obere kritische Lösungstemperatur (upper critical solution temperature)
VEGF	vaskulärer endotheliale Wachstumsfaktor (vascular endothelial growth factor)
WFS	Wirkstofffreisetzungssystem

Formelzeichen

A_0	Querschnittsfläche (mm^2)
C	Konzentration (mol/dm^3)
χ	Kristallinitätsgrad (%)
χ^*	Flory-Huggins-Parameter
ΔG	Gibb'sche Energie (J)
ΔH	Enthalpie (J)
ΔH_c	Enthalpie der Kaltkristallisation (J)
ΔH_m	Enthalpie der Schmelze (J)
ΔS	Entropie (J/K)
E	Elastizitätsmodul (MPa)
ε_B	Bruchdehnung (%)
F	Kraft (N)
k	Geschwindigkeitskonstante $(L/mol\ s)^{n-1}$
L	Länge (mm)
M_n	zahlenmittleres Molekulargewicht (g/mol)
M_w	gewichtsmittleres Molekulargewicht (g/mol)
$\tilde{\nu}$	Wellenzahl (rel. cm^{-1})
φ_i	Volumenanteil der Komponente i
q	Heizrate (K/min)
q_c	Abkühlgeschwindigkeit (K/min)
R	universelle Gaskonstante (J/mol K)
r_i	Anzahl der Kettensegmente
R_M	Zugfestigkeit (MPa)
σ_B	Bruchspannung (MPa)
t	Zeit (s)
T	Temperatur (K)
T_{cc}	Kristallisationstemperatur (°C)
$\mathrm{T_c}$	Kaltkristallisationstemperatur (°C)
T_g	Glasübergangstemperatur (°C)
T_m	Schmelztemperatur (°C)
w	Grenzflächenbreite (µm)

1. Einleitung und Zielstellung

Implantatkonzepte auf Polymerbasis haben aufgrund der Variabilität und vielfältigen physiko-chemischen Eigenschaften dieser Materialien einen immer größer werdenden Stellenwert in der Entwicklung von Medizinprodukten. Durch den demografischen Wandel und die damit verbundene Zunahme an kardiovaskulären Erkrankungen werden mehr langzeitfunktionale Implantate erforderlich [1]. Aufgrund der stetigen Entwicklung der Technik auf dem Gebiet und der Verbesserung in der Gesundheitsversorgung, ist die Zahl der Todesfälle rückläufig [2]. Dennoch ist die ischämische Herzkrankheit weiterhin weltweit die häufigste Todesursache und für 16 % aller Todesfälle verantwortlich [3].

Mit dem ersten erfolgreichen Einsatz von Herzschrittmacherimplantaten im Jahr 1958 [4], der Ballondilatation (PTCA) 1977 [5] und des selbstexpandierenden Stents 1986 [6] wurden wichtige Meilensteine in der Entwicklung von Therapiekonzepten erreicht. Durch die Entwicklung verbesserter Technologien, wie z. B. resorbierbare polymerbasierte Medizinprodukte, wird das Applikationsfeld der kardiovaskulären Implantate ständig erweitert [7]. Diese Produkte gelten aufgrund ihrer biologischen Abbaubarkeit, individuellen Anpassung und verbesserten Biokompatibilität als Alternative zu permanenten metallbasierten Implantaten [8]. Häufig finden Polymere in der Stenttechnologie Anwendung, u.a. als polymerbasierte Drug-Eluting Stents (DES) [9] oder Covered Stents [10]. Bei DES bzw. Covered Stents werden Polymere als Beschichtungsmaterial und Wirkstoffträger angewandt, um insbesondere aktive pharmazeutische Wirkstoffe (API) am Stent zu immobilisieren und gezielt im Patienten freizusetzen, Abb. 1 [11,12]. Ein darüber hinausgehender Entwicklungsschwerpunkt sind biodegradierbare Polymerstents [13,14].

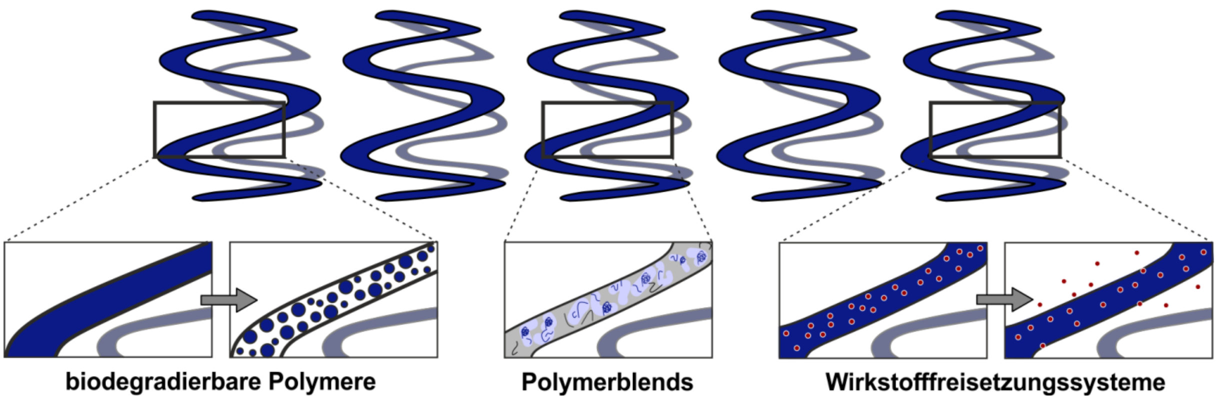

Abb. 1 Schematische Darstellung einer Stentstruktur für die kardiovaskuläre Gefäßintervention als Anwendungs-beispiel für Ein- (1-KS) bzw. Mehrkomponentensysteme (MKS) aus biodegradierbaren Polymeren, Polymerblends sowie polymerbasierten Wirkstofffreisetzungssystemen (WFS).

Diese haben den potentiellen Vorteil, dass sie u.a. eine bessere Voraussetzung für wiederholte interventionelle Eingriffe bieten und langfristig kein Fremdkörper im Gefäß verbleibt. An den verwendeten Werkstoff wird die Anforderung gestellt, dass dieser einen hohen E-Modul und

eine hohe Festigkeit aufweisen muss, damit der daraus entwickelte Stentgrundkörper die Stützwirkung des Gefäßes gewährleisten kann, bis dieser vom Körper resorbiert wird [15]. Dabei können sowohl polymerbasierte Einkomponentensysteme (1-KS) als auch Mehrkomponentensysteme (MKS) in Form von mehreren Polymeren, Zusätzen oder Polymer/Wirkstoff-Blends eingesetzt werden, um die erforderlichen Eigenschaften zu erreichen. Insbesondere das resorbierbare thermoplastische Poly(L-lactid) (PLLA) ist für biomedizinische Anwendungen weit verbreitet und weist im Bereich der Stenttechnologie sowohl vorteilhafte mechanische Eigenschaften als auch eine gute Biokompatibilität auf [16]. Aufgrund dessen ist PLLA vielseitig einsetzbar, u.a. als Stentbeschichtung [17], Wirkstoffdepotsystem [18] oder als Stentgrundkörper [19].
Um aus dem Werkstoff ein Implantat entwickeln zu können, bedarf es verschiedener Prozessschritte, die in Abb. 2 dargestellt sind und im Fokus der vorliegenden Arbeit stehen.

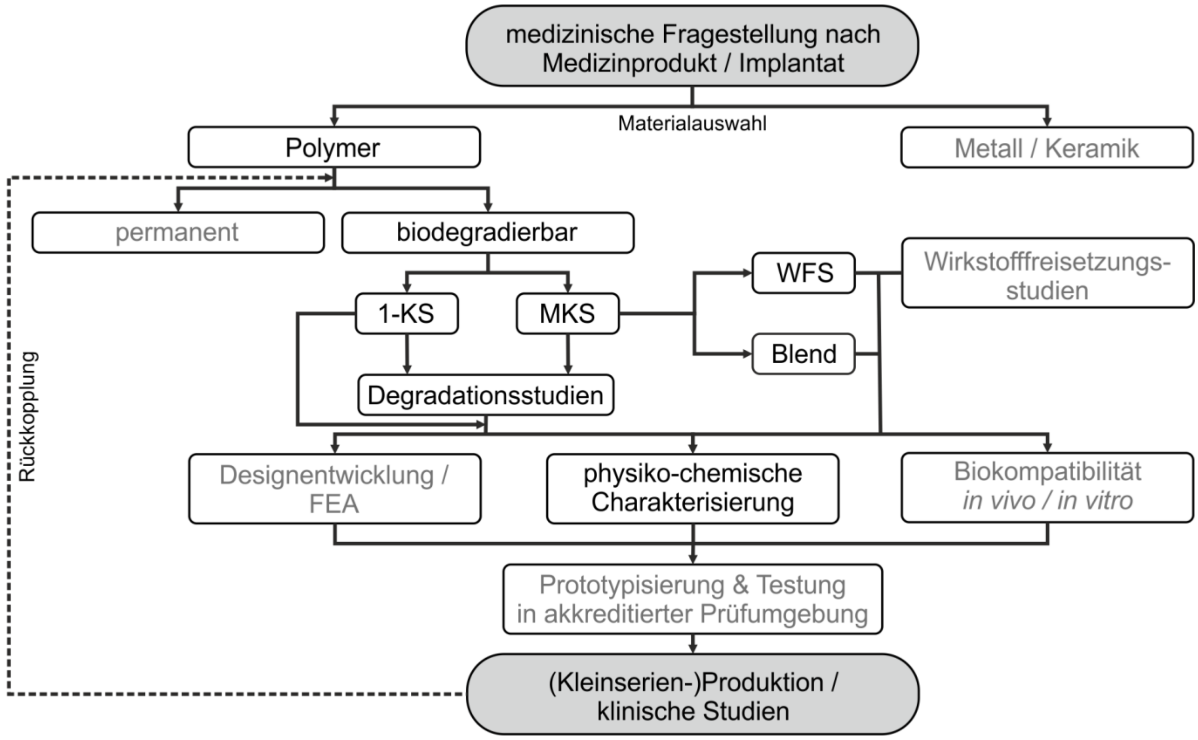

Abb. 2 Darstellung relevanter Schritte bei der Implantatentwicklung, ausgehend von der Auswahl eines biodegradierbaren 1-KS oder MKS, unter Einbeziehung wichtiger Entwicklungs- und Prüfabläufe für MKS aus Polymerblends bzw. polymerbasierten Wirkstofffreisetzungssystemen (WFS).

Ausgehend von der medizinischen Indikation für ein Implantat, ist eine Materialauswahl zu treffen, die den mechanischen und biologischen Anforderungen entspricht. Bei der Wahl eines Polymers als Grundmaterial ist zusätzlich die Entscheidung zu treffen, ob ein permanentes oder degradierbares Polymer die Anforderungen an den Einsatzzweck erfüllt. Zusätzlich ist zu prüfen, ob ein 1-KS bereits die benötigten Eigenschaften des Implantats erfüllt, oder ein MKS erforderlich ist, welches aus einem Blend oder polymerbasiertem Wirkstofffreisetzungssystem bestehen kann. Neben einem möglichen therapeutischen Nutzen spielen bei der

Entscheidungsfindung weitere Prozessschritte eine Rolle. Beispielsweise sind im Falle von degradierbaren Polymeren für eine klinische Zulassung zusätzlich *in vitro* Degradationsstudien im Labor durchzuführen, welche das *in vivo*-Abbauverhalten im Körper abbilden können. Für alle Implantatmaterialien sind im weiteren Verlauf der Entwicklung umfangreiche Prüfmethoden entsprechend den verfügbaren Normen und Standardisierungsverfahren durchzuführen, um die physiko-chemischen Eigenschaften, bestehend aus morphologischen, mechanischen und thermischen Komponenten, zu ermitteln. Die entwickelten Implantatprototypen sind mit standardisierten Prüfverfahren in gemäß der DIN EN ISO 25539-2 „Cardiovascular implants - endovascular devices: Part 2 - vascular stents“ speziellen Anwendungstests zu unterziehen [20]. Die Prüfverfahren sind in akkreditierter Prüfumgebung zu etablieren und für Produktzulassungen im Sinne der Richtlinie 93/42/EWG [21] und der Verordnung (EU) 2017/745 über Medizinprodukte (MDR) [22] zu validieren. Abschließend können diese in die Kleinserienproduktion überführt werden, um sie in klinischen Studien zu testen.

Basierend auf den genannten Prozessschritten wurden in der vorliegenden Arbeit PLLA-basierte MKS für den Einsatz im kardiovaskulären Bereich entwickelt und charakterisiert, um zum einen durch geeignete Postprozessierungsschritte eine Verbesserung der adaptiven Eigenschaften realisieren zu können und zum anderen den Einfluss von Zusätzen (Polymer oder API) auf die physiko-chemischen Eigenschaften der Prüfkörper beurteilen zu können. Zunächst wurde das Prüfmethodenspektrum hinsichtlich der Entwicklung von beschleunigten Degradationsprotokollen durch Temperaturerhöhung erweitert. Dazu wurde die beschleunigte Degradation von PLLA mit dem enzym-assoziierten Echtzeit-Abbau verglichen und anhand der Ergebnisse ein Korrelationsmodell entwickelt. Es wurde untersucht, ob die beschleunigten Protokolle unter Berücksichtigung der vorgegebenen Randbedingungen an *in vitro* Echtzeitstudien angepasst werden können.

In einer weiteren Studie wurde PLLA mit Poly(ε-caprolacton) (PCL) über ein Lösemittelverfahren in verschiedenen Mischungsverhältnissen kombiniert und thermisch nachbehandelt. Diese Kombination wurde gewählt, um durch die Verblendung des spröden PLLA mit einem flexiblen Polymer (PCL) die mechanischen Eigenschaften an die speziellen Anforderungen, die an ein Implantatmaterial gestellt werden, anzupassen. Durch die Änderung der Prozessprotokolle wurden die Materialeigenschaften modifiziert, wodurch sich die Möglichkeit eröffnet, generell auf weitere Zusätze, wie Weichmacher zu verzichten. Ergänzend dazu wurden dünne PLLA/Wirkstoff-Folien im Hinblick auf den Einfluss des Wirkstoffs auf die thermischen und mechanischen Eigenschaften der Polymermatrix untersucht. Als API wurden Sirolimus (SIR), Paclitaxel (PTX), Dexamethason (DEX) und Cyclosporin A (CYCLO) verwendet. Es wurde untersucht, inwiefern die Wirkstoffe die thermischen und mechanischen Eigenschaften von PLLA bestimmen und ob der Einfluss von verschiedenen APIs auf die

Polymermatrix vorhergesagt werden kann. Insbesondere wurde untersucht, ob eine zielgerichtete thermische Behandlung erforderlich ist, um die Lagerstabilität der daraus entwickelten Stents und deren erforderlichen mechanischen Eigenschaften zu gewährleisten.

2. Grundlagen zu Poly(L-lactid) als Implantatmaterial

Polylactid (PLA) ist eines der am vielfältigsten verwendeten Materialien in der Medizintechnik [23]. Die Gründe dafür liegen in der einfachen Verarbeitung und einer hohen Festigkeit mit einer Glasübergangstemperatur T_g und Schmelztemperatur T_m oberhalb der Körpertemperatur. Im Vergleich zu anderen Polymermaterialien liegen die Nachteile von PLA in der weniger optimalen Biokompatibiltät durch die sich bildenden Abbauprodukte während der Degradation des Materials. Klinische Studien zeigen, dass Implantate aus Polylactid nach längerer Implantationszeit Entzündungsreaktionen hervorrufen können [24]. Diese werden im Wesentlichen durch die Freisetzung saurer Degradationsprodukte verursacht, die während des Abbaus der Polymermatrix entstanden sind und das Puffervermögen des umliegenden Gewebes überschreiten [25]. Durch die Verwendung von hochmolekularem PLA soll diesem Effekt entgegengewirkt werden [26]. Weiterhin dient es als ein günstiger Blendpartner sowohl für andere Polymere als auch Wirkstoffsysteme. Somit findet PLA u.a. als Nahtmaterial sowie als orthopädisches Implantat und Wirkstofffreisetzungssystem Anwendung [27,28].

2.1. Struktur- und Gefügeeigenschaften

PLA zählt zur chemischen Gruppe der Poly(α-hydroxycarbonsäuren). Es ist ein steifes thermoplastisches Polymer, das je nach der Stereoreinheit des Polymergerüsts oder der thermischen Vorgeschichte des Polymers teilkristallin oder völlig amorph sein kann [25]. PLA kann durch Polykondensation von Milchsäure oder über Ringöffnungspolymerisation ausgehend von Lactid (L,L-Lactid zu PLLA, D,D-Lactid zu PDLA sowie *meso*-D,L-Lactid zu PDLLA) synthetisiert werden, siehe Abb. 3 a [29]. Die Rohstoffe können aus Depolymerisation von Milchsäureoligomeren gewonnen werden, welche beispielsweise ein Produkt der Fermentation von Biomasse, wie Mais, sind [30].

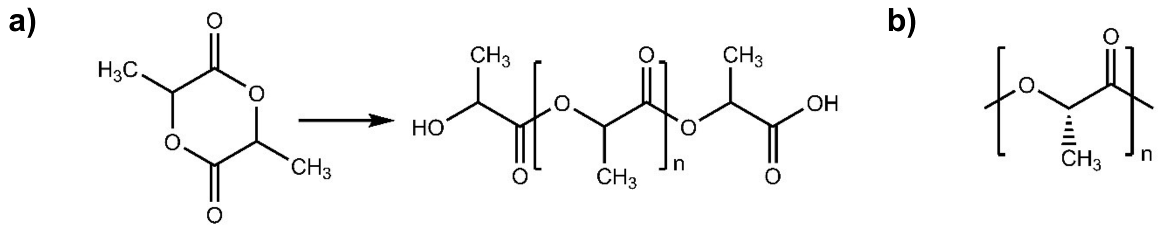

Abb. 3 a) Reaktionsschema zur Synthese des Polylactids aus dem cyclischen Dimer Lactid durch Ringöffnungspolymerisation. b) Strukturformel der enantiomeren L-(-)-Milchsäure-Wiederholeinheit.

Die Glasübergangstemperatur T_g und der Schmelzpunkt T_m sind wichtig für die Bestimmung der Einsatztemperaturen in verschiedenen Anwendungen. Beide Übergänge, T_g und T_m, werden von der Primärstruktur, der thermischen Vorgeschichte und dem Molekulargewicht M beeinflusst, wobei T_g üblicherweise um 60 °C liegt und T_m einen Bereich um 130-230 °C aufweisen kann. Während der Elastizitätsmodul E und die Zugfestigkeit R_M mit steigendem

Molekulargewicht M und zunehmender Kristallinität χ erhöht werden, können Restmonomere oder niedermolekulare Bestandteile als Weichmacher wirken, die eine Abnahme von E und R_M zur Folge haben können und überdies zu einer Beschleunigung des Degradationsprozesses beitragen.

Teilkristallines PLLA (Abb. 3 b) liegt sphärolithisch in einer Drei-Phasen-Form vor: die kristalline Form (CF - crystalline fraction), die mobile amorphe Form (MAF - mobile amorphous fraction) und die eingeschränkte oder starr amorphe Form (RAF - rigid amorphous fraction) [31,32]. Abb. 4 a zeigt schematisch den Aufbau eines polymeren Sphärolithen mit den entsprechenden Phasen. Die RAF resultiert aus der eingeschränkten Mobilität der amorphen Ketten aufgrund der Fixierung an der Grenzfläche der kristallinen Lamellen. Die Bildung einer RAF hängt von der Kristallgröße und dem Kristallisationsgrad ab. Weiterhin ausschlaggebend für die Bildung von RAF sind ebenso die Kristallisationsbedingungen. Diese beeinflussen sowohl die physiko-chemischen Eigenschaften des Polymers als auch deren Degradationsverhalten, was im Rahmen dieser Arbeit näher untersucht wird.

Die Kristallisation von PLLA ist ein thermodynamischer Prozess, der sowohl über die Schmelze als auch aus der Lösung erfolgen kann. Die von Hoffman und Lauritzen entwickelte Kristallisationstheorie legt dar, dass beide Prozesse über die Bildung von Kristallisationskeimen und anschließendem Kristallwachstum ablaufen [25,33]. Die Keimbildung ist erforderlich, um die Energiebarriere für die Bildung initialer metastabiler geordneter Mikrodomänen mit einer deutlichen Phasengrenze zu überwinden, die sie von der umgebenden Lösung (oder Schmelze) trennt. Die treibende Kraft für die Kristallkeimbildung sowie für das anschließende Wachstum zu größeren Kristallen ist die freie Kristallisationsenthalpie ΔG des Systems [33,34].

PLLA weist einen komplexen Polymorphismus auf und kann in α-, α'-, β- und γ- sowie Mischformen kristallisieren, einschließlich der unter bestimmten Kristallisationsbedingungen erhaltenen Mesophasenform [30,35–37]. Die stabile α-Phase von PLLA existiert in zwei Varianten: einer geordneten α-Phase mit antiparallelen Helices, die bei hoher Kristallisationstemperatur T_c erzeugt werden, und einer ungeordneteren Variante, die bei niedrigerer T_c erhalten wird und α'-PLLA genannt wird [38–40]. Abb. 4 b zeigt schematisch den Polymorphismus von PLLA. Bei niedrigen Temperaturen liegen in der PLLA-Matrix die Kristalle in der α'-Form vor [41,42]. Mit ansteigender Temperatur wurde der Übergang von ungeordneten α'-Kristallen zu geordneten α-Kristallen vor dem Einsetzen der Schmelze beobachtet [43,44]. Das Molekulargewicht M_w beeinflusst den Polymorphismus von PLLA nicht wesentlich und die α'- und α-Form-Kristalle werden unabhängig von der Kettenlänge gebildet. Allerdings wirkt sich M_w erheblich auf die Kristallisationskinetik aus und die Kristallisationsrate nimmt mit zunehmendem M_w stark ab [45]. Die β- und γ-Phase spielen für die praktische Anwendung eine untergeordnete Rolle [46,47].

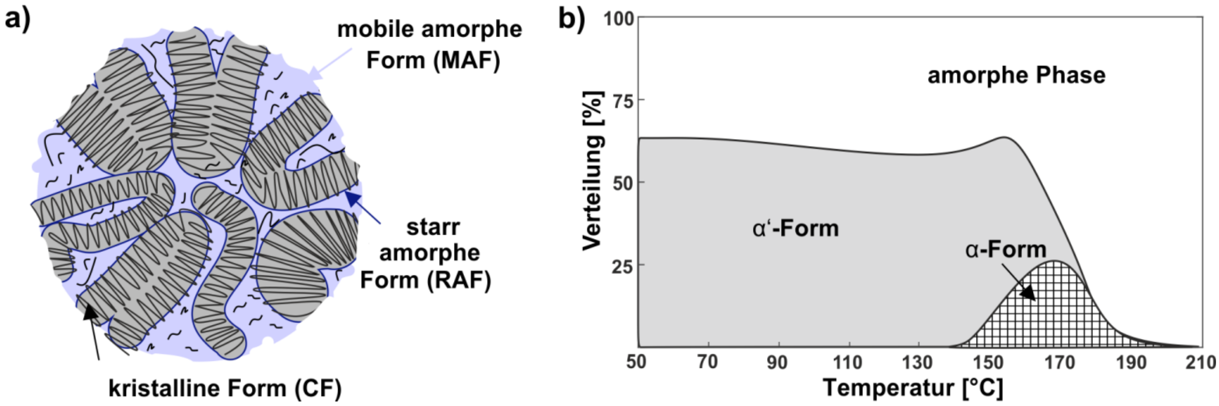

Abb. 4 a) Übergeordnete Kristallstruktur von PLLA in Form eines Sphärolithen. Gezeigt sind die Kristalllamellen (CF) sowie die mobile Form (MAF) und die an der Grenzfläche zwischen CF und MAF ausgebildeten starr amorphe Form (RAF) nach Hoffmann und Lauritzen [33,48]. b) Polymorphismus von PLLA, angelehnt an [49]. Dargestellt ist die relative Zusammensetzung der amorphen Phase sowie der *α*- und *α'*-Form, die sich in Abhängigkeit der Temperatur ausbildet.

2.2. Degradation

Eine wesentliche Fragestellung bei der Entwicklung von polymerbasierten Implantaten stellt die Charakterisierung der Alterung und des Abbauverhaltens im Körper dar. Üblicherweise wird eine *in vitro* Degradation durch Strahlung, Temperatur oder Hydrolyse initiiert [50]. Dabei kann die Hydrolyse rein hydrolytisch oder enzymkatalysiert ablaufen. PLLA wird durch Esterspaltung zu Oligomeren bis hin zu den niedermolekularen monomeren Ausgangsstoffen und anschließender Oxidation zu Pyruvat über den Zitronensäurezyklus abgebaut. Die relativ lange Degradationszeit von ca. zwei Jahren wird durch den hydrophoben Charakter des Polymers erklärt, welcher nur eine geringe Wasseraufnahme erlaubt und wiederum eine verminderte Abbaurate zur Folge hat [51].

Die Hydrolyse kann entweder am Kettenende oder zufällig in der Kettenmitte erfolgen, wobei die Polyesterketten zu Säuren und Alkoholen gespalten werden. Durch die Erhöhung der Konzentration an freien Carboxylgruppen sinkt der pH-Wert des Mediums [52,53]. Der hydrolytische Abbau von PLLA erfolgt weiterhin auch autokatalytisch, wobei durch die Bildung von freier Carbonsäure die weitere Kettenspaltung katalysiert wird [25].

Der PLLA-Abbau findet überwiegend in den amorphen Bereichen statt, da hier im Vergleich zu den kristallinen Bereichen das Wasser schneller hineindiffundieren kann. Während der Degradationsprozesse können infiltrierende Wassermoleküle die Mobilität der amorphen Ketten zusätzlich verstärken und sie in höher geordnete Strukturen umordnen [54]. Die Wassermoleküle sind dementgegen kaum in der Lage in die kristallinen Bereiche einzudringen, welche in der Folge während des Abbauprozesses kaum hydrolysiert werden. Der Abbau des kristallinen Rückstands erfolgt schließlich im Spätstadium der Hydrolyse, der sich in einer allmählichen Abnahme der Schmelztemperatur der Kristallite äußert [25].

Generell wird zwischen Masse- (Bulk-) und Oberflächenabbau unterschieden [55]. Beim Masseabbau diffundiert Wasser schneller in die Polymermatrix, als das Polymer abgebaut wird. Die hydrolysierbaren Bindungen werden über den gesamten Polymerkörper verteilt gleichmäßig gespalten. Daher nimmt die mittlere Molmasse des Polymers homogen ab. Die Abbauprodukte allerdings bleiben im Bulk eingeschlossen, wodurch ein Masseverlust erst mit fortgeschrittener Degradation beobachtet werden kann, siehe Abb. 5 oben.
Im Fall eines Oberflächenabbaus ist hingegen die Diffusionsgeschwindigkeit von Wasser in die Polymermatrix kleiner als die Abbaugeschwindigkeit des Polymers. Der Abbau findet daher hauptsächlich in einer dünnen Oberflächenschicht statt. Im Gegensatz zum Bulkabbau kann bereits zu Beginn der Degradation ein Masseverlust beobachtet werden, da Degradationsprodukte schnell abtransportiert werden können, während die Molmasse des Polymers im Bulk unverändert bleibt. Sowohl der Masse- als auch der Oberflächenabbau ist ein heterogener Prozess, dessen Geschwindigkeit von der Form des Probekörpers (z.B. Größe der Oberfläche) und der Hydrolysegeschwindigkeit der spaltbaren Bindungen im Polymer abhängt [56].

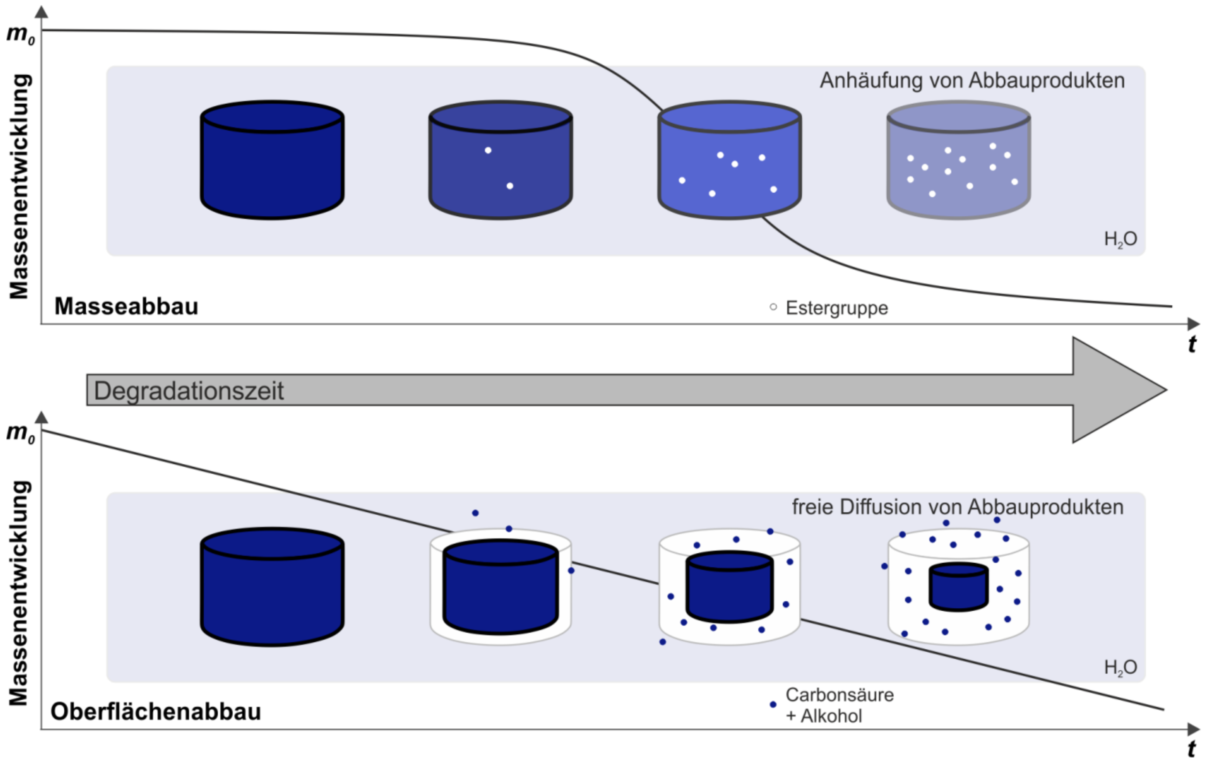

Abb. 5 Schematische Darstellung der beiden Abbaumechanismen bei Polyestern, nach [57,58]: Masse- und Oberflächenabbau. Die Abbauprodukte bestehen aus Carbonsäuren und Alkoholen, die sich im Material ansammeln können (Masseabbau) oder in das umgebende wässrige Medium diffundieren (Oberflächenabbau).

Ohne Einfluss von Enzymen findet die Degradation von PLLA über den Masseabbau statt [59]. Dennoch kann der Oberflächenabbau durch Enzyme beeinflusst werden [60], was im Rahmen dieser Arbeit näher betrachtet wird.

Durch die Hydrolyse zu niedermolekularen Abbauprodukten erhalten die PLLA Ketten zusätzliche Mobilität, sodass sich neue Kristallgitter ausbilden können, was zu einer Erhöhung des Kristallinitätsgrades führt [61]. Da die Kristallinität sowohl die Abbaugeschwindigkeit als auch die mechanischen Eigenschaften von PLLA beeinflusst, ist es wesentlich zu verstehen, wie sich die Kristallinität während des Abbauprozesses verändert [62,63]. Dies ist ebenso Gegenstand der vorliegenden Arbeit.

Autokatalytische vs. nicht-katalytische Hydrolyse

Im Allgemeinen ist der PLLA-Abbau in erster Linie auf die Hydrolyse der Esterbindungen zu Alkohol und Carbonsäure zurückzuführen. Sie erfordert die Anwesenheit von Wasser gemäß folgendem Reaktionsschema [25]:

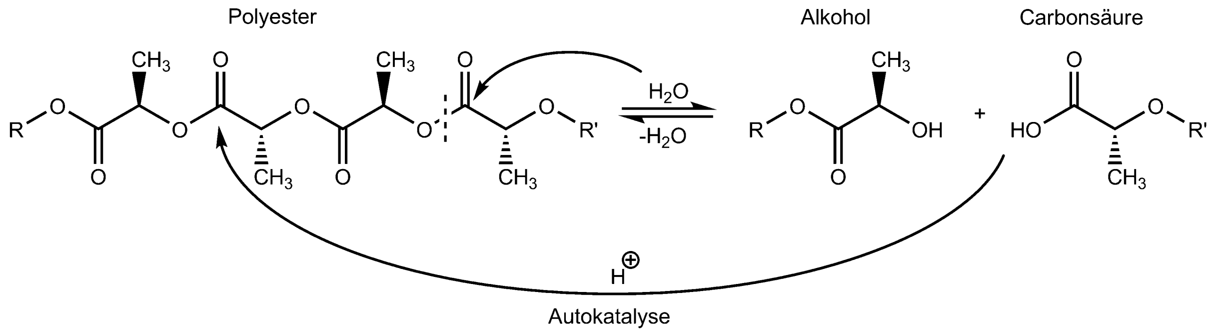

Abb. 6 Reaktionsschema des PLLA-Abbaus durch Hydrolyse der Esterbindungen entlang der Polymerkette, die nur durch Anwesenheit von Wasser stattfindet. Zusätzlich kann die Reaktion durch die sich während des Abbaus bildende freie Carbonsäure autokatalytisch verstärkt werden.

Die bei der Reaktion entstehende freie Säure kann nun wiederum die weitere Esterhydrolyse katalysieren. Bei dieser Autokatalyse hat das Endprodukt eine katalytische Wirkung auf die Reaktion selbst und beschleunigt diese mit fortlaufender Produktbildung. Diese lässt sich vereinfacht wie folgt beschreiben:

$$E + S = S + A \tag{1}$$

Wobei E = Ester, S = Säure und A = Alkohol darstellen. Gleichung 2 beschreibt den Reaktionsfortschritt über die Abnahme der Esterkonzentration im Laufe der Zeit [25]:

$$\frac{dC_E}{dt} = -\frac{dC_{COOH}}{dt} = -k \cdot C_{COOH} \cdot C_E \tag{2}$$

wobei C_{COOH}, C_{H_2O} und C_E die Konzentrationen der Carboxylendgruppen, des Wassers bzw. des Esters darstellen [25]. Anderson *et al.* [64] beschreiben eine mathematische Methode, um das Molekulargewicht mit der Hydrolysegeschwindigkeit in Beziehung zu setzen. Da das Molekulargewicht direkt mit der Spaltung der Polymerketten zusammenhängt gilt die zeitliche Änderung von M_n mit der Hydrolysegeschwindigkeit der Esterbindungen wie folgt:

$$\frac{dC_E}{dt} = \frac{d(1/M_n)}{dt} \tag{3}$$

Unter der Annahme, dass das Ausmaß des Molmassebbaus nicht groß ist, gaben sie die folgende kinetische Beziehung an:

$$\frac{1}{M_{n,t}} = \frac{1}{M_{n,0}} + k \cdot t \tag{4}$$

wobei $M_{n,t}$ das zahlenmittlere Molekulargewicht zum Zeitpunkt t, $M_{n,0}$ das zahlenmittlere Molekulargewicht zum Zeitpunkt Null und k die Geschwindigkeitskonstante der Hydrolysereaktion ist. Die Abbaugeschwindigkeit wird somit ausschließlich durch M_n beeinflusst. PLLA mit niedrigerem M_n wird dementsprechend schneller abgebaut als hochmolekulares PLLA.

Diese Methode berücksichtigt jedoch noch nicht die Möglichkeit der Autokatalyse, da die Bildung von freier Milchsäure ebenfalls die Geschwindigkeit des hydrolytischen Abbaus erhöht (siehe Abb. 6) [25,65].

Mit $C_{E,0}$ und $C_{S,0}$ als Konzentrationen des Esters bzw. der Säure als Katalysator zu Beginn der Reaktion (t = 0) ergibt sich folgendes Zeitgesetz:

$$C_{E,t} = \frac{C_{E,0} + C_{S,0}}{1 + \frac{C_{S,0}}{C_{E,0}} \cdot e^{-(C_{E,0} + C_{S,0})kt}} \tag{5}$$

Diese Gleichung beschreibt einen sigmoidalen Verlauf des Stoffumsatzes und ist in Abb. 7 a dargestellt [66]. Die Reaktion verläuft zu Beginn sehr langsam (Induktionsphase), da nur sehr wenig Katalysator vorhanden ist, nimmt dann mit fortschreitender Reaktion und zunehmender Katalysatormenge stetig zu und verlangsamt sich am Ende wieder, wenn der Ester verbraucht ist.

Unter der Annahme, dass die Ester- und Wasserkonzentrationen, da im Überschuss vorhanden, konstant bleiben und $C_{COOH} \propto \frac{1}{M_n}$, ist, ergibt sich folgender Zusammenhang [25]:

$$M_{n,t} = M_{n,0} \cdot e^{-kt} \tag{6}$$

Anhand dieser Gleichung lässt sich für den autokatalytischen Abbau eine Beziehung zwischen $\ln M_n$ und der Zeit wie folgt ableiten:

$$\ln M_{n,t} = - k \cdot t + \ln M_{n,0} \tag{7}$$

In diesem Fall wird die Degradation durch $\ln M_n$ abgebildet [30]. Abb. 7 zeigt schematisch die Abnahme des Molekulargewichts für die nicht-katalytische und autokatalytische Hydrolyse. Aus der Abbildung ist ersichtlich, dass eine starke autokatalytische Hydrolyse durch eine initial langsamere Verringerung des Molekulargewichts gekennzeichnet ist, während eine nicht-katalytische Hydrolyse durch eine anfänglich starke Verringerung des Molekulargewichts gekennzeichnet ist. Dies liegt daran, dass sich im Gegensatz zur nicht-katalytischen Kettenspaltung bei einer autokatalytischen Hydrolyse die Reaktionsgeschwindigkeit mit der Bildung kleiner Kettenfragmente im Reaktionsverlauf selbst beschleunigt. Trägt man die Molmassenentwicklung im Bulk für den nicht-katalytischen Reaktionsverlauf als Kehrwert ($1/M_n$) gegen die Zeit auf (Gleichung 4), so zeigt sie einen linearen Verlauf (siehe Abb. 7 b). Für die Autokatalyse gilt nach diesen Modellen eine lineare Beziehung zwischen $\ln M_n$ gegen die Zeit (aus Gleichung 7). Die Linearität für die beiden Auftragungen erlaubt eine Aussage darüber, welcher Reaktionsmechanismus zugrunde liegt. Das angewandte Modell basiert auf der Randbedingung, dass der Abbau noch nicht zu weit fortgeschritten ist und nur Daten bis zum ersten Masseverlust berücksichtigt werden können, damit der Abtransport von Reaktionsprodukten nicht in Betracht gezogen werden muss [64,67].

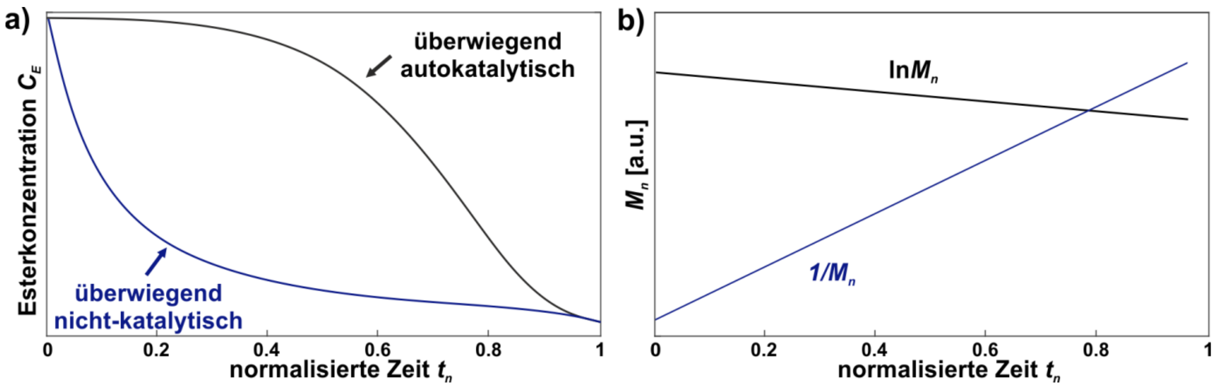

Abb. 7 a) Schematische Darstellung der Esterkonzentration in Abhängigkeit von der Zeit t_n (normalisiert auf den Zeitpunkt des ersten Masseverlustes) während der PLLA Hydrolyse. Abgebildet ist der sigmoidale Verlauf (überwiegend autokatalytische Hydrolyse) im Vergleich zum hyperbolischen Verlauf (überwiegend nicht-katalytische Hydrolyse) der C_E-Abnahme durch Degradation [25,65]. b) Logarithmische Darstellung der Molmassenentwicklung gegen die Abbauzeit (schwarze Kurve in b). Die so erhaltenen Daten sollten linear sein, wenn der Abbau autokatalytisch verläuft. Die blaue Kurve in b) stellt $1/M_n$ als Funktion der Abbaudauer dar. In diesem Fall verläuft die Degradation überwiegend nicht-katalytisch, wenn die aufgetragenen Daten linear sind [64].

2.3. Mehrkomponentensysteme auf Basis von Poly(L-lactid)

Blendmaterialien

Unter Polymerblends versteht man ein Gemisch aus zwei oder mehr Polymerkomponenten. Polymermischungen erlauben es, die Eigenschaften der Blendpartner in vorteilhafter Weise zu kombinieren, um so völlig neue Eigenschaftsbilder zu erstellen, die sich aus den Merkmalen der Einzelkomponenten nicht vorhersagen lassen und somit auch vorgegebene Eigenschaftsbilder optimal einzustellen [68]. Allerdings weisen Mischungen durchaus auch komplexes Mischphasenverhalten auf. Von entscheidender Bedeutung für die erzielbaren Eigenschaften eines Polymergemisches ist außer den Anteilen und der Beschaffenheit der Einzelkomponenten auch die Zahl der vorliegenden Phasen. So können Blends ein- oder mehrphasig sein. Im Falle der mehrphasigen Blends, d.h. Gemische aus unverträglichen Polymerbestandteilen, spielt daher die Wechselwirkung an den Grenzflächen der Phasen eine entscheidende Rolle [69].

Wenn zwei Polymere gemischt werden, ist das häufigste Ergebnis ein System, das aufgrund der abstoßenden Wechselwirkung zwischen den Komponenten eine vollständige Phasentrennung aufweist [70]. Eine vollständige Mischbarkeit in einer Mischung aus zwei Polymeren setzt voraus, dass die freie Energie ΔG_m folgende Bedingung erfüllt:

$$\Delta G_m = \Delta H_m - T\Delta S_m < 0 \tag{8}$$

wobei ΔH_m und ΔS_m die Enthalpie bzw. die Entropie der Mischung bei der Temperatur T sind. Der Wert von $T\Delta S_m$ ist immer positiv, da die Entropie beim Mischen ansteigt. Daher hängt das Vorzeichen von ΔG_m immer vom Wert der Mischungsenthalpie ΔH_m ab [71]. Die Polymerpaare vermischen sich nur dann zu einer einzigen Phase, wenn der entropische Beitrag zur freien Energie den enthalpischen Beitrag übersteigt:

$$\Delta H_m < T\Delta S_m \tag{9}$$

Die Mischbarkeit von Polymerblends lässt sich anhand eines Phasendiagramms erklären, das in Abb. 8 dargestellt ist. Es gibt drei Bereiche mit unterschiedlichem Grad der Mischbarkeit:

I. der einphasige mischbare Bereich zwischen den beiden Binodalen (homogene Mischphase)
II. die vier fragmentierten metastabilen Phasen zwischen Binodalen und Spinodalen (metastabile Phase)
III. die zweiphasig getrennten Bereiche der Unmischbarkeit (Phasenseparation), die von den Spinodalen begrenzt werden

Die Binodale trennen den mischbaren (einphasigen) und metastabilen Bereich, die Spinodale den metastabilen und zweiphasigen Bereich. Außerhalb der Mischungslücke liegt das Gemisch im Gleichgewicht als homogene Mischphase vor, während es innerhalb der Mischungslücke koexistierende Phasen bildet.

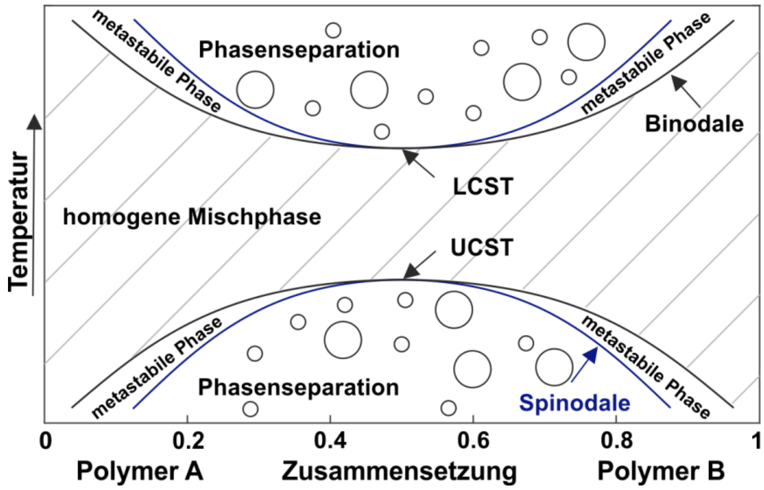

Abb. 8 Phasendiagramm eines Polymerblends aus zwei Komponenten, nach [72]. Dargestellt ist neben der Binodalen, die den einphasigen Bereich von dem metastabilen Bereich trennt, die Spinodale, welche den metastabilen vom zweiphasigen Bereich trennt. Außerhalb der Mischungslücke, in welcher beide Komponenten phasensepariert vorliegen, ist das Gemisch im Gleichgewicht als homogene Mischphase vorhanden. Dabei gibt die untere kritische Lösungstemperatur (LCST) das Minimum der Phasenseparationsgrenze an, während die obere kritische Lösungstemperatur (UCST) das Maximum der Phasenseparationsgrenze darstellt.

Das Diagramm zeigt auch zwei kritische Lösungstemperaturen: die Lower Critical Solution Temperature (LCST), und die Upper Critical Solution Temperature (UCST) [73]. Eine Phasentrennung von zwei Polymeren findet statt, wenn ein einphasiges System eine Änderung der Zusammensetzung, der Temperatur oder des Drucks erfährt, die es zwingt, in den binodalen Bereich einzutreten [74,75].

Die Flory-Huggins-Gittertheorie wurde entwickelt, um das Phasenverhalten von Polymermischungen und von Polymeren in Lösungsmitteln zu beschreiben [71]. Unter der Annahme einer zufälligen Mischung zweier Polymere kann für binäre Systeme der Ausdruck für die freie Energie der Mischung wie folgt beschrieben werden:

$$\Delta G_m = RT\left[\frac{\varphi_1}{r_1}\ln\varphi_1 + \frac{\varphi_2}{r_2}\ln\varphi_2 + \chi^*\varphi_1\varphi_2\right] \tag{10}$$

wobei φ_i der Volumenanteil der Komponente *i*, r_i die Anzahl der Kettensegmente und R die Gaskonstante ist. χ^* beschreibt den so genannten Flory-Huggins-Parameter für binäre Wechselwirkungen und T die absolute Temperatur. Die ersten beiden Terme der rechten Seite in Gleichung 10 beziehen sich auf die Mischungsentropie und der dritte Term ist der Mischungsenthalpie zugeordnet. Für Polymere mit unendlicher Molmasse, r_i ist unendlich, ist der entropische Beitrag sehr gering, und die Mischbarkeit oder Unmischbarkeit des Systems hängt hauptsächlich vom Wert der Mischungsenthalpie ΔH_m ab:

$$\Delta H_m = RT\chi^*\varphi_1\varphi_2 \tag{11}$$

Mischbarkeit kann nur erreicht werden, wenn χ^* negativ ist. Bei Polymeren kann die Mischbarkeit erreicht werden, wenn $\chi^* < \chi^*_{cr}$ ist, wobei χ^*_{cr} gegeben ist aus:

$$\chi_{cr}^{*}=\frac{1}{2}\left(\frac{1}{\sqrt{r_1}}+\frac{1}{\sqrt{r_2}}\right)^2 \tag{12}$$

Daraus ergibt sich, dass χ^* ausschließlich von der molaren Masse der beiden Polymerkomponenten abhängt. Darüber hinaus konnte ein Zusammenhang zwischen dem Flory-Huggins-Parameter und der Grenzflächenbreite w zwischen den Polymerblends wie folgt hergestellt werden [76,77]:

$$w\sim\left(\chi^{*}-\chi_{cr}^{*}\right)^{-0,5} \tag{13}$$

Die Bestimmung der Grenzflächenbreite über optische Messmethoden kann demnach Aufschluss über das Phasenverhalten von Polymermischungen geben [78,79]. Im Rahmen dieser Arbeit wurden sowohl rasterelektronische als auch Raman-Aufnahmen erstellt, um das Grenzflächenverhalten von dem Polymerblend PLLA/PCL in verschiedenen Mischungsverhältnissen und bei verschiedenen Tempertemperaturen zu untersuchen.

Wirkstofffreisetzungssysteme

Die Kombination von funktionalen Implantaten mit API ist in der Biomedizintechnik unverzichtbar geworden, wobei Stents ideale Trägerplattformen sind. Diese Drug-Eluting Stents (DES) sind als wirkstofffreisetzende Implantate Bare Metal Stents (BMS) in vielerlei Hinsicht überlegen [80–84]. Sie ermöglichen eine örtlich begrenzte und zeitlich gesteuerte Abgabe von Wirkstoffen und schirmen gleichzeitig die polymeren Implantatwerkstoffe effektiv gegenüber metabolischen Einflüssen des Organismus ab. Im Vergleich kommt es bei Verwendung von BMS bei 15-30 % durch eine übermäßige Intimaproliferation zu einer In-Stent-Restenose, welche durch Verwendung von DES auf unter 10 % reduziert werden konnte [85].

Eine der gebräuchlichsten Technologien ist die Inkorporation von API in eine auf das Stent aufgebrachte Polymerbeschichtung. Eine breite Palette von Polymeren ist als wirkstofftragende Matrix für DES im klinischen Einsatz [86–88]. Neben chemisch inerten Polymeren, wie z.B. (per)fluorierten Polymeren, wird vor allem PLA aufgrund der leichten Verarbeitbarkeit und Bioresorption als Beschichtungsmatrix verwendet [89,90]. Tab. 1 gibt einen Überblick über den Stand der Technik bei den verfügbaren DES. Zu den häufig verwendeten Pharmaka für kardiovaskuläre Implantate gehört die Substanzklasse der Limus-Familie, u.a. Sirolimus (SIR) [91–94], und Paclitaxel (PTX) [95,96]. SIR wird hauptsächlich wegen seiner mTOR-Inhibition eingesetzt, einer eigentlich immunsuppressiven Wirkung zur Verhinderung der Abstoßung von Organtransplantaten, wodurch aber auch die Zellproliferation und damit das Risiko einer Restenose im Stent verringert wird [97,98]. PTX wird als Beschichtung auf Ballons oder als Polymer/Wirkstoff-Depot von DES direkt in den Zielbereich appliziert [84]. Der Wirkmechanismus von PTX besteht in der Hemmung der

Migration und Proliferation glatter Muskelzellen [99]. Jedoch wird die Verwendung dieses Pharmakons aufgrund eines erhöhten Risikos der Spätmortalität in Frage gestellt [100].

Tab. 1 Übersicht über ausgewählte DES (modifiziert nach [87]), Daten zur Wirkstoffbeladung wurden aus [101] entnommen.

Stent / Hersteller	Stent-material	Polymer-beschichtung	Absorption-dauer	Wirkstoff	Wirkstoff-freisetzungs-dauer	Wirkstoff-beladung
CYPHER / Cordis	Edelstahl	PEVA/PBMA	Permanent	Sirolimus	90 Tage	140 µg/cm^2
TAXUS EXPRESS / Boston Scientific	Edelstahl	SIBS	Permanent	Paclitaxel	>180 Tage	100 µg/cm^2
XIENCE ALPINE / Abbott Laboratories	CoCr	PVDF-HFP	Permanent	Everolimus	120 Tage	100 µg/cm^2
RESOLUTE INTEGRITY / Medtronic	CoNi mit PtIr	BioLinx	Permanent	Zotarolimus	180 Tage	N/A
ORSIRO / Biotronik	CoCr	PLLA	15 Monate	Sirolimus	100–120 Tage	1.4 µg/mm^2
ULTIMASTER / Terumo Interventional Systems	CoCr	PDLLA-PCL	3–4 Monate	Sirolimus	3–4 Monate	N/A
SYNERGY / Boston Scientific	PtCr	PLGA	3–4 Monate	Everolimus	3 Monate	38–179 µg/stent
NOBORI / Terumo	Edelstahl	PDLLA	6–9 Monate	Biolimus	6–9 Monate	15.6 µg/mm^2

Weitere sogenannte Multi-Drug-Delivery-Strategien enthalten oft mehrere Wirkstoffe, wie PTX zur Verhinderung von Restenosen durch Hemmung des Fibroblastenwachstums gepaart mit Biomolekülen, nichtfreisetzenden Molekülen, Antikörpern, Proteinen, Peptiden oder Wachstumsfaktoren, die die Reendothelialisierung fördern sollen. Zu den bestehenden Strategien zählen zweischichtige Poly(lactid-*co*-glycolid)-Nanopartikel (PLGA), die vaskuläre endotheliale Wachstumsfaktoren (VEGF) und PTX enthalten [96,102–104]. Dazu gehören bereits mit elektrogesponnenen Fasern aus PLA bedeckte Stents, die PTX-geladene mesoporöse Siliziumdioxid-Nanopartikel enthalten und deren Oberfläche mit VEGF beschichtet ist [105,106]. Das hohe Oberflächen-Volumen-Verhältnis von Vliesstoffen kann die Oberflächenkonjugation maximieren und somit die Wirkstofffreisetzung verbessern [107–110]. Im Rahmen der durchgeführten Arbeiten wurden die thermischen Eigenschaften von dünnen wirkstoffinkorporierten Folien- mit Vliesmaterialien verglichen und der Einfluss verschieden inkorporierter Wirkstoffe auf die physiko-chemischen Eigenschaften der PLLA-Folien charakterisiert.

3. Methoden zur entwicklungsbegleitenden Charakterisierung polymerbasierter Implantatmaterialien

An polymerbasierte Implantatmaterialien werden unterschiedliche mechanische Anforderungen gestellt. Ein ballonexpandierender Polymerstent z.B. soll nicht nur plastisch verformbar sein, sondern auch eine hohe Stabilität aufweisen. Ein selbstexpandierender Polymerstent jedoch sollte elastisch verformbar sein. Daher muss der verwendete Werkstoff sowohl eine hohe Bruchdehnung als auch die erforderliche Festigkeit aufweisen, damit eine gute Einführbarkeit in das Gefäß als auch ausreichende radiale Stabilität gegenüber Gefäßspannungen gewährleistet ist [111]. Um vergleichbare mechanische Festigkeiten wie bei einem Metallgrundkörper zu erreichen, bei denen Strutdicken bereits zwischen 60 und 91 µm (CoCr) hergestellt werden können [112], sind bei Stentdesigns aus Polymermaterial bisher Strutdicken zwischen 98 und 170 µm realisiert worden [113]. Die dickeren Stentstreben führen jedoch zu einer verzögerten Endothelialisierung und einem erhöhten Thromboserisiko aufgrund der starken Beeinträchtigung der Hämodynamik [114]. Um die spezifischen Probleme polymerbasierter Stents zu lösen, ist eine Weiterentwicklung von Stentdesigns mit dünneren Streben in Verbindung mit adäquaten mechanischen Materialeigenschaften durch Fortschritte in der Werkstofftechnologie erforderlich [115].

Werden Polymermaterialien als DES-Beschichtung verwendet, neigen diese dazu, bei mechanischer Belastung während der Implantation, die durch das Einführen in das Gefäß und die Expansion des Stents verursacht wird, zu frakturieren oder z.T. in partikulärer Form, zu delaminieren [83,111]. Daher muss eine Wirkstoffbeschichtung neben dem erforderlichen Freisetzungsverhalten und der Biokompatibilität auch adäquate mechanische Eigenschaften in Kombination mit einer Widerstandsfähigkeit gegen Delamination aufweisen.

Diese Anforderungen sowohl an den Polymerstent als auch an die DES-Beschichtung sind in einer Reihe geeigneter technischer Prüfverfahren unter Anwendung der in Tab. 2 relevanten Prüfnormen nachzuweisen. Die Verfahren hierzu sind in DIN EN ISO 25539-2 definiert [20] und finden im Rahmen dieser Arbeit Anwendung.

Tab. 2 Übersicht über relevante Prüfnormen zur mechanischen und thermischen Charakterisierung von thermoplastischen Polymeren.

Prüfnorm	Titel	Bemerkung
ISO 527 / ASTM D 638 [116,117]	Kunststoffe - Bestimmung der Zugeigenschaften	beinhaltet sowohl die allgemeinen Grundsätze als auch die Prüfbedingungen für alle Prüfkörper
ASTM D 1708 [118]	Standard Test Method for Tensile Properties of Plastics by Use of Microtensile Specimens	umfasst die Bestimmung der vergleichenden Zugfestigkeit und der Dehnungseigenschaften von Standard-Mikrozugproben
ASTM D 882-18 [119]	Standard Test Method for Tensile Properties of Thin Plastic Sheeting	umfasst die Bestimmung der Zugeigenschaften von Kunststoffen in Form von dünnen Folien (d ≤ 1,0 mm)
ASTM D618-21 [120]	Standard Practice for Conditioning Plastics for Testing	legt Verfahren fest zur Konditionierung von Kunststoffen vor der Prüfung und die Bedingungen, unter denen sie geprüft werden
ISO 11357 / DIN 53765 [121,122]	Kunststoffe - Dynamische Differenz-Thermoanalyse (DSC)	beinhaltet alle Grundlagen der DSC und die zur Durchführung relevanten Prüfbedingungen
ASTM D3418(2012) [123] / ASTM E793[124]	Standard Test Method for Transition Temperatures of Polymers by Differential Scanning Calorimetry	umfasst übergeordnet die Bestimmung der Übergangstemperaturen und der Schmelz- und Kristallisationsenthalpien von Polymeren
ASTM E794(2018) [125]	Standard Test Method for Melting And Crystallization Temperatures By Thermal Analysis	beschreibt die Bestimmung der Schmelz- und Kristallisationstemperatur von reinen Materialien - Erweiterung zu ASTM D3418
ASTM E1356-08(2014) [126]	Standard Test Method for Assignment of the Glass Transition Temperatures by Differential Scanning Calorimetry	umfasst die Bestimmung der Glasübergangstemperaturen von Werkstoffen, welche sich im Glasübergangsbereich nicht zersetzen oder sublimieren

3.1. Polymer- und Wirkstoffverarbeitung – Auswahl der Fertigungsverfahren und Prüfkörperherstellung

Zu den hauptsächlich verwendeten Verarbeitungstechnologien von Polymeren gehören thermische und lösungsmittelbasierte Herstellungsprotokolle [127]. Beim thermischen Verfahren wie Extrusion, Spritzguss oder Schmelzgießen werden die Polymere bis zur flüssigen Phase erhitzt und in eine Form gegeben. Der anschließende Abkühlprozess des Formkörpers ist entscheidend für die Ausbildung und das Wachstum der Kristallstrukturen, die die Oberflächenmorphologie und Festigkeit des Prüfkörpers beeinflussen [68]. Diese thermischen Verfahren sind aufgrund der einfachen Prozessierung besonders geeignet zur Herstellung von Bulkmaterialien, wie beispielsweise Stenthalbzeugen.

Die andere Möglichkeit der Verarbeitung stellen lösungsmittelbasierte Herstellungsprotokolle dar. So beruhen in der Industrie viele Beschichtungsverfahren auf der Verwendung von Polymerlösungen. Das Lösen eines Polymers in einem geeigneten Lösungsmittel ermöglicht eine Vielzahl verschiedener Verfahren wie Gieß- und Tauchverfahren, Elektrospinnen und -sprühen, Airbrush, Spin-Coating und Ultraschallsprühprozesse zur Erzeugung homogener und reproduzierbarer Beschichtungen auf komplexen Implantatstrukturen [127–131]. Diese Verfahren eignen sich besonders für das Prototyping und die Kleinserienproduktion im Labormaßstab. Darüber hinaus ermöglichen lösungsmittelbasierte Protokolle das Einbringen thermisch empfindlicher Wirkstoffe, z.B. Pharmaka, Wachstumsfaktoren oder Partikel [88]. Im Vergleich dazu müssen diese bei der thermischen Verarbeitung eine Temperaturstabilität oberhalb T_m der Polymere aufweisen, wodurch die Auswahl von Zusätzen eingeschränkt wird [88,89,132]. Im Gegensatz zur thermischen Verarbeitung erfordern die Lösungsmittelverfahren jedoch eine zusätzliche Nachbehandlung der Materialien, die aus Waschen und/oder Tempern bestehen kann, um Lösungsmittelrückstände zu beseitigen ohne die API aus dem Verbund herauszulösen [133]. Diese müssen insbesondere in Bezug auf medizinische Anwendungen gewährleisten, dass sich die Restlösemittelgehalte nach der Postprozessierung unterhalb der ICH-Grenzwerte für Medizinprodukte befinden, um schädliche oder toxische Nebenwirkungen auszuschließen [134,135]. Jeder dieser Prozessschritte beeinflusst wiederum stark die physiko-chemischen Eigenschaften, beispielsweise durch Nachkristallisation des Materials oder Umstrukturierung des Gefüges, was auch bedeutet, dass die endgültigen charakteristischen Eigenschaften des gewünschten Materials bereits während der Produktion gezielt gesteuert werden müssen, z.B. durch Temperprotokolle, Wahl und Konzentration der Lösungsmittel, Sprühparameter und Waschverfahren [136,137]. Vor diesem Hintergrund wurden die verwendeten Herstellungsprotokolle zur Durchführung entwicklungsbegleitender Charakterisierungen in vorangegangenen Studien entwickelt und sind in den nächsten Abschnitten als auch in der Abb. 9 beschrieben.

Degradationsproben

Für die im Rahmen dieser Arbeit durchgeführten Degradationsstudien wurden Polymerfolien durch Gießverfahren, gemäß Abb. 9 a, aus Chloroform ($CHCl_3$) gegossen. Um eine vollständige Entfernung des Lösungsmittels aus den Folien zu gewährleisten, wurden diese nach dem Verdampfen des Lösungsmittels zwei Tage lang in Methanol (MeOH) und zwei Tage in entionisiertem Wasser gewaschen. Anschließend wurden die Folien für 7 Tage im Vakuumofen bei T = 40 °C gelagert [138]. Mit diesem Verfahren wurden Prüfkörper mit einer Dicke von d = 100 µm hergestellt.

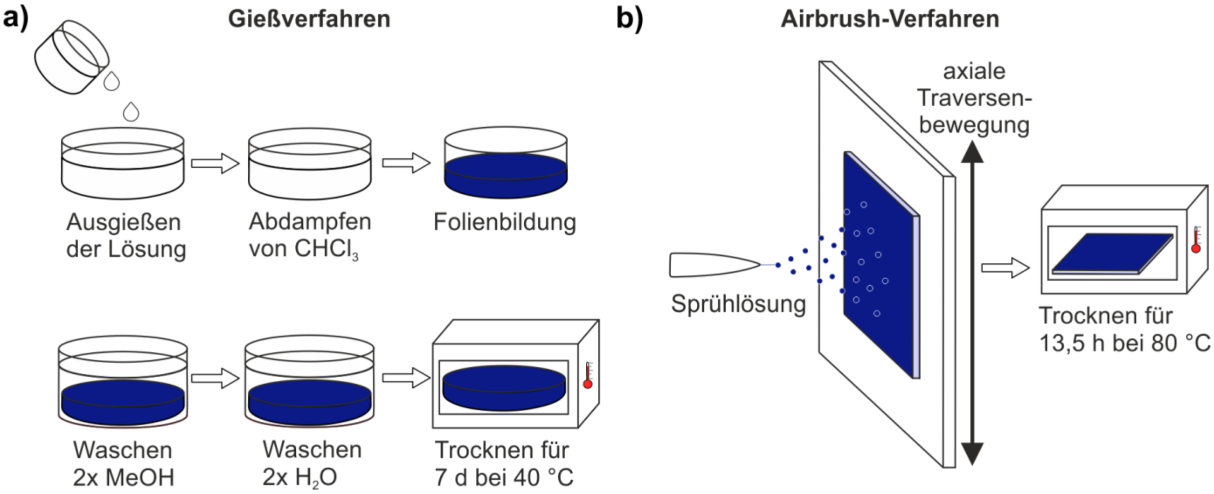

Abb. 9 a) Prüfkörperherstellung unter Verwendung des Gießverfahrens. Die hergestellten Folien mit einer Schichtdicke von ca. 100 µm werden einem Waschprozess mit Methanol (MeOH) und Wasser unterzogen und anschließend für 7 Tage in einem Ofen getrocknet, um den Restlösemittelgehalt unterhalb der geforderten Grenzwerte für Medizinprodukte zu reduzieren [138]. b) Herstellung einer Sprühfolie durch Airbrush-Verfahren. Während des Prozesses wird der zu besprühende Träger axial bewegt, um eine homogene Polymerschicht zu erzeugen. Die Sprühfolien werden anschließend für t = 13,5 h bei T = 80 °C unter vermindertem Druck getrocknet.

Blendherstellung

Für die Herstellung von Gießfolien wurden Polymerlösungen identisch zu der Probenpräparation der Degradationsstudien angesetzt, wobei neben den reinen Polymeren PLLA und PCL weiterhin deren Mischungen in verschiedenen Verhältnissen (90/10, 50/50, 10/90 %*w/w*) hergestellt wurden. Für weiterführende Untersuchungen unter verschiedenen Tempertemperaturen wurden die Proben von PLLA, PCL und deren Mischungen in einen Ofen gegeben und bei verschiedenen Temperaturen (40 °C, 80 °C und 200 °C) für 60 Minuten bei Umgebungsatmosphäre erhitzt (Abb. 10). Anschließend wurden alle Proben mit q_c = 1 K/min im Ofen abgekühlt.

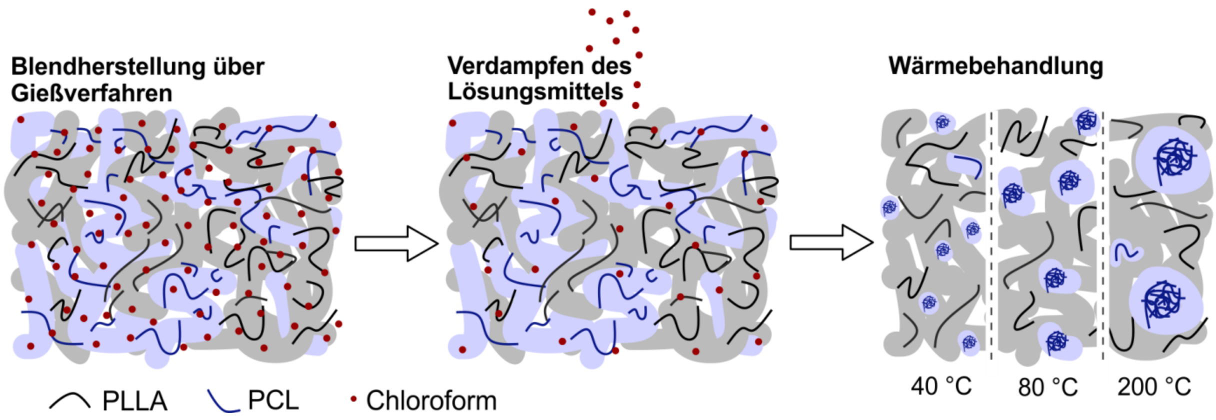

Abb. 10 Prüfkörperherstellung eines Polymerblends aus PLLA und PCL. Dieser wurde im Lösungsmittel-Gießverfahren hergestellt und verschiedenen Nachbehandlungsschritte unterzogen. Während Chloroform verdampft bilden sich PLLA- und PCL-reiche Domänen, deren Struktur sich durch die anschließende Wärmebehandlung bei 40 °C, 80 °C und 200 °C stark unterscheiden kann und somit Einfluss auf die physiko-chemischen Eigenschaften des Polymerblends nimmt.

Wirkstoffinkorporierte Probenherstellung

Mit Hilfe des Airbrush-Verfahrens, gemäß der Abb. 9 b, wurden dünne Folien aus PLLA mit inkorporierten Pharmaka hergestellt. Dazu wurde PLLA in $CHCl_3$ gelöst und eine Wirkstofflösung in MeOH (PTX, SIR, DEX und CYCLO) oder $CHCl_3$ (CYCLO) hinzugefügt. Für jedes Pharmakon wurde ein endgültiges Verhältnis von 10, 15 bzw. 20 %*w/w* in Bezug auf das gelöste Polymer eingestellt, um eine gezielte Freisetzung im therapeutischen Fenster zu gewährleisten [139,140]. Als Referenz wurde eine reine PLLA-Folie auf die gleiche Weise ohne Zugabe von Wirkstoffen hergestellt. Anschließend wurden aus den angefertigten Lösungen mit einem Airbrush-Gerät dünne Folien mit einer Materialstärke von etwa d = 7 µm auf rechteckigen Glasobjektträgern erzeugt, um *in vivo*-nahe Bedingungen zu realisieren. Die Lösungsmittelreste von den beschichteten Glasobjektträgern wurden unter reduziertem Druck bei T = 80 °C entfernt.
Für den Vergleich der thermischen Eigenschaften von PLLA-Folien (fPLLA) und -Nanofasern (nfPLLA) wurden fPLLA über das Airbrush-Verfahren und nfPLLA über Elektrospinningverfahren hergestellt. Zusätzlich wurde die Polymeroberfläche aller Proben mit Sauerstoffplasma aktiviert, um eine stabile Oberflächenimmobilisierung mit dem vaskulären endothelialen Wachstumsfaktor (VEGF) zu gewährleisten. Durch die Plasmabehandlung lassen sich polare und funktionelle Gruppen auf der Polymeroberfläche erzeugen, um so die Ankopplung mit weiteren Wirkstoffen zu vereinfachen.

3.2. *In vitro* Degradation

Um Degradationsexperimente von biodegradierbaren Polymermaterialien realistisch in den Entwicklungsprozess zu integrieren, sind beschleunigte *in vitro*-Abbauprotokolle erforderlich. Diese ermöglichen es, das Langzeitverhalten der Polymere in einem relativ kurzen Experiment zu reproduzieren. Ebenso spielen Enzyme beim *in vivo*-Abbau dieser Materialien eine wichtige Rolle, gerade in den späten Stadien des Polymerabbaus mit einem hohen Grad an Materialfragmentierung und bereits drastisch verringertem Molekulargewicht (< 20.000 g/mol) [141,142]. Daher wurden die Abbaubedingungen gemäß den Normen ISO 13781 und ISO 15814 mit einer Degradationstemperatur von T = 37 °C gewählt, um *in vivo*-Bedingungen zu simulieren und eine maximale Enzymaktivität zu gewährleisten [143,144]. Darüber hinaus wurde in Anlehnung an die Van't-Hoff-Regel eine Temperatur von T = 55 °C verwendet, um beschleunigte Abbaubedingungen zu schaffen. Hierdurch wurde es möglich, Polymere innerhalb einer sehr kurzen Zeit abzubauen, wofür sonst mehrere Jahre investiert werden müssen. Außerdem lag die gewählte Temperatur unterhalb der Glasübergangstemperatur T_g von PLLA, um dadurch strukturelle Veränderungen zu vermeiden, die durch den Abbau

oberhalb T_g verursacht werden und um die Vergleichbarkeit der beiden gewählten Abbaubedingungen zu gewährleisten.
Für die enzym-assoziierten Echtzeitstudien wurde Sørensen-Puffer verwendet, dem zusätzlich 5,0 mg/l Proteinase K, 5,0 mg/l Pseudomonas Lipase und 7,7 mg/l Aspergillus Lipase hinzugefügt wurde [145]. Die Proben wurden nach 2, 4, 12, 24, 36, 48, 60, 72, 84, 96 und 108 Wochen für weiterführende Untersuchungen entnommen. Jede Polymerprobe wurde mit destilliertem Wasser gewaschen und eine Woche lang bei T = 40 °C unter reduziertem Druck getrocknet.
Für die beschleunigten Untersuchungen wurde jede Probe einzeln in Sørensen-Puffer ohne Enzyme bei pH = 7,4 inkubiert, nach 0,2, 1, 2, 3, 4, 6, 8, 10, 12, 14 und 16 Wochen für weitere Untersuchungen entnommen und gemäß der Echtzeitstudie nachbehandelt.

3.3. Morphologische Charakterisierung

Um neben dem Phasenverhalten von Polymerblends ebenso übergeordnete Kristallstrukturen von PLLA mit verschiedenen inkorporierten Wirkstoffen beurteilen zu können, wurden im Rahmen dieser Arbeit die Morphologie der Polymerfolien rasterelektronenmikroskopisch (REM) mit einem SEM QUANTA FEG 250 (FEI Company, Deutschland) und rasterkraftmikroskopisch (AFM) mit einem NanoWizard II (JPK Instruments AG, Deutschland) untersucht.
Im Hinblick auf die Phasentrennung des Polymers und hinsichtlich der Verteilung des Wirkstoffes an der Oberfläche wurden die Polymerproben zusätzlich mittels Raman-Bildgebung mit einem konfokalen Raman-Mikroskop WITec alpha 300 (WITec GmbH, Deutschland) durchgeführt. Für die Visualisierung von Phasentrennungsphänomenen wurden Signale gewählt, die für die einzelnen Polymere und Wirkstoffe spezifisch sind.

3.4. Ermittlung der mechanischen Eigenschaften

Zur Bestimmung der mechanischen Eigenschaften der Polymere stellt der quasistatische, uniaxiale Zugversuch eine standardisierte Methode der Kunststoffprüfung dar und liefert Werkstoffkennwerte als Grundlage für die Materialauswahl [146]. Dafür wird eine Rechteckprobe oder ein genormter Zugstab gemäß der ISO 527-2 in einer Universalprüfmaschine mit konstanter Traversen-Geschwindigkeit langsam und stoßfrei gezogen [116]. Die auftretenden Kräfte werden auf die Querschnittsfläche A_0 bezogen und die daraus resultierenden Normalspannungen σ berechnet [147].

$$\sigma = \frac{F}{A_0} \tag{14}$$

Die Zugfestigkeit R_M eines Materials ergibt sich aus der maximalen Zugspannung, die während des Versuches registriert wird [148]. Die Dehnung ε lässt sich aus der Verlängerung ΔL bezogen auf die Ausgangslänge L_0 gemäß

$$\epsilon = \frac{\Delta L}{L_0} = \frac{L - L_0}{L_0} \tag{15}$$

berechnen. Die Bruchdehnung ε_B eines Materials ist als Dehnung beim Erreichen der Bruchspannung σ_B definiert [148].

Der mikroskopische Aufbau des thermoplastischen PLLA beeinflusst maßgeblich die mechanischen Eigenschaften des Polymers. Wird ein thermoplastischer Kunststoff unter einachsigem Zug beansprucht, können verschiedene Deformationsphasen unterschieden werden, Abb. 11. Für PLLA im speziellen bedeutet dies, dass es sich im ersten Teil der Deformation linear elastisch (reversibel) verhält. Gegen Ende des linear elastischen Bereiches beginnen erste Makromolekülkettenabschnitte sich gegeneinander zu verschieben und die Kurve wird flacher bzw. nichtlinear bis hin zum lokalen Maximum. Im zweiten Schritt verstrecken sich die amorphen Bereiche und nach Erreichen der Fließspannung fällt die Spannung ab, wobei sich die Probe einschnürt, die sich entlang der Probe ausbreitet. Das Spannungsniveau bleibt während dieser Phase annähernd konstant.

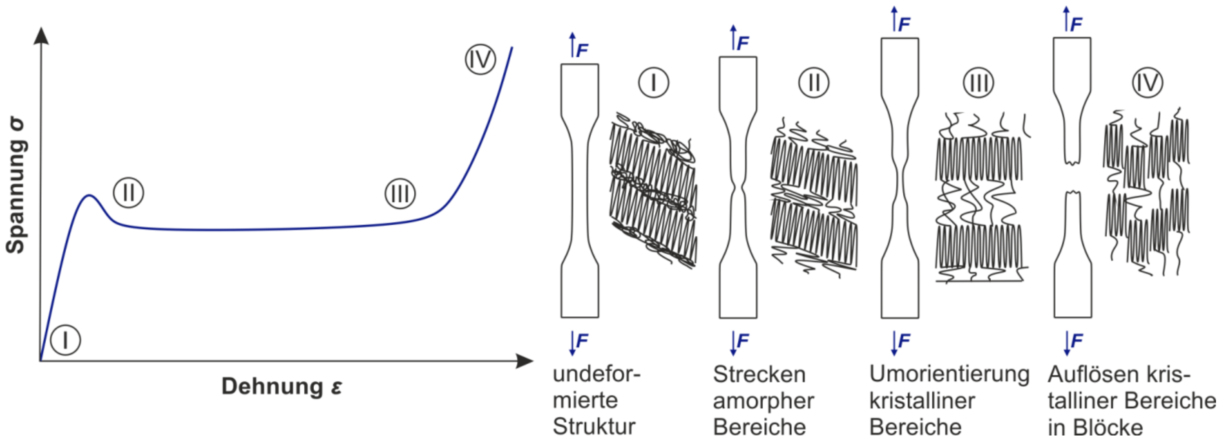

Abb. 11 Stadien der Verformung eines thermoplastischen Polymers unter quasistatischer uniaxialer Zugbelastung nach [149]. Zu Beginn wird der Probekörper elastisch verformt (I). Die amorphen Bereiche verstrecken sich und nach Erreichen der Fließspannung fällt die Spannung ab, wobei sich die Probe einschnürt (II). Bei größeren Dehnungen ordnen sich die kristallinen Bereiche so um, dass die Molekülketten in Belastungsrichtung orientiert werden (III). Sobald alle lasttragenden Molekülketten vollständig orientiert und gestreckt sind, führt jede weitere Belastungssteigerung zum mechanischen Bruchversagen der Probe (IV).

Die Moleküle orientieren sich entlang der Belastungsrichtung in den amorphen Bereichen und zusätzlich tritt eine Orientierung der Kristalle auf, bis diese vollständig gestreckt sind und der Prüfkörper reißt [115,150].

Die in der vorliegenden Arbeit durchgeführten Untersuchungen des Spannungs-Dehnungs-Verhaltens von PLLA erfolgten im quasistatischen Zugversuch bei Raumtemperatur (RT) mit einer Universalprüfmaschine Zwick ZN 2.5 (Zwick GmbH & Co. KG, Deutschland). Dafür wurden Prüfkörper gemäß DIN EN ISO 527-2 1BB mit den effektiven Abmessungen von l = 12 mm und b = 2 mm präpariert. Mit Hilfe des sogenannten Zeit-Temperatur-Verschiebungsprinzips kann das mechanische Verhalten für verschiedene Temperaturen und verschiedene Belastungsgeschwindigkeiten ineinander umgerechnet werden [146]. Die Zusammenhänge stellt die folgende Gleichung dar:

$$log\left(\frac{t}{t_{ref}}\right) = k \cdot \left(\frac{1}{T} - \frac{T}{T_{ref}}\right) \tag{16}$$

Auf Grundlage des zeitabhängigen Verhaltens von Polymeren bei einachsiger Zugbeanspruchung wurden die mechanischen Tests mit einer konstanten Traversengeschwindigkeit von v = 25 mm/min durchgeführt. Neben dem zeitabhängigen Verhalten spielt der Einfluss von Medium auf die Polymereigenschaften bei Zugbeanspruchung eine wichtige Rolle. Durch die Diffusion von Medium in die Polymermatrix kann diese wie ein Weichmacher wirken und die Polymereigenschaften nachhaltig beeinflussen. In dieser Arbeit wurden die Versuche dennoch in trockener Umgebung durchgeführt, um insbesondere bzgl. der Wirkstoffinkorporation die eingebrachten Wirkstoffe nicht herauszuwaschen, was das Messergebnis verfälschen könnte. Auf der Grundlage der erhaltenen Kraft-Verlängerungs-Messkurven wurde der Elastizitätsmodul E im linear elastischen Bereich berechnet. Außerdem wurde die Zugfestigkeit R_M und die Bruchdehnung ε_B bestimmt.

3.5. Thermische Analyse

Viele Faktoren wie M_w, Restmonomergehalt, aber auch äußere Faktoren wie Abkühlgeschwindigkeit, Lösemittel oder Nachprozessierungen wie Sterilisation beeinflussen die thermischen Eigenschaften von PLLA. Dies wiederum hat Einfluss auf die mechanischen Eigenschaften des Polymers und auf das Degradations- und Diffusionsverhalten der inkorporierten Pharmaka. Daher ist es von großer Wichtigkeit, die thermischen Eigenschaften von PLLA-basierten MKS zu charakterisieren.

Zur thermischen Charakterisierung von Polymeren dient die Dynamische Differenz Kalorimetrie (DSC), welche es ermöglicht, eine Reihe von physikalischen Prozessen zu untersuchen [151]. Aus dem Energieeintrag lassen sich Rückschlüsse auf Kristallisationsprozesse, das Schmelzverhalten und mit ihnen die Änderung im Enthalpie- ΔH und Entropieverhalten ΔS ziehen. Daneben können mit den kalorimetrischen Messungen sämtliche Prozesse untersucht werden, die eine Änderung der Wärmekapazität zeigen, wie z.B. der Glasübergang T_g. Bei dem in dieser Arbeit verwendeten Wärmestromkalorimeter werden der Proben- und Referenztiegel gemeinsam in einem Ofen erhitzt. Der sich ändernde Wärmestrom dQ ist proportional zur Temperaturdifferenz der beiden Tiegel und wird als

Messkurve über der Temperatur *T* aufgezeichnet. Die Schmelzwärme *ΔH* und der Kristallisationsgrad χ können mit der folgenden Gleichung 17 quantitativ bewertet werden:

$$\chi = 100\,\% \cdot \left[\frac{\Delta H_m}{\Delta H_{m0}}\right] \cdot \frac{1}{W} \tag{17}$$

wobei ΔH_{m0} der Enthalpiewert eines reinen kristallinen Materials, ΔH_m die dem Schmelzprozess entsprechende Enthalpie und *W* die Menge der einzelnen Komponenten bei polymerbasierten MKS ist. Die zeitlich nicht konstante Materialgröße der Kristallinität bestimmt maßgeblich das Eigenschaftsbild teilkristalliner Polymere.

Abb. 12 zeigt beispielhaft ein DSC-Thermogram für PLLA, welche mit einer Heizrate von *q* = 10 K/min aufgeheizt wurde. Das Diagramm veranschaulicht sowohl exotherme als auch endotherme Ereignisse, die während eines Temperaturscans von 40 °C bis 200 °C auftraten. Der endotherme Temperatursprung (Glasübergang) tritt im Scan zuerst bei ca. 60 °C auf, gefolgt von einem exothermen Peak um etwa 100 °C, der auch Kaltkristallisation genannt wird. Dieser ist immer Folge von thermodynamisch instabilen Zuständen (Eigenspannungen, Orientierungen, unvollkommene Kristallstruktur), die aus den verarbeitungsbedingten Abkühlbedingungen bei der Herstellung entstehen.

Um 180 °C tritt ein endothermer Peak durch Schmelzen auf. Anhand der erhaltenen exo- und endothermen Peaks wird der Kristallisationsgrad aus der latenten Kristallisations- und Schmelzwärme mittels Peakintegration bis zur Baseline bestimmt.

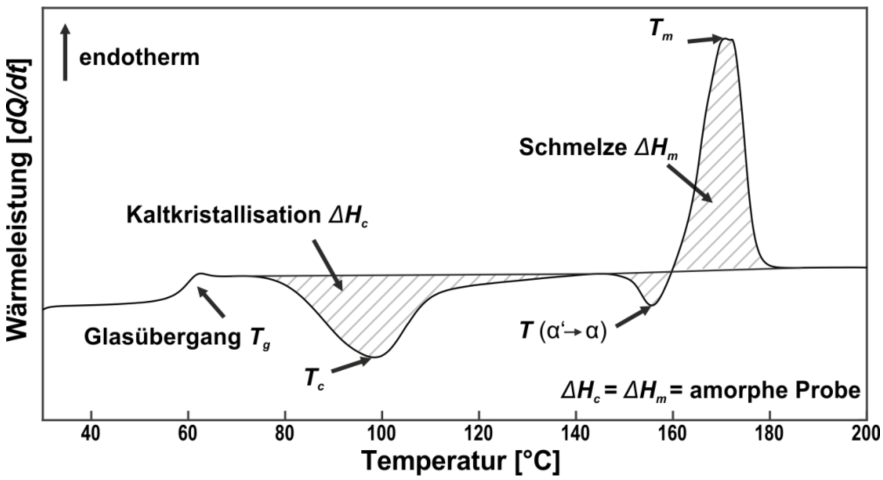

Abb. 12 DSC Aufheizkurve des teilkristallinen Polymers PLLA mit Darstellung wichtiger thermischer Effekte. Aufgetragen ist die Wärmeleistung über die Temperatur. Die Glasübergangstemperatur T_g ist als Stufe in der Messkurve zu erkennen. Je nach thermischer Vorgeschichte kann PLLA bei weiterer Temperaturerhöhung exotherm auskristallisieren (Kaltkristallisation ΔH_c). Das endotherme Schmelzen ΔH_m erfolgt bei weiterer Temperaturerhöhung, wobei T_m die Schmelztemperatur darstellt. Sind die Integrale der Kaltkristallisation und Schmelze identisch, so liegt das Polymer in amorpher Form vor. Der exotherme Peak vor dem Schmelzen zeigt den Übergang der kristallinen Form α' zu α.

Um eine geeignete thermische Charakterisierung der MKS vornehmen zu können, ist eine Kenntnis über die thermischen Übergänge der einzelnen Komponenten von hoher Bedeutung. Diese ermöglichen eine Beurteilung der thermischen Änderungen durch Bildung von

Mischphasen [152]. Ebenso können über DSC Messungen Aussagen über thermische Änderungen getroffen werden, welche beispielsweise durch Postprozessierungsschritte initiiert wurden [135].

Im Rahmen dieser Arbeit wurden die thermischen Eigenschaften mit einer DSC 1 (Mettler Toledo, Schweiz) untersucht. Es wurden konventionelle Kalibrierungsmethoden mit hochreinen Standards verwendet. Die Proben wurden mit einer Heizrate von q = 10 K/min unter Stickstoff bei atmosphärischem Umgebungsdruck erhitzt. Die Endtemperatur lag zwischen T = 210 °C und 280 °C, je nach Polymersystem und eingearbeitetem Wirkstoff. Die Proben wurden im Hinblick auf T_g, T_m und χ analysiert. Die Schmelz- und Kristallisationswärme wurde quantitativ bewertet, indem die endothermen Peakflächen bestimmt wurden, die mit der Schmelzpeakfläche von vollständig kristallinem PLLA (χ_{100} = 93,7 J/g) [153] verglichen wurden.

4. Physiko-chemische Untersuchung hochmolekularer Poly(L-lactid)-basierter Mehrkomponentensysteme

4.1. Studie 1: *In vitro* Degradation von PLLA unter *in vivo*-nahen und beschleunigten Bedingungen

Die Erarbeitung von Degradationsexperimenten im Labormaßstab für Biomaterialien auf Polymerbasis ist für die Entwicklung sicherer und funktioneller Implantate von entscheidender Bedeutung. Jedoch erfordern lange PLLA Degradationszeiten von mehr als zwei Jahren beschleunigte Untersuchungskonzepte, um diese realistisch in den Entwicklungsprozess zu integrieren. Daher war das Ziel dieser Studie, aus den erhaltenen Ergebnissen der enzym-assoziierten Echtzeit-Degradation und des beschleunigten Abbauprotokolls ein Korrelationsmodell zu entwickeln. Dazu wurden für den beschleunigten Abbau lösungsmittelgegossene PLLA-Folien bei T = 55 °C für 16 Wochen degradiert und mit der enzym-assoziierten (Proteinase K und Lipasen) Echtzeit-Degradation, die bei T = 37 °C für 108 Wochen durchgeführt wurde, verglichen. Es wurden PLLA mit unterschiedlichen Molgewichten (PLLA L210 mit M_w = 320.000 g/mol und PLLA L214 mit M_w = 700.000 g/mol) verwendet, um den Einfluss des Molekulargewichts M_w auf das Degradationsverhalten zu untersuchen. Unter beiden angewandten Bedingungen wurde eine wellenförmige Entwicklung der Kristallinität von PLLA beobachtet, wobei sich χ mit 75 % fast verdoppelte. Anhand der gewonnenen Ergebnisse konnte ein Korrelationsmodell entwickelt werden, das auf der Verringerung des Molekulargewichts basiert.

Enzym-assoziierte Degradation

Ansatz dieser Studien war es, unter Verwendung von Lipasen die *in vivo*-Situation für den PLLA-Abbau abzubilden. Im Ergebnis konnte ein linearer Masseverlust für PLLA L210 von etwa 30 % und für L214 von bis zu 73 % innerhalb des untersuchten Zeitraumes von 108 Wochen beobachtet werden. Für L214 wurde beim enzym-assoziierten Echtzeit-Abbau bei T = 37 °C nach 24 Wochen eine schnelle Abnahme der Masse beobachtet, während das Molekulargewicht nur eine geringe Abnahme zeigte [Pub1]. Dies kann auf den enzymatischen Oberflächenabbau zurückgeführt werden, Vgl. Abb. 5. Aufgrund des stärkeren Masseverlustes von PLLA L214 im Vergleich zu PLLA L210 wird geschlussfolgert, dass L214 schneller von Enzymen abgebaut wird, was ebenfalls durch Literaturdaten unterstützt wird [59].

Thermisches Verhalten während der Degradation

Beim Vergleich der Kristallinitäten beider PLLA Varianten wurden nur geringe Änderungen in χ während der ersten 36 Monate der Echtzeit-Degradation beobachtet. Nach 108 Wochen jedoch verdoppelte sich χ beider Polymere nahezu, von χ_{L210}(36 Wochen) = 31 ± 4 % auf einen Wert von χ_{L210}(108 Wochen) = 57 ± 4 %, und χ_{L214}(36 Wochen) = 26 ± 4 % auf χ_{L214}(108 Wochen) = 48 ± 5 %. Ein ähnlicher Trend wurde bei der Studie zur beschleunigten Degradation für beide PLLA-Arten festgestellt. Bis zur 8-wöchigen Degradation bei *T* = 55 °C blieb χ_{L210} nahezu konstant bei etwa 40 %, gefolgt von einem Anstieg auf χ_{L210} = 75 ± 7 %. Dieses Verhalten wurde auch bei L214 nachgewiesen, wenn auch nicht so ausgeprägt wie bei L210. Bis zu 6 Wochen lag χ_{L214} bei etwa 35 %, gefolgt von einem Anstieg bis zu 16 Wochen auf χ_{L214} = 44 ± 8 %. Zusätzlich wurde eine wellenförmige Entwicklung von χ beobachtet, was in Bezug auf den Vergleich beider Degradationsstudien Berücksichtigung finden muss.

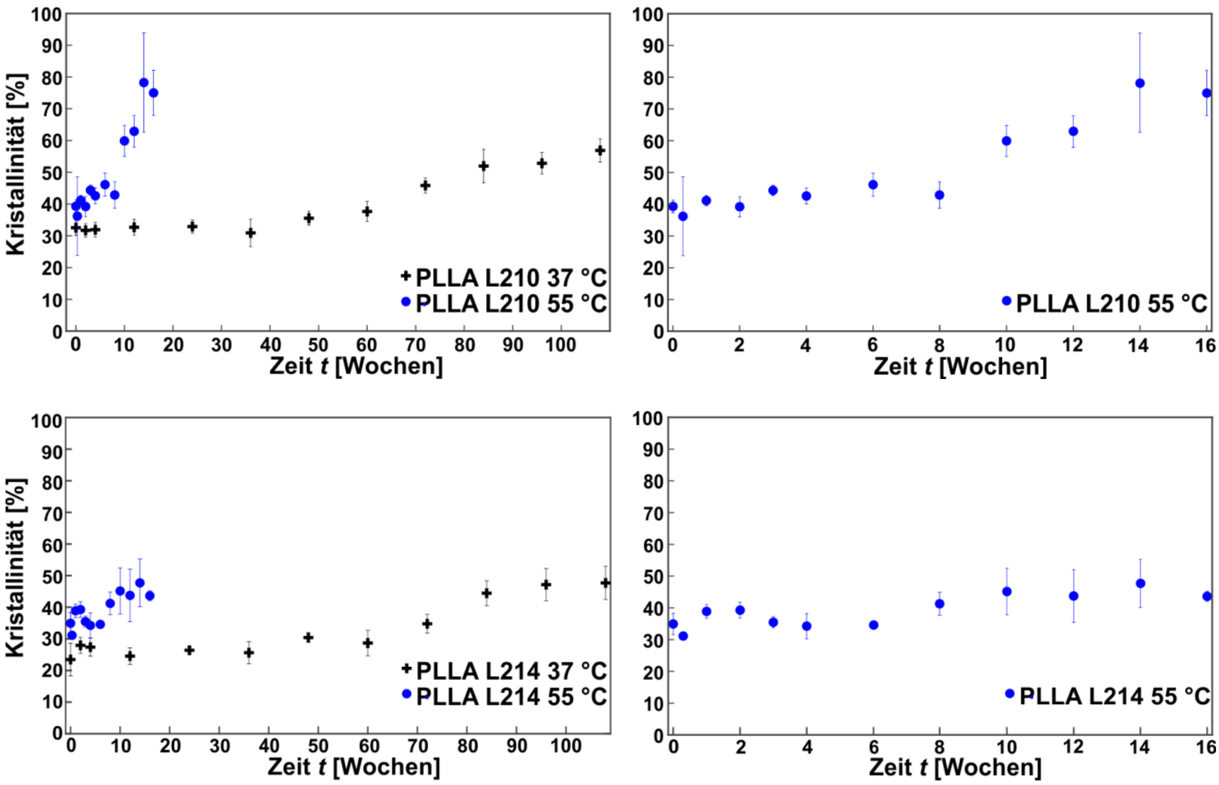

Abb. 13 Änderungen der Kristallinität während der Echtzeit-Degradation bei *T* = 37 °C (schwarz) im Vergleich zum beschleunigten Abbau (blau) von PLLA L210 (oben) und PLLA L214 (unten), n = 5.

Vergleich von Echtzeit-Experimenten mit beschleunigten Degradationsbedingungen

Um beschleunigte Experimente auf Echtzeitstudien abbilden zu können, wurde die Entwicklung des Molekulargewichtes M_w herangezogen. Zu diesem Zweck wurden die Abbauzeiten jeweils auf den Zeitpunkt des ersten Masseverlustes normiert. Dies ist relevant, um den Einfluss der Enzyme während der Echtzeit-Degradation auszuschließen und so eine Vergleichbarkeit der Studien gewährleisten zu können.

In Abb. 14 (links) wurde die Molekulargewichtsabnahme der Echtzeit- und beschleunigten Abbaustudien über die normierte Zeit aufgetragen und zur besseren Veranschaulichung mit linearen Trendlinien versehen. Aus den Molekulargewichten der beschleunigten Experimente und denen der Echtzeitstudie der erhaltenen normalisierten Zeitpunkte wurden die Quotienten *Q* bestimmt und über die Degradationszeit aufgetragen, siehe Abb. 14 rechts. Für einen erleichterten Vergleich beider Studien wurde eine Trendlinie für *Q* hinzugefügt.

Im Fall von PLLA L210 zeigte sich, dass eine Echtzeitstudie normiert auf den Zeitpunkt des ersten Masseverlustes von einem halben Jahr durch eine beschleunigte Studie von sechs Wochen abgebildet werden kann, wobei M_w unter beschleunigten Bedingungen im Vergleich zur Echtzeit-Degradation um das 1,5-fache abnahm. Bei PLLA L214 bildete eine 16-wöchige Degradation bei T = 55 °C eine 48-wöchige Degradation in Echtzeit ab, wobei sich M_w um das 1,3-fache reduzierte.

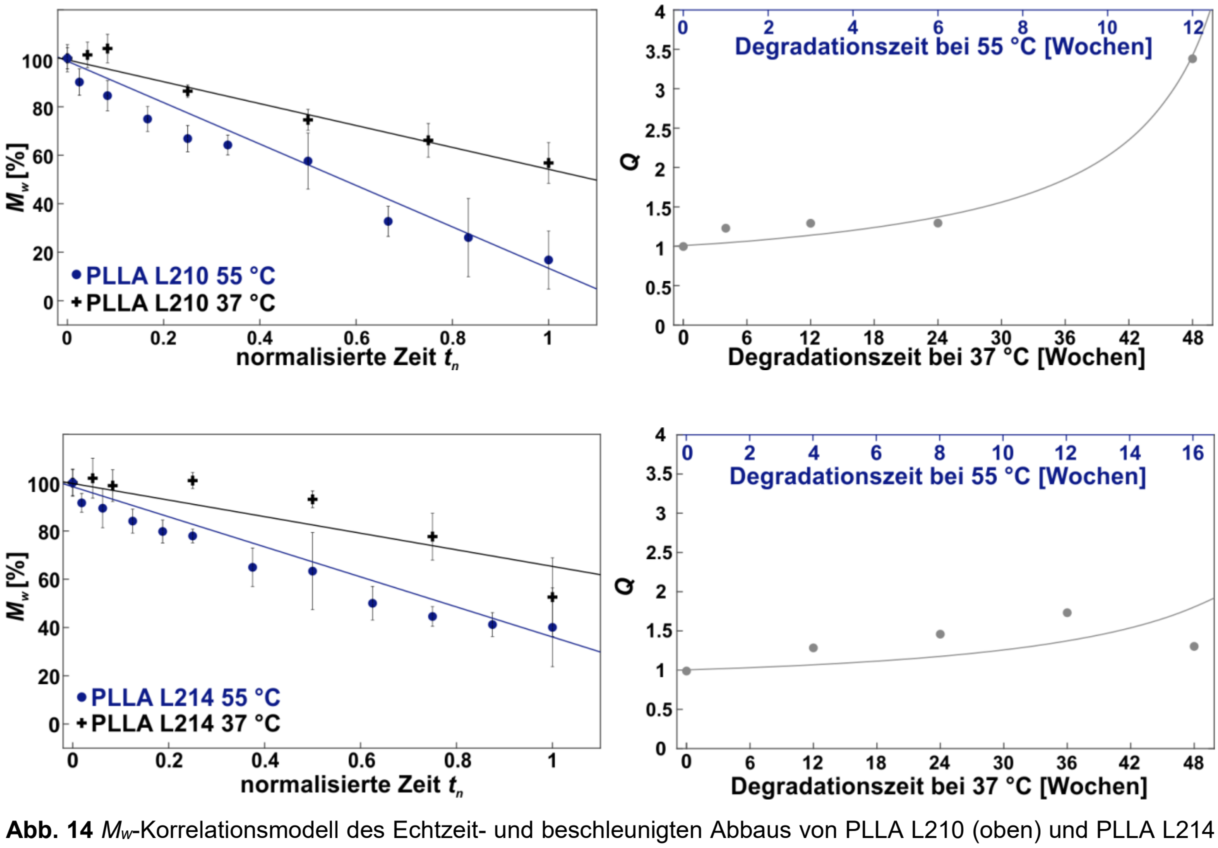

Abb. 14 M_w-Korrelationsmodell des Echtzeit- und beschleunigten Abbaus von PLLA L210 (oben) und PLLA L214 (unten). Dargestellt ist der Molekulargewichtsverlust der Echtzeit- und der beschleunigten Degradationsstudien über die Zeitpunkte t_n (normalisiert auf den Zeitpunkt des ersten Masseverlustes) (links). Zur Veranschaulichung wurden lineare Trendlinien hinzugefügt. Für die Abbildung der beschleunigten Studie auf die Echtzeitstudie wurde der Quotient aus den Molekulargewichten der beschleunigten Experimente und denen der Echtzeitstudie berechnet und über die Degradationszeit aufgetragen (rechts). Die durchgezogene Linie zeigt die Trendlinie für *Q* über die Abbauzeit.

Autokatalytischer Masseabbau im Vergleich zu nicht-katalytischem Abbau

Die Autokatalyse spielt eine wichtige Rolle bei der Degradation von Polyestern. Das Modell von Anderson *et al.* [64] kann verwendet werden, um abzuschätzen, ob die Esterhydrolyse stärker autokatalysiert oder nicht-katalysiert abläuft. Unter der Annahme, dass der enzym-assoziierte Abbau nur an der Probenoberfläche stattfindet und die gebildeten Polymerfragmente sofort ausgewaschen werden, können von beiden Degradationsbedingungen Untersuchungen zu diesen Degradationsmechanismen anhand der Molmassenentwicklung der Polymere durchgeführt werden. Dazu wurde die lineare Anpassung (R^2) an die Auftragung von lnM_n (Autokatalyse) und $1/M_n$ (nicht-katalytisch) gegen die Degradationszeit bis zum ersten Masseverlust bestimmt. Diese Beziehung ist für PLLA L210 und L214 in Abb. 15 dargestellt.

Beide PLLA-Varianten wiesen bereits zu Beginn der Studie einen Masseverlust aufgrund des enzym-assoziierten Abbaus auf, was eine Bestimmung des Endpunktes der Auftragung verhindert. Deshalb wurden die Zeitpunkte für den ersten Masseverlust (48 Wochen) von Weir *et al.* und Tsuji *et al.* [67,154] zur Berechnung von R^2 herangezogen.

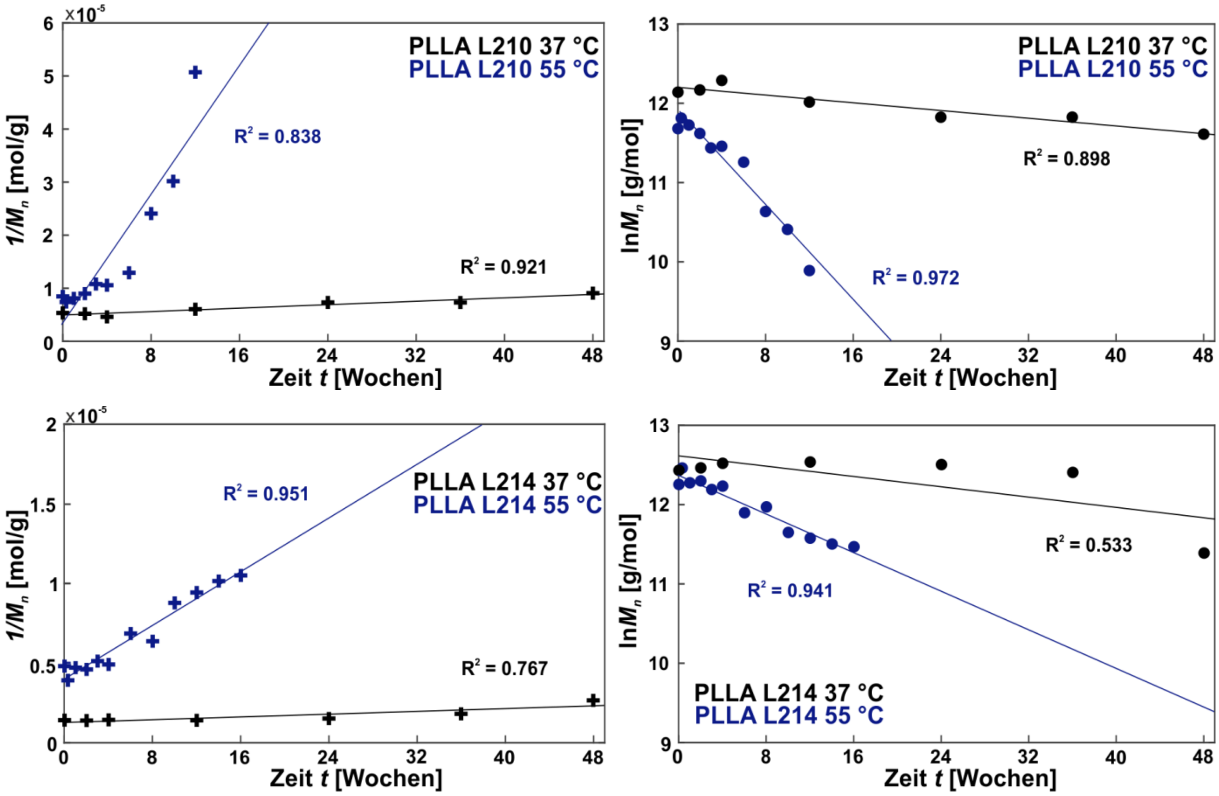

Abb. 15 Darstellung des nicht-katalysierten Modells (links) im Vergleich zu den autokatalysierten Modell (rechts) von PLLA L210 (oben) und PLLA L214 (unten) beim enzym-assoziierten Echtzeit-Abbau (schwarz) und beschleunigten Abbau (blau) [64,67,154].

Unter beschleunigten Bedingungen ohne Enzymeinwirkung begann der Masseverlust von PLLA L210 nach 12 Wochen und von PLLA L214 nach 16 Wochen. PLLA L210 zeigte sowohl für den beschleunigten Abbau als auch für die Echtzeit-Degradation für die R^2-Anpassung von

$1/M_n$ (entsprechend Gleichung 4) und $\ln M_n$ (entsprechend Gleichung 7) keine eindeutige Tendenz ($R^2_{1/Mn}$ = 0,921 und R^2_{lnMn} = 0,898 bei T = 37 °C, siehe Abb. 15). Für T = 55 °C wurden ähnliche Werte ermittelt ($R^2_{1/Mn}$ = 0,838 und R^2_{lnMn} = 0,972). Daraus lässt sich schließen, dass sowohl eine nicht-katalytische als auch eine autokatalytische Esterhydrolyse stattfindet.
Für PLLA L214 kann anhand der Daten von einer eher nicht-katalytischen Esterhydrolyse bei T = 37 °C ausgegangen werden ($R^2_{1/Mn}$ = 0,767 vs. R^2_{lnMn} = 0,533). Bei T = 55 °C zeigen die R^2-Anpassungen keinen klaren Unterschied ($R^2_{1/Mn}$ = 0,951vs. R^2_{lnMn} = 0,941), daher scheinen beide Hydrolysemechanismen vorzuliegen. Die generell niedrigen R^2-Werte für L214 in der Echtzeitstudie deuten jedoch darauf hin, dass die von Anderson *et al.* [64] entwickelte Theorie im Gegensatz zu L210 auf PLLA L214 aufgrund der sehr hohen Molmassen von 700.000 g/mol nicht anwendbar ist.

Einfluss des Herstellungsverfahrens auf die Degradation

Wie die Ergebnisse für PLLA L210 und L214 zeigen, hat das anfängliche Molekulargewicht einen deutlichen Einfluss auf die Geschwindigkeit der Oberflächenerosion unter Beteiligung von Enzymen. Aufgrund der Enzymdenaturierung können hingegen enzym-assoziierte Effekte bei höheren Temperaturen nicht abgebildet werden. Es findet somit keine Oberflächenerosion statt und Kettenfragmente aus dem Masseabbau bleiben im Körper eingeschlossen, was in frühen Versuchsstadien zu keinem beobachtbaren Masseverlust führt, vgl. Abb. 5.

Durch den Vergleich der durchgeführten Studie mit Literaturdaten [67,154] kann gefolgert werden, dass, unabhängig von der Probenvorbereitung, eine Vergleichbarkeit der *in vitro*-Abbaudaten sowohl mit lösungsmittelbasierten als auch mit Schmelzgussverfahren erreicht wird, sofern eine vergleichbare Anfangskristallinität vorliegt, vgl. Abb. 13. Hinsichtlich der Molekulargewichtsabnahme konnte nachgewiesen werden, dass für PLLA L210 eine 6 wöchige beschleunigte Degradationsstudie bei T = 55 °C eine 26-wöchige Echtzeitdegradation abbildet. Ebenso konnte aus den Ergebnissen geschlossen werden, dass für PLLA L214 eine 16 wöchige Abbaustudie bei T = 55 °C eine 48-wöchige Echtzeitdegradation abbildet. Jedoch muss berücksichtigt werden, dass der wellenförmige Verlauf der Kristallinität diesem entwickelten Modell Grenzen setzt. Ebenso spielt das Molekulargewicht eine entscheidende Rolle, wenn es um Enzym-assoziierte Oberflächenabbauprozesse und den damit verbundenen Massenverlust geht, und sollte bei der Planung von *in vitro*-Studien berücksichtigt werden.

4.2. Studie 2: Betrachtung der Phasenseparationseffekte von PLLA/PCL-Blends

Blends aus PLLA und PCL weisen in der Regel komplexes Phasentrennungs- und Kristallisationsverhalten auf, was sich stark auf ihre Eignung für bestimmte biomedizinische Anwendungen, wie abbaubare Beschichtungen oder Wirkstoffträger, auswirkt [155,156]. Daher ist es wichtig, die zugrunde liegenden Mechanismen zu verstehen. In Studie 2 [Pub2] wurde PLLA mit PCL in verschiedenen Masseanteilen (10, 50 und 90 %*w/w* PCL) in Lösung gemischt und anschließend zu Folien ausgegossen. Um den Einfluss eines zur Entfernung des Restlösemittels notwendigen Temperprotokolls auf die Materialeigenschaften des PLL/PCL-Blends zu ermitteln, wurden diese verschiedenen Temperaturen (40 °C, 80 °C und 200 °C) ausgesetzt, verbunden mit einer langsamen Abkühlung, um das thermodynamische Gleichgewicht im Blend zu erhalten. Mit Hilfe von Rasterelektronen-, Rasterkraft- und Raman-Mikroskopie sowie DSC wurden Struktur, Morphologie und thermische Eigenschaften der PLLA/PCL-Blends untersucht und mit Literaturdaten verglichen. Die ermittelten physiko-chemischen Eigenschaften der hergestellten PLLA/PCL-Blends unterschieden sich erheblich von denen, die durch Schmelzverfahren erreicht wurden [157–159]. So zeigte PLLA/PCL 90/10 bei T = 40 °C ein anderes Spannungs-Dehnungs-Verhalten im Vergleich zu einer Temperung bei T = 200 °C, was mit den Änderungen in der Kristallinität korrelierte, wobei χ_{PLLA} von 43 auf 61 % anstieg.

Einfluss der Tempertemperatur auf die Morphologie

Das morphologische Verhalten von reinem PLLA ist in Abb. 16 durch rasterelektronische (REM) und rasterkraftmikroskopische Aufnahmen (AFM) dargestellt. Morphologisch bildet PLLA beim Tempern von t = 60 min bei T = 40 °C ($PLLA_{T40}$) (Abb. 16 d) und T = 80 °C ($PLLA_{T80}$) (Abb. 16 e) eine einheitliche Phase mit Sphärolithen (Vergleich siehe Abb. 4 a) von etwa Ø = 20 µm. Im Vergleich dazu vergrößerte sich der Durchmesser solcher PLLA-Sphärolithe beim Tempern bei T = 200 °C ($PLLA_{T200}$) auf etwa Ø = 100 µm, was vergleichbar mit der Literatur ist [160–162].

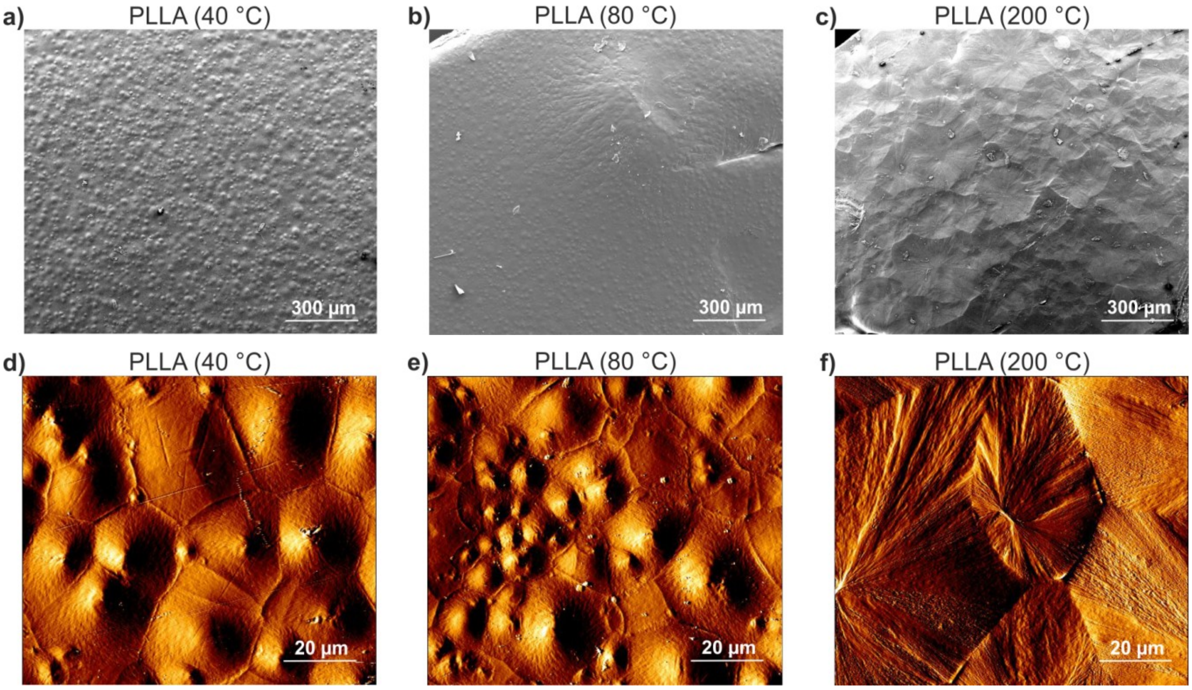

Abb. 16 Exemplarische rasterelektronische (a-c) und rasterkraftmikroskopische Aufnahmen (d-f) der reinen PLLA-Folie, welche 60 min bei Temperaturen von 40 °C, 80 °C und 200 °C getempert wurde. Durch die Wärmebehandlung mit immer höheren Temperaturen bilden sich zunehmend größere Sphärolithe aus.

Demgegenüber unterscheidet sich die Oberflächenmorphologie von PLLA/PCL 50/50 bei verschiedenen Temperbedingungen, welche in Abb. 17 durch REM-Aufnahmen dargestellt ist. Von einer anfänglich homogenen Oberfläche bei T = 40 °C (PLLA/PCL $50/50_{T40}$) (Abb. 17 a) geht die Oberfläche bei T = 80 °C (PLLA/PCL $50/50_{T80}$) in eine perforierte Struktur über (Abb. 17 b), die sich bei T = 200 °C (PLLA/PCL $50/50_{T200}$) in eine glatte und eine davon klar abgegrenzte mit Sphärolithen besetzte Domäne entwickelt (Abb. 17 c).

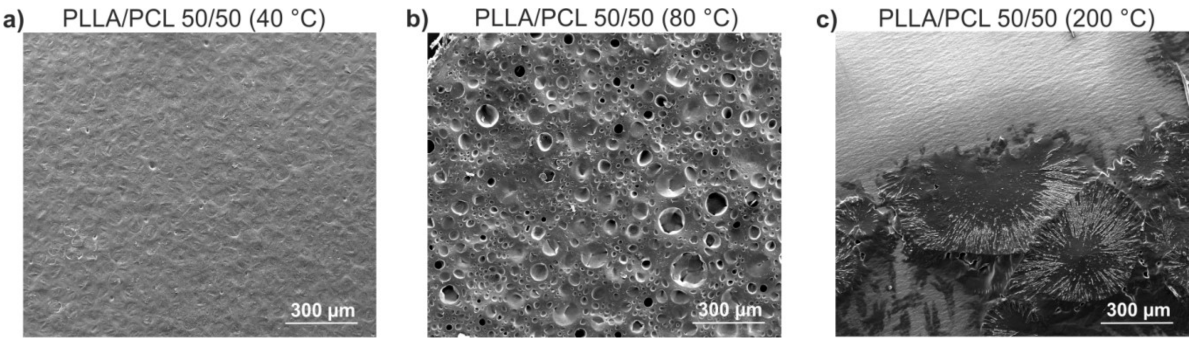

Abb. 17 Exemplarische rasterelektronische Aufnahmen des PLLA/PCL-Blends im Verhältnis 50/50 %*w/w*, welche 60 min bei Temperaturen von 40 °C, 80 °C und 200 °C getempert wurden. Durch die Wärmebehandlung bei T = 200 °C bilden sich zwei separate Strukturen aus, eine glatte und eine mit Sphärolithen besetzte Domäne.

Aufgrund der unterschiedlichen Schmelztemperaturen beider Polymerkomponenten bildet sich eine Mischungslücke von PLLA/PCL oberhalb von T = 80°C aus, wodurch das PLLA-Kristallwachstum bei Erreichen dieser Phasentrennung gefördert wird, was zu einer Bildung von PLLA-Sphärolithen und kleinen PCL-Kristallen führt, welche sich an der Oberfläche der Sphärolithen anlagern [163–165].

Zusätzlich wurden AFM-Aufnahmen angefertigt, die bei PLLA/PCL $50/50_{T40}$ lamellare Strukturen in kreisförmiger Anordnung von etwa Ø = 60 µm Größe zeigen, welche in eine glatte Oberfläche eingebettet sind (Abb. 18 a). Darüber hinaus sind etwa Poren mit einem Durchmesser von Ø = 5 µm zu beobachten. Bei PLLA/PCL $50/50_{T80}$ wird die Oberfläche zunehmend porös und zeigt Porendurchmesser von bis zu Ø = 50 µm (Abb. 18 b). Ähnliche AFM-Bilder und Porengrößen wurden nach Lösungsmittelätzung von PLLA/PCL-Blends beobachtet [164]. Dies ist darauf zurückzuführen, dass PCL im Gegensatz zu PLLA bei der thermischen Verarbeitung bei T = 80 °C aufgrund seiner niedrigeren Schmelztemperatur verflüssigt wird. Als Ergebnis dieses Prozesses würde man eine hochporöse Struktur erwarten, in der sich hauptsächlich PLLA-Strukturen um geschmolzene PCL-Domänen bilden. Bei PLLA/PCL $50/50_{T200}$ sind deutlich lamellare Strukturen zu erkennen, die mittels Raman-Mikroskopie als Teilsegmente von PCL-Sphärolithen interpretiert werden können.

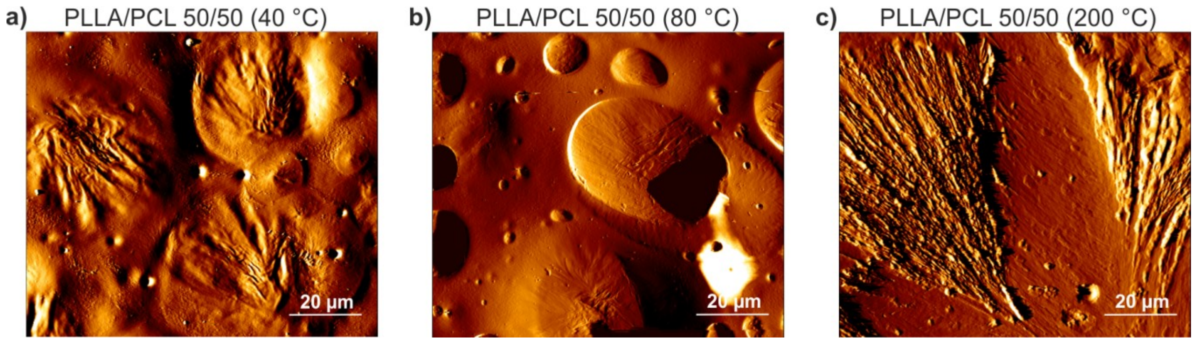

Abb. 18 Exemplarische rasterkraftmikroskopische Aufnahmen des PLLA/PCL-Blends im Verhältnis 50/50 %*w/w*, welche eine Stunde bei Temperaturen von 40 °C, 80 °C und 200 °C gelagert wurden.

In Ergänzung dazu konnte mit Hilfe der konfokalen Raman-Bildgebung nachgewiesen werden, dass alle drei verschiedenen Blends Phasentrennung aufweisen und dass insbesondere für PLLA/PCL $50/50_{T40}$ und PLLA/PCL $50/50_{T80}$ zwei gut differenzierte Bereiche jedes Polymers zu erkennen sind [Pub2]. Dies weist auf die Existenz großer Domänen jedes Homopolymers hin [166]. Gleichzeitig deutet eine schmale Grenzflächenbreite auf eine geringe Grenzflächenwechselwirkung und somit auf eine Unverträglichkeit zwischen PCL und PLLA hin.

Einfluss der Tempertemperatur auf die mechanischen Eigenschaften

Die Auswertung der mechanischen Kennwerte aus den uniaxialen Zugversuchen ist in Abb. 19 a dargestellt. Die Daten zeigen ein steifes und sprödes Verhalten von reinem PLLA. Es weist jedoch nach dem Tempern bei T = 40 °C im Vergleich zu T = 200 °C höhere Bruchdehnungen von ε_B = 60 ± 18 % auf, was sich auf die Kettenausrichtung während des Verdampfen des Lösungsmittels verbunden mit der zunehmenden Kettenmobilität durch die erhöhte Temperatur zurückführen lässt.

a)

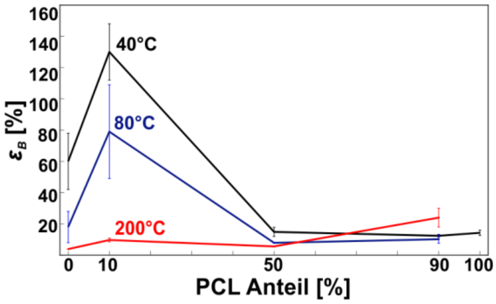

b)

PLLA/PCL 90/10	T = 40 °C	T = 80 °C	T = 200 °C
E (MPa)	998 ± 17	943 ± 19	810 ± 110
R_M (MPa)	38,1 ± 1,8	34,3 ± 1,4	27,5 ± 0,8
ε_B (%)	130 ± 18	79 ± 30	9,7 ± 1,2
χ (%)	43,3 ± 0,7	41,2 ± 1,2	61 ± 3
χ (%)	38 ± 3	28.1 ± 0,9	21 ± 6

Abb. 19 Bruchdehnung vom lösungsmittelgegossenen PLLA/PCL-Blend in Abhängigkeit vom PCL-Gehalt, welcher bei verschiedenen Temperaturen gelagert wurde (a). Mechanische und thermische Eigenschaften des PLLA/PCL-Blends 90/10 in Abhängigkeit der Lagertemperatur (b).

Durch Zugabe von 10 % PCL zu PLLA und die Temperung bei T = 40 °C konnte ein deutlicher Anstieg von ε_B beobachtet werden (Abb. 19 a), was mit Literaturdaten vergleichbar ist, in der von der Vermischung von PLLA mit PEG bekannt ist, dass aufgrund der Kristallisationskinetik vermutlich weiterhin eine Adhäsion zwischen PLLA und PEG besteht [158,167]. Auch eine Temperung bei 80 °C, oberhalb $T_{m,PCL}$, zeigt der 90/10 PLLA/PCL-Blend eine Erhöhung in ε_B, was darauf hindeutet, dass die Temperatur keinen signifikanten Einfluss auf die PLLA/PCL-Grenzflächen hat (siehe Abb. 19 b). Reines PCL_{T40} zeigt mit R_M = 15,2 ± 0,4 MPa und ε_B = 14,3 ± 1,7 % ein sprödes Verhalten im Gegensatz zu Literaturdaten (R_M = 12,5 ± 1,9 MPa, ε_B = 400 ± 19 % [168]). Dies kann mit der hohen Kristallinität von PCL (χ_{PCL} = 80,0 ± 0,2 %) erklärt werden, wobei Literaturdaten deutlich niedrigere Kristallinitätswerte (χ_{PCL} = 66,2 % [169]) aufweisen. Demzufolge kann es zu einer Erhöhung von ε_B kommen. Das Tempern von reinem PCL oberhalb dessen Schmelztemperatur führte zur Degradation der Proben, weshalb keine mechanischen Eigenschaften bestimmt werden konnten.

Zusammenfassend lässt sich sagen, dass in einem PLLA/PCL-Blend ein Anteil von 10 % an PCL ausreichend ist, um einen signifikanten Effekt in den mechanischen Kennwerten des Blends zu erzeugen. Dies ermöglicht die Modifikation der Materialeigenschaften lediglich durch Änderung der Prozessprotokolle und ohne weitere Zusätze, wie Weichmacher. Daher ist es umso wichtiger, die Temperaturen sorgfältig auszuwählen und über den gesamten Produktionsweg solcher Polymerblends beizubehalten, insbesondere im Hinblick auf Anwendungen im Bereich der Medizintechnik, da die Produktionsparameter nicht nur die mechanischen Eigenschaften der Blends beeinflussen, sondern auch einen Einfluss auf die Wirkstofffreisetzung und den Polymerabbau zeigen können.

4.3. Studie 3: Aspekte der Wirkstoffinkorporation in PLLA

Die lokale Freisetzung von Wirkstoffen ist zwar in vielen Bereichen der systemischen Verabreichung überlegen, doch kann deren Einbindung in Polymere die physiko-chemischen Eigenschaften der Matrix beeinflussen. Dies ist u.a. bei Stentanwendungen von besonderer Bedeutung, da die minimalinvasive Implantation häufig mit mechanischen Belastungen für das Implantat und die Wirkstoffbeschichtung einhergeht. Folglich kann die Inkorporation von Wirkstoffen in Polymeren zu einer Anfälligkeit für potenziell lebensbedrohliches Implantatversagen führen, wenn die Beschichtung durch das Einführen in das Gefäß und die Expansion des Stents frakturiert oder z.T. in partikulärer Form, delaminiert. Demnach war es das Ziel in Studie 3, PLLA-Wirkstoffblends mit Hilfe von thermischen Analysen und Zugversuchen zu untersuchen, um den Einfluss ausgewählter Wirkstoffe (SIR, PTX, DEX und CYCLO) auf die physiko-chemischen Eigenschaften des Polymers zu bestimmen [Pub3]. Diese wurden aufgrund ihrer unterschiedlichen strukturellen Merkmale wie Molekulargewicht, Größe, Polarität, Hydrophilie oder funktionelle Gruppen gewählt, was zu möglichen Wechselwirkungen mit der Polymermatrix führen kann. Die wirkstoffinkorporierten PLLA-Folien wurden mit Hilfe des Airbrush-Verfahrens, ausgehend von PLLA/Wirkstoff-Lösungen, hergestellt. Für alle PLLA/Wirkstoff-Blends konnte ein Anstieg der Zugfestigkeit beobachtet werden. Weiterhin wurden bei SIR und DEX Mischphasensysteme durch verschobene Wirkstoff-Schmelzpeaks bei T = 200 °C bzw. T = 240 °C identifiziert, während PTX und DEX zur Kaltkristallisation führten. Dahingegen konnte kein Einfluss von CYCLO auf die thermischen Eigenschaften der Matrix beobachtet werden.

Einfluss der Wirkstoffinkorporation auf die thermischen Eigenschaften

Abb. 20 veranschaulicht den Einfluss des inkorporierten Wirkstoffes auf die thermischen Eigenschaften von PLLA, welche mittels DSC untersucht wurden. Die API zeigen in der thermischen Analyse einen unterschiedlichen Einfluss auf PLLA. Beim PLLA/PTX-Blend wurde im Thermogramm kein PTX-Schmelzpeak beobachtet ($T_{m,PTX}$ = 217 °C), was darauf schließen lässt, dass der Wirkstoff vollständig mit dem Polymer vermischt ist (Abb. 20 a). Weiterhin wird eine leichte Verschiebung der T_g der Polymermatrix beobachtet. Dies lässt sich damit erklären, dass PTX mit den amorphen Domänen von PLLA mischbar ist, was zu einer Erweichung der Polymermatrix und damit zu einer Abnahme von T_g mit zunehmendem PTX Anteil führt. Darüber hinaus führt dies auch zur Kaltkristallisation, erkennbar durch einen exothermen Peak (T_c), der mit steigender PTX-Menge zunimmt, da das eingebettete PTX die Polymerrekristallisation verlangsamt [170,171]. Die Wasserstoffbrückenbindung zwischen PLLA und PTX bewirkt, dass PTX vermehrt in den amorphen Bereichen anreichert, wodurch es zu einer verringerten Diffusionsfähigkeit in der Polymerkette kommt und so die Kristallisation gehemmt werden kann [172].

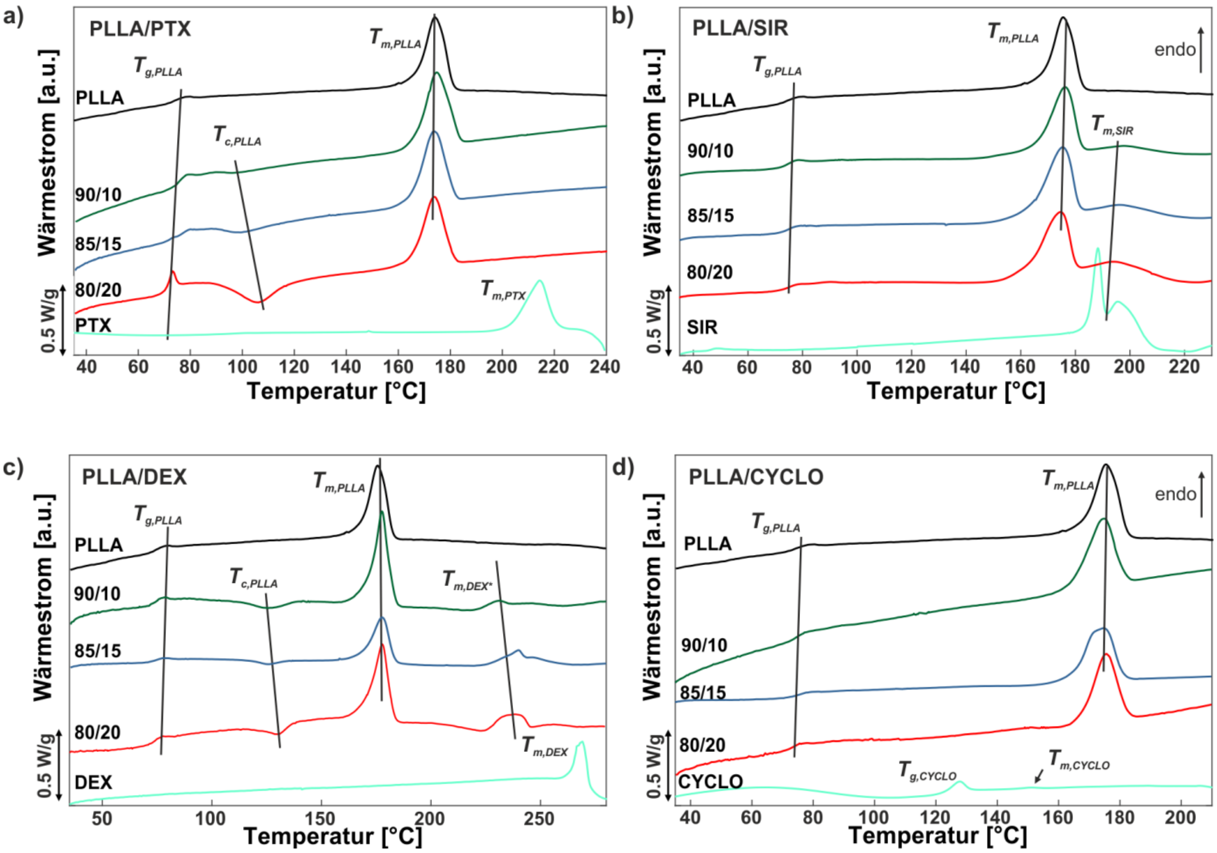

Abb. 20 DSC-Kurven von reinem PLLA (schwarz) im Vergleich mit reinem Wirkstoff (cyan) und mit PLLA/Wirkstoff-Blendkombinationen (a) PLLA/PTX, (b) PLLA/SIR, (c) PLLA/DEX und (d) PLLA/CYCLO) in verschiedenen Verhältnissen (90/10, 85/15, 80/20 %*w*/*w*). Die Trendlinien veranschaulichen den Einfluss der verschiedenen Wirkstoffe auf die thermischen Eigenschaften des PLLA.

Die Kaltkristallisation deutet ebenfalls darauf hin, dass das Tempern bei $T = 80$ °C für $t = 13{,}5$ h nicht ausreichend ist, um einen thermischen Gleichgewichtszustand zu erreichen. Dies kann einen Einfluss auf die Langzeiteigenschaften in Bezug auf die biomedizinische Anwendung einer solchen arzneimittelhaltigen Matrix, z. B. die Lagerfähigkeit, haben.

Für PLLA/SIR-Folien lässt das Vorhandensein eines SIR-Schmelzpeaks bis $T_m = 199{,}5 \pm 0{,}6$ °C, der über T_m der reinen SIR-Komponente mit $T_{m,SIR} = 183{,}9 \pm 0{,}5$ °C liegt, den Schluss zu, dass SIR nicht vollständig mit PLLA mischbar ist und phasensepariert vorliegt (Abb. 20 b). Eine ähnliche Beobachtung gab es für SIR in einem Blend aus Poly(butylmethacrylat)/Poly(ethylenvinylacetat) (PBMA/PEVA), was damit erklärt wurde, dass der Wirkstoff des verbreiterten Auftreten des SIR-Schmelzpeaks in der Nähe des Schmelzpeaks von reinem SIR hauptsächlich in einem Zustand mit nur geringer Kristallinität in der Polymermatrix verkapselt ist [173]. Es bleibt unklar, ob die SIR-Kristallbildung ein Effekt aufgrund einer generellen begrenzten Mischbarkeit von SIR mit PLLA ist oder aber bei der Herstellung der Testproben auftrat. Da SIR eine begrenzte Löslichkeit in $CHCl_3$ zeigt, wurde der Wirkstoff in MeOH gelöst und diese Lösung dann der $CHCl_3$-Polymer-Lösung zugesetzt. Während der weiteren Prozessschritte kann SIR aus dem komplexen Mehrkomponentengemisch (PLLA – $CHCl_3$ – MeOH – SIR) ausfallen, was zur Bildung von Mikrokristallen führen kann.

Im Falle der DEX-Inkorporation deutet die Verschiebung des endothermen Peaks von $T_{m,DEX}^{*}$ = 231,8 ± 1,5 °C auf $T_{m,DEX}^{*}$ = 240,1 ± 1,4 °C auf eine Wechselwirkung zwischen phasensepariertem DEX und PLLA hin (Abb. 20 c). Folglich muss DEX bis zu einem Schwellenwert in die PLLA-Matrix eingebaut worden sein, ab dem eine Phasentrennung stattfindet.

Das Fehlen eines deutlichen $T_{m,CYCLO}$-Signals im Vergleich zum Wirkstoff-T_m für SIR oder DEX zeigt, analog zu PTX, eine vollständige Vermischung des Wirkstoffs mit dem Polymer (Abb. 20 d).

Einfluss der Wirkstoffinkorporation auf die mechanischen und thermischen Eigenschaften

Wie sich die verschiedenen Wirkstoffanteile auf das mechanische Verhalten der Polymer/Wirkstoff-Blends auswirken, ist in Abb. 21 dargestellt. Im Vergleich zu den thermischen Eigenschaften wurden zum Teil widersprüchliche Ergebnisse beobachtet. So führt die Verblendung von PLLA mit PTX zu einer Verringerung der Kristallinität der PLLA-Matrix mit steigendem PTX Anteil, was eine Erweichung des Materials vermuten lässt. Ein Anstieg der Bruchdehnung von ε_B = 9,9 ± 0,7 % auf ε_B = 23 ± 16 % lässt ebenso diese Schlussfolgerung zu, jedoch erhöht sich der Elastizitätsmodul um bis zu 25 % im Vergleich zu reinem PLLA, welche mit einer Versprödung des Materials einhergeht (Abb. 21 c). Die Inkorporation von 10 % SIR führt zu einem Anstieg des Elastizitätsmoduls um etwa 34 %, was auf eine Wirkung als Hartmacher hinweist. Die Elastizitätsmodulwerte nehmen mit steigendem Wirkstoffgehalt ab und nähern sich bei 20 %*w/w* SIR dem ursprünglichen PLLA-Wert an. Die DSC-Daten zeigen eine Zunahme der Kristallinität von PLLA mit zunehmendem SIR-Gehalt. Zusätzlich zur Bildung von SIR-Kristalliten wirkt dieser Effekt dem Einfluss der SIR-Moleküle, die mit den Polymerketten interagieren, auf den Elastizitätsmodul entgegen. Es deutet darauf hin, dass sowohl PTX als auch SIR ein komplexes Verhalten im Polymer-Kristallgitter aufweisen. Der Einbau von DEX führt zu einer tendenziell geringeren Bruchdehnung bei hohen Wirkstoffkonzentrationen (Abb. 21 b). Dennoch wird eine Verringerung des Elastizitätsmoduls um etwa 10 % beobachtet. Dies lässt den Schluss zu, dass der Wirkstoff einerseits auf molekularer Ebene mit den PLLA-Polymerketten interagiert und somit als Weichmacher wirkt. Andererseits könnte die Bildung von Mikrokristallen zur Entwicklung von Sollbruchstellen und damit zu einem Rückgang der Bruchdehnung um etwa 31 % führen.

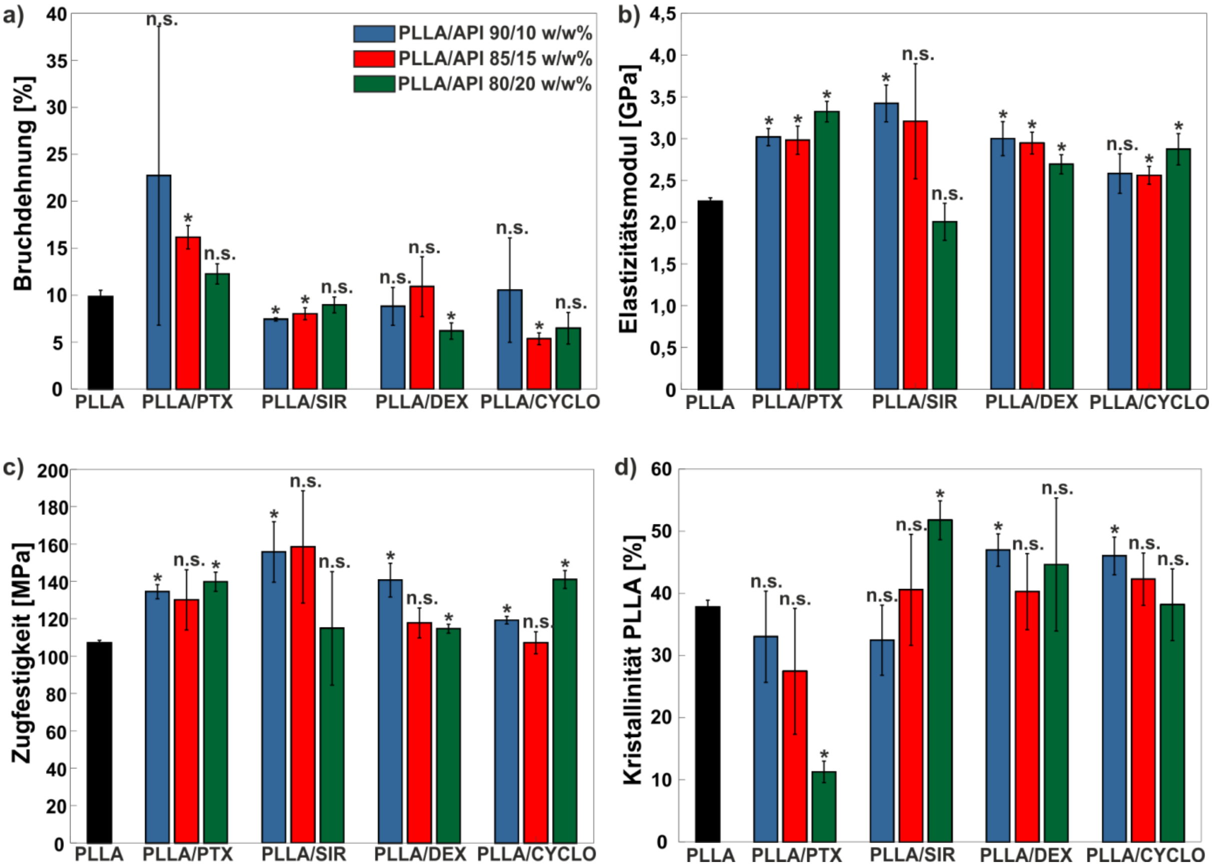

Abb. 21 Mechanische und thermische Eigenschaften (Bruchdehnung, Elastizitätsmodul, Zugfestigkeit und Kristallinität), ermittelt aus uniaxialen Zugversuchen von im Airbrush-Verfahren hergestellten PLLA/Wirkstoff-Folien mit verschiedenen Polymer-Wirkstoffverhältnissen (90/10, 85/15 und 80/20 %*w/w*). Sternchen markieren signifikante Unterschiede mit $p < 0{,}05$ (Nalimov-Test) zur PLLA-Referenz.

Die Untersuchung solcher Wechselwirkungen, speziell von PTX oder SIR mit PLLA, beides etablierte Wirkstoffe für Stentbeschichtungen, ist von hohem praktischen Interesse, da die Bildung mehrerer Phasen die für biomedizinische Anwendungen relevanten Eigenschaften, wie das Freisetzungsverhalten, entscheidend verändert. Darüber hinaus sind solche Effekte besonders wichtig für das Dilatationsverhalten und die Integrität der wirkstofftragenden Beschichtung nach mechanischer Belastung.

Vergleich der thermischen Eigenschaften von PLLA/PTX-Folien mit PLLA/PTX-Vliesen

Das diffusionsgesteuerte Freisetzungsverhalten des Wirkstoffes wird durch das Oberflächen- zu Volumenverhältnis des Depots bestimmt. Daher wurde in einem weiteren Teil der Studie untersucht, welchen Einfluss die Herstellung durch Airbrush-Verfahren im Vergleich zum Elektrospinningverfahren auf die thermischen Eigenschaften des MKS haben [Pub4]. Es wurden PLLA-Folien (fPLLA) über das Airbrush-Verfahren und PLLA-Nanofasern (nfPLLA) über Elektrospinningverfahren hergestellt und die thermischen Eigenschaften dieser miteinander verglichen. Zusätzlich wurde die Polymeroberfläche aller Proben mit Sauerstoffplasma aktiviert, um eine stabile Oberflächenimmobilisierung mit dem vaskulären endothelialen Wachstumsfaktor (VEGF) zu gewährleisten.

Das thermische Verhalten der durch Airbrush- und Elektrospinningverfahren und anschließender Oberflächenbehandlung hergestellten PLLA/PTX-Prüfkörper ist sowohl in Abb. 22 als auch in Tab. 3 dargestellt. Durch die Zugabe von PTX erhöhten sich die Glasübergangstemperaturen der PLLA-Folien leicht von T_g = 68,6 ± 2,2 °C auf T_g = 71,7 ± 0,2 °C und der PLLA-Vliese von T_g = 71,2 ± 0,4 °C auf T_g = 74,5 ± 0,6 °C. Die untersuchten Systeme sind nahezu unbeeinflusst von der O_2-Plasmabehandlung (siehe Tab. 3), was durch die rein oberflächliche Behandlung auch zu erwarten war.

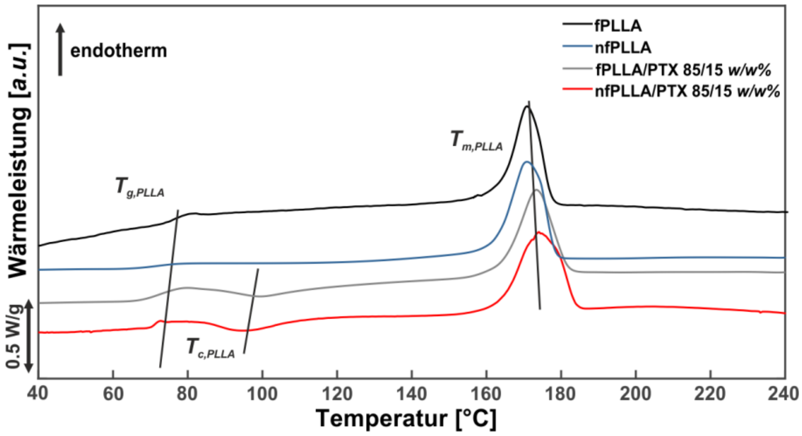

Abb. 22 Vergleich der DSC Kurven von einer reinen PLLA-Folie (schwarz) mit einem PLLA-Vlies (blau) und eines Blends aus PLLA/PTX im Verhältnis 85/15 *m/m*, sowohl aus einem Airbrush-Verfahren als Folie (grau) und über Elektrospinning als Vliesmaterial (rot) hergestellt. Die Linien veranschaulichen den Einfluss der Herstellung auf die thermischen Eigenschaften des PLLA.

Für beide Herstellungsvarianten ist eine leichte Verschiebung der T_g der Polymermatrix beobachtet worden, was durch die Mischbarkeit von PTX mit den amorphen Domänen von PLLA begründet werden kann [172]. Dies gleicht den Ergebnissen aus dem ersten Teil der Studie 3. Die dort untersuchten Sprühfolien aus PLLA mit verschiedenen Mengen an inkorporiertem PTX verursachten mit steigendem PTX-Anteil eine T_g Verschiebung zu niedrigeren Temperaturen, was mit der Mischbarkeit von PTX mit den amorphen Domänen von PLLA zusammenhängt.

Tab. 3 Thermische Eigenschaften (T_g (°C), χ (%)) von modifizierten PLLA-Folien (fPLLA) im Vergleich zu PLLA-Faservliesen (nfPLLA) mit und ohne O_2-Plasmabehandlung.

Probe	**T_g [°C]**	**χ [%]**		**T_g [°C]**	**χ [%]**
fPLLA	68.6 ± 2.2	35.6 ± 1.4	nfPLLA	71.2 ± 0.4	42.3 ± 1.3
fPLLA O_2 plasma	71.8 ± 0.2	34.6 ± 2.7	nfPLLA O_2 plasma	71.0 ± 0.2	41.0 ± 1.0
fPLLA-PTX	71.7 ± 0.2	33.3 ± 0.5	nfPLLA-PTX	74.5 ± 0.6	39.6 ± 3.6
fPLLA-PTX O_2 plasma	72.3 ± 1.0	32.9 ± 1.8	nfPLLA-PTX O_2 plasma	73.4 ± 1.4	37.3 ± 2.3

Darüber hinaus führt dies auch zur Bildung eines exothermen Peaks (T_c), der ebenfalls sowohl in den Sprühfolien als auch in den PLLA-Vliesen ausgeprägt ist. Mit steigender Temperatur konnte kein PTX-Schmelzpeak beobachtet werden, was darauf schließen lässt, dass PTX

vollständig mit dem Polymer vermischt ist. Auch hier hatte die Art der Probenherstellung keinen Einfluss auf die thermischen Eigenschaften der Proben.
Trotz der Unterschiede im Herstellungsprotokoll wurden nahezu identische thermische Eigenschaften hinsichtlich Kristallinität und T_g beider PLLA-Probekörper festgestellt. Des Weiteren konnte gezeigt werden, dass PTX, unabhängig von der Prüfkörperherstellung, eine Kaltkristallisation ausbildet.

Zusammenfassend zeigen die Ergebnisse in Abhängigkeit vom eingebrachten Wirkstoff komplexe Phasenübergangsprozesse während der Herstellung. Da es sich um ein Wirkstoff-Polymer-Lösungsmittel-System handelt, müssen die Wechselwirkungen zwischen den drei Komponenten in der Lösung sowie bei der Verdampfung des Lösungsmittels und damit die Verschiebung der Löslichkeiten bei der Herstellung und Anwendung berücksichtigt werden, da sich dadurch entscheidende Parameter wie die Wirkstofffreisetzung oder die mechanische Belastbarkeit ändern können. Die Echtzeitanalyse solcher Prozesse ist jedoch nach wie vor technisch anspruchsvoll. So stellt die Handhabung von Polymerfolien mit einer Dicke von etwa d = 10 µm eine Herausforderung dar, da minimale Defekte oder eine unzureichende Befestigung in der Prüfvorrichtung die Ergebnisse stark beeinflussen können. Allerdings ist auch die Herstellung dickerer Proben, z.B. durch Lösungsmittelgießverfahren, ungeeignet, da eine Zunahme der Probendicke zu einer unvollständigen Entfernung des Restlösungsmittels durch Verdunstung führt. Das verbleibende Lösungsmittel kann als Weichmacher wirken und damit die Ergebnisse zum Einfluss des Wirkstoffs auf die Schichteigenschaften verfälschen.
Insgesamt leisten die Daten einen Beitrag zum Verständnis der komplexen Wechselwirkung zwischen PLLA und verschiedenen API. So zeigen die Ergebnisse die Notwendigkeit einer zielgerichteten thermischen Behandlung, um die Lagerstabilität und mechanische Belastbarkeit von Stentbeschichtungen zu gewährleisten.

5. Zusammenfassung und Ausblick

Auf Grundlage der in Kapitel 1 dargestellten Prozessschritten für die Entwicklung von kardiovaskulären Implantaten wurden in der vorliegenden Arbeit PLLA-basierte Ein- und Mehrkomponentensysteme charakterisiert. Dabei sollte zum einen durch geeignete Postprozessierungsschritte eine Verbesserung der Eigenschaften realisiert werden und zum anderen der Einfluss von Zusätzen (Polymer oder Wirkstoff) auf die physiko-chemischen Eigenschaften der Prüfkörper beurteilt werden, um hieraus geeignete Prozessschritte für die Stententwicklung abzuleiten.

Dazu wurde in einer ersten Studie [Pub1] der beschleunigte Abbau von lösemittelgegossenen PLLA-Folien bei T = 55 °C mit dem enzym-assoziierten Echtzeit-Abbau bei T = 37 °C verglichen, um weiterführend ein Korrelationsmodell auf der Grundlage der Molekulargewichtsabnahme zu entwickeln. Aus den Ergebnissen und im Kontext einer umfangreichen Literaturrecherche konnte geschlossen werden, dass die Probenherstellung im Lösemittelgießverfahren, verglichen mit der Herstellung aus der Schmelze, nur einen geringen Einfluss auf das Abbauverhalten hat. Im Gegensatz dazu spielt die anfängliche Polymerkristallinität eine entscheidende Rolle. Bezogen auf die Molekulargewichtsabnahme konnte eine Echtzeitstudie durch eine beschleunigte Studie abgebildet werden. Allerdings ist anhand der Ergebnisse zu beachten, dass die Startbedingungen, wie Molekulargewicht und Kristallinität der gewählten Materialien identisch sind, um die *in vivo*-Abbauprozesse im Labormaßstab abbilden und weiterführend realistisch in den Entwicklungsprozess für degradierbare Polymerstents integrieren zu können.

In einer zweiten Studie [Pub2] wurden Polymerblends aus hochmolekularem PLLA und niedermolekularem PCL über ein Lösemittelverfahren in verschiedenen Mischungsverhältnissen kombiniert und thermisch nachbehandelt mit dem Ziel, die Anwendbarkeit von PLLA/PCL-Polymerblends zu optimieren. Diese bilden komplexe Mischphasen und Morphologien, die zu stark veränderten Eigenschaften des resultierenden Materials führen. Das Zusammenspiel der Polymere ist abhängig von deren Mischungsverhältnis, der Wahl des Herstellungsprotokolls sowie von Nachbearbeitungsverfahren. Diesbezüglich wurde untersucht, wie die Temperatur während der Nachbearbeitung die Eigenschaften und damit die Eignung von lösungsmittelgegossenen PLLA/PCL-Blends für biomedizinische Produkte beeinflusst.

Für die Gewährleistung der Patientensicherheit sind die toxischen Produkte aus der Probe zu entfernen. Dies beinhaltete beim angewandten Gießverfahren eine Verdampfung unter reduziertem Druck, einen Waschprozess, um das restliche Lösungsmittel vollständig aus dem Polymer zu entfernen und eine anschließende Temperung bei verschiedenen Temperaturen. Um eine Kaltkristallisation des Materials zu vermeiden und ein thermodynamisches

Gleichgewicht der Proben zu erhalten, wurden diese nach der Temperaturbehandlung mit einer sehr geringen Geschwindigkeit abgekühlt. Es konnte gezeigt werden, dass die Temperprozesse die Oberflächenmorphologie, die mechanischen und thermischen Eigenschaften von PLLA, PCL und deren Blends stark beeinflussen. So führte die Verblendung zu einer Verbesserung der mechanischen Eigenschaften der Polymere, wie z.B. Erhöhung der Duktilität. Eine Zugabe von 10 % PCL und Temperung bei T = 40 °C verdoppelte die Bruchdehnung des Materials. Die Temperatur als Nachbehandlungsform ermöglicht damit die Modifikation der Materialeigenschaften ohne weitere Zusätze, wie Weichmacher, sondern lediglich durch Änderung der verwendeten Prozessprotokolle.

Weiterhin wurden in einer dritten Studie [Pub3] dünne PLLA/Wirkstoff-Folien im Hinblick auf den Einfluss des Wirkstoffs auf die thermischen und mechanischen Eigenschaften der Polymermatrix untersucht. Als Wirkstoffe wurden SIR, PTX, DEX und CYCLO gewählt, da sie insgesamt ein relevantes Spektrum unterschiedlicher struktureller Merkmale wie Molekulargewicht, Größe, Polarität, Hydrophilie oder funktionelle Gruppen und damit auch mögliche Wechselwirkungen mit der Polymermatrix abdecken. Zusätzlich wurden PLLA/Wirkstoff-Vliese über Elektrospinning erzeugt und die physiko-chemischen Eigenschaften mit den PLLA/Wirkstoff-Folien verglichen. Die lokale Wirkstoffabgabe ist in der Biomedizintechnik unverzichtbar geworden, wobei Stents ideale Trägerplattformen darstellen. Während aus medizinischer Perspektive die lokale Wirkstofffreisetzung der systemischen Verabreichung in vielen Bereichen überlegen ist, muss aus werkstoffwissenschaftlicher Sicht der Einfluss der Einarbeitung des Wirkstoffes in das Polymerbeschichtung auf die physiko-chemischen Eigenschaften der genannten Matrix berücksichtigt werden. Dies ist insofern von besonderer Relevanz, da die minimalinvasive Implantation häufig mit mechanischen Belastungen des Implantats und der Wirkstoffbeschichtung einhergeht. So kann die Inkorporation von Wirkstoffen in die Polymermatrix beim Einführen in das Gefäß zu einem Ablösen der Beschichtung und zur Partikelfreisetzung führen. In dieser Studie wurde für alle Wirkstoffe und PLLA/Wirkstoff-Verhältnisse eine Erhöhung der Zugfestigkeit im Vergleich zu reiner PLLA-Folie beobachtet. In den thermischen Eigenschaften wurde bei SIR und DEX im PLLA/Wirkstoff-Mehrphasensystem ein verschobener Wirkstoff-Schmelzpeak bei T = 200 °C bzw. T = 240 °C beobachtet. Zusätzlich wiesen die PLLA/Wirkstoff-Mehrphasensysteme mit PTX und DEX eine Kaltkristallisation auf. Insgesamt zeigen die Ergebnisse die Notwendigkeit einer zielgerichteten thermischen Nachbehandlung, um die Haltbarkeit und Leistungsfähigkeit von Stentbeschichtungen zu gewährleisten. Insbesondere für PTX und DEX ist eine zusätzliche thermische Behandlung erforderlich, um die Lagerstabilität des Implantats und deren mechanische Belastbarkeit zu gewährleisten. Diese Ergebnisse wurden sowohl für die PLLA/Wirkstoff-Folien als auch für die Vliese erhalten [Pub4], wodurch die Nachprozessierung unabhängig von der Herstellungsmethode notwendig ist.

Im Rahmen der durchgeführten Arbeiten wurden mit Hilfe thermischer, mechanischer und morphologischer Charakterisierungsmethoden PLLA-basierte 1-KS und MKS untersucht, welche basierend auf der Prozesskette für die Entwicklung von kardiovaskulären Implantaten relevant sind. Unter anderem lieferten die durchgeführten Untersuchungen Ergebnisse zu Degradationseinflüssen, Unterschieden in Herstellungsprotokollen und dem Einfluss von Nachprozessierungsschritten. Neben Homopolymer-basierten MKS finden auch immer mehr Copolymer-basierte MKS Anwendung als Implantatmaterial, deren Charakterisierung durch die strukturelle Komplexität zusätzliche Herausforderungen birgt.

Zusammenfassend konnte in der vorliegenden Arbeit gezeigt werden, dass in der Kombination physiko-chemischer Analysen, bestehend aus thermischen, mechanischen und morphologischen Untersuchungen, wichtige Erkenntnisse bezüglich Degradations-bedingungen, Phasenseparation und Wirkstoffinkorporationen polymerbasierter Biomaterialien gewonnen werden. Diese können als Ausgangspunkt für prozessbegleitende Untersuchungen kardiovaskulärer Implantatmaterialien im Industriemaßstab dienen.

Grundsätzlich ist in der Medizintechnik davon auszugehen, dass entwicklungsbegleitende Untersuchungen von polymerbasierten Mehrkomponentensystemen an Bedeutung gewinnen werden. Sowohl Forschungseinrichtungen als auch Unternehmen müssen sich den dargestellten Problemkreisen verstärkt widmen, um den weiterhin zunehmenden Anforderungen aufgrund der aktuell insbesondere im europäischen Markt für Medizinprodukte steigenden Regulierungsdichte durch die MDR [22] gewachsen zu sein und somit letztendlich zur Steigerung der Patientensicherheit beizutragen.

Literaturverzeichnis

1. Timmis, A.; Vardas, P.; Townsend, N.; Torbica, A.; Katus, H.; Smedt, D. de; Gale, C.P.; Maggioni, A.P.; Petersen, S.E.; Huculeci, R.; et al. European Society of Cardiology: cardiovascular disease statistics 2021. Eur. Heart J. 2022, 43, 716–799, doi:10.1093/eurheartj/ehab892.
2. Deutsche Gesellschaft für Thorax-, Herz- und Gefäßchirurgie. Deutscher Herzbericht 2020 dokumentiert: Herzchirurgische Patientinnen und Patienten sind bundesweit hervorragend versorgt, 2021.
3. World Health Organisation. World Health Statitics 2021: Monitoring health for the SDGs (sustainable development goals), Switzerland, 2021.
4. Callaghan, J.C.; Bigelow, W.G. An electrical artificial pacemaker for standstill of the heart. Ann. Surg. 1951, 134, 8–17, doi:10.1097/00000658-195107000-00003.
5. Grüntzig, A.R.; Senning, A.; Siegenthaler, W.E. Nonoperative dilatation of coronary-artery stenosis: percutaneous transluminal coronary angioplasty. N. Engl. J. Med. 1979, 301, 61–68, doi:10.1056/NEJM197907123010201.
6. Sigwart, U.; Puel, J.; Mirkovitch, V.; Joffre, F.; Kappenberger, L. Intravascular stents to prevent occlusion and restenosis after transluminal angioplasty. N. Engl. J. Med. 1987, 316, 701–706, doi:10.1056/NEJM198703193161201.
7. Nappi, F.; Nenna, A.; Larobina, D.; Martuscelli, G.; Singh, S.S.A.; Chello, M.; Ambrosio, L. The Use of Bioactive Polymers for Intervention and Tissue Engineering: The New Frontier for Cardiovascular Therapy. Polymers 2021, 13, doi:10.3390/polym13030446.
8. Lin, C.; Liu, L.; Liu, Y.; Leng, J. Recent developments in next-generation occlusion devices. Acta Biomaterialia 2021, 128, 100–119, doi:10.1016/j.actbio.2021.04.050.
9. Garg, S.; Bourantas, C.; Serruys, P.W. New concepts in the design of drug-eluting coronary stents. Nat. Rev. Cardiol. 2013, 10, 248–260, doi:10.1038/nrcardio.2013.13.
10. Mwipatayi, B.P.; Ouriel, K.; Anwari, T.; Wong, J.; Ducasse, E.; Panneton, J.M.; Vries, J.-P.P.M. de; Dave, R. A systematic review of covered balloon-expandable stents for treating aortoiliac occlusive disease. J. Vasc. Surg. 2020, 72, 1473-1486.e2, doi:10.1016/j.jvs.2020.01.084.
11. König, A.; Leibig, M.; Rieber, J.; Schiele, T.M.; Theisen, K.; Siebert, U.; Gothe, R.M.; Klauss, V. Randomized comparison of dexamethasone-eluting stents with bare metal stent implantation in patients with acute coronary syndrome: serial angiographic and sonographic analysis. Am. Heart J. 2007, 153, 979.e1-8, doi:10.1016/j.ahj.2007.03.032.
12. Majewska, P.; Oledzka, E.; Sobczak, M. Overview of the latest developments in the field of drug-eluting stent technology. Biomater. Sci. 2020, 8, 544–551, doi:10.1039/C9BM00468H.
13. Yaojun, Z.; Runlin, G.; Bo, X.; Cummins, P.; Serruys, P.W. Bioresorbable scaffolds for coronary artery disease: current status and future prospective. Chin. Med. J. 2014, 127, 1141–1148, doi:10.3760/cma.j.issn.0366-6999.20140015.
14. Cockerill, I.; See, C.W.; Young, M.L.; Wang, Y.; Zhu, D. Designing Better Cardiovascular Stent Materials - A Learning Curve. Adv. Funct. Mater. 2021, 31, doi:10.1002/adfm.202005361.
15. Colombo, A.; Karvouni, E. Biodegradable stents : "fulfilling the mission and stepping away". Circulation 2000, 102, 371–373, doi:10.1161/01.CIR.102.4.371.
16. Hamad, K.; Kaseem, M.; Yang, H.W.; Deri, F.; Ko, Y.G. Properties and medical applications of polylactic acid: A review. Express Polym. Lett. 2015, 9, 435–455, doi:10.3144/expresspolymlett.2015.42.
17. Kukreja, N.; Onuma, Y.; Daemen, J.; Serruys, P.W. The future of drug-eluting stents. Pharmacol. Res. 2008, 57, 171–180, doi:10.1016/j.phrs.2008.01.012.

18. Tyler, B.; Gullotti, D.; Mangraviti, A.; Utsuki, T.; Brem, H. Polylactic acid (PLA) controlled delivery carriers for biomedical applications. Adv. Drug Deliv. Rev. 2016, 107, 163–175, doi:10.1016/j.addr.2016.06.018.
19. Grabow, N.; Martin, D.P.; Schmitz, K.-P.; Sternberg, K. Absorbable polymer stent technologies for vascular regeneration. J. Chem. Technol. Biotechnol. 2010, 85, 744–751, doi:10.1002/jctb.2282.
20. DIN EN ISO 25539-2:2019-07. Cardiovascular implants - endovascular devices: Part 2 - vascular stents; Beuth: Berlin, 2019 (25539-2).
21. Richtlinie 93/42/EWG des Rates vom 14. Juni 1993 über Medizinprodukte: 93/42/EWG, 1993.
22. Verordnung (EU) 2017/ 745 des europäischen Parlaments und des Rates - vom 5. April 2017 - über Medizinprodukte, zur Änderung der Richtlinie 2001/ 83/ EG, der Verordnung (EG) Nr. 178/ 2002 und der Verordnung (EG) Nr. 1223/ 2009 und zur Aufhebung der Richtlinien 90/ 385/ EWG und 93/ 42/ EWG des Rates: 2017/745, 2017.
23. Ebrahimi, F.; Ramezani Dana, H. Poly lactic acid (PLA) polymers: from properties to biomedical applications. International Journal of Polymeric Materials and Polymeric Biomaterials 2021, 1–14, doi:10.1080/00914037.2021.1944140.
24. Bergsma, J. Late degradation tissue response to poly(?-lactide) bone plates and screws. Biomaterials 1995, 16, 25–31, doi:10.1016/0142-9612(95)91092-D.
25. Henton, D.; Gruber, P.; Lunt, J.; Randall, J. Natural Fibers, Biopolymers, and Biocomposites: Polylactic Acid Technology; Taylor & Francis Group: Boca Raton, FL, 2005, ISBN 084931741x.
26. Lincoff, A.; Furst, J.G.; Ellis, S.G.; Tuch, R.J.; Topol, E.J. Sustained Local Delivery of Dexamethasone by a Novel Intravascular Eluting Stent to Prevent Restenosis in the Porcine Coronary Injury Model. J. Am. Coll. Cardiol. 1997, 29, 808–816, doi:10.1016/s0735-1097%2896%2900584-0.
27. Baiardo, M.; Frisoni, G.; Scandola, M.; Rimelen, M.; Lips, D.; Ruffieux, K.; Wintermantel, E. Thermal and mechanical properties of plasticized poly(L-lactic acid). J. Appl. Polym. Sci. 2003, 90, 1731–1738, doi:10.1002/app.12549.
28. Labinaz, M.; Zidar, J.P.; Stack, R.S.; Phillips, H.R. Biodegradable stents: the future of interventional cardiology? J. Interv. Cardiol. 1995, 8, 395–405, doi:10.1111/j.1540-8183.1995.tb00565.x.
29. Garlotta, D. A Literature Review of Poly(Lactic Acid). J. Polym. Environ. 2001, 9, 63–84, doi:10.1023/A:1020200822435.
30. Puchalski, M.; Kwolek, S.; Szparaga, G.; Chrzanowski, M.; Krucińska, I. Investigation of the Influence of PLA Molecular Structure on the Crystalline Forms (α' and α) and Mechanical Properties of Wet Spinning Fibres. Polymers 2017, 9, doi:10.3390/polym9010018.
31. Alsleben, M.; Schick, C. The melting of polymers — a three-phase approach. Thermochim. Acta 1994, 238, 203–227, doi:10.1016/S0040-6031(94)85211-1.
32. Ehrenstein, G.W. Polymer-Werkstoffe: Struktur - Eigenschaften - Anwendung, 3. Aufl.; Hanser: München, 2011, ISBN 3446422838.
33. Lauritzen, J.I.; Hoffman, J.D. Theory of Formation of Polymer Crystals with Folded Chains in Dilute Solution. J. Res. Natl. Bur. Stand. A Phys. Chem. 1960, 64A, 73–102, doi:10.6028/jres.064A.007.
34. Petzold, A. Kettendynamik in der Polymerschmelze und Kristallisation in teilkristallinem Polyethylenoxid. Dissertation; Martin-Luther-Universität, Halle-Wittenberg, 2011.
35. Limsukon, W.; Auras, R.; Smith, T. Effects of the Three-Phase Crystallization Behavior on the Hydrolysis of Amorphous and Semicrystalline Poly(lactic acid)s. ACS Appl. Polym. Mater. 2021, 3, 5920–5931, doi:10.1021/acsapm.1c01080.

36. Zhang, R.-C.; Sun, D.; Lu, A.; Zhong, M.; Xiong, G.; Wan, Y. Equilibrium Melting Temperature of Polymorphic Poly(l-lactide) and Its Supercooling Dependence on Growth Kinetics. Polymers 2017, 9, 625, doi:10.3390/polym9110625.
37. Di Lorenzo, M.L.; Androsch, R. Influence of α′-/α-crystal polymorphism on properties of poly(l -lactic acid). Polym. Int. 2019, 68, 320–334, doi:10.1002/pi.5707.
38. Wasanasuk, K.; Tashiro, K.; Hanesaka, M.; Ohhara, T.; Kurihara, K.; Kuroki, R.; Tamada, T.; Ozeki, T.; Kanamoto, T. Crystal Structure Analysis of Poly(l -lactic Acid) α Form On the basis of the 2-Dimensional Wide-Angle Synchrotron X-ray and Neutron Diffraction Measurements. Macromolecules 2011, 44, 6441–6452, doi:10.1021/ma2006624.
39. Zhang, N.; Yu, X.; Duan, J.; Yang, J.; Huang, T.; Qi, X.; Wang, Y. Comparison study of hydrolytic degradation behaviors between α′- and α-poly(l -lactide). Polym. Degrad. Stab. 2018, 148, 1–9, doi:10.1016/j.polymdegradstab.2017.12.014.
40. Zhang, L.; Zhao, G.; Wang, G. Investigation on the α/δ Crystal Transition of Poly(l-lactic Acid) with Different Molecular Weights. Polymers 2021, 13, doi:10.3390/polym13193280.
41. Wasanasuk, K.; Tashiro, K. Crystal structure and disorder in Poly(l-lactic acid) δ form (α′ form) and the phase transition mechanism to the ordered α form. Polymer 2011, 52, 6097–6109, doi:10.1016/j.polymer.2011.10.046.
42. Stępak, B.; Gazińska, M.; Nejbauer, M.; Stepanenko, Y.; Antończak, A. Diverse nature of femtosecond laser ablation of poly(L-lactide) and the influence of filamentation on the polymer crystallization behaviour. Sci. Rep. 2019, 9, 3069, doi:10.1038/s41598-019-39640-1.
43. Pan, P.; Zhu, B.; Kai, W.; Dong, T.; Inoue, Y. Polymorphic Transition in Disordered Poly(l -lactide) Crystals Induced by Annealing at Elevated Temperatures. Macromolecules 2008, 41, 4296–4304, doi:10.1021/ma800343g.
44. Xue, B.; Xie, L.; Zhang, J. Detailed molecular movements during poly(l -lactic acid) cold-crystallization investigated by FTIR spectroscopy combined with two-dimensional correlation analysis. RSC Adv 2017, 7, 47017–47028, doi:10.1039/C7RA08921J.
45. Pan, P.; Kai, W.; Zhu, B.; Dong, T.; Inoue, Y. Polymorphous Crystallization and Multiple Melting Behavior of Poly(l -lactide): Molecular Weight Dependence. Macromolecules 2007, 40, 6898–6905, doi:10.1021/ma071258d.
46. Lotz, B.; Li, G.; Chen, X.; Puiggali, J. Crystal polymorphism of polylactides and poly(Pro-alt -CO): The metastable beta and gamma phases. Formation of homochiral PLLA phases in the PLLA/PDLA blends. Polymer 2017, 115, 204–210, doi:10.1016/j.polymer.2017.03.018.
47. Wang, H.; Zhang, J.; Tashiro, K. Phase Transition Mechanism of Poly(l -lactic acid) among the α, δ, and β Forms on the Basis of the Reinvestigated Crystal Structure of the β Form. Macromolecules 2017, 50, 3285–3300, doi:10.1021/acs.macromol.7b00272.
48. Monnier, X.; Cavallo, D.; Righetti, M.C.; Di Lorenzo, M.L.; Marina, S.; Martin, J.; Cangialosi, D. Physical Aging and Glass Transition of the Rigid Amorphous Fraction in Poly(l -lactic acid). Macromolecules 2020, 53, 8741–8750, doi:10.1021/acs.macromol.0c01182.
49. Hsieh, Y.-T.; Nozaki, S.; Kido, M.; Kamitani, K.; Kojio, K.; Takahara, A. Crystal polymorphism of polylactide and its composites by X-ray diffraction study. Polym. J. 2020, 52, 755–763, doi:10.1038/s41428-020-0343-8.
50. Fuoco, T.; Cuartero, M.; Parrilla, M.; García-Guzmán, J.J.; Crespo, G.A.; Finne-Wistrand, A. Capturing the Real-Time Hydrolytic Degradation of a Library of Biomedical Polymers by Combining Traditional Assessment and Electrochemical Sensors. Biomacromolecules 2021, 22, 949–960, doi:10.1021/acs.biomac.0c01621.
51. Göpferich, A. Mechanisms of polymer degradation and erosion. Biomaterials 1996, 17, 103–114.
52. Lyu, S.; Untereker, D. Degradability of polymers for implantable biomedical devices. Int. J. Mol. Sci. 2009, 10, 4033–4065, doi:10.3390/ijms10094033.

53. Vieira, A.C.; Vieira, J.C.; Ferra, J.M.; Magalhães, F.D.; Guedes, R.M.; Marques, A.T. Mechanical study of PLA-PCL fibers during in vitro degradation. J. Mech. Behav. Biomed. Mater. 2011, 4, 451–460, doi:10.1016/j.jmbbm.2010.12.006.
54. Bergsma, J.E.; Rozema, F.R.; Bos, R.R.M.; Boering, G. In vitro predegradation at elevated temperatures of poly(lactide). J. Mater. Sci. Mater. Med. 1995, 642–646, doi:10.1007/BF00123445.
55. Tamada, J.A.; Langer, R. Erosion kinetics of hydrolytically degradable polymers. Proc. Natl. Acad. Sci. U. S. A. 1993, 90, 552–556, doi:10.1073/pnas.90.2.552.
56. Burkersroda, F.v.; Schedl, L.; Göpferich, A. Why degradable polymers undergo surface erosion or bulk erosion. Biomaterials 2002, 4221–4231.
57. Herzog, K.; Müller, R.-J.; Deckwer, W.-D. Mechanism and kinetics of the enzymatic hydrolysis of polyester nanoparticles by lipases. Polym. Degrad. Stab. 2006, 91, 2486–2498, doi:10.1016/j.polymdegradstab.2006.03.005.
58. Larrañaga, A.; Lizundia, E. A review on the thermomechanical properties and biodegradation behaviour of polyesters. Eur. Polym. J. 2019, 121, 109296, doi:10.1016/j.eurpolymj.2019.109296.
59. Cam, D.; Hyon, S.; Ikada, Y. Degradation of high molecular weight poly(l-lactide) in alkaline medium. Biomaterials 1995, 16, 833–843, doi:10.1016/0142-9612(95)94144-A.
60. Li, S.; Vert, M. Biodegradable Polymers, Principles & Applications: Biodegradation of aliphatic polyesters; Chapman & Hall, London, 1995, ISBN 0-412-59010-7.
61. Tsuji, H.; Ikada, Y. Properties and morphology of poly(l-lactide) 4. Effects of structural parameters on long-term hydrolysis of poly(l-lactide) in phosphate-buffered solution. Polym. Degrad. Stab. 2000, 67, 179–189, doi:10.1016/S0141-3910(99)00111-1.
62. Gleadall, A.; Pan, J.; Kruft, M.-A.; Kellomaki, M. Degradation mechanisms of bioresorbable polyesters. Part 1. Effects of random scission, end scission and autocatalysis. Acta Biomaterialia 2014, 10, 2223–2232, doi:10.1016/j.actbio.2013.12.039.
63. Gleadall, A.; Pan, J.; Kruft, M.-A.; Kellomaki, M. Degradation mechanisms of bioresorbable polyesters. Part 2. Effects of initial molecular weight and residual monomer. Acta Biomaterialia 2014, 10, 2233–2240, doi:10.1016/j.actbio.2014.01.017.
64. Anderson, J.M. Perspectives on the in vivo responses of biodegradable polymers.; CRC Press, Boca Raton, FL, USA, 1995, ISBN 978-0849348969.
65. Siparsky, G.L.; Voorhees, K.J.; Miao, F. Hydrolysis of Polylactic Acid (PLA) and Polycaprolactone (PCL) in Aqueous Acetonitrile Solutions: Autocatalysis. Journal of Polymers and the Environment 1998, 6, 31–41, doi:10.1023/A:1022826528673.
66. Moore, J.W.; Pearson, R.G. Kinetics and mechanism, 3. ed.; Wiley: New York, NY, 1981, ISBN 0471035580.
67. Weir, N.A.; Buchanan, F.J.; Orr, J.F.; Dickson, G.R. Degradation of poly-L-lactide. Part 1: in vitro and in vivo physiological temperature degradation. Proc. Inst. Mech. Eng. H 2004, 218, 307–319, doi:10.1243/0954411041932782.
68. Kaiser, W. Kunststoffchemie für Ingenieure: Von der Synthese bis zur Anwendung, 3. Aufl.; Hanser: München, 2011, ISBN 9783446430471.
69. Keller, A.; Cheng, S.Z. The role of metastability in polymer phase transitions. Polymer 1998, 39, 4461–4487, doi:10.1016/S0032-3861(97)10320-2.
70. Ajitha A. R.; Sabu, T. Compatibilization of Polymer Blends: Chapter 1 - Introduction: Polymer blends, thermodynamics, miscibility, phase separation, and compatibilization; Elsevier: Switzerland, 2020, ISBN 9780128160060.
71. Utracki, L.A.; Wilkie, C.A. Polymer Blends Handbook, 2nd ed.; Springer Netherlands: Dordrecht, 2014, ISBN 978-94-007-6063-9.
72. Robeson, L.M. Polymer blends: A comprehensive review; Hanser: Munich, Cincinnati, 2007, ISBN 9781569904084.

73. Strobl, G. The physics of polymers: Concepts for unterstanding their structures and behavior, 3rd ed.; Springer, 2007, ISBN 978-3-540-25278-8.
74. Mannella, G.A.; Carfì Pavia, F.; La Carrubba, V.; Brucato, V. Phase separation of polymer blends in solution: A case study. Eur. Polym. J. 2016, 79, 176–186, doi:10.1016/j.eurpolymj.2016.04.025.
75. Genzer, J.; Composto, R.J. The interface between immiscible polymers studied by low-energy forward recoil spectrometry and neutron reflectivity. Polymer 1999, 40, 4223–4228, doi:10.1016/S0032-3861(98)00664-8.
76. Kacar, G.; Peters, E. A. J. F.; With, G. de. A generalized method for parameterization of dissipative particle dynamics for variable bead volumes. Eurphys. Lett. 2013, 102, 40009, doi:10.1209/0295-5075/102/40009.
77. Zhu, B.; Wang, Y.; Liu, H.; Ying, J.; Liu, C.; Shen, C. Effects of interface interaction and microphase dispersion on the mechanical properties of PCL/PLA/MMT nanocomposites visualized by nanomechanical mapping. Compos. Sci. Technol. 2020, 190, 108048, doi:10.1016/j.compscitech.2020.108048.
78. Pillin, I.; Montrelay, N.; Grohens, Y. Thermo-mechanical characterization of plasticized PLA: Is the miscibility the only significant factor? Polymer 2006, 47, 4676–4682, doi:10.1016/j.polymer.2006.04.013.
79. Wu, D.; Zhang, Y.; Yuan, L.; Zhang, M.; Zhou, W. Viscoelastic interfacial properties of compatibilized poly(ε-caprolactone)/polylactide blend. J. Polym. Sci. B Polym. Phys. 2010, 48, 756–765, doi:10.1002/polb.21952.
80. Fotaki, N.; Klein, S. In vitro drug release testing of special dosage forms: Drug Eluting Stents, First edition; Wiley: Hoboken, NJ, 2020, ISBN 9781118341476.
81. Torii, S.; Jinnouchi, H.; Sakamoto, A.; Kutyna, M.; Cornelissen, A.; Kuntz, S.; Guo, L.; Mori, H.; Harari, E.; Paek, K.H.; et al. Drug-eluting coronary stents: insights from preclinical and pathology studies. Nat. Rev. Cardiol. 2020, 17, 37–51, doi:10.1038/s41569-019-0234-x.
82. Wu, J.J.; Way, J.A.H.; Kritharides, L.; Brieger, D. Polymer-free versus durable polymer drug-eluting stents in patients with coronary artery disease: A meta-analysis. Ann. Med. Surg. 2019, 38, 13–21, doi:10.1016/j.amsu.2018.12.003.
83. Schmidt, W.; Lanzer, P.; Behrens, P.; Brandt-Wunderlich, C.; Öner, A.; Ince, H.; Schmitz, K.-P.; Grabow, N. Direct comparison of coronary bare metal vs. drug-eluting stents: same platform, different mechanics? Eur. J. Med. Res. 2018, 23, 2, doi:10.1186/s40001-017-0300-y.
84. Ali, R.M.; Abdul Kader, M.; Wan Ahmad, W.A.; Ong, T.K.; Liew, H.B.; Omar, A.-F.; Mahmood Zuhdi, A.S.; Nuruddin, A.A.; Schnorr, B.; Scheller, B. Treatment of Coronary Drug-Eluting Stent Restenosis by a Sirolimus- or Paclitaxel-Coated Balloon. JACC Cardiovasc. Interv. 2019, 12, 558–566, doi:10.1016/j.jcin.2018.11.040.
85. Schömig, A.; Neumann, F.J.; Kastrati, A.; Schühlen, H.; Blasini, R.; Hadamitzky, M.; Walter, H.; Zitzmann-Roth, E.M.; Richardt, G.; Alt, E.; et al. A randomized comparison of antiplatelet and anticoagulant therapy after the placement of coronary-artery stents. N. Engl. J. Med. 1996, 334, 1084–1089, doi:10.1056/NEJM199604253341702.
86. Parker, T.; Davé, V.; Falotico, R. Polymers for drug eluting stents. Curr. Pharm. Des. 2010, 16, 3978–3988, doi:10.2174/138161210794454897.
87. Lee, D.-H.; La Torre Hernandez, J.M.d. The Newest Generation of Drug-eluting Stents and Beyond. Eur. Cardiol. Rev. 2018, 13, 54, doi:10.15420/ecr.2018:8:2.
88. Shanshan, C.; Lili, T.; Yingxue, T.; Bingchun, Z.; Ke, Y. Study of drug-eluting coating on metal coronary stent. Mater. Sci. Eng. C Mater. Biol. Appl. 2013, 33, 1476–1480, doi:10.1016/j.msec.2012.12.049.
89. Gnanasekaran, D. Green Biopolymers and their Nanocomposites: Opportunities for PLA and Its Blends in Various Applications, 1st ed. 2019; Springer Singapore: Singapore, 2019, ISBN 978-981-13-8063-1.

90. Grabow, N.; Bünger, C.M.; Kischkel, S.; Timmermann, J.H.; Reske, T.; Martin, D.P.; Williams, S.F.; Schareck, W.; Sternberg, K.; Schmitz, K.-P. Development of a sirolimus-eluting poly (L-lactide)/poly(4-hydroxybutyrate) absorbable stent for peripheral vascular intervention. Biomed. Tech. (Berl) 2013, 58, 429–437, doi:10.1515/bmt-2012-0050.
91. Birgelen, C. von; Buiten, R.A. Superiority of biodegradable polymer sirolimus-eluting stents in STEMI. The Lancet 2019, 394, 1208–1210, doi:10.1016/S0140-6736(19)31955-5.
92. Grubman, D.; Saito, Y.; Lansky, A. The Firehawk stent: a review of a novel abluminal groove-filled biodegradable polymer sirolimus-eluting stent. Rev. arg, cardioangiol. interv. 2019, 10, 73–77, doi:10.30567/RACI/201902/0073-0077.
93. Yoshioka, G.; Nishihira, K.; Asada, Y.; Node, K. In-stent restenosis following third-generation sirolimus-eluting stent implantation: first report analysed from imaging modalities and histopathological findings. Eur. Heart J. 2020, doi:10.1093/eurheartj/ehaa142.
94. Bünger, C.M.; Grabow, N.; Sternberg, K.; Kröger, C.; Ketner, L.; Schmitz, K.-P.; Kreutzer, H.J.; Ince, H.; Nienaber, C.A.; Klar, E.; et al. Sirolimus-eluting biodegradable poly-L-lactide stent for peripheral vascular application: a preliminary study in porcine carotid arteries. J. Surg. Res. 2007, 139, 77–82, doi:10.1016/j.jss.2006.07.035.
95. Stone, G.W.; Ellis, S.G.; Cox, D.A.; Hermiller, J.; O'Shaughnessy, C.; Mann, J.T.; Turco, M.; Caputo, R.; Bergin, P.; Greenberg, J.; et al. A polymer-based, paclitaxel-eluting stent in patients with coronary artery disease. N. Engl. J. Med. 2004, 350, 221–231, doi:10.1056/NEJMoa032441.
96. Yang, J.; Zeng, Y.; Zhang, C.; Chen, Y.-X.; Yang, Z.; Li, Y.; Leng, X.; Kong, D.; Wei, X.-Q.; Sun, H.-F.; et al. The prevention of restenosis in vivo with a VEGF gene and paclitaxel co-eluting stent. Biomaterials 2013, 34, 1635–1643, doi:10.1016/j.biomaterials.2012.11.006.
97. Wessely, R. New drug-eluting stent concepts. Nat. Rev. Cardiol. 2010, 7, 194–203, doi:10.1038/nrcardio.2010.14.
98. Wessely, R.; Schömig, A.; Kastrati, A. Sirolimus and Paclitaxel on polymer-based drug-eluting stents: similar but different. J. Am. Coll. Cardiol. 2006, 47, 708–714, doi:10.1016/j.jacc.2005.09.047.
99. Vos, N.S.; Fagel, N.D.; Amoroso, G.; Herrman, J.-P.R.; Patterson, M.S.; Piers, L.H.; van der Schaaf, R.J.; Slagboom, T.; Vink, M.A. Paclitaxel-Coated Balloon Angioplasty Versus Drug-Eluting Stent in Acute Myocardial Infarction: The REVELATION Randomized Trial. JACC Cardiovasc. Interv. 2019, 12, 1691–1699, doi:10.1016/j.jcin.2019.04.016.
100. Dash, A.K. The dark side of paclitaxel. Oncol. Rev. 2010, 4, 71–72, doi:10.1007/s12156-010-0052-1.
101. Hu, T.; Yang, J.; Cui, K.; Rao, Q.; Yin, T.; Tan, L.; Zhang, Y.; Li, Z.; Wang, G. Controlled Slow-Release Drug-Eluting Stents for the Prevention of Coronary Restenosis: Recent Progress and Future Prospects. ACS Appl. Mater. Interfaces 2015, 11695–11712, doi:10.1021/acsami.5b01993.
102. Zhu, X.; Xie, H.; Liang, X.; Li, X.; Duan, J.; Chen, Y.; Yang, Z.; Liu, C.; Wang, C.; Zhang, H.; et al. Bilayered Nanoparticles with Sequential Release of VEGF Gene and Paclitaxel for Restenosis Inhibition in Atherosclerosis. ACS Appl. Mater. Interfaces 2017, 9, 27522–27532, doi:10.1021/acsami.7b08312.
103. Bachmann, B.O.; Luetjen-Drecoll, E.; Bock, F.; Wiegand, S.J.; Hos, D.; Dana, R.; Kruse, F.E.; Cursiefen, C. Transient postoperative vascular endothelial growth factor (VEGF)-neutralisation improves graft survival in corneas with partly regressed inflammatory neovascularisation. Br. J. Ophthalmol. 2009, 93, 1075–1080, doi:10.1136/bjo.2008.145128.
104. Nasuno, T.; Tokura, M.; Kageyama, M.; Toyoda, S.; Sakuma, M.; Komatsu, T.; Taguchi, I.; Abe, S.; Inoue, T. The wound healing response after implantation of a drug-eluting stent

is impaired persistently in the long term. Heart Vessels 2016, 31, 985–989, doi:10.1007/s00380-015-0676-y.

105. Zhang, Y.; Wang, J.; Xiao, J.; Fang, T.; Hu, N.; Li, M.; Deng, L.; Cheng, Y.; Zhu, Y.; Cui, W. An electrospun fiber-covered stent with programmable dual drug release for endothelialization acceleration and lumen stenosis prevention. Acta Biomaterialia 2019, 94, 295–305, doi:10.1016/j.actbio.2019.06.008.
106. Rawal, M.; Singh, A.; Amiji, M.M. Quality-by-Design Concepts to Improve Nanotechnology-Based Drug Development. Pharm. Res. 2019, 36, 153, doi:10.1007/s11095-019-2692-6.
107. Gao, S.; Tang, G.; Hua, D.; Xiong, R.; Han, J.; Jiang, S.; Zhang, Q.; Huang, C. Stimuli-responsive bio-based polymeric systems and their applications. J. Mater. Chem. B 2019, 7, 709–729, doi:10.1039/C8TB02491J.
108. Pant, B.; Park, M.; Park, S.-J. Drug Delivery Applications of Core-Sheath Nanofibers Prepared by Coaxial Electrospinning: A Review. Pharmaceutics 2019, 11, 305, doi:10.3390/pharmaceutics11070305.
109. Herrero-Herrero, M.; Gómez-Tejedor, J.A.; Vallés-Lluch, A. PLA/PCL electrospun membranes of tailored fibres diameter as drug delivery systems. Eur. Polym. J. 2018, 99, 445–455, doi:10.1016/j.eurpolymj.2017.12.045.
110. Ismail, H.M.; Zamani, S.; Elrayess, M.A.; Kafienah, W.; Younes, H.M. New Three-Dimensional Poly(decanediol-co-tricarballylate) Elastomeric Fibrous Mesh Fabricated by Photoreactive Electrospinning for Cardiac Tissue Engineering Applications. Polymers 2018, 10, 455, doi:10.3390/polym10040455.
111. Wissgott, C.; Schmidt, W.; Brandt, C.; Behrens, P.; Andresen, R. Preliminary Clinical Results and Mechanical Behavior of a New Double-Layer Carotid Stent. J. Endovasc. Ther. 2015, 22, 634–639, doi:10.1177/1526602815593490.
112. Foin, N.; Lee, R.D.; Torii, R.; Guitierrez-Chico, J.L.; Mattesini, A.; Nijjer, S.; Sen, S.; Petraco, R.; Davies, J.E.; Di Mario, C.; et al. Impact of stent strut design in metallic stents and biodegradable scaffolds. Int. J. Cardiol. 2014, 177, 800–808, doi:10.1016/j.ijcard.2014.09.143.
113. Peng, X.; Qu, W.; Jia, Y.; Wang, Y.; Yu, B.; Tian, J. Bioresorbable Scaffolds: Contemporary Status and Future Directions. Front. Cardiovasc. Med. 2020, 7, doi:10.3389/fcvm.2020.589571.
114. Kastrati, A.; Mehilli, J.; Dirschinger, J.; Dotzer, F.; Schühlen, H.; Neumann, F.J.; Fleckenstein, M.; Pfafferott, C.; Seyfarth, M.; Schömig, A. Intracoronary stenting and angiographic results: strut thickness effect on restenosis outcome (ISAR-STEREO) trial. Circulation 2001, 103, 2816–2821, doi:10.1161/01.CIR.103.23.2816.
115. Schultze, C. Bioabsorbierbare koronare Polymerstents - Strukturmechanische und experimentelle Untersuchungen. Dissertation; Universität, Rostock, 2010.
116. DIN EN ISO 527-2. Kunststoffe - Bestimmung der Zugeigenschaften: Teil 2: Prüfbedingungen für Form- und Extrusionsmassen; Beuth: Berlin, 2012 (527-2).
117. ASTM D638-14. Test Method for Tensile Properties of Plastics; ASTM International: West Conshohocken, PA (D638-14).
118. ASTM D 1708. Prüfung der Zugeigenschaften von Kunststoffen an Mikrozugproben; ASTM International: West Conshohocken, PA, 2018 (D 1708).
119. ASTM D882-18. Test Method for Tensile Properties of Thin Plastic Sheeting; ASTM International: West Conshohocken, PA, 2018 (D882-18).
120. ASTM D618-21. Practice for Conditioning Plastics for Testing; ASTM International: West Conshohocken, PA, 2021 (D618-21).
121. ISO 11357. Kunststoffe – Dynamische Differenz-Thermoanalyse (DSC); Beuth: Berlin, 2017 (11357).

122. DIN 53765. Prüfung von Kunststoffen und Elastomeren; Thermische Analyse; Dynamische Differenzkalorimetrie (DDK); Beuth: Berlin, 1994 (53765).
123. ASTM D 3418. Test Method for Transition Temperatures and Enthalpies of Fusion and Crystallization of Polymers by Differential Scanning Calorimetry; ASTM International: West Conshohocken, PA, 2021 (D 3418).
124. ASTM E793-06. Standard Test Method for Enthalpies of Fusion and Crystallization by Differential Scanning Calorimetry; ASTM International: West Conshohocken, PA, 2018 (E793-06).
125. ASTM E794-06. Standard Test Method for Melting And Crystallization Temperatures By Thermal Analysis; ASTM International: West Conshohocken, PA, 2018 (E794-06).
126. ASTM E1356-08. Standard Test Method for Assignment of the Glass Transition Temperatures by Differential Scanning Calorimetry; ASTM International: West Conshohocken, PA, 2014 (E1356-08).
127. Hopmann, C. Einführung in die Kunststoffverarbeitung, 8. Aufl.; Hanser: München, 2017, ISBN 978-3-446-45355-5.
128. Scriven, L.E. Physics and Applications of DIP Coating and Spin Coating. MRS Proc. 1988, 121, doi:10.1557/PROC-121-717.
129. Bose, S.; Keller, S.S.; Alstrøm, T.S.; Boisen, A.; Almdal, K. Process optimization of ultrasonic spray coating of polymer films. Langmuir 2013, 29, 6911–6919, doi:10.1021/la4010246.
130. Bhardwaj, N.; Kundu, S.C. Electrospinning: a fascinating fiber fabrication technique. Biotechnol. Adv. 2010, 28, 325–347, doi:10.1016/j.biotechadv.2010.01.004.
131. Illner, S.; Ortelt, J.; Arbeiter, D.; Khaimov V.; Wulf, K.; Oschatz, S.; Reske, T.; Senz, V.; Schmitz, K.-P.; Grabow, N. Adaptable Superfibers as Implant Material. Curr. Dir. Biomed. Eng. 3120, 465–468.
132. Siewert, S.; Falke, K.; Luderer, F.; Reske, T.; Schmidt, W.; Pfensig, S.; Stiehm, M.; Hinze, U.; Chichkov, B.; Grabow, N.; et al. Development of a biodegradable flow resisting polymer membrane for a novel glaucoma microstent. Biomed. Microdevices 2017, 19, 78, doi:10.1007/s10544-017-0218-8.
133. Takayama, T.; Todo, M.; Tsuji, H. Effect of annealing on the mechanical properties of PLA/PCL and PLA/PCL/LTI polymer blends. J. Mech. Behav. Biomed. Mater. 2011, 4, 255–260, doi:10.1016/j.jmbbm.2010.10.003.
134. European Medicines Agency. Q3C (R6) Step 5 - impurities: guideline for residual solvents 2016.
135. Teske, M.; Arbeiter, D.; Schober, K.; Eickner, T.; Grabow, N. Systemic analysis about residual chloroform in PLLA films. Curr. Dir. Biomed. Eng. 2016, 2, 1929, doi:10.1515/cdbme-2016-0014.
136. Teske, M.; Arbeiter, D.; Schober, K.; Eickner, T.; Grabow, N. Systematic analysis about residual chloroform removal from PCL films. Curr. Dir. Biomed. Eng. 2018, 4, 567–569, doi:10.1515/cdbme-2018-0136.
137. Arbeiter, D.; Schümann, K.; Sahmel, O.; Eickner, T.; Schmitz, K.-P.; Grabow, N. The effect of thermal treatment on the mechanical properties of PLLA tubular specimens. Curr. Dir. Biomed. Eng. 2016, 2, 26, doi:10.1515/cdbme-2016-0009.
138. Grabow, N.; Schlun, M.; Sternberg, K.; Hakansson, N.; Kramer, S.; Schmitz, K.-P. Mechanical properties of laser cut poly(L-lactide) micro-specimens: implications for stent design, manufacture, and sterilization. J. Biomech. Eng. 2005, 127, 25–31, doi:10.1115/1.1835349.
139. Finkelstein, A.; McClean, D.; Kar, S.; Takizawa, K.; Varghese, K.; Baek, N.; Park, K.; Fishbein, M.C.; Makkar, R.; Litvack, F.; et al. Local drug delivery via a coronary stent with programmable release pharmacokinetics. Circulation 2003, 107, 777–784, doi:10.1161/01.CIR.0000050367.65079.71.

140. Petersen, S.; Hussner, J.; Reske, T.; Grabow, N.; Senz, V.; Begunk, R.; Arbeiter, D.; Kroemer, H.K.; Schmitz, K.-P.; Meyer zu Schwabedissen, H.E.; et al. In vitro study of dual drug-eluting stents with locally focused sirolimus and atorvastatin release. J. Mater. Sci.: Mater. Med. 2013, 24, 2589–2600, doi:10.1007/s10856-013-5001-7.
141. Iannace, S.; Maffezzoli, A.; Leo, G.; Nicolais, L. Influence of crystal and amorphous phase morphology on hydrolytic degradation of PLLA subjected to different processing conditions. Polymer 2001, 42, 3799–3807, doi:10.1016/S0032-3861(00)00744-8.
142. Mukai, K.; Doi, Y.; Sema, Y.; Tomita, K. Substrate specificities in hydrolysis of polyhydroxyalkanoates by microbial esterases. Biotechnol. Lett. 1993, 15, 601–604, doi:10.1007/BF00138548.
143. ISO 13781. Implants for surgery - Homopolymers, copolymers and blends on poly(lactide) - In vitro degradation testing; Beuth: Berlin, 2017 (13781:2017(E)).
144. ISO 15814. Implants for surgery - Copolymers and blends based on poly(lactide) - In vitro degradation testing; Beuth: Berlin, 1999 (15814:1999(E)).
145. Liu, L.; Li, S.; Garreau, H.; Vert, M. Selective enzymatic degradations of poly(L-lactide) and poly(epsilon-caprolactone) blend films. Biomacromolecules 2000, 1, 350–359, doi:10.1021/bm000046k.
146. Menges, G.; Haberstroh, E.; Michaeli, W.; Schmachtenberg, E. Menges Werkstoffkunde Kunststoffe, 1. Aufl.; Hanser: München, 2014, ISBN 3446427627.
147. Bonten, C. Kunststofftechnik: Einführung und Grundlagen, 2. Aufl.; Hanser: München, 2016, ISBN 9783446449176.
148. Grellmann, W. Kunststoffprüfung, 3. Aufl.; Hanser: München, 2015, ISBN 978-3-446-44350-1.
149. Rösler, J.; Harders, H.; Bäker, M. Mechanisches Verhalten der Werkstoffe, 6. Aufl.; Springer: Wiesbaden, 2019, ISBN 978-3-658-26801-5.
150. Frick, A.; Stern, C. Einführung in die Kunststoffprüfung: Prüfmethoden und Anwendungen; Hanser: München, 2017, ISBN 9783446443518.
151. Koltzenburg, S.; Maskos, M.; Nuyken, O. Polymere: Synthese, Eigenschaften und Anwendungen; Springer: Berlin, Heidelberg, 2014, ISBN 978-3-642-34772-6.
152. Botlhoko, O.J.; Ramontja, J.; Ray, S.S. A new insight into morphological, thermal, and mechanical properties of melt-processed polylactide/poly(ε -caprolactone) blends. Polym. Degrad. Stab. 2018, 154, 84–95, doi:10.1016/j.polymdegradstab.2018.05.025.
153. Fischer, E.W.; Sterzel, H.J.; Wegner, G. Investigation of the structure of solution grown crystals of lactide copolymers by means of chemical reactions. Kolloid-Z. u. Z. Polymere 1973, 980–990.
154. Tsuji, H.; Mizuno, A.; Ikada, Y. Properties and morphology of poly(L-lactide). III. Effects of initial crystallinity on long-termin vitro hydrolysis of high molecular weight poly(L-lactide) film in phosphate-buffered solution. J. Appl. Polym. Sci. 2000, 77, 1452–1464, doi:10.1002/1097-4628(20000815)77:7<1452:AID-APP7>3.0.CO;2-S.
155. Meredith, J.C.; Amis, E.J. LCST phase separation in biodegradable polymer blends: poly(D,L-lactide) and poly(ε-caprolactone). Macromol. Chem. Phys. 2000, 201, 733–739.
156. Maglio, G.; Malinconico, M.; Migliozzi, A.; Groeninckx, G. Immiscible Poly(L-lactide)/Poly(ε-caprolactone) Blends: Influence of the Addition of a Poly(L-lactide)-Poly(oxyethylene) Block Copolymer on Thermal Behavior and Morphology. Macromol. Chem. Phys. 2004, 205, 946–950, doi:10.1002/macp.200300150.
157. Hilianen-Vainio M.; Varpomaa P. Modification of poly(L-lactides) by blending: mechanical and hydrolytic behavior. Macromol. Chem. Phys. 1995, 1503–1523.
158. Todo, M.; Park, S.-D.; Takayama, T.; Arakawa, K. Fracture micromechanisms of bioabsorbable PLLA/PCL polymer blends. Eng. Fract. Mech. 2007, 74, 1872–1883, doi:10.1016/j.engfracmech.2006.05.021.

159. Migliaresi, C.; Lollis, A. de; Fambri, L.; Cohn, D. The effect of thermal history on the crystallinity of different molecular weight PLLA biodegradable polymers. Clin. Mater. 1991, 8, 111–118, doi:10.1016/0267-6605(91)90018-B.

160. Tsuji, H. Properties and morphologies of poly(L-lactide): 1. Annealing condition effects on properties and morphologies of poly(L-lactide). Polymer 1995, 36, 2709–2716, doi:10.1016/0032-3861(95)93647-5.

161. Carvalho, J.R.G.; Conde, G.; Antonioli, M.L.; Dias, P.P.; Vasconcelos, R.O.; Taboga, S.R.; Canola, P.A.; Chinelatto, M.A.; Pereira, G.T.; Ferraz, G.C. Biocompatibility and biodegradation of poly(lactic acid) (PLA) and an immiscible PLA/poly(ε-caprolactone) (PCL) blend compatibilized by poly(ε-caprolactone-b-tetrahydrofuran) implanted in horses. Polym. J. 2020, 52, 629–643, doi:10.1038/s41428-020-0308-y.

162. Grigoriev, T.E.; Bukharova, T.B.; Vasilyev, A.V.; Leonov, G.E.; Zagoskin, Y.D.; Kuznetsova, V.S.; Gomzyak, V.I.; Salikhova, D.I.; Galitsyna, E.V.; Makhnach, O.V.; et al. Effect of Molecular Characteristics and Morphology on Mechanical Performance and Biocompatibility of PLA-Based Spongious Scaffolds. BioNanoScience 2018, 8, 977–983, doi:10.1007/s12668-018-0557-9.

163. Broz, M. Structure and mechanical properties of poly(D,L-lactic acid)/poly(ε-caprolactone) blends. Biomaterials 2003, 24, 4181–4190, doi:10.1016/S0142-9612(03)00314-4.

164. Ostafinska, A.; Fortelny, I.; Nevoralova, M.; Hodan, J.; Kredatusova, J.; Slouf, M. Synergistic effects in mechanical properties of PLA/PCL blends with optimized composition, processing, and morphology. RSC Adv. 2015, 5, 98971–98982, doi:10.1039/C5RA21178F.

165. Dell'Erba, R.; Groeninckx, G.; Maglio, G.; Malinconico, M.; Migliozzi, A. Immiscible polymer blends of semicrystalline biocompatible components: thermal properties and phase morphology analysis of PLLA/PCL blends. Polymer 2001, 42, 7831–7840, doi:10.1016/S0032-3861(01)00269-5.

166. Murphy, S.H.; Marsh, J.J.; Kelly, C.A.; Leeke, G.A.; Jenkins, M.J. CO 2 assisted blending of poly(lactic acid) and poly(ε-caprolactone). Eur. Polym. J. 2017, 88, 34–43, doi:10.1016/j.eurpolymj.2016.12.013.

167. Farah, S.; Anderson, D.G.; Langer, R. Physical and mechanical properties of PLA, and their functions in widespread applications - A comprehensive review. Adv. Drug Deliv. Rev. 2016, 107, 367–392, doi:10.1016/j.addr.2016.06.012.

168. López-Rodríguez, N.; López-Arraiza, A.; Meaurio, E.; Sarasua, J.R. Crystallization, morphology, and mechanical behavior of polylactide/poly(ε-caprolactone) blends. Polym. Eng. Sci. 2006, 46, 1299–1308, doi:10.1002/pen.20609.

169. Kesel, C. de; Lefèvre, C.; Nagy, J.B.; David, C. Blends of polycaprolactone with polyvinylalcohol: a DSC, optical microscopy and solid state NMR study. Polymer 1999, 40, 1969–1978, doi:10.1016/S0032-3861(98)00253-5.

170. Mandelkern, L. The crystallization kinetics of polymer-diluent mixtures: The temperature coefficient of the process. Polymer 1964, 637–648, doi:10.1016/0032-3861(64)90214-9.

171. Hobzova, R.; Hampejsova, Z.; Cerna, T.; Hrabeta, J.; Venclikova, K.; Jedelska, J.; Bakowsky, U.; Bosakova, Z.; Lhotka, M.; Vaculin, S.; et al. Poly(d,l-lactide)/polyethylene glycol micro/nanofiber mats as paclitaxel-eluting carriers: preparation and characterization of fibers, in vitro drug release, antiangiogenic activity and tumor recurrence prevention. Mater. Sci. Eng. C Mater. Biol. Appl. 2019, 98, 982–993, doi:10.1016/j.msec.2019.01.046.

172. Liggins, R.T.; Burt, H.M. Paclitaxel-loaded poly(L-lactic acid) microspheres 3: blending low and high molecular weight polymers to control morphology and drug release. Int. J. Pharm. 2004, 282, 61–71, doi:10.1016/j.ijpharm.2004.05.026.

173. Nukala, R.K.; Boyapally, H.; Slipper, I.J.; Mendham, A.P.; Douroumis, D. The application of electrostatic dry powder deposition technology to coat drug-eluting stents. Pharm. Res. 2010, 27, 72–81, doi:10.1007/s11095-009-0008-y.

Verzeichnis der Abbildungen und Tabellen

Danksagung

Eine Doktorarbeit zu schreiben ist immer eine Herausforderung und erfordert vielerlei Unterstützung. An dieser Stelle möchte ich mich bei allen bedanken, die zum Gelingen dieser Arbeit beigetragen haben.

Besonders danken möchte ich Prof. Grabow für die Bereitstellung des spannenden Themas und die Betreuung während der gesamten Zeit. Auch möchte ich mich dafür bedanken, dass er mir das Vertrauen geschenkt hat, meine eigenen Ideen zu verwirklichen und mir nicht nur jederzeit mit Rat und Tat, sondern auch immer mit einem hervorragenden Espresso zur Seite stand.

Darüber hinaus möchte ich insbesondere Herrn Dr. Stefan Oschatz für die enorme Unterstützung bei der Durchführung dieser Arbeit danken. Es war zugegebenermaßen nicht immer einfach, aber mit seinem Humor und seiner Zuversicht gab er mir den Mut und die Kraft, durchzuhalten. Vielleicht lag es aber auch an dem guten Essen. Ein ganz lieber Dank geht auch an seine Frau Sophie, die es, selbst im Weihnachtsurlaub, mit einem Lächeln zugelassen hat, Stefan’s Hilfe in Anspruch zu nehmen. Ich hoffe, Kristian und ich konnten uns mit einer super Gartenparty revangieren.

Dem gesamten IBMT und IIB e.V. möchte ich für die tolle Zusammenarbeit, konstruktiven Gespräche und kreativen Auszeiten danken. Ein besonderer Dank dabei geht an Prof. Schmitz, der mit seiner vollen Unterstützung und seinem unermüdlichen Antrieb den Grundstein für den Erfolg dieser Arbeit gelegt hat. Dr. Kerstin Lebahn danke ich herzlichst für die konstruktiven Gespräche, nicht nur im Büro, sondern auch auf den gemeinsamen BMT Tagungen. Der gesamten AG Chemie danke ich, dass sie immer ein offenes Ohr für mich haben. Weiterhin geht ein großer Dank an Konstanze Jäh und Volkmar Senz, die mir, insbesondere in der letzten Phase meiner Arbeit, Ihr vollstes Verständnis zeigten. Zudem möchte ich Caroline Dudda, Andrea Rohde, Katja Hahn und Babette Hummel danken, ohne deren Probenpräparation und die tollen REM Aufnahmen diese Arbeit nicht zustande gekommen wäre.

An Dani, Tina und Mady geht ebenfalls ein riesen Dank, deren Herzlichkeit und Lebensfreude Genuss pur sind. Danke für die Auszeiten, die mir so viel Energie geschenkt haben. Und die extra Portion Glitzer gab es noch gratis obendrauf.

Meinen Eltern Uschi und Axel, meiner Schwester Anja und meiner Familie Jan, Sarah, Leah und Brian möchte ich ganz besonders herzlich für eure durchweg uneingeschränkte Unterstützung und Liebe danken.

Zuletzt und von ganzem Herzen danke ich Krischi, dafür, dass du mir während der gesamten Phase den Rücken frei gehalten und nie an mir gezweifelt hast, auch wenn ich es manchmal tat. Jeder Tag mit dir ist ein Erlebnis, besonders samstags.

Förderungshinweis

Die vorliegende Dissertation wurde im Rahmen des Forschungsprojektes "Card-ii-Omics - Kardiovaskuläre Implantatentwicklung-Infektionen-Proteomics: Prävention, Diagnostik und Therapie von Implantatinfektionen“ angefertigt. Die Förderung des Projektes erfolgt aus Mitteln des Europäischen Sozialfonds (ESF) im Rahmen des Qualifikationsprogrammes "Förderung von Nachwuchswissenschaftlern in exzellenten Forschungsverbünden - Exzellenzforschungsprogramm des Landes Mecklenburg-Vorpommern“. (ESF/14-BM-A55-0040/16).

EUROPÄISCHE UNION
Europäischer Sozialfonds

Europäische Fonds EFRE, ESF und ELER
in Mecklenburg-Vorpommern 2014-2020

Erklärung

Ich erkläre, dass ich die eingereichte Dissertation selbstständig und ohne fremde Hilfe verfasst, andere als die von mir angegebenen Quellen und Hilfsmittel nicht benutzt und die den benutzten Werken wörtlich oder inhaltlich entnommenen Stellen als solche kenntlich gemacht habe.

Des Weiteren erkläre ich, dass ich mich bisher noch keinem Promotionsverfahren unterzogen oder um eine Zulassung zu solchem beworben habe. Die eingereichte Schrift wurde an keiner anderen Hochschule vorgelegt.

Rostock, Mai 2022

Daniela Arbeiter

Verwendete Originalarbeiten zur kumulativen Dissertation mit Darstellung des eigenen Beitrags an den Publikationen

Folgende Arbeiten wurden für die kumulative Dissertation herangezogen:

Studie 1: *In vitro* Degradation von PLLA unter *in vivo*-nahen und beschleunigten Bedingungen

[Pub1] **Arbeiter D**, Lebahn K , Reske T, Senz V, Eickner T, Schmitz K-P, Grabow N, Oschatz S. Comparison of accelerated and enzyme-associated real-time degradation of HMW PLLA and HMW P3HB films.
Polymer Testing (**2022**) 107.
DOI: 10.1016/j.polymertesting.2021.107471 (IF = 4,282)

In der Veröffentlichung hauptverantwortlich erarbeitet wurden:
Konzept und Studiendesign
Degradationsstudie
Rasterelektronenmikroskopie
Thermische Untersuchungen
Ergebnisanalyse und Diskussion
Manuskripterstellung

Studie 2: Betrachtung der Phasenseparationseffekte von PLLA/PCL-Blends

[Pub2] **Arbeiter D**, Eickner T, Oschatz S, Specht O, Reske T, Teske M, Senz V, Schmitz K-P, Grabow N. Physico chemical characterization of phase separated PLLA PCL blends obtained from solvent cast processes in a biomedical background.
Mater. Res. Express 7 (**2020**) 095302.
DOI: 10.1088/2053-1591/abb2c9 (IF = 1,449)

In der Veröffentlichung hauptverantwortlich erarbeitet wurden:
Konzept und Studiendesign
Rasterelektronenmikroskopie
Rasterkraftmikroskopie
Thermische Untersuchungen
Mechanische Untersuchungen
Ergebnisanalyse und Diskussion
Manuskripterstellung

Studie 3: Aspekte der Wirkstoffinkorporation in PLLA

[Pub3] **Arbeiter D**, Reske T, Teske M, Bajer D, Senz V, Schmitz K-P, Grabow N, Oschatz S. Influence of drug incorporation on the physico-chemical properties of poly(L-lactide) implant coating – a systematic study.
Polymers (**2021**) 13(2):292.
DOI: 10.3390/polym13020292
PMID: 33477626 (IF = 3,426)

In der Veröffentlichung hauptverantwortlich erarbeitet wurden:
Konzept und Studiendesign
Thermische Untersuchungen
Mechanische Untersuchungen
Ergebnisanalyse und Diskussion
Manuskripterstellung

[Pub4] Wulf K, **Arbeiter D**, Matschegewski C, Teske M, Huling J, Schmitz KP, Grabow N, Kohse S. Smart releasing electrospun nanofibers-poly: L.lactide fibers as dual drug delivery system for biomedical application.
Biomed. Mater. 16 (**2021**).
DOI: 10.1088/1748-605X/abbec8 (IF = 3,174)

In der Veröffentlichung hauptverantwortlich erarbeitet wurden:
Thermische Untersuchungen
Ergebnisanalyse und Diskussion
Manuskripterstellung: Artikelabschnitt zur thermischen Analyse

Publikation 1

Polymer Testing (**2022**) 107.

Comparison of accelerated and enzyme-associated real-time degradation of HMW PLLA and HMW P3HB films.

Arbeiter D, Lebahn K , Reske T, Senz V, Eickner T, Schmitz K-P, Grabow N, Oschatz S.

Eingereicht: 24.08.2021, veröffentlicht: 06.01.2022

DOI: 10.1016/j.polymertesting.2021.107471 (IF = 4,282)

Abstract: Designing laboratory-scale degradation experiments for polymer-based biomaterials is crucial for the development of safe and functional implants, in particular regarding high molecular weight polyesters. Within this work, we compared accelerated degradation of solvent-cast HMW-PLLA and HMW-P3HB films at 55 °C (16 weeks) with enzyme-associated (proteinase K and lipases) real-time degradation at 37 °C (108 weeks). During real-time degradation, PLLA showed mass loss up to 83 %, in contrast to accelerated conditions, where no changes occurred. Moreover, we observed wave-shape development of crystallinity for PLLA and PHB for both degradation conditions applied, whereby PLLA χ value nearly doubled to up to 75 %. These results were used to develop a correlation model based on molecular weight decrease and were furthermore discussed in light of a detailed literature review. In summary, real-time in vitro studies could be adapted to accelerated protocols providing the same limiting conditions such as molecular weight and initial crystallinity are given.

Polymer Testing 107 (2022) 107471

Contents lists available at ScienceDirect

Polymer Testing

journal homepage: www.elsevier.com/locate/polytest

Comparison of accelerated and enzyme-associated real-time degradation of HMW PLLA and HMW P3HB films

Daniela Arbeiter [a,*], Kerstin Lebahn [a], Thomas Reske [b], Volkmar Senz [a], Thomas Eickner [a], Klaus-Peter Schmitz [a,b], Niels Grabow [a], Stefan Oschatz [a]

[a] Institute for Biomedical Engineering, Rostock University Medical Center, Friedrich-Barnewitz-Straße 4, 18119, Rostock-Warnemünde, Germany
[b] Institute for Implant Technology and Biomaterials e.V, Friedrich-Barnewitz-Straße 4, 18119, Rostock-Warnemünde, Germany

ARTICLE INFO

Keywords:
Poly-L-lactide
Poly-3-hydroxybutyrate
Enzyme-associated degradation
Accelerated degradation
Molecular weight
Crystallinity

ABSTRACT

Designing laboratory-scale degradation experiments for polymer-based biomaterials is crucial for the development of safe and functional implants, in particular regarding high molecular weight polyesters. Within this work, we compared accelerated degradation of solvent cast HMW-PLLA and HMW-P3HB films at 55 °C (16 weeks) with enzyme-associated (proteinase K and lipases) real-time degradation at 37 °C (108 weeks). During real-time degradation, PLLA showed mass loss up to 83%, in contrast to accelerated conditions, where no changes occurred. Moreover, we observed wave-shape development of crystallinity for PLLA and PHB for both degradation conditions applied, whereby PLLA χ value nearly doubled to up to 75%. These results were used to develop a correlation model based on molecular weight decrease and were furthermore discussed in light of a detailed literature review. In summary, real-time *in vitro* studies could be adapted to accelerated protocols providing the same limiting conditions such as molecular weight and initial crystallinity are given.

1. Introduction

Accelerated *in vitro* degradation protocols for polymeric materials allow to reproduce long-term behavior in a relatively short experiment [1]. In general, the hydrolytic degradation rate of biodegradable polymers is raised by increasing temperature or altering pH. Ideally, finding a correlation between real-time and accelerated conditions, according to the relevant standards e.g. ISO 10993 [2], would allow process-related analytics and the development of a validation protocol of absorbable polymers which can substantially accelerate future degradation studies, saving resources and research funds. However, as various factors, such as the involvement of enzymes, play a role in *in vivo* degradation, the realistic situation can only be represented to a limited extent by *in vitro* experiments, especially under accelerated conditions.

In the field of biodegradable polyesters, poly-L-lactide (PLLA) and poly-3-hydroxybutyrate (P3HB) exhibit a still increasing importance [3–6]. PLLA can be applied as implant coating [7], drug carrying matrix [8], surgical sutures [9] or solid implant material [10,11]. As for the latter, currently several ultrathin strut PLLA-based biodegradable stents are under clinical and preclinical investigation [12–16]. P3HB in turn is used, among other applications, as porous patches for pericardial replacement in fields of cardiology for example [17] or as bone graft material [18].

Due to their inherent properties, PLLA and P3HB can be processed by several methods, such as extrusion [7] or melt electrospinning [19], as well as solvent-based manufacturing methods. In general, solvent-based manufacturing protocols are in particular relevant, as most industrial coating techniques rely on the use of polymer solutions. Dissolving a polymer in an adequate solvent enables a variety of different processes such as electrospinning and -spraying, air-brush [20], spin coating [21] and ultrasonic spraying to generate homogeneous and reproducible coatings on complex structures, such as stents, TAVR or cardiac pacemakers. Dipcoating [22,23] is another noteworthy method to access films or cylindrical semi-finished products, whereas the latter can furthermore be processed into implants, e.g. stents by laser cutting [7]. This process is especially suitable for lab scale prototyping. Moreover, compared to thermal processing, solvent-based protocols allow for the incorporation of active compounds, e.g. drugs, growth factors, or particles for various reasons [24–26].

Notably, processing methods have a considerable influence on the properties of the resulting material, e.g. surface morphology, crystallinity, polymer chain alignment and distribution of crystalline and

* Corresponding author.
E-mail address: daniela.arbeiter@uni-rostock.de (D. Arbeiter).

https://doi.org/10.1016/j.polymertesting.2021.107471
Received 24 August 2021; Received in revised form 15 November 2021; Accepted 30 December 2021
Available online 6 January 2022

amorphous domains [27,28]. Compared to thermal processing, solvent cast techniques require additional post-treatment of the materials, which can be either washing or annealing or a combination of both, to remove solvent residues as those may alter material properties or even show toxic effects [25,29]. In addition, molecular weight of the polymer material influences material properties.

Despite similar chemical composition with P3HB exhibiting just one additional CH_2-group compared to PLLA, PLLA and P3HB differ considerably regarding their degradation behavior. Whereas PLLA undergoes plain hydrolytic degradation within about 3 years, it is reported in the literature that scission of P3HB chains at physical conditions requires support by enzymatic catalysis and takes place over a period of about 4 years [30,31]. Moreover, effects such as autocatalysis [32,33] or mid-chain ester hydrolysis versus end-group scission have to be taken into account [34]. For more detailed predictions on auto and non-catalytic hydrolysis, Gleadall et al. [35] developed reaction kinetic models accounting the nature of the chain scissions (random or end). As reported by Scaffaro et al., PLLA degradation proceeds in 3 stages. Stage 1 describes surface degradation, while stage 2 explains the degradation penetration. They suggested that in the case of complete autocatalytic degradation or remarkable bulk depletion during long-term immersion, a third stage could be observed, often associated with pronounced erosional phenomena [36]. Real-time degradation studies for investigation of such behavior, however, remain challenging as degradation takes place over up to several years.

Literature overview on degradation experiments for PLLA

Due to complexity of the topic and the sheer amount of factors to be considered, a remarkable amount of experiments have been conducted to understand the degradation of PLLA. Yet, those studies vary in used molecular mass, specimen manufacturing protocol as well as choice of degradation medium and conditions. A brief overview on selected degradation studies on PLLA is given in Table 1.

Early studies on the degradation of PLLA mainly focused on morphology of the material and its influence on degradation behavior. In 1990, Li et al. prepared PLLA samples via compression molding followed by subsequent quenching or annealing to yield amorphous and semi crystalline specimens, respectively [37]. They pointed out that the early stage of degradation is independent of the initial morphology and rather depends on the thermal history and crystallinity of the material. However, remaining polymer residues appeared to be very resistant at the end of the degradation. Extensive investigations were focused on the crystallization behavior during the degradation process [37,48].

Tsuji et al. studied the hydrolysis of solution cast PLLA films showing different degrees of crystallinity, which was adjusted by previous annealing processes [28]. One of their results was that PLLA hydrolysis took place dominantly in the amorphous region in between the

Table 1
Overview on selected degradation studies performed on PLLA as reported in the literature.

	molecular weight M_W (Da)	manufacturing process	crystallinity χ (%)	degradation conditions		
				media	temperature	time[a]
Li et al. (1990) [37]	1.3×10^5	injection molding & quenched	0	saline & PBS, pH = 7.4	not specified	2 years
		injection molding & annealed at 130 °C for 2 h	73	PBS, pH = 7.4		
Pistner et al. (1993) [38]	4.5×10^5	injection molding	36	*in vivo* (rats)		2 years
	9.5×10^5	as-polymerized PLLA block	73			
Gogolewski et al. (1993) [39]	2.75×10^5	injection molding	52	*in vivo* (mouse)		6 months
Cam et al. (1995) [40]	3×10^5	CH_2Cl_2 without further process	30	0.01 M NaOH	37 °C	175 days
	4.5×10^5		15			
	6.5×10^5		5			
	3×10^6		3			
Bergsma et al. (1995) [1]	8.8×10^5	granulate	64	PBS; pH = 7.4	90 °C	6 weeks
Tsuji et al. (2000) [28]	1.3×10^6	CH_2Cl_2 washed in Methanol and 1 week in vacuum oven, melted at 200 °C & quenched at 0 °C	0	PBS; pH = 7.4	37 °C	2 years
		annealed for 15 min	2			
		annealed for 30 min	30			
		annealed for 45 min	45			
		annealed for 60 min	54			
Iannace et al. (2001) [41]	6×10^5	solvent cast in $CHCl_3$, evaporated & isothermal crystallization at 90 °C	46	PBS; pH = 7.02	37 °C	40 weeks
		as above at 130 °C	44			
Weir et al. (2004) [42]	4.24×10^5	compression molding, annealed at 120 °C for 4 h	40	PBS; pH = 7.4	37 °C	57 weeks
Weir et al. (2004) [43]	4.24×10^5	compression molding, annealed at 120 °C for 4 h	47	PBS; pH = 7.4	50 °C	115 days
			57.5	PBS; pH = 7.4	70 °C	23 days
Salguero et al. (2012) [44]	n.a.	commercial available polymer	36	PBS; pH = 7.02	37 °C	40 days
Deplaine et al. (2014) [45]	1.65×10^5	freeze extraction and porogen-leaching methods	13	PBS; pH = 7.02	37 °C	12 months
Felfel et al. (2015) [46]	1.2×10^5	compression molding, melted at 210 °C for 10 min	9.2	PBS; pH = 7.4	21 °C 37 °C 50 °C 65 °C 75 °C 85 °C	56 days
Wang et al. (2016) [47]	5.0×10^4	compression molding at 190 °C and 15 MPa, annealed at 115 °C for 1 h	19.5 ± 5.3	*in vivo* (rabbits)		1 year
Porfyris et al. (2018) [48]	1.79×10^5	compression molding at 190 °C for semi-crystalline	50	80% RH	70 °C	140 h
	1.49×10^5	160 °C for amorphous	0			
Fuoco et al. (2021) [49]	2.65×10^5	solvent cast in $CHCl_3$	76	PBS; pH = 7.4	60 °C	15–20 days

[a] Degradation times are extracted from the original literature and thus cannot be easily harmonized.

crystalline regions and hydrolysis rate was higher in that specific domain in comparison to free amorphous region. In general, they presumed that higher crystallinity and hence higher crystal thickness lead to more defects in the amorphous domain, promoting hydrolysis by enhanced water diffusion.

Cam et al. analyzed PLLA samples with a broad range of molecular weights in terms of their degradation behavior [40]. They showed that an increase in molecular weight leads to a decrease of initial crystallinities, yet the degradation rate increased. This may be contradictory compared to the aforementioned influence of crystallinity, but the authors stated that residual solvent could have influenced degradation behavior. They concluded that it is necessary to remove the solvent completely from the polymer.

Weir et al. analyzed the degradation of compression molded PLLA samples in an accelerated time period and compared the data with real time degradation [42,43]. Thus, at higher temperature, degradation proceeds by a very similar mechanism to that observed at 37 °C, *in vitro* as well as *in vivo*.

Still, concerns remained about the validity of testing above glass transition temperature T_g of PLLA when predicting results at degradation temperatures below T_g and the significance of autocatalysis as temperature is increased [43]. Thus, Weir et al. contradicted Bergsma's statement [1] that, although degradation temperature is well above glass transition temperature and not comparable to physiological temperatures, there seems to be good correlation between *in vitro* degraded and physiologically degraded material.

Moreover, conditions for performing *in vitro* degradation of PLLA have been standardized by ISO 13781:2017, specifying the use of Sørensen buffer (0.012 M KH_2PO_4, 0.055 M Na_2HPO_4 in water) with pH adjusted to 7.4 ± 0.2 at 37 °C ± 1 °C. The minimum solution volume has to be 10 ml and is recommended to be more than 30:1 to the test sample mass [50].

Literature overview on degradation experiments for P3HB

Regarding the *in vitro* degradation of P3HB, a summary on relevant degradation studies is given in Table 2.

Compared to PLLA, similar studies have been performed with P3HB. Doi et al. investigated the effects of polymer composition on the degradation rates of different PHB variations at different temperatures [51]. They concluded that hydrolytic degradation of PHB occurs in two steps: first random hydrolytic chain scission of the ester groups, followed by weight loss just at low M_w. Kurcok et al. concluded that the degree of crystallinity of P3HB due to chain orientation influences the rate of its hydrolytic degradation, with atactic P3HB showed faster degradation compared to semicrystalline polymer [52].

Regarding the need for enzymatic support in the P3HB degradation, Freier et al. [30] observed a slower pure hydrolytic degradation of P3HB in comparison to PLLA but a threefold accelerated loss in M_w when using porcine pancreatin, a mixture of lipases, amylases α-chymotrypsin, trypsin and proteases. Still, it remained uncertain if P3HB degradation behavior observed in their study was based on enzymatic catalysis.

In a very recent study, Zhuikov et al. [54] observed a wave-shape change of crystallinity during degradation of P3HB due to the fact that amorphous regions degrade faster than crystalline domains, leading to an increase of crystallinity. By hydrolysis of crystalline regions, amorphous components are formed, leading to an up-and-down in χ during degradation experiments. Overall, P3HB has not as extensively been investigated regarding accelerated degradation behavior as PLLA.

Objective of this study

Biodegradable polyesters with high molecular weight (HMW) are of particular interest in biomedical engineering, as mechanical and physico-chemical properties can be enhanced by increasing M_w [55,56].

Yet, in the case of HMW PLLA, with $M_w > 300$ kDa, and HMW P3HB with $M_w > 700$ kDa, no studies for solvent cast materials concerning the comparison of accelerated and enzyme-associated real-time degradation have been reported in the literature. Depicting the *in vivo* degradation allows for analyzing biomaterials in terms of changes in deflection, fatigue and tensile strength, changes in surface roughness and thus fluid mechanics, or fragmentation and particle formation.

Aim of our work is to contribute to the understanding of the degradation behavior of solvent cast HMW PLLA and HMW P3HB film materials. We investigated polymer film degradation in a real-time study with the use of lipases and proteinase K degradation in comparison to accelerated conditions at 55 °C. In addition to gravimetric measurements, morphological as well as thermal analyses and gel-permeation chromatography (GPC) were performed in order to be able to compare the results with literature data and to evaluate the accelerated degradation protocol. Two key findings of this work are that our choice of lipases did not catalyze the degradation of HMW P3HB but affected HMW PLLA. Moreover, we were able to observe that accelerated PLLA degradation induces more drastic changes in crystallinity compared to enzyme-associated real-time conditions. Overall, our results hold implications regarding the setup of test parameters and thus for the conclusions drawn from *in vitro* data.

2. Materials and methods

Materials: Poly-L-lactide (PLLA L210, M_w = 320.000 g/mol and PLLA L214, M_w = 700.000 g/mol) was purchased from Boehringer Ingelheim Pharma (Ingelheim, Germany). Poly-3-hydroxybutyrate (P3HB, M_w = 750.000 g/mol) was supplied by

Table 2
Overview on selected degradation studies performed on P3HB as reported in the literature.

	molecular weight M_W (Da)	manufacturing process	crystallinity χ (%)	degradation conditions: media	temperature	time[a]
Doi et al. (1989) [51]	n.a.	solvent cast in $CHCl_3$	59	PBS, pH = 7.4	37 °C 70 °C	200 days
Gogolewski et al. (1993) [39]	1.29×10^5	injection molding	60.7	*in vivo* (mouse)		6 months
Kurcok et al. (1995) [52]	2.34×10^4	granulate	n.a.	PBS; pH = 7.4	70 °C	80 days
Canetti et al. (1999) [53]	1.66×10^5	solvent cast in CH_2Cl_2, melted at 185 °C for 2 min & crystallization at 50 °C	51	Potassium phosphate buffer; pH = 7.0	37 °C	300 h
Freier et al. (2002) [30]	6.4×10^5	solvent cast in $CHCl_3$, 1 week in vacuum oven	69	PBS; pH = 7.4; porcine pancreatin	37 °C 70 °C	1 year
Salguero et al. (2012) [44]	6.0×10^5	solvent cast in $CHCl_3$ at 62 °C	53	PBS; pH = 7.02	37 °C	40 days
Zhuikov et al. (2020) [54]	1.1×10^6	solvent cast in $CHCl_3$, 72 h in vacuum oven	63	PBS; pH = 7.4; porcine pancreatic lipase	37 °C	6 months

[a] Degradation times are extracted from the original literature and thus cannot be easily harmonized.

Umweltforschungszentrum Leipzig-Halle GmbH (Leipzig-Halle, Germany).

Sample preparation: Degradation studies were performed using films cast from chloroform (Merck, Darmstadt, Germany) solutions (1 g polymer in 25 ml chloroform) employing petri dishes (Ø = 9 cm). After evaporation of the solvent, films were washed for two days in methanol (Merck, Darmstadt, Germany) and two days in deionized water at 25 °C, and dried for 7 days in a vacuum oven, model Scientific 45001 (Bioblock Fisher Scientific, Schwerte, Germany), at 40 °C. Polymer samples were punched in form of round slices of Ø = 5 mm. For real-time degradation study the following initial thickness was obtained (mean ± sample standard deviation of n = 3 samples with 3 measurements each): d = 133 ± 6 μm (PLLA L210), d = 118 ± 2.6 μm (PLLA L214) and d = 155 ± 5 μm (P3HB). For the accelerated study, sample thickness was: d = 101 ± 15 μm (PLLA L210), d = 104 ± 7 μm (PLLA L214) and d = 124 ± 12 μm (P3HB).

Degradation conditions: The degradation conditions were chosen according to the standards ISO 13781 [57] and ISO 15814 [50,58]. 37 °C were chosen as established temperature to simulate *in vivo* conditions and to ensure maximum enzyme activity. Furthermore, following Van't Hoff rule, a temperature of 55 °C was chosen to generate accelerated degradation conditions that allow us to degrade polymers within a very short time, for which several years would normally have to be invested. In addition, the studies had to be performed below the glass transition temperature of PLLA to avoid structural changes caused by degradation above T_g and to ensure comparability of the two chosen degradation conditions. Degradation assays for enzyme-associated real-time studies were conducted using Sørensen buffer at pH = 7.4 (MORPHISTO, Frankfurt am Main, Germany) containing 5.0 mg/l proteinase K (a ≥30 U/mg; Sigma-Aldrich, Darmstadt, Germany), 5.0 mg/l pseudomonas lipase (a ≥30 U/mg; Sigma-Aldrich, Darmstadt, Germany), and 7.7 mg/l aspergillus lipase (a = 181 U/mg; Sigma-Aldrich, Darmstadt, Germany). Each sample was incubated individually in 2 ml buffer at 37 °C and shaken with 100 rpm. Every two weeks, Sørensen buffer was changed in each vial. Specimens were taken out for investigations after 2, 4, 12, 24, 36, 48, 60, 72, 84, 96 and 108 weeks. Each polymer specimen wwas washed three times with distilled water and then dried for one week at 40 °C under reduced pressure.

For accelerated studies, each sample was incubated individually in 2 ml Sørensen buffer without enzymes at pH = 7.4 (MORPHISTO, Frankfurt am Main, Germany). Samples were shaken with 100 rpm at 55 °C. Every week, Sørensen buffer was changed in each vial. For investigations, specimens were taken out after 0.2, 1, 2, 3, 4, 6, 8, 10, 12, 14 and 16 weeks. The buffer solution was changed every week. After removal, specimens were treated precisely as in real-time study.

Microscopy: The polymer films were analyzed by means of light microscopic photography using an Olympus SC50 digital camera mounted on an Olympus SZX10 stereo microscope and cellSens Standard imaging software (Olympus, Tokyo, Japan). Scanning electron microscopy (SEM) was carried out using a SEM Quanta FEG 250 (FEI Company, Frankfurt, Germany). For SEM imaging, the samples were fixed onto aluminum trays with conductive carbon pads. The SEM investigations were performed using high vacuum and 10 kV with a working distance of approx. 10 mm. The images were taken at 800× magnification.

Mass change: Prior to degradation study, the polymer film sample mass was determined using an electronic microbalance XP6U (Mettler Toledo, Zurich, Switzerland). On removal, the same specimens were being weighed after washing three times with distilled water and drying for one week at 40 °C under reduced pressure. The overall percentage mass change was calculated from the mass before degradation.

GPC measurements: The molecular weight (M_w) and number average molecular weights (M_n) of polymer samples at different degradation time points were obtained at 30 °C using a PSS SECcurity SEC system (Polymer Standard Services, Mainz, Germany) including a RI detector combined with a WGE Dr. Bures g 2010 viscosity detector (WGE Dr. Bures, Dallgow, Germany). Separation was carried out with three PSS SDV columns (103, 105 and 106 Å, respectively). Chloroform stabilized with ethanol was the eluent with a flow rate of 1 ml/min. The samples were prepared with a concentration of 1.5 mg/ml in chloroform with hexylbenzene as internal standard and the injection volume was 0.1 ml. The molecular weights were calculated by the universal calibration method using twelve polystyrene calibration standards in a range between 376 and 2570.000 g/mol.

Thermal analysis: Thermal properties were investigated in a DSC FP84HT (Mettler Toledo, Zurich, Switzerland) for real-time degradation and DSC 1 (Mettler Toledo, Zurich, Switzerland) for accelerated degradation. Conventional calibration methods with highly pure standards were used. Real-time degradation samples were heated from +40 °C up to 225 °C with a heating rate of q = 10 K/min (FP84HT without active cooling system) operating at ambient atmospheric pressure. Accelerated degradation samples were heated from −40 °C up to 225 °C with a heating rate of q = 10 K/min (DSC 1 with intracooling system) operating under nitrogen at ambient atmospheric pressure. Sample weights were in the range of 3–6 mg. We analyzed the samples with respect to glass transition (T_g), melting temperature (T_m), and degree of crystallinity (χ). The heats of fusion and crystallization were quantitatively evaluated by determining the endothermic peak areas, which were compared with the melting peak area of totally crystalline PLLA (χ_{100} = 93.7 J/g) [59] and P3HB (χ_{100} = 146 J/g) [60].

FTIR-ATR-measurements: FTIR-ATR-measurements were performed using a Bruker Vertex 70 IR-Spectrometer (Bruker, Leipzig, Germany) equipped with a DLaTGS-detector. Data were collected in the range of $\tilde{\nu}$ = 500 cm^{-1} to 4000 cm^{-1} with a resolution of $\tilde{\nu}$ = 4 cm^{-1} averaged over 100 scans in reflection mode using a Graseby Golden Gate Diamond ATR-unit. Atmospheric compensation has been performed. All spectra were subsequently baseline corrected and finally normalized with OPUS vector-normalization-function for better visualization.

3. Results and discussion

General properties of the investigated polymers prior to degradation as taken from DSC and GPC experiments are summarized in Table 3.

To address the *in vivo* situation, our approach was the use of lipases for PLLA and proteinase K for P3HB as this protocol has been described before [30,61]. The role of enzymes in *in vivo* degradation of polymer biomaterials is being broadly discussed in the literature [31,53,62–65]. Some authors reported about enzyme contribution during the late stages of polymer degradation, with a high grade of material fragmentation and already drastically decreased molecular weight (<20.000 g/mol) [42,66]. Cam et al. stated that enzyme catalysis is nearly negligible regarding the biodegradation of PLLA [40]. Moreover, they illustrated that enzymes, being macromolecules themselves, are inhibited to penetrate into the polymer bulk due to their molecular size, thus bulk degradation by chain scissoring takes place just by hydrolysis. Still, surface degradation may be influenced by enzymes [67]. This, without bulk hydrolysis, would lead to the observation that M_w remains constant during degradation, whereas sample mass decreases as surface degradation products are easily washed out. In contrast, bulk hydrolysis without enzyme contribution on surface degradation would lead to M_w

Table 3
Material properties of polymers addressed in this study.

	PLLA		P3HB
	L210	L214	
molecular weight M_w	320.000 g/mol	700.000 g/mol	750.000 g/mol
glass transition temperature T_g	62 °C	65 °C	0 °C
melting temperature T_m	175 °C	178 °C	180 °C
crystallinity χ	37%	24%	68%

decrease at constant sample mass as hydrolysis products remain entrapped in the polymer. This assumption is taken into concern for the following analyses, as PLLA initial mass loss observed during our study must derive from enzymatic surface degradation, as molecular weight decrease proceeds considerable slower.

Surface morphology during degradation

First, changes in morphology during enzyme-associated *in vitro* degradation process at 37 °C and accelerated degradation at 55 °C were investigated by means of macrophotography and SEM. Within both degradation studies, PLLA L210 showed considerable visual changes (Fig. 1). The samples turned opaque and showed clear cracks after 16 weeks (accelerated) and 108 weeks (real-time), respectively. PLLA L214 became only opaque after 2 weeks in the real-time study but no further macroscopic changes were observed. In contrast to this, L214 samples did not show any optical changes during accelerated degradation. P3HB showed no optical changes during both degradation studies. Macro photography documentation of the degradation process of PLLA can be found in supporting information (Figs. S1–S6).

For a more detailed view, SEM imaging has been used to investigate the microscopic appearance of the degraded polymer samples. At 800× magnification, no such thing as microcrystals or other inhomogeneities as well as changes in surface morphology could be observed for PLLA L214 and P3HB, each for both degradation conditions. These samples appeared smooth and comparable to the initial state before degradation (images can be found in supporting information (Figs. S7–S12). PLLA L210 appeared to have one uniform rough surface, which did not change during real-time degradation. However, during accelerated degradation, growth of small spherulite crystals could be observed. After 16 weeks of degradation at 55 °C, continuous cracks at spherulite phase-phase-interfaces could be detected (Fig. 2f), presumably indicating propagation of hydrolytic degradation processes [36]. Fig. 2d) and e) each show the side which was attached to the surface of the Petri dish, thus resulting in a generally smoother surface.

Changes in mass during degradation

During enzyme-associated real-time degradation, PLLA L210 and L214 showed an almost linear mass loss from 10 weeks on to a residual of 71% and 27% of the starting mass after 108 weeks, respectively (Fig. 3). Accelerated degradation at 55 °C exhibited almost no mass loss with residual mass of 98% for L210 and 99% for L214 after 16 weeks. In the case of P3HB, there was no mass loss observable during both studies, real-time and accelerated degradation.

For enzyme-associated real-time degradation at 37 °C, L214 showed fast decrease in residual sample mass whereas M_w showed only low decrease until 24 weeks. Overall, we observed linear mass loss for film materials of PLLA L210 of about 30% and for L214 up to 73%, respectively. However, the increasing standard deviations can be explained by the advancing degradation due to the disintegration of the samples and the removal of free floating fragments during the media changes.

Regarding P3HB, enzyme-associated real-time at 37 °C, as well as accelerated degradation at 55 °C, did not result in a considerable mass loss of the samples.

Molecular mass loss during degradation

The molecular mass of PLLA L210 remained stable for the first 4 weeks. For PLLA L214, decrease in molecular mass could just be observed after 12 weeks of real-time degradation. In the following, both polymers exhibited an almost linear degradation behavior during the remaining time. After 108 weeks, both PLLA species retained 11–12% of their initial molecular mass. The real-time degradation of PLLA L210 and PLLA L214 was almost congruent in the end stage of degradation.

The initial molecular weight of P3HB showed fast decrease already during the first weeks of real-time degradation compared to PLLA (Fig. 4), reaching 80% of the initial value after 12 weeks. The molecular mass of P3HB decreased in an almost linear fashion until the end of the study. The mean values of the relative loss after 108 weeks were 53% for P3HB.

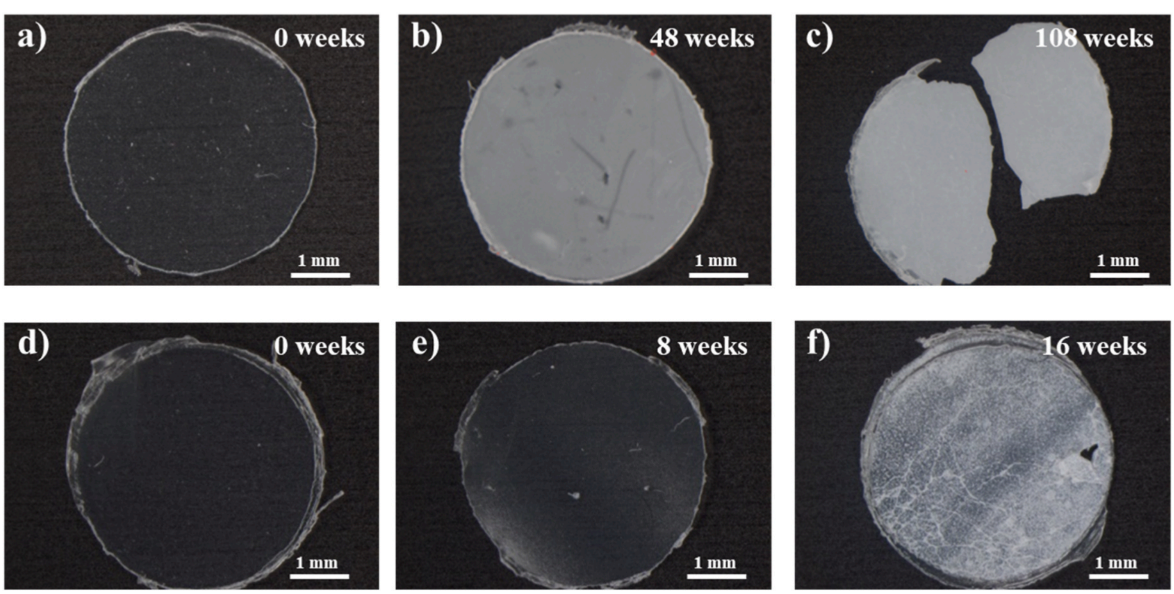

Fig. 1. Macroscopic documentation of real-time (a–c) and accelerated (d–f) degradation-induced changes of PLLA L210 morphology: (a,d) initial state, (b) after 48 weeks, (c) after 108 weeks, (e) after 8 weeks and (f) after 16 weeks.

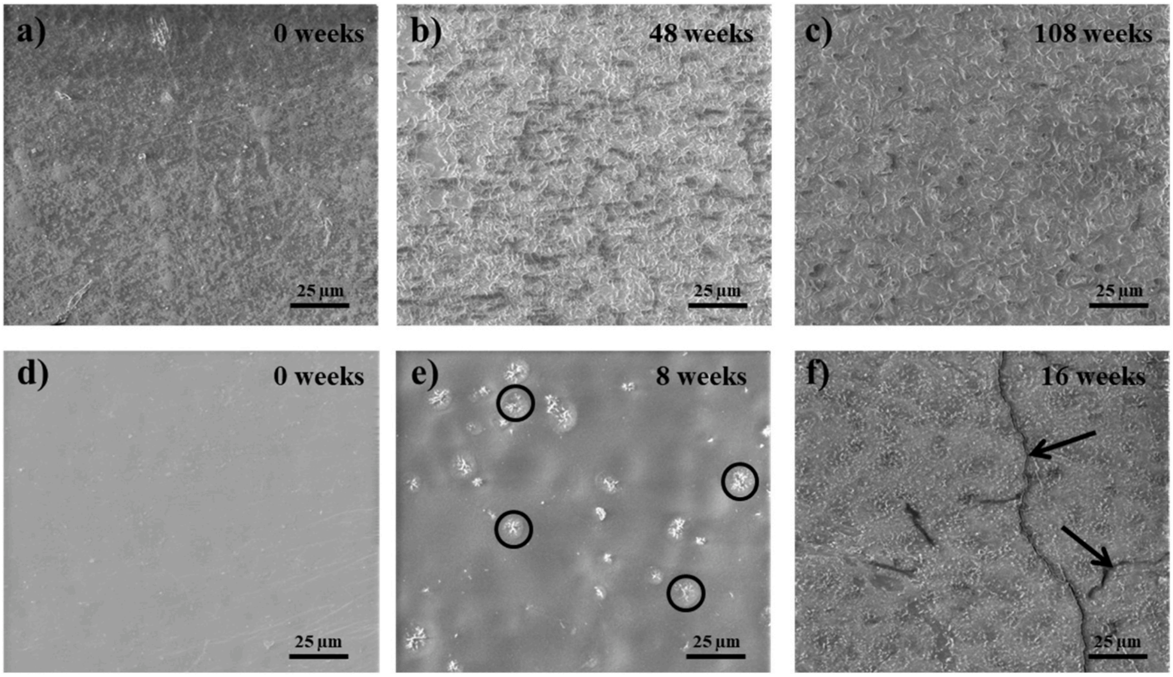

Fig. 2. SEM documentation of real-time (a–c) and accelerated (d–f) degradation-induced changes of PLLA L210 morphology: (a,d) initial state, (b) after 48 weeks, (c) after 108 weeks, (e) after 8 weeks and (f) after 16 weeks (800× magnification). The encircled structures in e) and arrows in f) show changes induced by accelerated degradation study.

After 12 weeks of degradation at 55 °C, molecular weight of PLLA L210 was reduced to less than 20% of its initial value. The linear degradation curve also appears to flatten out towards the end due to fragmentation of the material. Similar behavior was observed for PLLA L214, resulting in linear decrease in M_w, although not quite as fast when compared to PLLA L210. Comparable to L210, L214 M_w plots showed an increased standard deviation at the last time points and flattening of the curve. Accelerated degradation of P3HB at 55 °C resulted in 31% residual M_w after 16 weeks. Loss in M_w showed exponential decrease during degradation. Molecular weight (g/mol), polydispersity PI and mass loss (%) for all time points for both, real-time and accelerated degradation, (Tables S1–S3), as well as exemplary chromatograms of the GPC measurements from beginning, middle of end of degradation can be found in the supporting information (Figs. S13–S18).

When combining data for mass loss and M_w decrease, literature data for PLLA real-time degradation without enzymes, conducted by Weir et al. (compression molding sample preparation) [42] and Tsuji et al. (solvent cast sample preparation) [28], did not show mass loss during early stages of degradation, albeit decrease in M_w. The collateral decrease of M_w indicated furthermore additional bulk degradation by hydrolysis. PLLA L214 with higher M_w showed to be more affected by enzymes when compared to PLLA L210. Our results are consistent with those of Cam et al. [40] showing that due to the higher mass loss in L214, enzymes favor surface degradation with consistently decreasing M_w.

Regarding P3HB, our results indicated a decrease in M_w up to 70% but no considerable mass loss. Therefore, we assumed that the lipases we used did not catalyze P3HB chain scissoring, but simple bulk hydrolysis occurred.

Changes in thermal properties during degradation

The DSC curves of all polymers are shown in Fig. 5. The degree of crystallinity versus time is presented in Fig. 6. The χ values, glass transitions (T_g) and melting temperature (T_m) for all time points for both, real-time and accelerated degradation, can be found in the supplement data (Tables S4–S6).

PLLA L210 and PLLA L214 showed comparable thermal behavior during real-time degradation study. The DSC heating curves of PLLA cast films for both molecular weights exhibited a glass transition temperature of approximately $T_g = 65$ °C before degradation. No exothermic peak, but an endothermic melting peak at $T_m = 179$ °C was observed for L210 and L214, which was comparable to reported T_m data for HMW PLLA [4], see Table 3.

Decrease in T_m by hydrolysis for more than 12 months in both PLLAs (values in Tables S4–S5) was consistent with the literature [28,32,68]. Still noteworthy is that we measured T_g from dried samples and therefore is not reflective of T_g in the medium. Faster increase in crystallization values may be attributed to the fact that medium temperature is in the range of T_g. The amorphous portions were thus more mobile, allowing water to diffuse more rapidly through it, causing faster degradation. Regarding T_m, P3HB remained unaffected, due to the fact that degradation has not occurred yet in the crystallites, but only chain scission started in the amorphous regions.

Regarding crystallinity development, both HMW PLLA species, L210 and L214, exhibited a wave-shaped behavior during real-time degradation, whereas χ showed only little changes during the first 36 weeks. After 108 weeks, χ of both polymers nearly doubled, from χ_{L210} (36 weeks) = 31 ± 4% to χ_{L210} (108 weeks) = 57 ± 4%, and χ_{L214} (36 weeks) = 26 ± 4% to χ_{L214} (108 weeks) = 48 ± 5%. A similar trend was observed for the accelerated degradation study for both PLLA species.

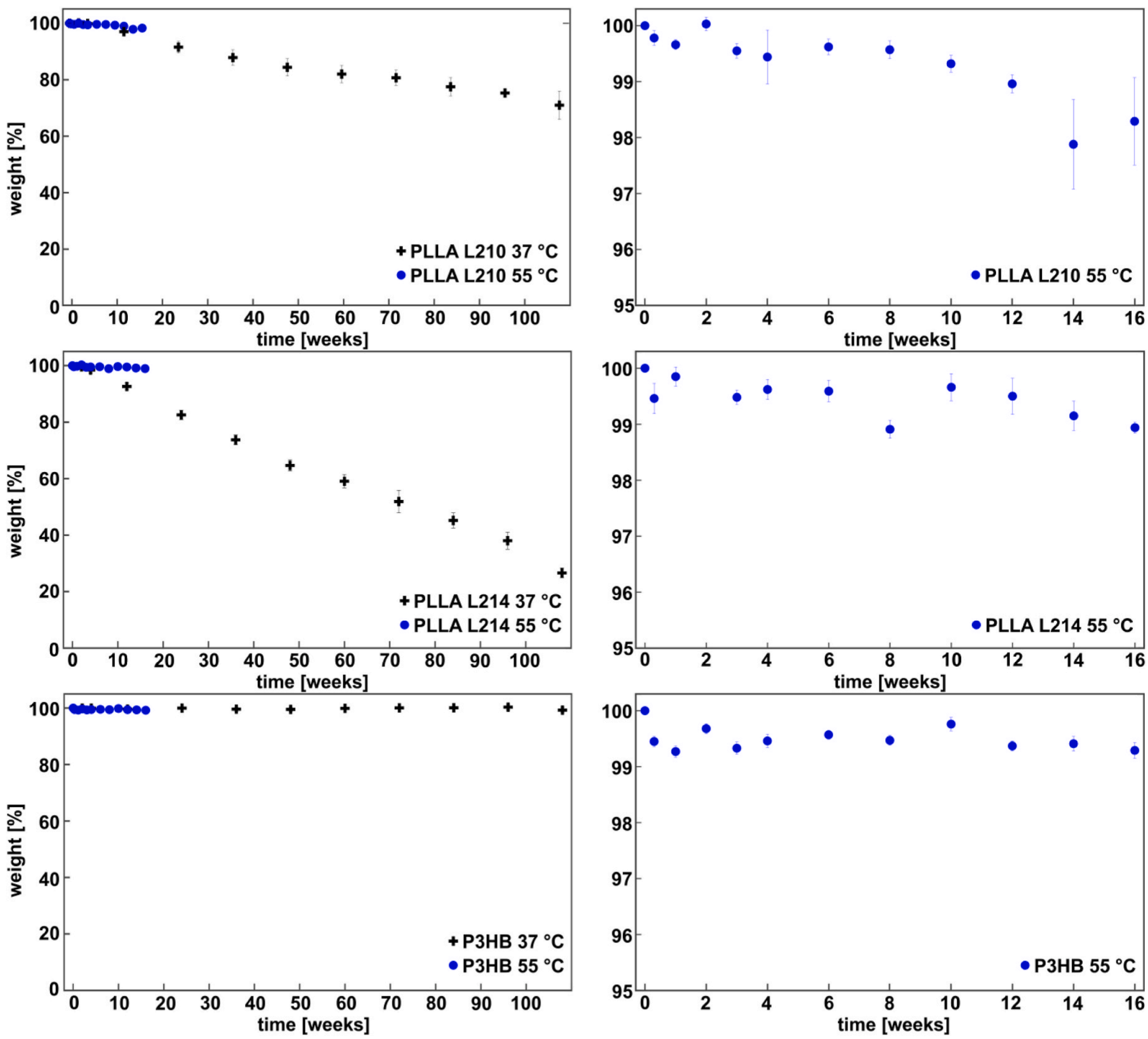

Fig. 3. Changes in mass of PLLA L210 (top), PLLA L214 (middle) and P3HB (bottom) during real-time degradation at 37 °C (black points) and accelerated degradation at 55 °C (blue points). All data points are means of n = 8 measurements except n = 7 at 10 weeks, L210 and 12 weeks, L210. For a better view, mass loss during accelerated degradation has been magnified on the right. (For interpretation of the references to colour in this figure legend, the reader is referred to the Web version of this article.)

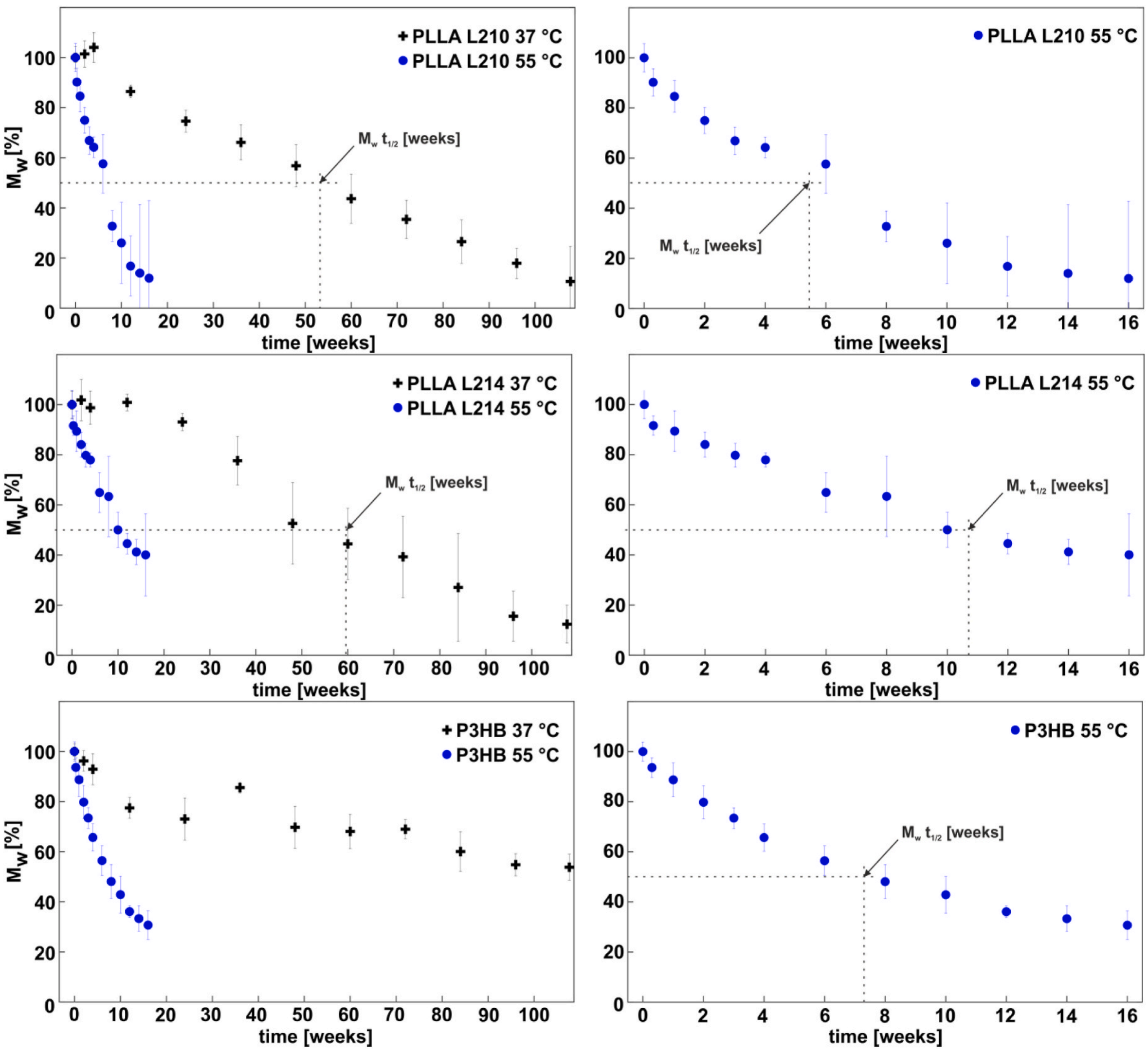

Fig. 4. Decrease in molecular weight of PLLA L210 (top), PLLA L214 (middle) and P3HB (bottom) during real-time degradation at 37 °C (black points) and accelerated degradation at 55 °C (blue points). Intersection of dotted lines represents molecular weight half-life ($M_w\ t_{1/2}$) with $Mw\ t_{1/2}$ (L210) = 53 weeks (37 °C) and $Mw\ t_{1/2}$ (L210) = 5.5 weeks (55 °C), and $Mw\ t_{1/2}$ (L214) = 59 weeks (37 °C) and $Mw\ t_{1/2}$ (L214) = 10.5 weeks (55 °C). $M_w\ t_{1/2}$ of P3HB during real-time degradation at 37 °C has not been reached after 108 weeks and $Mw\ t_{1/2}$ (P3HB) = 7.5 weeks (55 °C). All data points are mean values of 3 (accelerated degradation) and 5 measurements (real-time degradation), respectively. (For interpretation of the references to colour in this figure legend, the reader is referred to the Web version of this article.)

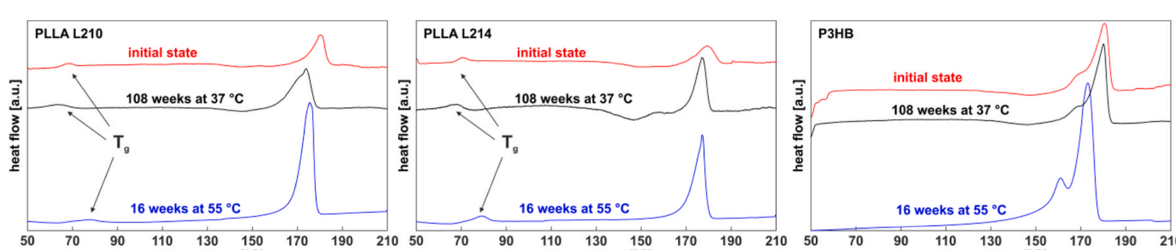

Fig. 5. DSC thermograms of PLLA L210 (left), PLLA L214 (middle) and P3HB (right) during real-time degradation at 37 °C (black line) and accelerated degradation at 55 °C (blue line). The red curve corresponds to the initial state before degradation. (For interpretation of the references to colour in this figure legend, the reader is referred to the Web version of this article.)

Until 8 weeks of degradation at $T = 55$ °C, χ_{L210} remained almost constant at approximately 40%, followed by an increase in χ up to 75 ± 7%, This behavior was also apparent with L214, although not as pronounced as for L210. Until 6 weeks, χ_{L214} is about 35%, followed by an increase until 16 weeks to $\chi_{L214} = 44 \pm 8\%$.

P3HB showed an initial crystallinity of $\chi_{P3HB} = 68 \pm 5\%$. During real-time and accelerated degradation study, also wave-shaped changes in thermal properties, T_g, T_m, and χ_{P3HB}, could be observed. This alternation can be attributed to degradation initially affecting predominantly amorphous regions, which exhibited a degradation rate of up to 20-fold

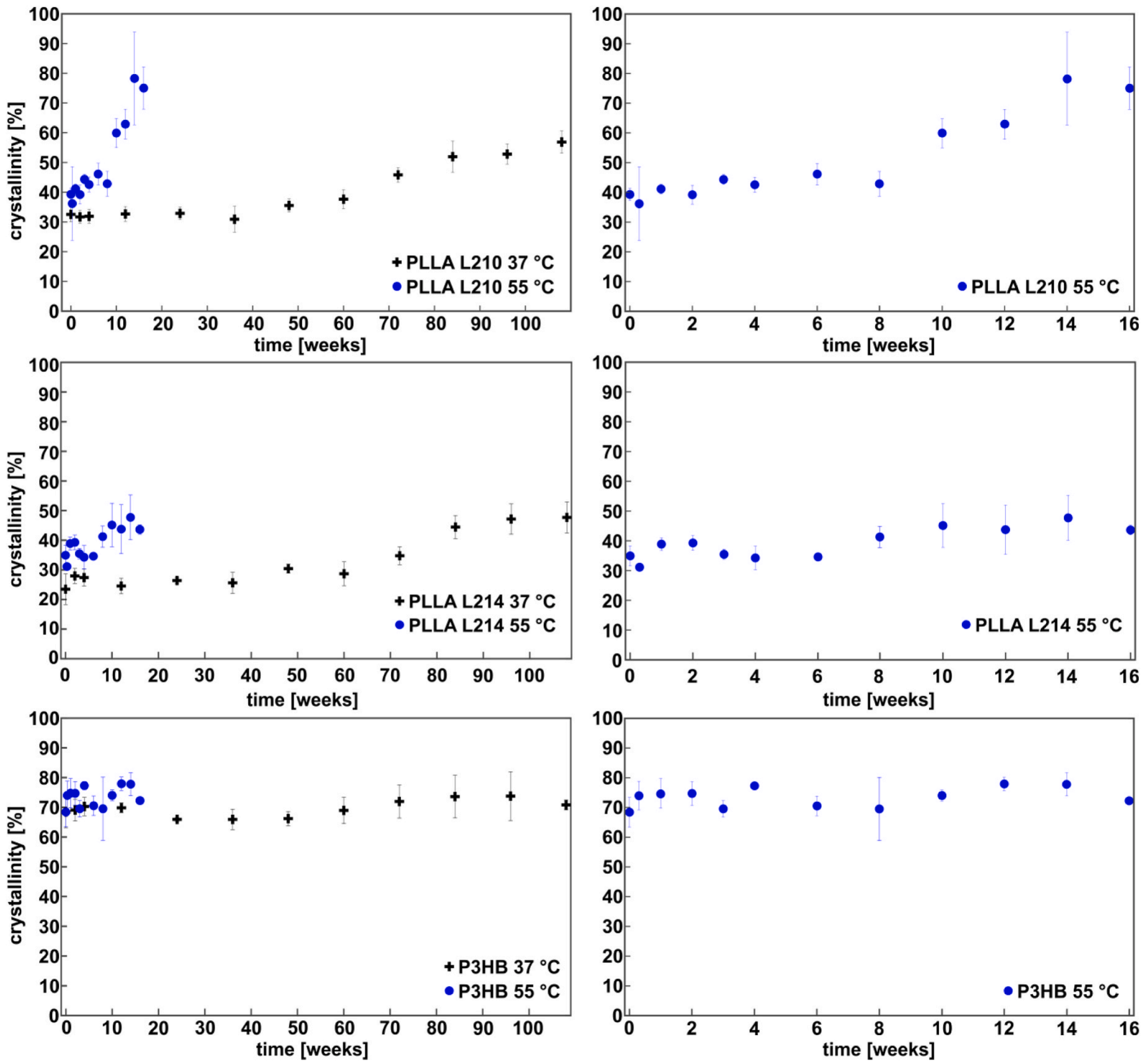

Fig. 6. Changes in χ of PLLA L210 (top), PLLA L214 (middle) and P3HB (bottom) during real-time degradation at 37 °C (black points) and accelerated degradation at 55 °C (blue points). All data points are means of 5 measurements. (For interpretation of the references to colour in this figure legend, the reader is referred to the Web version of this article.)

compared to the crystalline ones [1,69]. Polymer chain fragments in such regions are washed out more quickly due to the fact that water could easily migrate into amorphous domains, resulting in a decrease in amorphous fractions [38]. Fischer et al. quantified the decrease of average distance of crystalline regions during hydrolysis and showed that the loss of amorphous fractions leads to an increase in enthalpy of fusion and melting temperature decrease (see, Table S4) [59]. In accordance to this, our data show the same development in T_m and in ΔH, thus, we conclude the same mechanistic background. However, as hydrolysis is undirected, also crystalline domains were affected. This again led to a subsequent decrease in crystalline domains and reformation of amorphous regions due to short chain polymer fragments and secondary crystallites.

Comparison of real-time experiments with accelerated conditions

Qualitative FTIR-ATR spectroscopy has been performed to compare enzyme-associated real-time degradation with accelerated degradation at selected sampling points (t = 0/60/112 w (37 °C) and t = 0/6/16 w (55 °C)). All spectra can be found in the supplements (Figs. S19–24). According to literature findings [70], changes in bands at $\tilde{\nu} = 1210$ cm^{-1} and $\tilde{\nu} = 1230$ cm^{-1}, which are associated to asymmetric C–O–C stretching and asymmetric CH_3 rocking vibrations, respectively, were examined for PLLA L210 and L214 to follow the degradation progress at 37 °C and 55 °C. As for P3HB, FTIR spectra for both degradation conditions showed a comparable decrease in the amorphous C–O–C band at $\tilde{\nu} = 1183$ cm^{-1} [71]. The data show a similar progression of spectra changes for both degradation conditions for all polymers, thus real-time and accelerated degradation yield a comparable outcome.

For the comparison of enzyme-associated real-time degradation with accelerated degradation at 55 °C based on molecular weight and crystallinity, degradation times have been normalized to the point of first mass loss, respectively. However, one boundary condition was set that the initial crystallinity is similar in both studies and exhibits comparable behavior over time.

For comparison, molecular weight loss is plotted in Fig. 7 (left) with

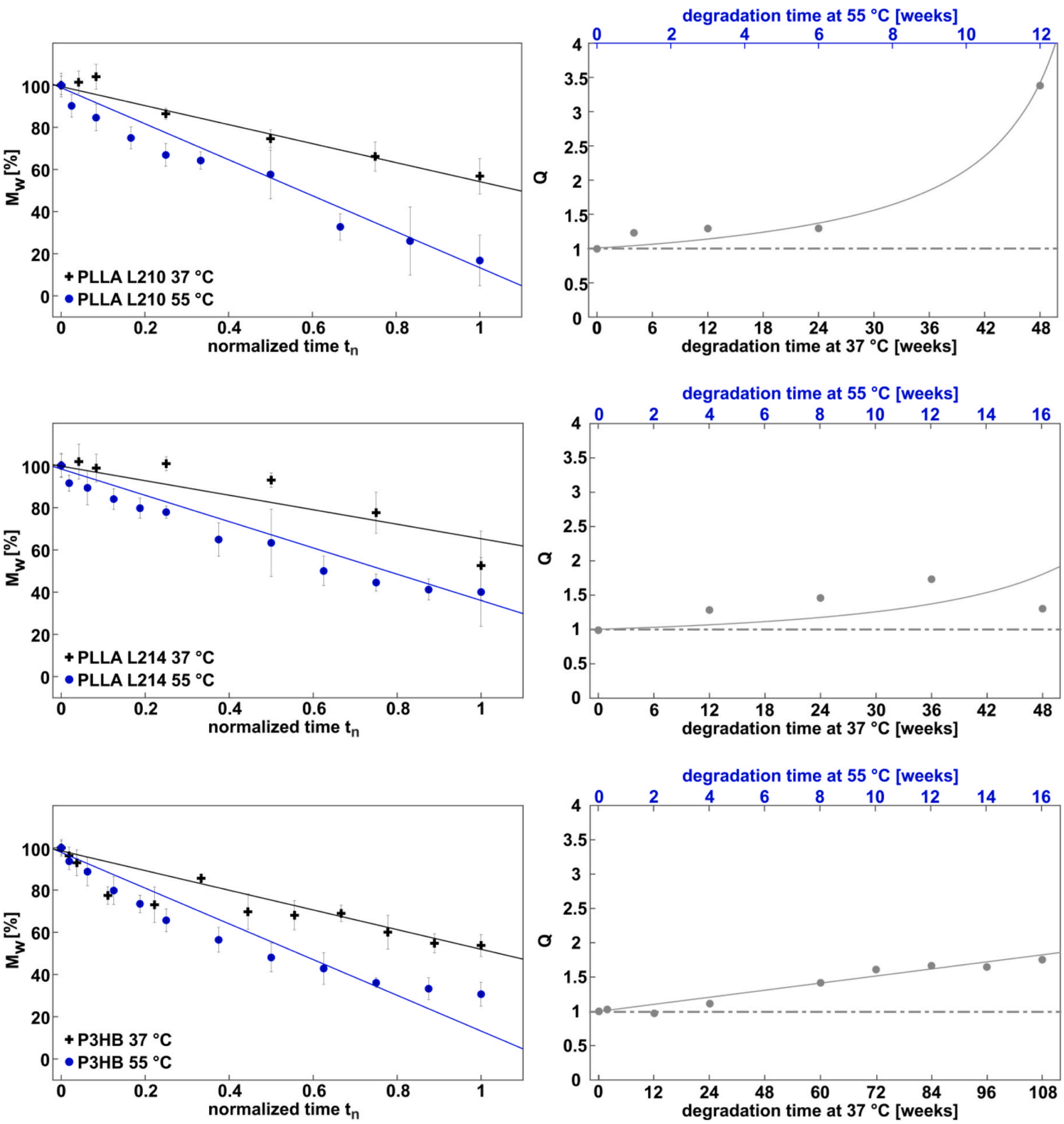

Fig. 7. M_w-correlation model of real-time and accelerated degradation of PLLA L210 (top), PLLA L214 (middle) and P3HB (bottom). Left: Plots of molecular weight loss of the real-time and accelerated degradation studies over normalized time points (t_n). For better illustration, linear trend lines have been added. Right: Plots of calculated quotient of the molecular weights of the accelerated experiments to those of the real-time study. The solid line presents the correlation trend line for Q over degradation time, while the dashed line represents idealized correlation.

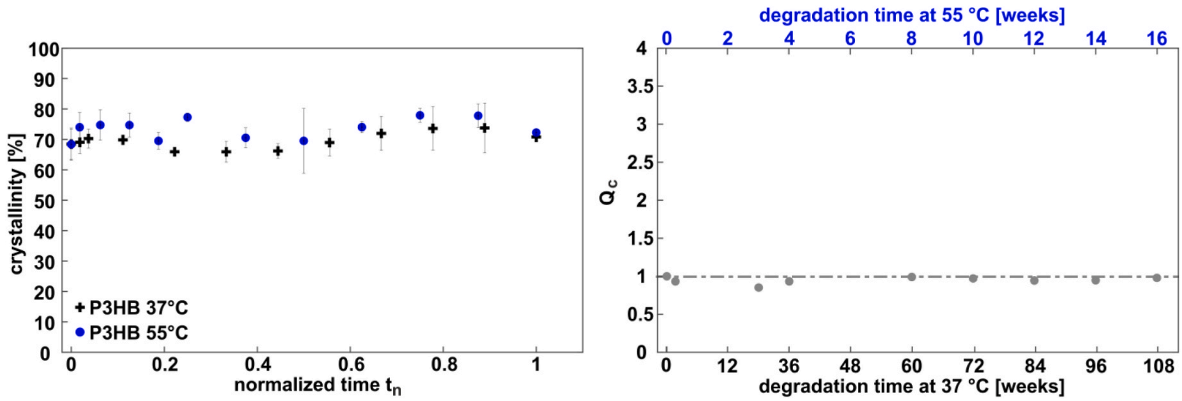

Fig. 8. χ-correlation model of real-time and accelerated degradation of P3HB. Left: Plots of crystallinity of the real-time and accelerated degradation studies over normalized time points (t_n). Right: Plots of calculated quotient of the crystallinity of accelerated experiments to those of real-time study. The dashed line represents idealized correlation.

added with linear trend lines for better illustration. The resulting overlapping normalized time points for the polymers based on the normalized curves were subsequently taken into account for further calculations.

Using the resulting data, quotients of the molecular weights of the accelerated experiments to those of the real-time study were determined by calculating

$$Q = \frac{M_w\ (37\ ^\circ C;\ t_n)}{M_w\ (55\ ^\circ C;\ t_n)} \tag{1}$$

And plotted in Fig. 7 (right).

A correlation trend line for Q over degradation time was generated. In the case of PLLA L210, it was indicated that a real-time study of half a year can be reproduced by an accelerated study of 6 weeks, yielding 1.5 fold decrease in M_w for accelerated conditions compared to real-time degradation. As for PLLA L214, 16 weeks degradation at 55 °C reproduce 48 weeks of real-time degradation, resulting in a 1.3 fold loss in M_w. However, the progression of PLLA crystallinity over time at 37 °C vs. 55 °C, showing a non-linear but wave-shaped progression, must be considered as limitation for the model (Fig. 6).

Real-time studies over 2 years on P3HB were reproduced by 16 weeks degradation under accelerated conditions, giving a 1.3 fold decrease in M_w.

Regarding crystallinity, P3HB showed, in contrast to PLLA, a well matching development when degradation times are normalized (108 versus 16 weeks). When forming the quotient

$$Q_c = \frac{\chi\ (37\ ^\circ C;\ t_n)}{\chi\ (55\ ^\circ C;\ t_n)} \tag{2}$$

Acorrelation with respect to thermal properties with a correlation factor of 1 over the entire degradation time was found (Fig. 8).

For P3HB, 16 weeks of accelerated degradation were suitable to reproduce 108 weeks of real-time degradation, in particular with respect to development of crystallinity over time. However, further investigations are necessary for validation of these findings. As for M_w decrease, it must be noted that with the correlation of 108 to 16 weeks, the M_w change increased 1.3 fold during accelerated degradation.

Autocatalytic versus non-catalytic bulk degradation

Regarding reaction kinetics of polymer chain scission with respect to autocatalysis, plotting $1/M_n$ and ln M_n versus time has been reported to be used for modeling the non-catalyzed and autocatalyzed degradation mechanisms [42,72]. In summary, a linear relationship between $1/M_n$ vs. t should exist for non-catalytic ester hydrolysis and a linear relationship between ln M_n vs. t should exist for the autocatalytic model. The applied model is based on the boundary condition that degradation has not progressed too far. Thus, only data until first mass loss can be considered and erosion phenomena cannot be taken into account. The corresponding plots of PLLA and P3HB are shown in Fig. 9 including linear regression lines and R^2 correlation coefficients displayed.

Autocatalysis plays an important role for the degradation of polyesters. The model by Anderson et al. [72] may be used to consider the contribution of autocatalyzed or non-catalyzed ester hydrolysis. With the assumption that bulk degradation occurs just by hydrolysis, we determined the fitting (R^2) to either lnM_n (autocatalysis) or $1/M_n$ (non-catalytic) during degradation until first mass loss (Fig. 9).

As both PLLA species already exhibited mass loss from the beginning of the study due to enzyme-associated degradation, time points for first mass loss (48 weeks) were taken from Weir et al. and Tsuji et al. [42,68] to calculate R^2. Under accelerated conditions, PLLA L210 mass loss started after 12 weeks and PLLA L214 after 16 weeks. Regarding P3HB, normalization was performed until the end of the study, as there was no mass loss observed over the entire test period.

Concerning PLLA L210, R^2 fitting of $1/M_n$ and ln M_n showed no distinct tendency. R^2 values for 37 °C gave $1/M_n$ = 0,921 and ln M_n = 0,898. As for 55 °C, R^2 values were $1/M_n$ = 0,838 and ln M_n = 0,972. Weir et al. [42] observed similar values for PLLA degradation and reported R^2 values of 0.85 (tensile samples) and 0.95 (extruded rod samples) for the autocatalyzed model and 0.63 (tensile samples) and 0.90 (extruded rod samples) for the non-catalyzed model. They concluded that both non-catalytic and autocatalytic ester hydrolysis are present.

For PLLA L214, however, we assume a more non-catalytic ester hydrolysis at 37 °C (R^2 = 0.767 vs. 0.533). As R^2 fittings show no clear difference at 55 °C (R^2 = 0.951 vs. 0.941), both hydrolysis mechanisms appear to be present. However, the low R^2 values for L214 (M_w = 700.000 g/mol) real-time study suggest that, in contrast to L210 (M_w =

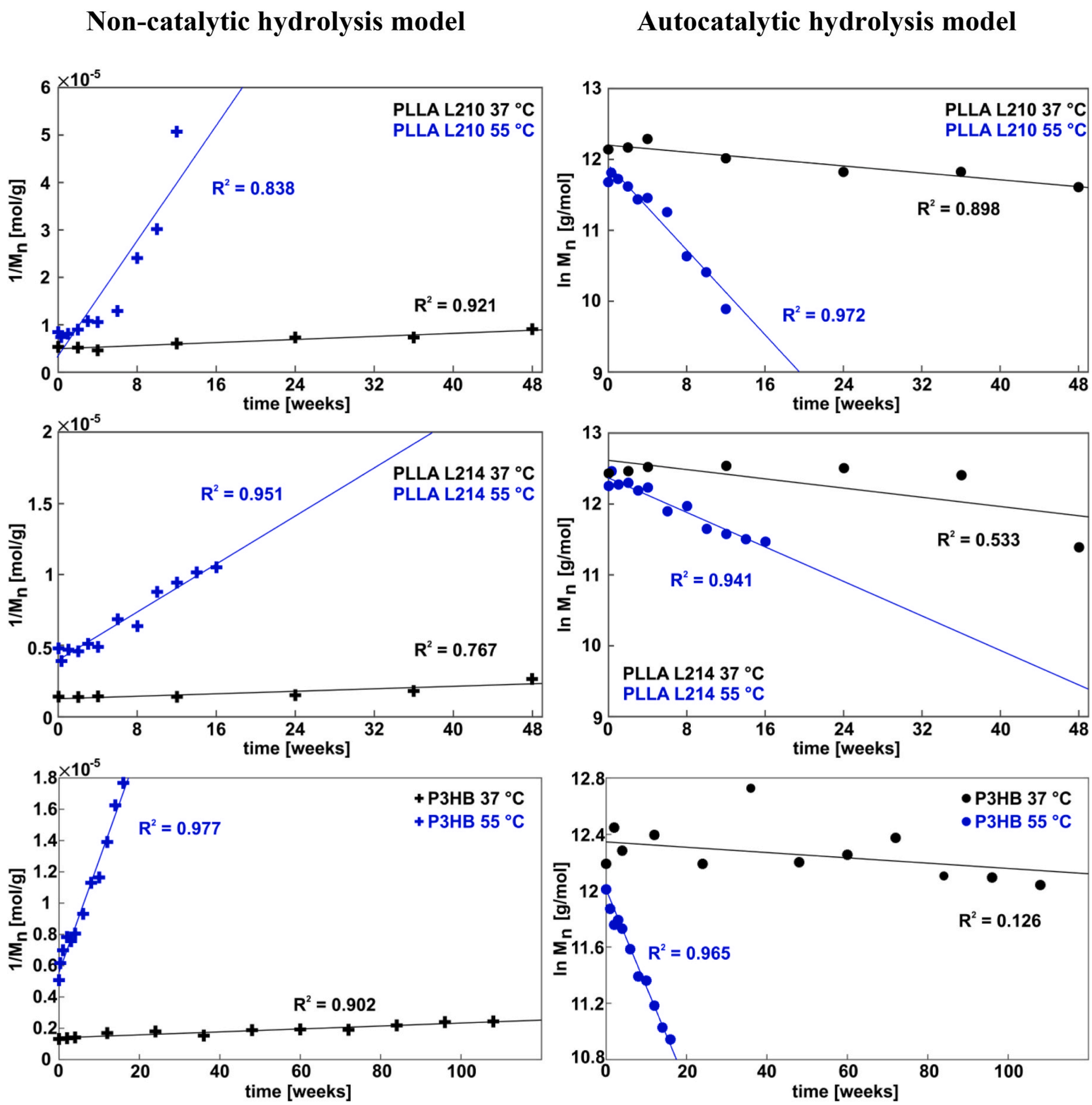

Fig. 9. Comparison of non-catalyzed and autocatalyzed models of PLLA L210 (top), PLLA L214 (middle) and P3HB (bottom) at enzyme-associated real-time degradation (black) and accelerated degradation (blue) following Weir et al. [42]. (For interpretation of the references to colour in this figure legend, the reader is referred to the Web version of this article.)

320.000 g/mol), the theory developed by Anderson et al. [72] may not be applicable. In consequence, although chemically similar, degradation behavior concerning autocatalysis cannot be easily predicted for equivalent polymers with different molecular weights.

For P3HB, the results showed distinct differences in R^2 fitting at 37 °C. P3HB is expected to undergo non-catalytic ester hydrolysis at 37 °C ($R^2 = 0.902$ vs. 0.126). In contrast, R2 fitting shows no differences at 55 °C, therefore both mechanisms appear to be apparent.

Influence of processing protocol on degradation of PLLA

In comparison to our work, Weir et al. [42] used compression molded samples in their real-time degradation studies with nearly the same initial M_w (4.24×10^5 g/mol) and χ (40.7%). Their reported results are comparable in means of M_w decrease (83%) and mass loss (constant until 57 weeks) during 65 weeks of degradation at 37 °C. Tsuji et al., however, used solvent cast PLLA from $CHCl_3$ with considerably higher molecular weight ($M_w = 1.3 \times 10^6$ g/mol) [68]. Regarding M_w and χ development during degradation, their results showed a comparable outcome as our data. However, they did not observe any mass loss during the first 24 months of degradation at 37 °C, which, with respect to our data, implies that enzymes are critical factors for surface degradation. As our results for PLLA L210 and L214 indicate, initial molecular weight has a pronounced influence on the rate of surface erosion with enzyme participation. This is particularly relevant considering the comparability of the outcome of accelerated experiments with *in vivo* studies. Enzyme-associated effects cannot be reproduced at higher temperatures due to enzyme denaturation. Thus, no surface erosion takes part and chain fragments from bulk degradation remain entrapped in the body, leading to no observable mass loss at early experimental stages.

In terms of accelerated degradation at increased temperature, a study by Felfel et al. showed no mass loss on compression molded PLLA with lower molecular weight ($M_w = 1.2 \times 10^5$ g/mol) after 8 weeks of accelerated degradation at 50 °C [46]. However, it should be noted, that these data are only comparable to a certain extent, as no M_w development was specified. According to this, our studies on solvent cast PLLA showed that sample mass remained nearly constant (≥99%) until 12 weeks (L210) and 16 weeks (L214). These findings were also consistent with the results of Weir et al. for degradation at 50 °C using compression molded HMW PLLA [43]. They also showed a decrease in M_w of 95% over 16 weeks, which was in a comparable range as our findings at 55 °C for 16 weeks (decrease in M_w of 90%). In contrast to this, accelerated studies performed by Fuoco et al. on solvent cast PLLA ($M_w = 1.18 \times 10^4$ g/mol) showed early sample mass loss of 10% after only 20 days even without the use of enzymes [49]. Although their processing protocol was similar to ours, however, specimens with substantially higher initial crystallinity ($\chi = 76\%$) were obtained. This indicates that crystallinity affects the degradation rate, although it must be taken into account that their degradation temperature has been very close to T_g.

Based on these data, independent of sample preparation, comparability of *in vitro* degradation data can be achieved using either solvent based or compression mold methods, provided comparable initial crystallinity. Noteworthy, molecular mass plays a crucial role when it comes to enzyme-associated surface degradation processes and related mass loss and should be taken into account for *in vitro* study design.

4. Conclusion

The aim of this study was to compare real-time enzyme-associated degradation with accelerated degradation at increased temperatures in order to contribute an understanding of the degradation processes of PLLA and P3HB. Analyzing the degradation of HMW PLLA (L210 and L214) and HMW P3HB films we found that our choice of enzymes, comprising proteinase K, pseudomonas lipase and aspergillus lipase, did not show to affect degradation of P3HB but did have an effect on PLLA degradation. In summary, according to our results and in comparison with the literature, we conclude that in contrast to the initial polymer crystallinity, the manufacturing processes show only a minor impact on the degradation behavior. Regarding molecular weight decrease of both degradation studies, it was found that a real-time study can be reproduced by an accelerated study, such that for PLLA L210 6 weeks at 55 °C reproduces a 26 weeks real-time degradation and for PLLA L214 16 weeks at 55 °C reproduces a 48 weeks real-time degradation. In the case of P3HB, 16 weeks of accelerated degradation can reproduce 108 weeks of real-time degradation. However, it must be considered that wave-like progression of χ limits this developed model. Consequently, accelerated experiments require boundary conditions in terms of identical molecular weight, initial crystallinity, and degradation parameters in order to reproduce degradation processes more realistically.

Author statement

Conceptualization: D.A. and S·O.; methodology: D.A., T.E., K.L. and S·O.; SEM imaging: V·S.; gravimetric analysis, K.L.; GPC measurements: T.R.; DSC analysis: D.A.; writing—original draft preparation: D.A. and S·O.; writing—review and editing: all; project administration: K.-P.S. and N.G.; funding acquisition: K.-P.S. and N.G. All authors have read and agreed to the published version of the manuscript.

Declaration of competing interest

The authors declare that they have no known competing financial interests or personal relationships that could have appeared to influence the work reported in this paper.

Acknowledgements

The authors thank Andrea Rohde, Katja Hahn and Caroline Dudda for their expert technical assistance. Furthermore, financial support by the Federal Ministry of Education and Research (BMBF) within RESPONSE “Partnership for Innovation in Implant Technology” (03ZZ0921A, 03ZZ0922G, 03ZZ0926A) is gratefully acknowledged.

Appendix A. Supplementary data

Supplementary data to this article can be found online at https://doi.org/10.1016/j.polymertesting.2021.107471.

References

[1] J.E. Bergsma, F.R. Rozema, R.R.M. Bos, G. Boering, In vitro predegradation at elevated temperatures of poly(lactide), J. Mater. Sci. Mater. Med. (1995) 642–646, https://doi.org/10.1007/BF00123445.
[2] International Standard Organisation, 10993-13:2019: Biological Evaluation of Medical Devices - Part 13: Identification and Quantification of Degradation Products from Polymeric Medical Devices, 2019.
[3] T. Barrows, Degradable implant materials: a review of synthetic absorbable polymers and their applications, Clin. Mater. 1 (1986) 233–257, https://doi.org/10.1016/S0267-6605(86)80015-4.
[4] C. Migliaresi, A. de Lollis, L. Fambri, D. Cohn, The effect of thermal history on the crystallinity of different molecular weight PLLA biodegradable polymers, Clin. Mater. 8 (1991) 111–118, https://doi.org/10.1016/0267-6605(91)90018-B.
[5] M. Prakasam, J. Locs, K. Salma-Ancane, D. Loca, A. Largeteau, L. Berzina-Cimdina, Biodegradable materials and metallic implants-A review, J. Funct. Biomater. 8 (2017), https://doi.org/10.3390/jfb8040044.
[6] M. Vert, Degradable and bioresorbable polymers in surgery and in pharmacology: beliefs and facts, J. Mater. Sci. Mater. Med. 20 (2009) 437–446, https://doi.org/10.1007/s10856-008-3581-4.
[7] N. Grabow, D.P. Martin, K.-P. Schmitz, K. Sternberg, Absorbable polymer stent technologies for vascular regeneration, J. Chem. Technol. Biotechnol. 85 (2010) 744–751, https://doi.org/10.1002/jctb.2282.
[8] K. Wulf, M. Teske, C. Matschegewski, D. Arbeiter, D. Bajer, T. Eickner, K.-P. Schmitz, N. Grabow, Novel approach for a PTX/VEGF dual drug delivery system in cardiovascular applications-an innovative bulk and surface drug immobilization, Drug Deliv. and Transl. Res. 8 (2018) 719–728, https://doi.org/10.1007/s13346-018-0507-7.
[9] C. Bigalke, F. Luderer, K. Wulf, T. Storm, M. Löbler, D. Arbeiter, B.M. Rau, H. Nizze, B. Vollmar, K.-P. Schmitz, E. Klar, K. Sternberg, VEGF-releasing suture material for enhancement of vascularization: development, in vitro and in vivo study, Acta Biomater. 10 (2014) 5081–5089, https://doi.org/10.1016/j.actbio.2014.09.002.
[10] L.-D. Hou, Z. Li, Y. Pan, M. Sabir, Y.-F. Zheng, L. Li, A review on biodegradable materials for cardiovascular stent application, Front. Mater. Sci. 10 (2016) 238–259, https://doi.org/10.1007/s11706-016-0344-x.
[11] C. Mc Conville, I. Major, D.R. Friend, M.R. Clark, A.D. Woolfson, R.K. Malcolm, Development of polylactide and polyethylene vinyl acetate blends for the manufacture of vaginal rings, J. Biomed. Mater. Res. B Appl. Biomater. 100 (2012) 891–895, https://doi.org/10.1002/jbm.b.31919.
[12] L. Song, Z. Sun, C. Guan, H. Yan, M. Yu, J. Cui, C. Mu, H. Qiu, Y. Tang, Y. Zhao, S. Qiao, H. Suryapranata, R. Gao, B. Xu, First-in-man study of a thinner-strut sirolimus-eluting bioresorbable scaffold (FUTURE-I): three-year clinical and imaging outcomes, Catheter, Cardiovasc. Interv. 95 (1) (2020) 648–657, https://doi.org/10.1002/ccd.28722.
[13] C.J. Li, B. Xu, L. Song, M.Y. Yu, H.B. Yan, H. Qiu, C.W. Mu, J.G. Cui, C.D. Guan, Z. W. Sun, S.B. Qiao, R.L. Gao, The safety and efficacy of Firesorb bioresorbable scaffold in first-in-man study for coronary artery disease: the four-year outcomes, Zhonghua Xinxueguanbing Zazhi 49 (2021) 128–135, https://doi.org/10.3760/cma.j.cn112148-20201110-00897.
[14] A. Chieffo, S.A. Khawaja, A. Latib, B. Vesga, M. Moncada, J.A. Delgado, J. Fonseca, L. Testa, G. Esposito, M. Ferrone, B. Cortese, A. Maehara, J.F. Granada, A. Colombo, First-in-human evaluation of a novel sirolimus-eluting ultra-high molecular weight APTITUDE bioresorbable scaffold: 9- and 24-month imaging and clinical results of the RENASCENT II trial, EuroIntervention 16 (2020) e133–e140, https://doi.org/10.4244/EIJ-D-19-00600.
[15] P. Gasior, Y. Cheng, J. Xia, G.B. Conditt, J.C. McGregor, R. Virmani, J.F. Granada, G.L. Kaluza, Two-year longitudinal evaluation of a second-generation thin-strut sirolimus-eluting bioresorbable coronary scaffold with hybrid cell design in porcine coronary arteries, Cardiol. J. 27 (2020) 115–125, https://doi.org/10.5603/CJ.a2018.0095.
[16] X. Peng, W. Qu, Y. Jia, Y. Wang, B. Yu, J. Tian, Bioresorbable scaffolds: contemporary status and future directions, Front. Cardiovasc. Med. 7 (2020), https://doi.org/10.3389/fcvm.2020.589571.
[17] T. Malm, S. Bowald, A. Bylock, T. Saldeen, C. Busch, Regeneration of pericardial tissue on absorbable polymer patches implanted into the pericardial sac. An immunohistochemical, ultrastructural and biochemical study in the sheep, Scand. J. Thorac. Cardiovasc. Surg. 26 (1992) 15–21, https://doi.org/10.3109/14017439209099048.
[18] P.A. Holmes, Applications of PHB-a microbially produced biodegradable thermoplastic, Phys. Technol. (1985), https://doi.org/10.1088/0305-4624/16/1/305.
[19] H. Zhou, T.B. Green, Y.L. Joo, The thermal effects on electrospinning of polylactic acid melts, Polymer 47 (2006) 7497–7505, https://doi.org/10.1016/j.polymer.2006.08.042.
[20] D. Arbeiter, T. Reske, M. Teske, D. Bajer, V. Senz, K.-P. Schmitz, N. Grabow, S. Oschatz, Influence of drug incorporation on the physico-chemical properties of poly(l-lactide) implant coating matrices-A systematic study, Polymers 13 (2021), https://doi.org/10.3390/polym13020292.

[21] K. Wulf, U. Tschierschky, T. Eickner, N. Grabow, R.G. Mundkowski, Studies on the interaction of polylactid-based planar and nanoparticular biomaterials with serum albumin and fibrinogen, Colloids Surf. B Biointerfaces 159 (2017) 1–6, https://doi.org/10.1016/j.colsurfb.2017.07.002.
[22] M. Grau, J. Matena, M. Teske, S. Petersen, P. Aliuos, L. Roland, N. Grabow, H. Murua Escobar, N.-C. Gellrich, H. Haferkamp, I. Nolte, In vitro evaluation of PCL and P(3HB) as coating materials for selective laser melted porous titanium implants, Materials 10 (2017), https://doi.org/10.3390/ma10121344.
[23] H. Gollwitzer, P. Thomas, P. Diehl, E. Steinhauser, B. Summer, S. Barnstorf, L. Gerdesmeyer, W. Mittelmeier, A. Stemberger, Biomechanical and allergological characteristics of a biodegradable poly(D,L-lactic acid) coating for orthopaedic implants, J. Orthop. Res. (2005) 802–809, https://doi.org/10.1016/j.orthres.2005.02.003.
[24] T.M. Bedair, W. Park, B.-J. Park, M.-W. Moon, K.-R. Lee, Y.K. Joung, D.K. Han, Dual-layer coated drug-eluting stents with improved degradation morphology and controlled drug release, Macromol. Res. 26 (2018) 641–649, https://doi.org/10.1007/s13233-018-6110-4.
[25] A. Rudolph, M. Teske, S. Illner, V. Kiefel, K. Sternberg, N. Grabow, A. Wree, M. Hovakimyan, Surface modification of biodegradable polymers towards better biocompatibility and lower thrombogenicity, PLoS One 10 (2015), e0142075, https://doi.org/10.1371/journal.pone.0142075.
[26] R.T. Liggins, H.M. Burt, Paclitaxel-loaded poly(L-lactic acid) microspheres 3: blending low and high molecular weight polymers to control morphology and drug release, Int. J. Pharm. 282 (2004) 61–71, https://doi.org/10.1016/j.ijpharm.2004.05.026.
[27] D. Arbeiter, T. Eickner, S. Oschatz, T. Reske, O. Specht, M. Teske, V. Senz, K.-P. Schmitz, N. Grabow, Physico chemical and phase separation characterization of high molecular PLLA blended with low molecular PCL obtained from solvent cast processes, Mater. Res. Express 7 (2020) 95302, https://doi.org/10.1088/2053-1591/abb2c9.
[28] H. Tsuji, Y. Ikada, Properties and morphology of poly(l-lactide) 4. Effects of structural parameters on long-term hydrolysis of poly(l-lactide) in phosphate-buffered solution, Polym. Degrad. Stabil. 67 (2000) 179–189, https://doi.org/10.1016/S0141-3910(99)00111-1.
[29] A.C. Renouf-Glauser, J. Rose, D.F. Farrar, R.E. Cameron, The effect of crystallinity on the deformation mechanism and bulk mechanical properties of PLLA, Biomaterials 26 (2005) 5771–5782, https://doi.org/10.1016/j.biomaterials.2005.03.002.
[30] T. Freier, C. Kunze, C. Nischan, S. Kramer, K. Sternberg, M. Saß, U.T. Hopt, K.-P. Schmitz, In vitro and in vivo degradation studies for development of a biodegradable patchbased on poly(3-hydroxybutyrate), Biomaterials (2002) 2649–2657.
[31] M.R. Roohi, M. Kuddus Zaheer, PHB (poly-β-hydroxybutyrate) and its enzymatic degradation, Polym. Adv. Technol. 29 (2018) 30–40, https://doi.org/10.1002/pat.4126.
[32] H. Tsuji, Autocatalytic hydrolysis of amorphous-made polylactides: effects of l-lactide content, tacticity, and enantiomeric polymer blending, Polymer 43 (2002) 1789–1796, https://doi.org/10.1016/S0032-3861(01)00752-2.
[33] G.L. Siparsky, K.J. Voorhees, F. Miao, Hydrolysis of polylactic acid (PLA) and polycaprolactone (PCL) in aqueous acetonitrile solutions: autocatalysis, J. Environ. Polym. Degrad. 6 (1998) 31–41, https://doi.org/10.1023/A:1022826528673.
[34] C. Shih, Chain-end scission in acid catalyzed hydrolysis of poly (d,l-lactide) in solution, J. Contr. Release 34 (1995) 9–15, https://doi.org/10.1016/0168-3659(94)00100-9.
[35] A. Gleadall, J. Pan, M.-A. Kruft, M. Kellomaki, Degradation mechanisms of bioresorbable polyesters. Part 2. Effects of initial molecular weight and residual monomer, Acta Biomater. 10 (2014) 2233–2240, https://doi.org/10.1016/j.actbio.2014.01.017.
[36] R. Scaffaro, A. Maio, E.F. Gulino, Hydrolytic degradation of PLA/Posidonia Oceanica green composites: a simple model based on starting morpho-chemical properties, Compos. Sci. Technol. 213 (2021) 108930, https://doi.org/10.1016/j.compscitech.2021.108930.
[37] S. Li, H. Garreau, M. Vert, Structure-property relationships in the case of the degradation of massive poly(α-hydroxy acids) in aqueous media, J. Mater. Sci. Mater. Med. 1 (1990) 198–206, https://doi.org/10.1007/BF00701077.
[38] H. Pistner, D.R. Bendix, J. Mühling, J.F. Reuther, Poly(L-lactide): a long-term degradation study in vivo, Biomaterials 14 (1993) 291–298, https://doi.org/10.1016/0142-9612(93)90121-H.
[39] S. Gogolewski, M. Jovanovic, S.M. Perren, J.G. Dillon, M.K. Hughes, Tissue response and in vivo degradation of selected polyhydroxyacids: polylactides (PLA), poly(3-hydroxybutyrate) (PHB), and poly(3-hydroxybutyrate-co-3-hydroxyvalerate) (PHB/VA), J. Biomed. Mater. Res. 27 (1993) 1135–1148, https://doi.org/10.1002/jbm.820270904.
[40] D. Cam, S. Hyon, Y. Ikada, Degradation of high molecular weight poly(l-lactide) in alkaline medium, Biomaterials 16 (1995) 833–843, https://doi.org/10.1016/0142-9612(95)94144-A.
[41] S. Iannace, A. Maffezzoli, G. Leo, L. Nicolais, Influence of crystal and amorphous phase morphology on hydrolytic degradation of PLLA subjected to different processing conditions, Polymer 42 (2001) 3799–3807, https://doi.org/10.1016/S0032-3861(00)00744-8.
[42] N.A. Weir, F.J. Buchanan, J.F. Orr, G.R. Dickson, Degradation of poly-L-lactide. Part 1: in vitro and in vivo physiological temperature degradation, Proc. Inst. Mech. Eng. H 218 (2004) 307–319, https://doi.org/10.1243/0954411041932782.
[43] N.A. Weir, F.J. Buchanan, J.F. Orr, D.F. Farrar, G.R. Dickson, Degradation of poly-L-lactide. Part 2: increased temperature accelerated degradation, Proc. Inst. Mech. Eng. H 218 (2004) 321–330, https://doi.org/10.1243/0954411041932809.
[44] N.G. Salguero, M.F. del Grosso, H. Durán, P.J. Peruzzo, J.I. Amalvy, C. R. Arbeitman, G. García Bermúdez, Characterization of biodegradable polymers irradiated with swift heavy ions, Nucl. Instrum. Methods Phys. Res. B 273 (2012) 47–50, https://doi.org/10.1016/j.nimb.2011.07.035.
[45] H. Deplaine, V.A. Acosta-Santamaría, A. Vidaurre, J.L. Gómez Ribelles, M. Doblaré, I. Ochoa, G. Gallego Ferrer, Evolution of the properties of a poly(l -lactic acid) scaffold with double porosity during in vitro degradation in a phosphate-buffered saline solution, J. Appl. Polym. Sci. 131 (2014), https://doi.org/10.1002/app.40956 n/a-n/a.
[46] R.M. Felfel, K.M.Z. Hossain, A.J. Parsons, C.D. Rudd, I. Ahmed, Accelerated in vitro degradation properties of polylactic acid/phosphate glass fibre composites, J. Mater. Sci. 50 (2015) 3942–3955, https://doi.org/10.1007/s10853-015-8946-8.
[47] Z. Wang, Y. Wang, Y. Ito, P. Zhang, X. Chen, A comparative study on the in vivo degradation of poly(L-lactide) based composite implants for bone fracture fixation, Sci. Rep. 6 (2016) 20770, https://doi.org/10.1038/srep20770.
[48] A. Porfyris, S. Vasilakos, C. Zotiadis, C. Papaspyrides, K. Moser, L. van der Schueren, G. Buyle, S. Pavlidou, S. Vouyiouka, Accelerated ageing and hydrolytic stabilization of poly(lactic acid) (PLA) under humidity and temperature conditioning, Polym. Test. 68 (2018) 315–332, https://doi.org/10.1016/j.polymertesting.2018.04.018.
[49] T. Fuoco, M. Cuartero, M. Parrilla, J.J. García-Guzmán, G.A. Crespo, A. Finne-Wistrand, Capturing the real-time hydrolytic degradation of a library of biomedical polymers by combining traditional assessment and electrochemical sensors, Biomacromolecules 22 (2021) 949–960, https://doi.org/10.1021/acs.biomac.0c01621.
[50] International Standard Organisation, 13781:2017(E): Implants for Surgery - Homopolymers, Copolymers and Blends on Poly(lactide) - in Vitro Degradation Testing, 2017. Switzerland.
[51] Y. Doi, Y. Kanesawa, Y. Kawaguchi, M. Kunioka, Hydrolytic degradation of microbial poly(hydroxyalkanoates), Makromol. Chem. Rapid Commun. (1989) 227–230, https://doi.org/10.1002/marc.1989.030100506.
[52] P. Kurcok, M. Kowalczuk, G. Adamus, Z. Jedliński, R.W. Lenz, Degradability of poly(β-hydroxybutyrate)s. Correlation with chemical microstructure, J. Macromol. Sci. Phys. 32 (1995) 875–880, https://doi.org/10.1080/10601329508010300.
[53] M. Canetti, M. Urso, P. Sadocco, Influence of the morphology and of the supermolecular structure on the enzymatic degradation of bacterial poly(3-hydroxybutyrate), Polymer (1999) 2587–2594, https://doi.org/10.1016/S0032-3861(98)00503-5.
[54] V.A. Zhuikov, Y.V. Zhuikova, T.K. Makhina, V.L. Myshkina, A. Rusakov, A. Useinov, V.V. Voinova, G.A. Bonartseva, A.A. Berlin, A.P. Bonartsev, A. L. Iordanskii, Comparative structure-property characterization of poly(3-hydroxybutyrate-Co-3-Hydroxyvalerate)s films under hydrolytic and enzymatic degradation: finding a transition point in 3-hydroxyvalerate content, Polymers 12 (2020), https://doi.org/10.3390/polym12030728.
[55] F. Li, S. Rastogi, D. Romano, Synthesis of ultrahigh molecular weight PLAs using a phenoxy-imine Al(III) complex, ACS Omega 5 (2020) 24230–24238, https://doi.org/10.1021/acsomega.0c01952.
[56] T. Casalini, F. Rossi, A. Castrovinci, G. Perale, A perspective on polylactic acid-based polymers use for nanoparticles synthesis and applications, Front. Bioeng. Biotechnol. 7 (2019) 259, https://doi.org/10.3389/fbioe.2019.00259.
[57] International Standard Organisation, 13781:1997(E): Poly(L-Lactide) Resins and Fabricated Forms for Surgicals Implants - in Vitro Degradation Testing, 1997. Switzerland.
[58] International Standard Organisation, 15814:1999(E): Implants for Surgery - Copolymers and Blends Based on Poly(lactide) - in Vitro Degradation Testing, 1999. Switzerland.
[59] E.W. Fischer, H.J. Sterzel, G. Wegner, Investigation of the structure of solution grown crystals of lactide copolymers by means of chemical reactions, Kolloid-Z.u.Z. Polymere (1973) 980–990, https://doi.org/10.1007/BF01498927.
[60] P.J. Barham, A. Keller, E.L. Otun, P.A. Holmes, Crystallization and morphology of a bacterial thermoplastic: poly-3-hydroxybutyrate, J. Mater. Sci. 19 (1984) 2781–2794, https://doi.org/10.1007/BF01026954.
[61] K. Herzog, R.-J. Müller, W.-D. Deckwer, Mechanism and kinetics of the enzymatic hydrolysis of polyester nanoparticles by lipases, Polym. Degrad. Stabil. 91 (2006) 2486–2498, https://doi.org/10.1016/j.polymdegradstab.2006.03.005.
[62] M. Żenkiewicz, A. Richert, R. Malinowski, K. Moraczewski, A comparative analysis of mass losses of some aliphatic polyesters upon enzymatic degradation, Polym. Test. 32 (2013) 209–214, https://doi.org/10.1016/j.polymertesting.2012.10.011.
[63] A. Banerjee, K. Chatterjee, G. Madras, Enzymatic degradation of polymers: a brief review, Mater. Sci. Technol. 30 (2014) 567–573, https://doi.org/10.1179/1743284713Y.0000000503.
[64] G. Tomasi, M. Scandola, B.H. Briese, D. Jendrossek, Enzymatic degradation of bacterial poly(3-hydroxybutyrate) by a depolymerase from Pseudomonas lemoignei, Macromolecules 29 (1996) 507–513, https://doi.org/10.1021/ma951067n.
[65] K. Mukai, Y. Doi, Y. Sema, K. Tomita, Substrate specificities in hydrolysis of polyhydroxyalkanoates by microbial esterases, Biotechnol. Lett. 15 (1993) 601–604, https://doi.org/10.1007/BF00138548.
[66] S.C. Woodward, P.S. Brewer, F. Moatamed, A. Schindler, C.G. Pitt, The intracellular degradation of poly(epsilon-caprolactone), J. Biomed. Mater. Res. 19 (1985) 437–444, https://doi.org/10.1002/jbm.820190408.
[67] S. Li, M. Vert, Biodegradable Polymers, Principles & Applications: Biodegradation of Aliphatic Polyesters, Chapman & Hall, London, 1995, ISBN 0-412-59010-7.
[68] H. Tsuji, A. Mizuno, Y. Ikada, Properties and morphology of poly(L-lactide). III. Effects of initial crystallinity on long-termin vitro hydrolysis of high molecular weight poly(L-lactide) film in phosphate-buffered solution, J. Appl. Polym. Sci. 77

(2000) 1452–1464. https://doi.org/10.1002/1097-4628(20000815)77:7<1452:AID-APP7>3.0.CO;2-S.
[69] K. Sudesh, H. Abe, Y. Doi, Synthesis, structure and properties of polyhydroxyalkanoates: biological polyesters, Prog. Polym. Sci. (2000) 1503–1555, https://doi.org/10.1016/S0079-6700(00)00035-6.
[70] A. Leroy, S. Ribeiro, C. Grossiord, A. Alves, R.H. Vestberg, V. Salles, C. Brunon, K. Gritsch, B. Grosgogeat, Y. Bayon, FTIR microscopy contribution for comprehension of degradation mechanisms in PLA-based implantable medical devices, J. Mater. Sci. Mater. Med. 28 (2017) 87, https://doi.org/10.1007/s10856-017-5894-7.
[71] A. Tapadiya, N. Vasanthan, Crystallization and alkaline hydrolysis of poly(3-hydroxybutyrate) films probed by thermal analysis and infrared spectroscopy, Int. J. Biol. Macromol. 102 (2017) 1130–1137, https://doi.org/10.1016/j.ijbiomac.2017.04.095.
[72] J.M. Anderson, Perspectives on the in Vivo Responses of Biodegradable Polymers, CRC Press, Boca Raton, FL, USA, 1995, ISBN 084934896X.

Publikation 2

Mater. Res. Express (**2020**), *7*, 095302.

Physico chemical characterization of phase separated PLLA PCL blends obtained from solvent cast processes in a biomedical background.

Arbeiter D, Eickner T, Oschatz S, Specht O, Reske T, Teske M, Senz V, Schmitz K-P, Grabow N.

Eingereicht: 18.05.2020, veröffentlicht: 04.09.2020

DOI: 10.1088/2053-1591/abb2c9 (IF = 1,449)

Abstract: Blends of PLLA and PCL yielded by solvent casting usually exhibit phase separation and crystallization behavior which have a strong impact on their suitability for certain biomedical applications such as degradable coatings or drug carriers. Therefore, it is important to understand the underlying mechanisms. In this study, high-molecular biodegradable semi-crystalline poly(L-lactide) (PLLA) (M_w = 320 kDa) was blended with low-molecular biodegradable semi-crystalline poly(ε caprolactone) (PCL) (M_w = 40 kDa) in various combinations (10, 50 and 90 wt.% PCL) by solvent casting. The yielded blends were subjected to annealing at 40 °C, 80 °C and 200 °C and cooled down slowly to maintain thermodynamic equilibrium. Scanning electron microscopy, atomic force microscopy, Raman images and differential scanning calorimetry were used to investigate the structure, morphology and thermal properties of the solvent cast PLLA/PCL blends. It was shown that the physico-chemical properties of PLLA/PCL blends prepared by solvent casting differ substantially compared to those accessed by melt manufacturing processes. In summary, the blends showed a complex phase separation behavior, which is completely dependent on the method of preparation and the adjusted temperature during production process.

IOP Publishing Mater. Res. Express 7 (2020) 095302 https://doi.org/10.1088/2053-1591/abb2c9

Materials Research Express

CrossMark

OPEN ACCESS

RECEIVED
18 May 2020

REVISED
16 July 2020

ACCEPTED FOR PUBLICATION
26 August 2020

PUBLISHED
4 September 2020

PAPER

Physico chemical and phase separation characterization of high molecular PLLA blended with low molecular PCL obtained from solvent cast processes

Daniela Arbeiter[1,3], Thomas Eickner[1], Stefan Oschatz[1], Thomas Reske[2], Olaf Specht[2], Michael Teske[1], Volkmar Senz[1], Klaus-Peter Schmitz[1,2] and Niels Grabow[1]

[1] Institute for Biomedical Engineering, Rostock University Medical Center Friedrich-Barnewitz-Straße 4, 18119 Rostock, Germany
[2] Institute for ImplantTechnology and Biomaterials e.V., Friedrich-Barnewitz-Straße 4, 18119 Rostock-Warnemünde, Germany
[3] Author to whom any correspondence should be addressed.

E-mail: daniela.arbeiter@uni-rostock.de, thomas.eickner@uni-rostock.de, stefan.oschatz@uni-rostock.de, thomas.reske@uni-rostock.de, olaf.specht@uni-rostock.de, michael.teske@uni-rostock.de, volkmar.senz@uni-rostock.de, schmitz@iib-ev.de and niels.grabow@uni-rostock.de

Keywords: phase separation, solvent cast blends, morphological, mechanical and thermal properties, PCL, PLLA

Supplementary material for this article is available online

Abstract

Blends of PLLA and PCL yielded by solvent casting usually exhibit phase separation and crystallization behavior which have a strong impact on their suitability for certain biomedical applications such as degradable coatings or drug carriers. Therefore, it is important to understand the underlying mechanisms. In this study, high-molecular biodegradable semi-crystalline poly(L-lactide) (PLLA) (M_w = 320 kDa) was blended with low-molecular biodegradable semi-crystalline poly(ε-caprolactone) (PCL) (M_w = 40 kDa) in various combinations (10, 50 and 90 wt.% PCL) by solvent casting. The yielded blends were subjected to annealing at 40 °C, 80 °C and 200 °C and cooled down slowly to maintain thermodynamic equilibrium. Scanning electron microscopy, atomic force microscopy, Raman images and differential scanning calorimetry were used to investigate the structure, morphology and thermal properties of the solvent cast PLLA/PCL blends. It was shown that the physico-chemical properties of PLLA/PCL blends prepared by solvent casting differ substantially compared to those accessed by melt manufacturing processes. In summary, the blends showed a complex phase separation behavior, which is completely dependent on the method of preparation and the adjusted temperature during production process.

Introduction

PLLA and PCL are both widespread and highly relevant materials in biomedical engineering, either individually as well as in combination as blends. In fact, however, blend formation leads to additional matrix effects which alter the material properties such as mechanical resilience, drug release behavior or degradation rate. This impact not only depends on the polymer combination to form a blend but furthermore on the underlying manufacturing process. Polymer based materials can be processed thermally, e.g. by extrusion or melt electro spinning. However, for medical applications, the focus recently shifted to solvent cast processes such as dip coating, airbrush and spin coating. Contrary to thermal processing, the solvent cast processes require additional post-treatment of the materials, which can be either washing or annealing or both, to eliminate solvent residues [1, 2]. However, solvent cast processes are usually more versatile and easy to handle compared to thermal extrusion and allow for a wider variety of substrates or temperature susceptible additives such as drug molecules since no adverse effects from high temperature treatment are involved. Each step of the process influences the physico-chemical properties, which also means that the final characteristic properties of the desired material can already be specifically controlled during production, e.g. by annealing protocol, choice of solvent and washing procedure [3–5].

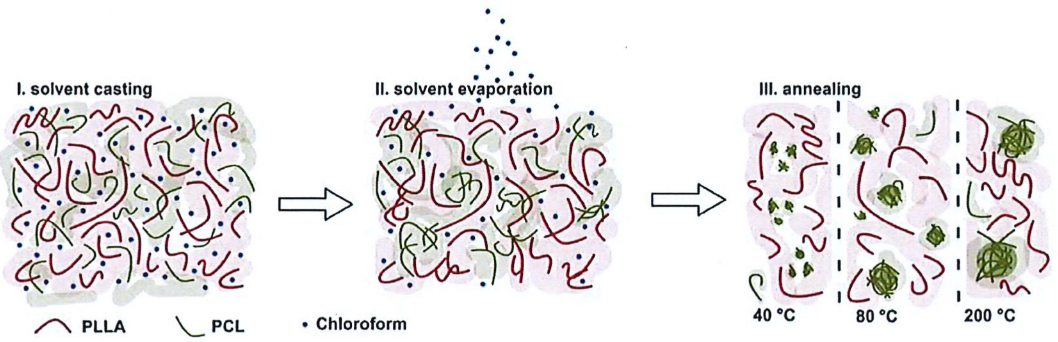

Figure 1. Schematic view of the phase separation of PLLA and PCL blends, prepared by solvent cast processes.

Solvent cast processes allow for the generation of polymer blends which may exhibit improved adaptive properties for certain fields of application. For example, elastic components can be combined with stiffer ones by blending to obtain ductile yet resilient materials [6, 7]. In this background, the preferred and main biodegradable polymers used for blend generation are aliphatic polyesters, such as poly(L-lactide) (PLLA) and poly(ε-caprolactone) (PCL). It is well known that PLLA exhibits a relatively brittle fracture, because glass transition temperature is above room temperature [8]. On the other hand, PCL, a ductile biodegradable thermoplastic polymer with a much lower glass transition temperature, has been shown to be a promising blend partner for PLLA to obtain a more ductile material. López-Rodriguez *et al* observed that PLLA and PCL are immiscible, but that a certain adhesion at the PLLA/PCL interface can be achieved if the main phase is PCL [6, 9]. Todo *et al* also demonstrated that even a PCL of 5% can significantly change the mechanical properties [10]. Both research groups used PLLA with a lower molecular weight ($M_w < 200$ kDa) and prepared blends by melt extrusion. Studies with high-molecular PLLA blended with low-molecular PCL are not further known in the literature.

Broz *et al* concluded that the immiscibility of PLLA and PCL causes phase separation in PLLA/PCL blend, see figure 1, leading to a suppression of an improved toughness, especially with increasing PCL content.

Notably, these effects significantly vary depending on the production protocol in a way that melt processes lead to different equilibration states on a molecular level compared to solvent cast processes making blend manufacturing a complex matter. Nevertheless, blending can radically alter the resultant properties, which depend sensitively on the mechanical properties of the components as well as the blend microstructure and the interface between the phases [9].

Flory Huggins model is an important theory regarding interactions in polymer solutions and miscibility of polymer blends [11–14]. This lattice model describes the thermodynamics of polymer solutions and polymer blends. For our PLLA/PCL blend system, low miscibility leads to a complex situation with various phases and mixed crystals, even more when solvents are taken into account [15, 16]. Therefore, theoretical considerations such as the determination of parameters such as χ are not trivial. Pillin *et al* determined the interaction parameter via thermal analysis using several approximations, revealing that miscibility also yields some changes in crystallization and melting temperatures with the decrease of the integrated enthalpies [13]. Therefore, we used thermal analysis via DSC measurements to describe PLLA/PCL blends. A more basic question concerns the phase morphology and the nature of the interphase. Uncontrolled morphology and a weak interphase lead to poor mechanical properties and therefore to ineligibility [6]. Aim of our work was the investigation of PLLA/PCL blends in respect to the processibility of these polymers and their suitability for biomedical applications such as implant coatings or drug delivery systems.

Another effect that influences the mechanical properties of PLLA/PCL was reported by Takayama *et al*. They observed that annealing of the blends is linked to an increase in crystallinity, which effectively improves the strength of the blends [1].

A stable and controlled application of PLLA/PCL blends requires detailed knowledge of their phase separation behavior and morphology. A deeper understanding of the thermal and mechanical properties of the combined polymers is required. In this work, we investigated the properties of solvent cast films in comparison to melting cast films. However, to eliminate solvent effects during annealing, washing processes were performed to completely remove the solvent from the blends. This was established in in-house studies and resulted in residual solvent contents below the ICH limits for medical devices [4, 5]. Afterwards, the blends were thermally treated to investigate the influence of temperature on the physicochemical properties of the blends previously produced from solvents.

Therefore, we have investigated high-molecular biodegradable semi-crystalline PLLA ($M_w = 320$ kDa), low-molecular PCL ($M_w = 40$ kDa) and their blends (10, 50 and 90 wt.% PCL contents) prepared by solvent

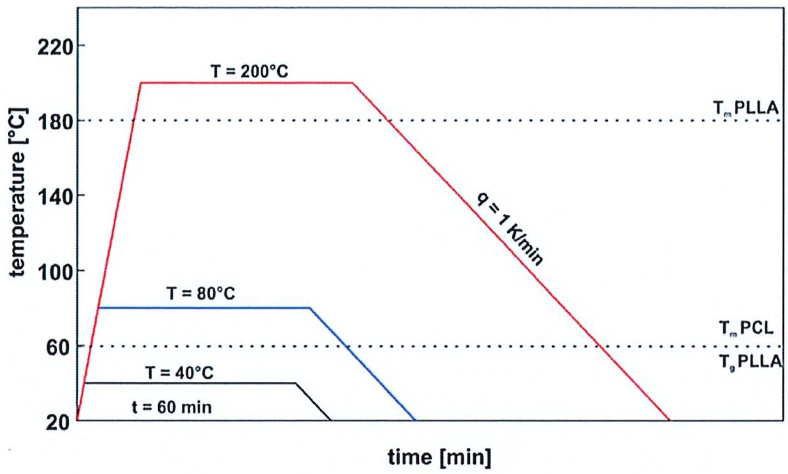

Figure 2. Temperature time profile for sample preparation; PLLA, PCL and their blends were heated up with q = 10 K min^{-1} to different temperatures (black line 40 °C, blue line 80 °C and red line 200 °C) and hold isothermally for 60 min. Then, all samples were cooled down with a cooling rate of q = 1 K min^{-1} to crystallize the samples.

casting. The samples were subjected to annealing at 40 °C, 80 °C and 200 °C, respectively. Both polymers have been widely used in a variety of medical applications and, to our knowledge, there has not been a systematic investigation of the morphology and thermal properties after a different annealing process of high-molecular PLLA combined with low-molecular PCL as solvent cast blends. Scanning electron microscopy (SEM), atomic force microscopy (AFM), Raman images and differential scanning calorimetry (DSC) were used to investigate the structure, morphology and thermal properties of the solvent cast PLLA/PCL blends.

Materials and methods

Materials

Poly(L-lactide) (PLLA, intrinsic viscosity in chloroform: 3.8 dl g^{-1}, M_w = 320 kDa) was purchased from Evonik Industries AG (Darmstadt, Germany). Poly-ε-caprolactone (PCL, intrinsic viscosity in chloroform: 0.8 dl g^{-1}, M_w = 40 kDa) was supplied by LACTEL Absorbable Polymers (Birmingham, AL, USA). Chloroform was purchased from Baker (Fisher Scientific GmbH, Austria, Vienna). All chemicals were used as received without further purification.

Blend preparation

For cast film production, polymer solutions (1 g Polymer in 25 ml chloroform) of PLLA, PCL and their blends in different ratios (90/10, 50/50, 10/90 w/w) were poured into glass petri dishes (Ø = 9 cm). After evaporation of the solvent under ambient conditions in a fume hood, films were washed for 2 days in methanol (LiChrosolv, Merck KGaA) with daily exchange, two days in distilled water (MilliQ Ultrapure, R = 18.2 MΩ.cm at 25 °C) with daily exchange, and dried for 7 days in a vacuum oven (Memmert GmbH + Co.KG) at 40 °C and 40 mbar. With this preparation method film samples with a thickness of ~100 μm were achieved. For annealing experiments, samples of PLLA, PCL and their blends were placed in a chamber furnace and kept at different temperatures (40 °C, 80 °C and 200 °C) for 60 min at ambient atmosphere (KLS 05/13 Thermconcept). An annealing temperature of 40 °C was selected that corresponds to a temperature lower than the melting temperature (T_m) of PCL and PLLA. 80 °C were used due to the temperature lower than T_m of PLLA but higher than T_m of PCL. Furthermore 200 °C was selected, since this temperature exceeded the melting temperature for both polymers. Subsequently, all samples were cooled down with 1 K min^{-1} in the furnace, see figure 2. The PLLA/PCL blend samples were kept in the laboratory refrigerator at 8 °C until the investigations were completed.

Morphology analysis

SEM

Morphology of the polymer films was examined with scanning electron microscopy SEM QUANTA FEG 250 (FEI Company, Germany) with an accelerating voltage of 10 kV and a proprietary spot size value of 3.0. The samples were fixed onto aluminum trays with conductive tape and sputter coated with gold. The images were taken at magnification x500.

AFM

Atomic force microscopy was performed with a NanoWizard II from JPK Instruments AG (Berlin, Germany). Commercial Si cantilevers (CSC37) were applied for the contact mode experiments. Height and deflection images with a resolution of 512 × 512 pixels in a 100 μm × 100 μm area were simultaneously observed with a scan rate of 0.6 Hz under ambient conditions (IGain: 150 Hz, PGain: 0.0048, Setpoint: 0.6 V). Images were taken at five different measuring points for each sample. In each image the heights were determined by Peak to valley roughness (R_t) at five different positions.

Raman imaging

Test samples were investigated with regard to polymer phase separation at the surface by means of Raman imaging. Therefore, a WITec alpha 300 confocal Raman microscope from WITec GmbH (Ulm, Germany) with 10× magnification and an input laser wavelength of 532 nm was used (excitation energy = 17.6 mW). For Raman area scans, a 500 μm × 500 μm field with 50 dots per row and column was used. Signals that are specific for the distinct polymers (PLLA: 878 rel. cm^{-1}, PCL: 1727 rel. cm^{-1}) were chosen for visualizing phase separation phenomena. According to the manufacturer's specification the typical resolution of the Raman system is 300 nm in xy direction and <1000 μm in z direction.

Mechanical characterization

Uniaxial tensile testing was performed with a Zwicki ZN 2.5 (Zwick, Ulm, Germany). Tests were conducted with a 50 N load cell and a crosshead speed of 25 mm min^{-1}. During the procedure samples were kept at room temperature. Dumbbell-shaped tensile test specimens with effective dimensions of 12 mm × 2 mm × 0.1 mm were prepared with a blanking tool according to DIN EN ISO 527-2 1BB standards [17]. An image with the detailed dumbbell-shaped size is given in the supplementary data available online at stacks.iop.org/MRX/7/095302/mmedia. The tensile force as a function of elongation was measured. Based on these data the elastic modulus (E) was calculated in the linear elastic region. Furthermore, the tensile strength (σ_{max}) and elongation at break (ε_B) were determined. All results were averaged over n = 6 samples.

Thermal analysis

The thermal behavior of the polymer films was investigated in a DSC 1 system (Mettler Toledo, Schwerzenbach, Switzerland) using the conventional calibration methods with highly pure standards. The specimens were heated at a rate of 10 K min^{-1} operating under nitrogen at atmospheric pressure. The samples were heated from −90 °C up to 200 °C. The sample weights were in the range of 3–6 mg. Samples were analyzed with respect to glass transition (T_g), melting temperature (T_m), and degree of crystallinity (χ). The T_g were determined by the midpoint of the inflection of the measured heating curve. The heats of fusion ΔH and crystallization χ_C were quantitatively evaluated by means of equation (1)

$$\chi_c = 100\% \cdot \left[\frac{\Delta H_m}{\Delta H_{m0}}\right] \cdot \frac{1}{W} \quad (1)$$

where ΔH_{m0} is the enthalpy value of a pure crystalline material, ΔH_m is the enthalpy corresponding to the fusion process and W the amount of each homopolymer in the blend. The reference value taken for ΔH_{m0} of PLLA was $\chi_{100} = 93.7$ J g^{-1} [18] and for PCL $\chi_{100} = 135.44$ J g^{-1} [19]. All results were averaged over n = 6 samples.

Results and discussion

Influence of annealing temperature on the morphology measured by SEM

Figure 3 shows SEM documentation of the polymer morphology with increasing PCL content after 40 °C, 80 °C and 200 °C annealing temperature. Pure PLLA appears to have one uniform phase with spherulite crystals of about 20 μm at an annealing temperature of T = 40 °C ($PLLA_{T40}$) and T = 80 °C ($PLLA_{T80}$). In comparison to this, the radius of such spherulites of PLLA annealed at T = 200 °C ($PLLA_{T200}$) increased dramatically to about 100 μm. These results are comparable with the literature, which show that PLLA spherulites increase with increasing temperature [7, 20, 21]. The smaller crystal size of PLLA film obtained from solution compared to PLLA film from melt may be explained by the surrounding solvent and evaporation processes during thermal annealing. PLLA/PCL 90/10 blends show significant increase in crystal size with increasing annealing temperature. However, two separated phases could not be clearly observed.

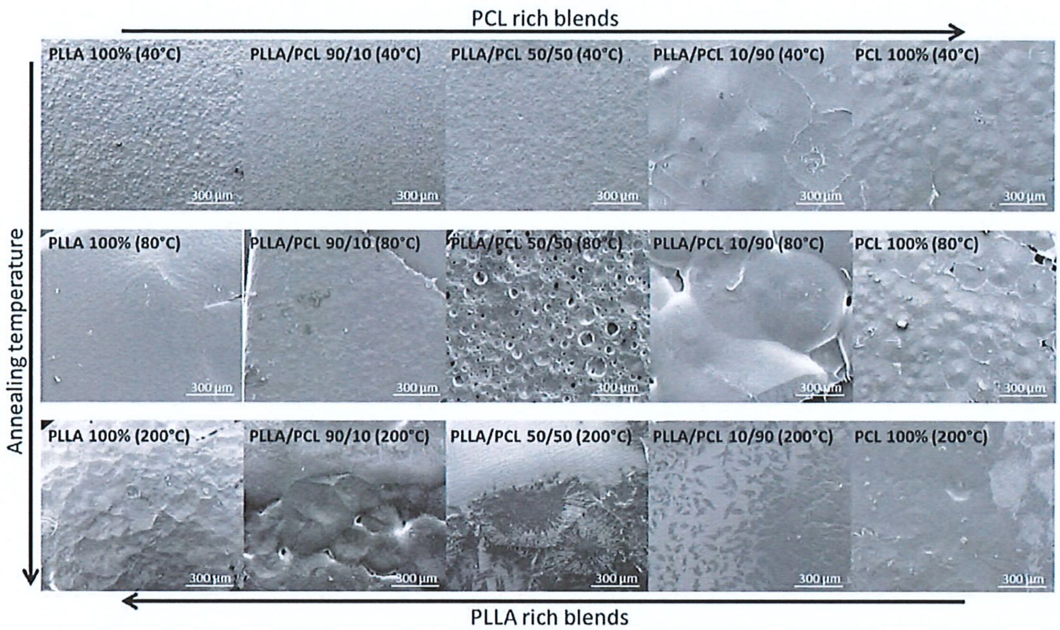

Figure 3. SEM images of various PLLA, PCL and their blends in different ratios (90/10, 50/50, 10/90 w/w) treated at different annealing temperatures (40 °C, 80 °C and 200 °C).

Interestingly, the surface morphology of PLLA/PCL 50/50 differs with different annealing conditions, see figure 3. From an initial smooth surface at T = 40 °C (PLLA/PCL 50/50$_{T40}$), the surface at T = 80 °C (PLLA/PCL 50/50$_{T80}$) changes to a perforated structure, which develops into two phases at T = 200 °C (PLLA/PCL 50/50$_{T200}$), a smooth and a spherulite-seeded structure. It is known from literature that a mixing gap of PLLA/PCL occurs from 80 °C and higher. When reaching mixing gap, PLLA spherulites are formed and small PCL crystals are deposited on the surface of the spherulite, thereby enhancing PLLA crystal growth [9]. This can also be found considering the solubility parameters of the two polymers which show a difference of approximately 0.9. Coleman *et al* describe a relatively weak favorable intermolecular interaction, if the difference between the solubility parameters of these polymer pairs is $\Delta\delta = 1.0$ (cal cm^{-3})$^{0.5}$, respectively [16]. They conclude in their work, that for high molecular polymers $\Delta\delta$ should be much smaller than 1 to ensure that the components are miscible. The fact that the value of PLLA and PCL are $\delta_{PLLA} = 10.1$ (cal cm^{-3})$^{0.5}$ and $\delta_{PCL} = 9.2$ (cal cm^{-3})$^{0.5}$ and therefore $\Delta\delta = 0.9$ suggests that the blend has only weak intermolecular interactions.

PLLA/PCL 10/90 shows large spherulites of about 300 μm at an annealing temperature of T = 40 °C (PLLA/PCL 10/90$_{T40}$) and T = 80 °C (PLLA/PCL 10/90$_{T80}$). The crystal shape of PLLA/PCL 10/90 at T = 200 °C (PLLA/PCL 10/90$_{T200}$) changes from circular to oval and the diameter decreased dramatically to about 50 μm.

Pure PCL exhibits remarkably smaller spherulites compared to PLLA/PCL 10/90 with diameters of about 200 μm at annealing temperatures of T = 40 °C (PCL$_{T40}$) and T = 80 °C (PCL$_{T80}$). The radii of spherulites of PCL at T = 200 °C (PCL$_{T200}$) increased dramatically to about 300 μm and the crystal height seems to regrade to a smooth surface.

Influence of annealing temperature on the morphology measured by AFM

Figure 4 shows a typical error, used for topography interpretation and height image of PLLA$_{T200}$ (image size 100 μm × 100 μm), which are used for the roughness evaluation R_t, see table 1. PLLA that was annealed at 200 °C forms spherulites with different sizes and heights.

Figure 5 shows error signal images of the tested polymer samples with a picture size of 100 μm × 100 μm. The top row represents the polymers and their blends at an annealing temperature of T = 40 °C. In the middle, the samples are shown at T = 80 °C and below at T = 200 °C. Pure PLLA, annealed at 40 °C, crystallizes into small conical spherulites between 10 and 30 μm in size. The size of the crystals increases drastically at T = 200 °C. Based on the height profiles, an increase from 2.68 ± 0.14 μm to 4.2 ± 0.8 μm is determined. PLLA/PCL 90/10, annealed at 40 °C, exhibits a smoother substructure, which is pervaded with approximately 5 μm pores and suggestively of small PCL inclusions. Chloroform diffuses rapidly through the PCL, leading to higher chloroform concentrations in PCL areas, which leads to pore formation during evaporation. The pore size increases at an annealing temperature of 200 °C. Dell'Erba *et al* discovered that low interfacial tensions are

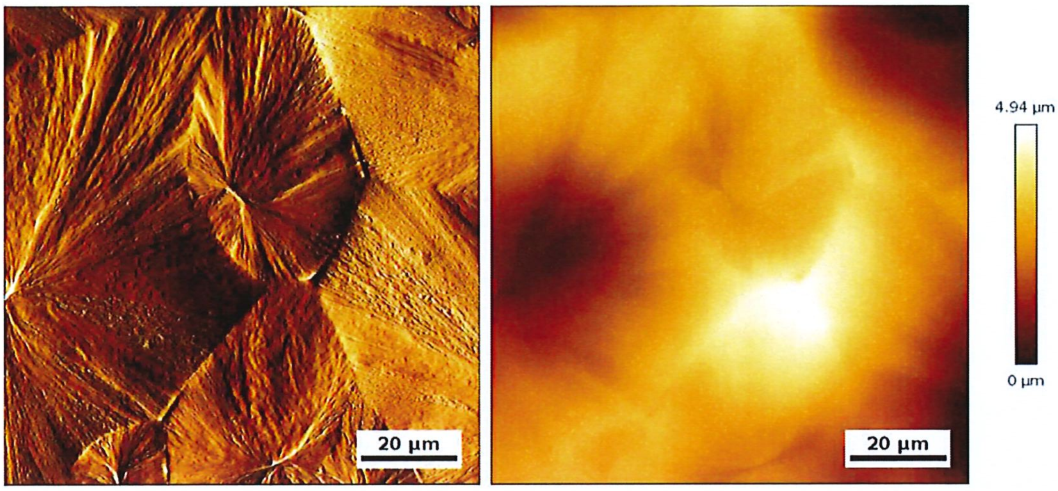

Figure 4. Representative AFM images of 100 × 100 μm^2 area. Contact mode error signal (left) and topography image (right) of PLLA, annealed at T = 200 °C for 60 min are shown.

Table 1. Mechanical properties (elastic modulus (E), tensile strength (σ_{max}), elongation at break (ε_B)), determined from uniaxial tensile tests, roughness (R_t), determined from AFM images and spherulite sizes, obtained from all morphology methods, of PLLA/PCL blends in different ratios (90/10, 50/50, 10/90 w/w) treated at different annealing temperatures. Due to low melting temperature PCL could not be observed (n.a. = not available).

T = 40 °C Composition (PLLA/PCL)	E (MPa)	σ_{max} (MPa)	ε_B (%)	R_t (μm)	$\varnothing_S$ (μm)
100/0	2090 ± 80	75.9 ± 1.3	60 ± 18	2.68 ± 0.14	10–20
90/10	998 ± 17	38.1 ± 1.8	130 ± 18	3.40 ± 0.11	n.a.
50/50	696 ± 15	24.5 ± 0.3	14.9 ± 2.9	4.0 ± 0.6	50
10/90	419 ± 9	19.8 ± 0.9	12.4 ± 0.9	5.7 ± 0.5	200–400
0/100	302 ± 16	15.2 ± 0.4	14.3 ± 1.7	5.2 ± 0.4	50–200

T = 80 °C Composition (PLLA/PCL)	E (MPa)	σ_{max} (MPa)	ε_B (%)	R_t (μm)	$\varnothing_S$ (μm)
100/0	2015 ± 22	75.5 ± 1.9	18 ± 10	2.35 ± 0.15	10–30
90/10	943 ± 19	34.3 ± 1.4	79 ± 30	4.54 ± 0.21	n.a.
50/50	850 ± 23	28.05 ± 0.02	7.86 ± 0.11	16.2 ± 0.9	50–100
10/90	230 ± 27	8.6 ± 1.0	10.2 ± 2.6	5.7 ± 1.4	300–600
0/100	n.a.	n.a.	n.a.	5.12 ± 0.12	100–200

T = 200 °C Composition (PLLA/PCL)	E (MPa)	σ_{max} (MPa)	ε_B (%)	R_t (μm)	$\varnothing_S$ (μm)
100/0	2250 ± 70	73.1 ± 2.9	3.90 ± 0.08	4.2 ± 0.8	100–200
90/10	810 ± 110	27.5 ± 0.8	9.7 ± 1.2	5.3 ± 1.2	200–400
50/50	861 ± 12	29.2 ± 0.9	5.58 ± 0.23	7.9 ± 0.5	300–500
10/90	160 ± 27	4.2 ± 1.2	24 ± 6	5.7 ± 1.0	50–500
0/100	n.a.	n.a.	n.a.	3.5 ± 0.4	300–500

obtained in binary PLLA/PCL blends due to the similar chemical nature of the blends components, which allows interpolymer polar interactions across phase boundaries [22]. This can be also observed at PLLA/PCL 50/50. In PLLA/PCL 50/50, annealed at 40 °C, lamellar structures in circular arrangements of about 60 μm in size are embedded in a smooth surface. In addition, approximately pores with a diameter of 5 μm can be observed. With PLLA/PCL 50/50$_{T80}$, the surface becomes very porous exhibiting pore diameters up to 50 μm. The height difference increases drastically to R_t = 16.2 ± 0.9 μm at T = 80 °C. Similar SEM images and pore sizes have been observed after solvent etching of PLLA/PCL blends [23]. This may be due to the melting of PCL in contrast to PLLA at the thermal processing step at 80 °C due to its lower melting temperature. Hence, PCL is liquefied, similar to the etching process where PCL is solved. As a result of this liquefying process a highly porous structure mainly built by PLLA would be expected. Such pores are not observed at T = 40 °C, where PCL remains solid and at T = 200 °C, where both polymers are melted, which results in a smooth surface without

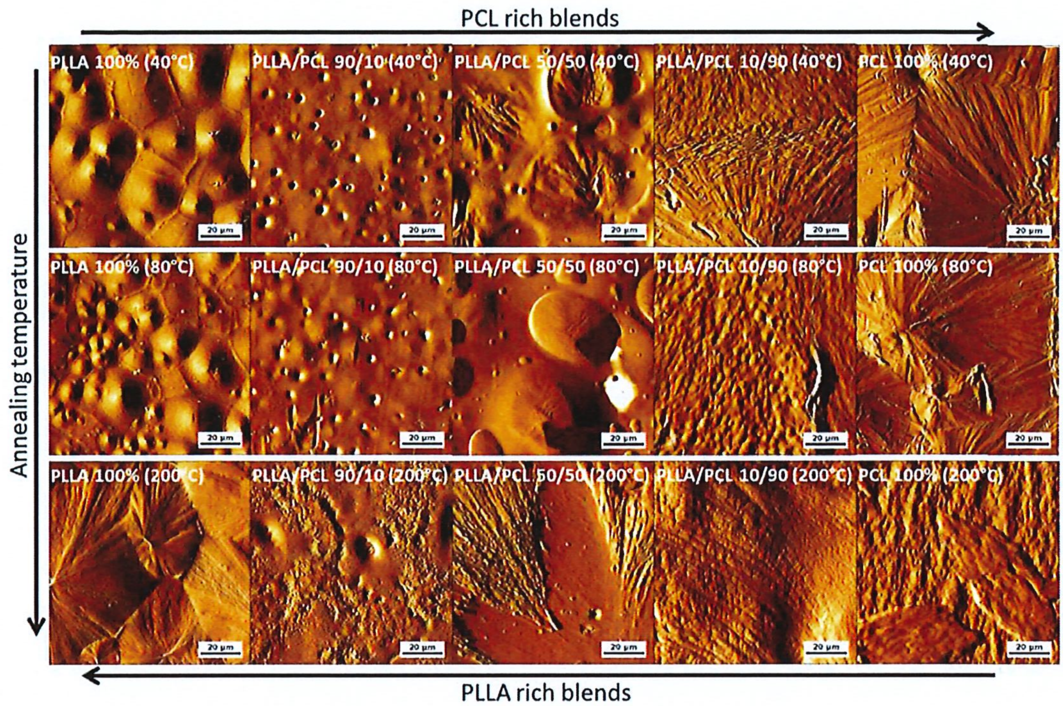

Figure 5. AFM contact mode error signal images of various PLLA, PCL and their blends in different ratios (90/10, 50/50, 10/90 w/w) treated at different annealing temperatures (40 °C, 80 °C and 200 °C).

pores. For the PLLA/PCL 10/90$_{T80}$ also a smooth surface is expected, due to the low amount of PLLA, witch rather forms particles than a connected structure. At T = 200 °C height difference drops down to 7.9 ± 0.5 μm. Clearly, two types of structures are visible: First, a smooth surface combined with a lamellar structure which corresponds to PCL crystals was observed in accordance to [22]. However, PLLA/PCL 10/90 exhibits a rough surface that can be interpreted as partial segments of spherulites. In part, the crystal boundaries are still visible. The height values (seen in table 1) show the same results of approx. 5.7 μm at all annealing temperatures. A similar picture is visible with pure PCL. When applying an annealing temperature of 200 °C, the structure changed. Plate-shaped structures were formed on a generally rough base structure. The AFM results obtained are consistent with the SEM images.

Influence of annealing temperature on the morphology measured using Raman images

Confocal Raman imaging was used in order to detect the phase separation in the different polymeric blends. In figure 6 the Raman images received by mapping the PLLA/PCL samples and their blends are shown. The corresponding Raman spectra are given in the supplementary data. In particular, the yellow area is related to the intensity of PLLA signal from the band centered at 878 rel. cm^{-1}. The red area is related to the intensity of the PCL signal, centered in the band at 1727 rel. cm^{-1}. The dark regions of the Raman images correspond to regions out of focus plane. From this analysis it becomes clear that phase separated morphology exists for all the three different blends, and it is possible to detect both, the PLLA-rich phase and the PCL-rich phase. For PLLA/PCL 90/10 it can be supposed that PLLA forms a continuous phase with dispersed spheres of PCL with different sizes (red regions of figure 6). Most interestingly, for PLLA/PCL 50/50 $_{T40}$ and PLLA/PCL 50/50$_{T80}$, two well differentiated areas of each homopolymer are detected, indicating the existence of large domains of each homopolymer. It is known from the literature that if polymer components are being phase separated, the interface width (w) can be related to the Flory-Huggins parameters (χ) by a general relation in the form $w \sim (\chi - \chi crit)^{-0.5}$ [14]. That means for our PLLA/PCL system a narrow interfacial width indicates relatively low interface interactions, which is consistent with the reported results of incompatibility between PCL and PLA [24]. López *et al* noted that in phase-separated PLA/PCL blends sharp interfaces are existing in the microstructure, whereas Broz *et al* found poor adhesion at the phase boundary interface and confirmed immiscibility and phase separation through NMR [6, 9]. It was hypothesized that to improve the mechanical properties of the blend, the samples should be annealed in the single-phase region of the LCST phase-diagram to enhance interfacial adhesion. It was concluded that interfacial adhesion may occur when the majority phase is PCL [25]. This could be also seen at T = 200 °C, but it is a more dominant PLLA phase in that case. Finally,

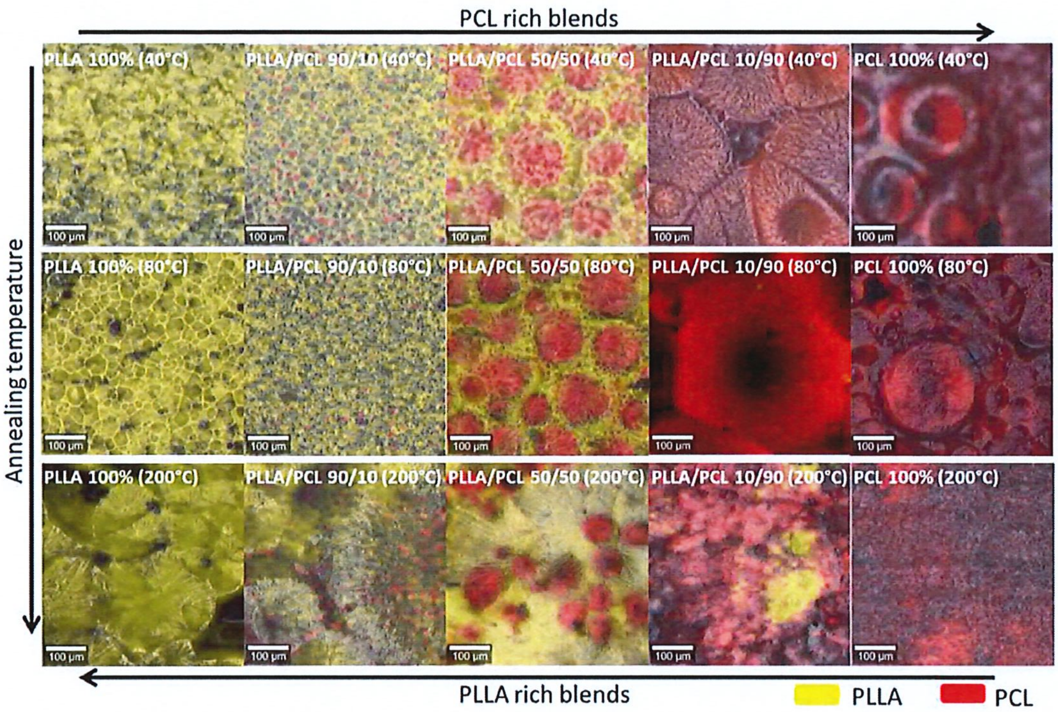

Figure 6. Raman images of various PLLA, PCL and their blends in different ratios (90/10, 50/50, 10/90 w/w) treated at different annealing temperatures (40 °C, 80 °C and 200 °C).

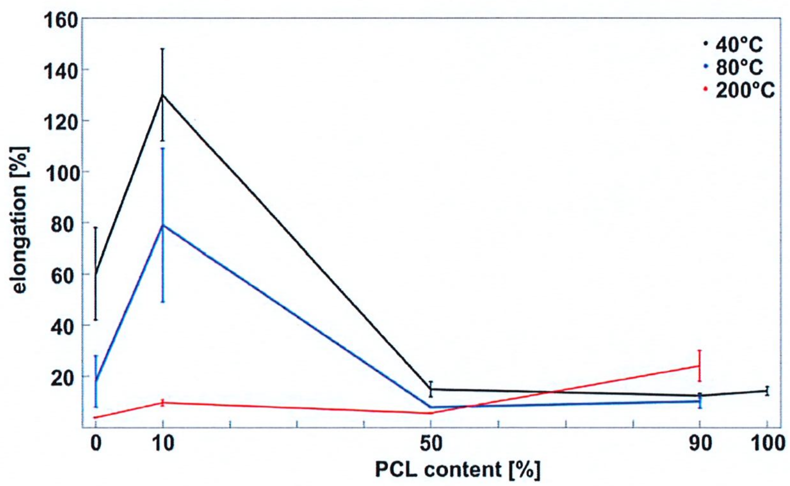

Figure 7. Elongation at break of solvent cast PLLA/PCL blends treated at different annealing temperatures as a function of PCL content, n=6. Tensile strength of solvent cast PLLA/PCL blends as a function of PCL content are given in the supplementary data.

PLLA/PCL $10/90_{T200}$ presents the PCL continuous region with small irregular PLLA domains of different sizes. At $T = 40$ °C, red regions indicating PCL phases are overlayed with yellow phases of PLLA, hence the areas appear orange. Thus, Raman maps are well related with the morphology previously received from the SEM and AFM images.

Influence of annealing temperature on the mechanical properties

The mechanical properties of the PLLA/PCL blends are plotted in figure 7. In this graphic, pure PLLA shows a stiff and brittle behavior, but after annealing to a temperature of 40 °C PLLA shows an elongation at break of $60 \pm 18\%$. This is probably due to the chain alignment during solvent evaporation [26]. Annealing above melting point (200 °C) reduces the elongation at break of pure PLLA down to a value of approximal 3%, which is known from literature [27].

PCL shows, in contrast to the literature, a brittle behavior. This can be associated with its high crystallinity, as described later in this work. Due to the washing and annealing processes, PCL reached such a high degree of crystallization and as a result the mechanical properties varied. Comparing the elongation values of PCL at 80 °C and 200 °C [6], it is evident that the crystallization values are significantly lower and consequently the elongation at break increases. Annealing of pure PCL above the melting temperature led to the degradation of the samples, which is why no mechanical properties could be determined. Addition of 10% PCL to PLLA and annealing to 40 °C results in a substantial increase in elongation at break, decreasing again with further addition of PCL (figure 7). From the literature, it is known from blending PLLA with PEG, that there is probably still an adhesion between PLLA and PEG based on the crystallization kinetics [27]. After annealing at 80 °C the 90/10 PLLA/PCL blend reveals the same effect, which indicates that the temperature has no significant effect on the PLLA/PCL boundary interfaces. Table 1 shows all mechanical properties of PLLA/PCL obtained by solvent casting, followed by an annealing process. The corresponding stress strain curves are given in the supplementary data. With further addition of PCL tensile strength (table 1) and elastic modulus decreases, which is comparable with the reported results [6, 9]. In summary, blending can substantially change the mechanical properties by influencing factors such as crystallization kinetics. To address this issue, thermal properties of the blends were investigated.

Influence of annealing temperature on the thermal properties

As typical examples, figure 8 shows the DSC traces of PLLA, PCL, and their blends in different ratios (90/10, 50/50, 10/90 w/w) of the cast film samples recorded by the first heating scan. The DSC spectrum of pure PLLA film exhibits a glass transition temperature at approximal 67 °C, see table 2 for all annealing temperatures and are consistent compared to literature values [26]. No exothermic peak, but an endothermic melting peak at 179 °C for an annealing temperature of 40 °C and 80 °C is observed. At 200 °C the melting peak of pure PLLA decreases to 173.4 $\pm$ 1.4 °C. With increasing annealing temperature two PLLA melting peaks are formed, see figure 8(c). The DSC spectrum of pure PCL film exhibits a glass transition temperature at -64.66 ± 0.03 °C for an annealing temperature of 40 °C (figure 8(a)) and increases with increasing annealing temperature up to $-61{,}6 \pm 1{,}9$ °C, see table 2. Pure PCL and all blends show a different melting behavior at 200 °C compared to annealing temperatures of 40 °C and 80 °C. For an annealing temperature of 200 °C, two melting peaks are formed for PCL (figure 8(c)). The appearance of two PCL and two PLLA melting peaks might be an indication of formation of mixed crystalline structures. There are some explanations for the PCL and PLLA double melting peaks phenomenon in the literature. Finotti *et al* state that the lower peak temperature can be associated with the partial migration of PLLA molecules to the PCL phase. The low molecular weight allows the diffusion of PLLA from the PLLA/PCL interface to the interior of the PCL rich-phase, decreasing the size and degree of perfection of the crystalline lamellae, hence lowering the T_M of the PCL. They also described the second melting peak at 56 °C as typical of pure PCL [28]. Regarding PLLA, Zhou *et al* stated the possibility to crystallize into two different crystal structures, the α-form, melting at higher temperature and the β-form, melting at lower temperature [29]. They also pointed out that the presence of the two endothermic peaks can also be explained by the growth of small crystals, which at low heating rates melt and recrystallize before melting again. Shan *et al* suggested the higher temperature peak may be a result of the melting of the thicker lamellae, possibly generated during the production process. In contrast, the lower temperature peak is attributed to the crystallization of the sample during the annealing process [30].

Table 2 shows the peak temperatures T_m and the T_g of PLLA and PCL as determined from the DSC curves as well as the percentage PLLA and PCL crystallinity, χ_{PLLA} (%) and χ_{PCL} (%) values as determined according to equation (1). Heat of fusion (ΔH) of PLLA, PCL and their blends are given in the supplementary data. T_g is not discussed here due to insufficient heating rate (10 K min^{-1}) and some overlay characteristics.

Thus, it can be concluded that blending PLLA with PCL changes the inherent crystallization behaviors of both polymers in combination. χ_{PLLA} at T_{40} is about 39.3 $\pm$ 1.7% and increases with increasing annealing temperature up to 62.8 $\pm$ 0.9%. The crystallinity of $PLLA_{T80}$ in the blend decreases at PLLA/PCL 90/10 and increases with higher PCL content. This can be explained in a way that PCL separates from the PLLA crystal due to the PLLA/PCL mixing gap, which is known from the literature [31]. This approaches the original crystallinity of PLLA 100. At T_{200} χ_{PLLA} in the 10/90 blend decreases from 62 $\pm$ 4% to 43 $\pm$ 8%. Other studies report an increase in the crystallinity of PLLA in the presence of PCL obtained from melt processes, probably due to the increase in nucleation rate [22, 32, 33]. However, this effect could not be observed in this work which may be explained by the fact that a solvent casting process was chosen in this paper. This has a different effect on the crystallization mechanism of PLLA and underlines the impact of the manufacturing process of such blend materials. The trend of increasing crystallinity with increasing PCL content in the blend can be seen in the case of all applied annealing temperatures, in a way that the high temperature thermal treatment at 200 °C approximates melt cast conditions.

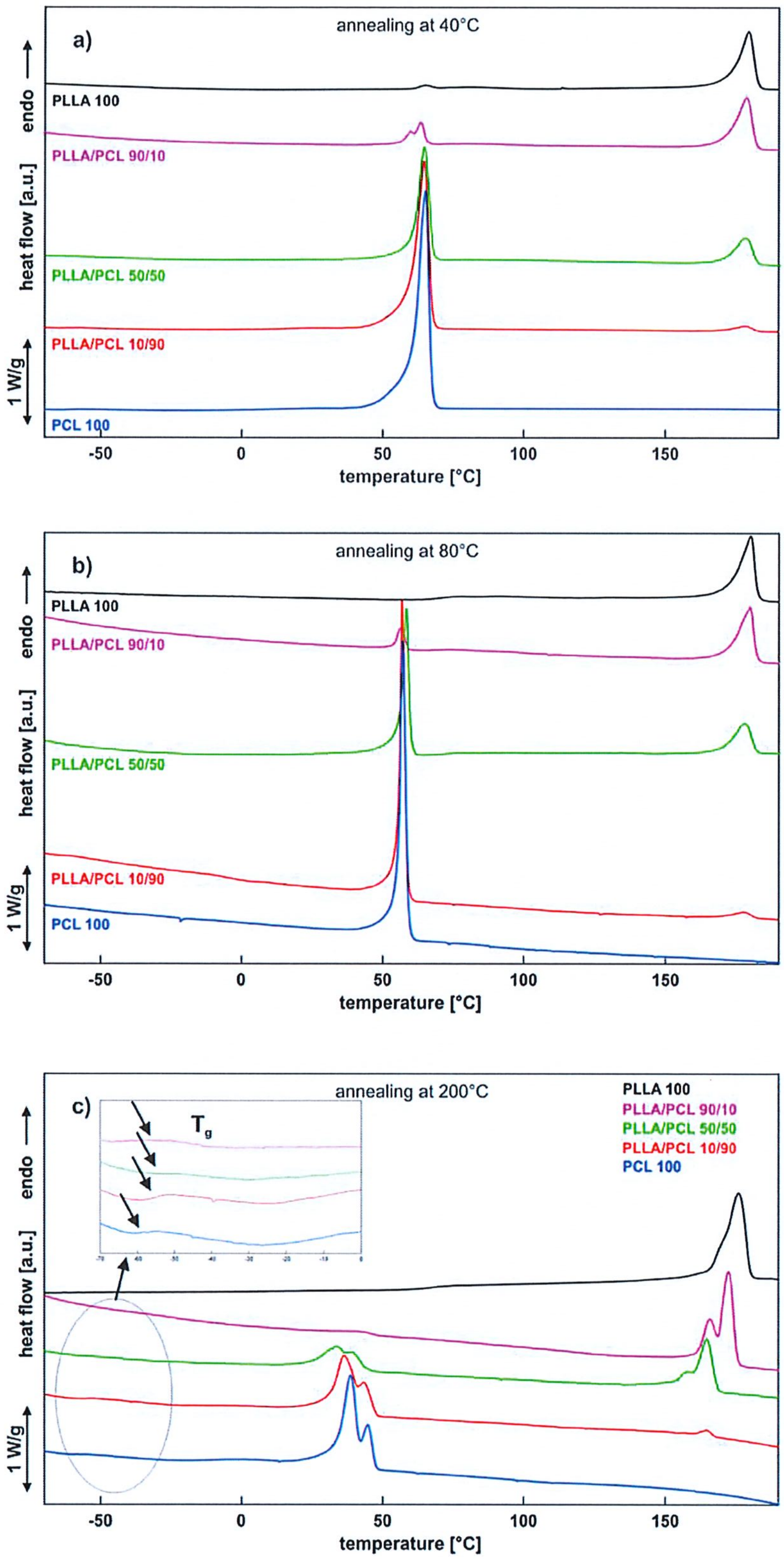

Figure 8. DSC curves of PLLA, PCL and their blends in different ratios (90/10, 50/50, 10/90 w/w) treated at different annealing temperatures (a = 40 °C, b = 80 °C and c = 200 °C).

Annealing at 200 °C is comparable to the thermally induced equilibration from melting process, which is widely applied for the investigation of crystalline polymers. Notably, it can be seen in figure 9 that the degree of crystallinity of PCL gradually decreases with increasing PLLA content, while the crystallinity of PLLA increases slowly with increasing PCL content (see table 2). Liu *et al* showed that a higher crystallization rate coefficient (CRC) of the blend in comparison to pure PLLA causes faster crystallization [34]. Therefore, χ_{PLLA} increases

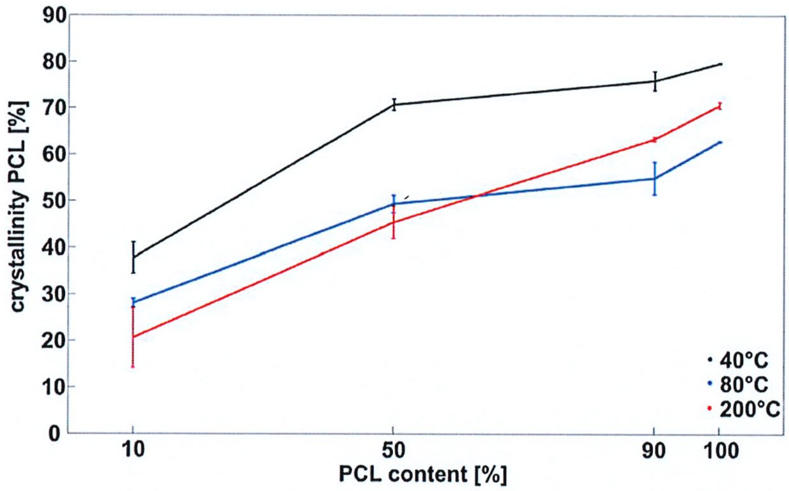

Figure 9. Crystallization behavior of PCL and their blends in different ratios (10/90, 50/50, 90/10 w/w) treated at different annealing temperatures, n = 6 Crystallization behavior of PLLA and their blends in different ratios (10/90, 50/50, 90/10 w/w) are given in the supplementary data.

Table 2. DSC results (glass transition (T_g), melting temperature (T_m) and degree of crystallinity (χ)) of PLLA/PCL blends in different ratios (90/10, 50/50, 10/90 w/w) treated at different annealing temperatures (n = 6 for each group, n.a. = not available).

T = 40 °C	PLLA			PCL		
Composition (PLLA/PCL)	T_g (°C)	χ (%)	T_m (°C)	T_g (°C)	χ (%)	T_m (°C)
100/0	67.25 ± 0.08	39.3 ± 1.7	179.51 ± 0.24			
90/10	75.4 ± 0.5	43.3 ± 0.7	180.14 ± 0.11	n.a.	38 ± 3	60.64 ± 0.08
50/50	74.65 ± 0.18	42.5 ± 0.9	178.61 ± 0.28	−62.95 ± 0.14	70.7 ± 1.2	65.04 ± 0.11
10/90	n.a.	37.7 ± 1.8	178.42 ± 0.10	−60.5 ± 0.8	75.9 ± 2.0	64.48 ± 0.11
0/100				−64.66 ± 0.03	79.66 ± 0.15	65.5 ± 0.5
T = 80 °C	PLLA			PCL		
Composition (PLLA/PCL)	T_g (°C)	χ (%)	T_M (°C)	T_g (°C)	χ (%)	T_M (°C)
100/0	68.2 ± 0.6	45.0 ± 1.7	179.80 ± 0.15			
90/10	71.6 ± 0.5	41.2 ± 1.2	179.56 ± 0.14	n.a.	28.1 ± 0.9	55.7 ± 0.3
50/50	71.7 ± 0.4	40.0 ± 1.2	178.18 ± 0.06	−63.9 ± 0.9	49.4 ± 1.9	57.74 ± 0.12
10/90	n.a.	40 ± 5	178.49 ± 0.12	−64.1 ± 0.8	55 ± 3	57.40 ± 0.09
0/100				−63.00 ± 0.23	62.81 ± 0.12	57.28 ± 0.05
T = 200 °C	PLLA			PCL		
Composition (PLLA/PCL)	T_g (°C)	χ (%)	T_M (°C)	T_g (°C)	χ (%)	T_M (°C)
100/0	66.1 ± 0.8	62.8 ± 0.9	173.4 ± 1.4			
90/10	66.5 ± 0.7	61 ± 3	173.7 ± 1.4	−63.59 ± 0.20	21 ± 6	45.8 ± 2.8
50/50	n.a.	62 ± 4	169.8 ± 2.6	−63.1 ± 1.0	45 ± 3	46 ± 3
10/90	n.a.	43 ± 8	174.89 ± 0.23	−62.7 ± 0.4	63.3 ± 0.5	55.6 ± 0.6
0/100				−61.6 ± 1.9	70.6 ± 0.7	54.64 ± 0.11

with increasing PCL content. Clearly, high PCL content substantially decreases the crystallinity of PLLA/PCL blends. This means that the large nucleus formation induced by PCL molecules inhibit the mobility of PLLA chains. As a result, chain rearrangement is limited, so low χ_{PLLA} are noted. Our assumption is that similar processes on the surface of the PLLA nuclei lead to a decrease in the crystallinity of the PCL when raising the PLLA concentration. Due to the increase in the annealing temperature, the crystal sizes of both polymers may decrease, resulting in a decrease in the melting temperature.

In general, solvent cast processes followed by low thermal annealing lead to substantially different properties of the yielded films in comparison to melt cast process data from the literature [22, 35, 36]. In addition to thermal equilibration, solvent evaporation plays an important role and can lead to different crystal growth rates compared to the cooling rate.

Conclusion

Polymer blends, in our case PLLA/PCL, may form complex structures and morphologies, leading to drastically altered properties of the resulting material. The interplay of the polymers depends on the material composition, the choice of preparation protocol, as well as on postprocessing procedures, such as washing or thermal annealing. Our aim was the investigation regarding the applicability of high-molecular PLLA blended with low-molecular PCL, e.g. as implant coating or drug delivery matrix. In this context, the thermal and mechanical properties are of great interest to ensure the formation of a functional biomaterial. With respect to this, we investigated how annealing temperature during postprocessing influences the properties and therefore the suitability of solvent cast PLLA/PCL blends for biomedical products.

In general, the applied solvent cast process used included evaporation under reduced pressure and a washing process to completely remove residual solvent from the polymer, which impacted the morphological and thermal properties of the material. Furthermore, during thermal analysis, to investigate crystallization and phase separation processes, the materials were cooled down with a very low cooling rate after annealing process in order to avoid cold crystallization of the material and to maintain thermodynamic equilibrium. Interestingly, it could be demonstrated that annealing processes strongly influence surface morphology, mechanical and thermal characteristic of PLLA, PCL and their blends. Blending led to an improvement of the mechanical performance of polymers, such as increase in ductility and therefore elongation at break or mechanical resilience overall. PLLA/PCL 90:10 has shown different stress strain behavior when tempered at 40 °C compared to 200 °C and correlated with changes in crystallinity, where χ_{PLLA} increased from 43 to 61%. This allows the modification of material properties without further additives such as plasticizers, only by changing the process protocols.

Furthermore, solution cast versus melt cast processes have been investigated. It was demonstrated that the thermal properties changed with the annealing temperature.

Our results shown that the method of preparation has great influence on the resulting polymer film and should be considered when developing polymer based implant materials.

In summary, we have demonstrated the influence of different annealing temperatures on the morphological, mechanical and thermal properties of PLLA/PCL blends. Thus, it is important to carefully choose and to maintain temperatures throughout the production path of such coatings, in particular regarding applications in the field of medical engineering, since production parameters not only affects the mechanical properties of the blends, but can also show an effect on drug release and polymer degradation. In order to verify this, further studies are necessary, especially regarding storage stability, degradation and drug release.

Acknowledgments

The authors thank Andrea Rohde, Katja Hahn, Caroline Dudda and Nathalie Böttcher for their expert technical assistance. Furthermore, partial financial support by the Federal Ministry of Education and Research (BMBF) within RESPONSE 'Partnership for Innovation in Implant Technology' and by the European Social Fund (ESF) within the excellence research program of the state Mecklenburg-Vorpommern Card-ii-Omics is gratefully acknowledged.

Conflict of interest

The authors declare that they have no conflict of interest.

ORCID iDs

Daniela Arbeiter https://orcid.org/0000-0002-4088-9145

References

[1] Takayama T, Todo M and Tsuji H 2011 *J Mech Behav Biomed Mater* 4 255–60
[2] European Medicines Agency 2016 ICH guideline Q3C (R6) on impurities: guideline for residual solvents EMA/CHMP/ICH/82260/2006
[3] Arbeiter D, Schümann K, Sahmel O, Eickner T, Schmitz K-P and Grabow N 2016 *Curr. Dir. Biomed. Eng.* 2 26
[4] Teske M, Arbeiter D, Schober K, Eickner T and Grabow N 2018 *Curr. Dir. Biomed. Eng.* 4 567–9

[5] Teske M, Arbeiter D, Schober K, Eickner T and Grabow N 2016 *Curr. Dir. Biomed. Eng.* **2** 1929
[6] López-Rodríguez N, López-Arraiza A, Meaurio E and Sarasua J R 2006 *Polym. Eng. Sci.* **46** 1299–308
[7] Tsuji H and Ikada Y 1994 *Polymer* **14** 2709–16
[8] Park S D, Todo M, Arakawa K and Koganemaru M 2006 *Polymer* **47** 1357–63
[9] Broz M 2003 *Biomaterials* **24** 4181–90
[10] Todo M, Park S-D, Takayama T and Arakawa K 2007 *Eng Fract Mech* **74** 1872–83
[11] Mannella G A, Carfì Pavia F, La Carrubba V and Brucato V 2016 *Eur. Polym. J.* **79** 176–86
[12] Genzer J and Composto R J 1999 *Polymer* **40** 4223–8
[13] Pillin I, Montrelay N and Grohens Y 2006 *Polymer* **47** 4676–82
[14] Kacar G, Peters E A J F and de With G 2013 *EPL* **102** 40009
[15] Letchford K, Liggins R and Burt H 2008 *J Pharm Sci-US* **97** 1179–90
[16] Coleman M M, Serman C J, Bhagwagar D E and Painter P C 1990 *Polymer* **31** 1187–203
[17] International Standard Organisation 527-2 2012 *Plastics-Determination of Tensile Properties* - Parts 2: Test conditions for moulding and extrusion plastic
[18] Fischer E W, Sterzel H J and Wegner G 1973 *Kolloid-Z. u. Z. Polymere* **251** 980–90
[19] Crescenzi V, Manzini G, Calzolari G and Borri C 1972 *Eur. Polym. J.* **8** 449–63
[20] Grigoriev T E *et al* 2018 *BioNanoSci.* **8** 977–83
[21] Carvalho J R G, Conde G, Antonioli M L, Dias P P, Vasconcelos R O, Taboga S R, Canola P A, Chinelatto M A, Pereira G T and Ferraz G C 2020 *Polym J* **101** 8493
[22] Dell'Erba R, Groeninckx G, Maglio G, Malinconico M and Migliozzi A 2001 *Polymer* **42** 7831–40
[23] Ostafinska A, Fortelny I, Nevoralova M, Hodan J, Kredatusova J and Slouf M 2015 *RSC Adv.* **5** 98971–82
[24] Zhu B, Wang Y, Liu H, Ying J, Liu C and Shen C 2020 *Comp. Sci. Tech.* **190** 108048
[25] Murphy S H, Marsh J J, Kelly C A, Leeke G A and Jenkins M J 2017 *Eur. Polym. J.* **88** 34–43
[26] Migliaresi C, Lollis A, de, Fambri L and Cohn D 1991 *Clinical Materials* **8** 111–8
[27] Farah S, Anderson D G and Langer R 2016 *Advanced Drug Delivery Reviews* **107** 367–92
[28] Finotti P F M, Costa L C, Capote T S O, Scarel-Caminaga R M and Chinelatto M A 2017 *J Mech Behav Biomed Mater* **68** 155–62
[29] Zhou H, Green T B and Joo Y L 2006 *Polymer* **47** 7497–505
[30] Shan G-F, Yang W, Tang X-G, Yang M-B, Xie B-H, Fu Q and Mai Y-W 2010 *Polymer Testing* **29** 273–80
[31] Maglio G, Malinconico M, Migliozzi A and Groeninckx G 2004 *Macromol. Chem. Phys.* **205** 946–50
[32] Can E, Udenir G, Kanneci A I, Kose G and Bucak S 2011 *AAPS PharmSciTech* **12** 1442–53
[33] Liu T-Y, Lin W-C, Yang M-C and Chen S-Y 2005 *Polymer* **46** 12586–94
[34] Navarro-Baena I, Sessini V, Dominici F, Torre L, Kenny J M and Peponi L 2016 *Polym. Degrad. Stab.* **132** 97–108
[35] Hamad K, Kaseem M, Yang H W, Deri F and Ko Y G 2015 *Express Polym. Lett.* **9** 435–55
[36] Botlhoko O J, Ramontja J and Ray S S 2018 *Polym. Degrad. Stab.* **154** 84–95

Publikation 3

Polymers (**2021**), *13(2)*, 292.

Influence of drug incorporation on the physico-chemical properties of poly(L-lactide) implant coating – a systematic study.

Arbeiter D, Reske T, Teske M, Bajer D, Senz V, Schmitz K-P, Grabow N, Oschatz S.

Eingereicht: 23.12.2020, veröffentlicht: 18.01.2021

DOI: 10.3390/polym13020292 (IF = 3,426)

Abstract: Local drug delivery has become indispensable in biomedical engineering with stents being ideal carrier platforms. While local drug release is superior to systemic administration in many fields, the incorporation of drugs into polymers may influence the physico-chemical properties of said matrix. This is of particular relevance as minimally invasive implantation is frequently accompanied by mechanical stresses on the implant and coating. Thus, drug incorporation into polymers may result in a susceptibility to potentially life-threatening implant failure. We investigated spray-coated poly(L-lactide) (PLLA)/drug blends using thermal measurements (DSC) and tensile tests to determine the influence of selected drugs, namely sirolimus, paclitaxel, dexamethasone, and cyclosporine A, on the physico-chemical properties of the polymer. For all drugs and PLLA/drug ratios, an increase in tensile strength was observed. As for sirolimus and dexamethasone, PLLA/drug mixed phase systems were identified by shifted drug melting peaks at 200 °C and 240 °C, respectively, whereas paclitaxel and dexamethasone led to cold crystallization. Cyclosporine A did not affect matrix thermal properties. Altogether, our data provide a contribution towards an understanding of the complex interaction between PLLA and different drugs. Our results hold implications regarding the necessity of target-oriented thermal treatment to ensure the shelf life and performance of stent coatings.

polymers

MDPI

Article

Influence of Drug Incorporation on the Physico-Chemical Properties of Poly(L-Lactide) Implant Coating Matrices—A Systematic Study

Daniela Arbeiter [1,*], Thomas Reske [2], Michael Teske [1], Dalibor Bajer [1], Volkmar Senz [1], Klaus-Peter Schmitz [1,2], Niels Grabow [1] and Stefan Oschatz [1]

[1] Institute for Biomedical Engineering, Rostock University Medical Center, Friedrich-Barnewitz-Straße 4, 18119 Rostock, Germany; michael.teske@uni-rostock.de (M.T.); dalibor.bajer@uni-rostock.de (D.B.); volkmar.senz@uni-rostock.de (V.S.); schmitz@iib-ev.de (K.-P.S.); niels.grabow@uni-rostock.de (N.G.); stefan.oschatz@uni-rostock.de (S.O.)

[2] Institute for Implant Technology and Biomaterials e.V., Friedrich-Barnewitz-Straße 4, 18119 Rostock, Germany; thomas.reske@uni-rostock.de

* Correspondence: daniela.arbeiter@uni-rostock.de; Tel.: +49-381-54345-554

Abstract: Local drug delivery has become indispensable in biomedical engineering with stents being ideal carrier platforms. While local drug release is superior to systemic administration in many fields, the incorporation of drugs into polymers may influence the physico-chemical properties of said matrix. This is of particular relevance as minimally invasive implantation is frequently accompanied by mechanical stresses on the implant and coating. Thus, drug incorporation into polymers may result in a susceptibility to potentially life-threatening implant failure. We investigated spray-coated poly-L-lactide (PLLA)/drug blends using thermal measurements (DSC) and tensile tests to determine the influence of selected drugs, namely sirolimus, paclitaxel, dexamethasone, and cyclosporine A, on the physico-chemical properties of the polymer. For all drugs and PLLA/drug ratios, an increase in tensile strength was observed. As for sirolimus and dexamethasone, PLLA/drug mixed phase systems were identified by shifted drug melting peaks at 200 °C and 240 °C, respectively, whereas paclitaxel and dexamethasone led to cold crystallization. Cyclosporine A did not affect matrix thermal properties. Altogether, our data provide a contribution towards an understanding of the complex interaction between PLLA and different drugs. Our results hold implications regarding the necessity of target-oriented thermal treatment to ensure the shelf life and performance of stent coatings.

Keywords: drug-eluting stent (DES); poly-L-lactide; drug delivery coatings; mechanical properties; thermal properties; surface morphology; paclitaxel; sirolimus; dexamethasone; cyclosporine A

check for updates

Citation: Arbeiter, D.; Reske, T.; Teske, M.; Bajer, D.; Senz, V.; Schmitz, K.-P.; Grabow, N.; Oschatz, S. Influence of Drug Incorporation on the Physico-Chemical Properties of Poly(L-Lactide) Implant Coating Matrices—A Systematic Study. *Polymers* **2021**, *13*, 292. https://doi.org/10.3390/polym13020292

Received: 23 December 2020
Accepted: 13 January 2021
Published: 18 January 2021

1. Introduction

Drug-eluting stents (DES), in particular those of newer generations, are superior to bare metal stents in the treatment of coronary artery stenosis [1–5]. Among others, frequently used drugs are from the Limus family, especially sirolimus (SIR) [6–9], but also paclitaxel (PTX) [10], dexamethasone (DEX) [11,12], and cyclosporine A (CYCLO) [13,14]. SIR is mainly used for its immunosuppressant effects to inhibit organ transplant rejection, but also shows mammalian target of rapamycin (mTOR) inhibition, reducing cell proliferation and thus the risk of in-stent restenosis [15,16]. PTX is being applied directly to the target area with drug-eluting balloons or in polymer coatings of DES [3,17], however this has recently been questioned [18]. The mechanism of action for PTX is the inhibition of smooth muscle cell (SMC) migration and proliferation by suppression of spindle microtubule assembly during mitosis cycle [16,19]. Dexamethasone (DEX), a corticosteroid, is used for its immunosuppressive and anti-inflammatory properties [20]. Another active pharmaceutical ingredient (API) for potential DES application is CYCLO, which blocks calcineurin-cyclophylin complexation and thus inhibits SMC proliferation and migration [21,22].

Besides polymer-free DES, one of the most common technologies is the drug incorporation into a polymer coating applied to the stent [23]. A wide range of polymers are in clinical use regarding drug carrying matrices for DES [24,25]. Alongside chemically inert polymers, such as fluorinated polymers, polylactide (PLA) and its derivatives are widely used as coating matrices due to the easy processability and their biodegradable nature [26]. Table 1 gives a brief overview about the state-of-the-art of available DES.

Table 1. Overview on selected commercially available DES (modified according to [25], drug loading data was taken from [27]).

Stent	Stent Material	Polymer	Absorption Time	Drug	Drug-Eluting Time	Manufacturer	Drug Loading
Cypher	Stainless steel	PEVA/PBMA	Permanent	Sirolimus	90 days	Cordis	140 μg/cm^2
Taxus Express	Stainless steel	SIBS	Permanent	Paclitaxel	>180 days	Boston Scientific	100 μg/cm^2
Xience Alpine	CoCr	PVDF-HFP	Permanent	Everolimus	120 days	Abbott Laboratories	100 μg/cm^2
Resolute Integrity	CoNi with Pt-Ir	BioLinx	Permanent	Zotarolimus	180 days	Medtronic	-
Orsiro	CoCr	PLLA	15 months	Sirolimus	100–120 days	Biotronik	1.4 μg/mm^2
Ultimaster	CoCr	PDLLA-PCL	3–4 months	Sirolimus	3–4 months	Terumo Interventional Systems	-
Synergy	PtCr	PLGA	3–4 months	Everolimus	3 months	Boston Scientific	38–179 μg/stent
Nobori	Stainless steel	PDLLA	6–9 months	Biolimus	6–9 months	Terumo	15.6 μg/mm^2

PEVA = poly(ethylene-co-vinyl acetate); PBMA = poly(n-butyl methacrylate); SIBS = poly(styrene-*b*-isobutylene-*b*-styrene); PVDF-HFP = poly(vinylidene fluoride-co-hexafluoropropylene); BioLinx = blend of methacrylate and vinylpyrrolidone based polymers; PLLA = poly-L-lactide; PDLLA-PCL = poly(DL-lactide-co-caprolactone); PLGA = poly(lactic-co-glycolic acid); PDLLA = poly(DL-lactide).

In this context, effort has been taken, including work from our group, to understand and modify drug release behavior from polymer/drug matrices. Several reports regarding the release profile of PTX loaded PLA film coatings can be found in the literature [28–32]. Furthermore, in particular SIR loaded DES has been investigated to an extent [33–36]. Also, release profiles of DEX/PLLA [37] and CYCLO/PLLA [13] are well known from the literature.

As DES coatings usually possess a thickness in a range of only 10 μm for hemodynamic reasons, they are prone for fracturing or peeling off due to mechanical stress during implantation which is caused by stent insertion and dilatation [4,38]. Therefore, a drug containing coating does not only have to show appropriate release and biocompatibility, but furthermore a suitable mechanical performance paired with resilience against delamination and particle detachment, which is required e.g., in DIN EN ISO 25539-2 [39].

For relatively stiff and rigid polymers such as PLLA, blending with other polymers, e.g., PCL, is a frequently used technique to create suitable and sufficient ductile coatings [40–42]. In a recent work, we investigated the influence of PCL fraction on the mechanical, morphological and thermal behavior of high molecular weight (HMW) PLLA film materials [43]. Another way to modify the polymer properties is the use of small molecular additives. The fact that the incorporation of such additives into a polymer may lead to plasticizing or hardening effects by intermolecular interactions is well known [44–48]. As for that, Ljungberg and Wesslén reported on the influence of several additives on the mechanical and thermal properties of *PLA*. Triacetine and tributyl citrate proved to be effective plasticizers up to an extent of 25 *w*/*w*% where saturation occurred and the polymer-additive mixture showed phase separation upon heating, accompanied by an increase in PLA crystallinity due to enhanced molecular mobility [49].

However, even the incorporation of a drug alone, being a small molecule, the API may lead to the desired increase in flexibility and resilience against fracturing. Regarding the influence on the material properties of drugs incorporated into a polymer matrix, Siepmann, le Brun, and Siepmann reported on acrylic acid copolymers mixed with ibuprofen, chlorpheniramine maleate and metoprolol tartrate [50]. One of their findings was that by the addition of 20 w/w% ibuprofen, the glass transition temperature (T_g) of the polymer was decreased from 80 °C down to 20 °C accompanied by a strong increase of elongation at break. An innovative concept to overcome such effects, which are not always beneficial or even unwanted, is the encapsulation of the API in a hollow PLA nanoparticles, as reported by Lai's group [51,52]. Using DSC and IR measurements, they showed that this approach allows a physical separation between the drug and the carrier matrix, so that the drug does not interact with the polymer chains and matrix properties are not altered. Furthermore, due to the diffusion barrier, the encapsulation leads to a decreased burst release.

All those effects are of certain interest regarding a functional implant, especially in the field of stent devices, which have to be crimped and diluted and are even exposed to intense mechanical stress during the implantation process. Still, only little is known on how the integration of drugs as small molecules into the polymer matrix alters the physico-chemical and mechanical properties of a DDS coating in its entirety.

In the current literature, mostly release behavior of drug containing PLA has been addressed. Although it can be estimated, the influence a drug has on the matrix, such as a shift in T_g or changes in crystallinity, can differ greatly [53,54]. The present study addresses the outcome of the incorporation of selected drugs, SIR, PTX, DEX, and CYCLO, which are approved or under investigation for the local treatment regarding stent related complications, on the mechanical, thermal and morphological properties of PLLA thin films regarding the functionality as DES coatings.

The drug inclusion criterion for our study was to identify candidates with a high relevance in DES applications, but at the same time representing substantially different chemical base structures. While SIR is a macrocyclic lactone, PTX is a diterpene, DEX possesses a sterol backbone, and CYCLO is a cyclic peptide. Overall, the selected API cover a relevant range of different structural properties in terms of molecular weight, size, polarity, hydrophilicity or functional groups and therefore possible ways of interacting with the polymer matrix. Some indicators for these parameters are polar surface area (PSA) and partition coefficient (logP). Selected characteristics of SIR, PTX, DEX and CYCLO have been summarized in Table 2. To visualize how the drugs used differ in terms of molecular size and shape, structural formulas and space-filling model illustrations were included.

Table 2. An overview concerning the drugs used in this study for blending with PLLA and their selected properties.

Drug	Structural Formula	Space Filling Model Illustration	PSA (in Å^2) [1]	logP	M_W (g/mol)
PACLITAXEL (PTX)	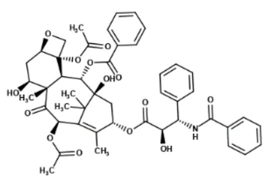	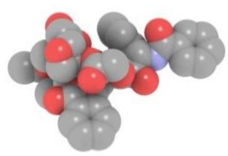	221	3 [18]	853.9
SIROLIMUS (SIR)	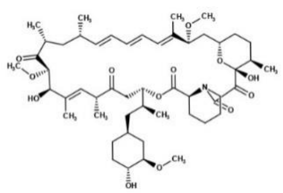	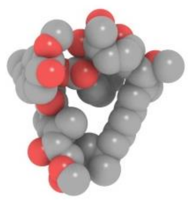	195	7.45 [55]	914.2
DEXAMETHASONE (DEX)	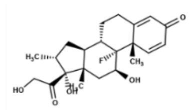	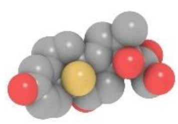	95	1.83 [56]	392.5

Table 2. *Cont.*

Drug	Structural Formula	Space Filling Model Illustration	PSA (in Å^2) [1]	logP	M_W (g/mol)
CYCLOSPORINE (CYCLO)	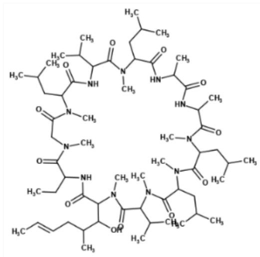	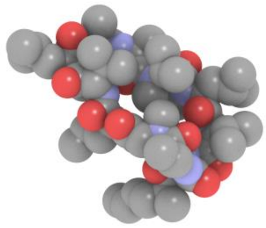	279	1.4 [57]	1202.6

[1] Polar surface area (PSA) values were taken from PubChem and calculated via CACTVS [58], according to the information on the website. MarvinSketch was used for molecular structure drawing (Marvin v.20.11, 2020, ChemAxon, Budapest, Hungary). Space filling models were created with QuteMol (v. 0.4.1) [59] using pdb-files created from MarvinSketch.

Our interest was to what extent blending PLLA with different drugs alone may influence or even have beneficial effects on the polymer properties. As shown in Table 1, commercially available DES vary in drug loading. This is both dependent on stent design, as well as on the incorporated API, as different drugs show different therapeutic windows. Thus, literature reports on incorporated drugs for DES technology range from 1 *w*/*w*% for PTX [60] up to 200 *w*/*w*% for DEX [37]. In order to generate comparable data for the selected drugs, we decided to investigate the alteration of polymer properties after incorporation of 10, 15, and 20 *w*/*w*% of drug in PLLA, knowing that certain drug coatings for clinical use may contain lower or higher drug amounts.

It must be noted that the topic of drug incorporation becomes even more complex when considering the effect of additives on polymer/drug matrices. There are several reports in the literature on how the addition of stabilizers or supporting molecules may enhance drug release, mechanical resilience or stability of the carrying matrix on a high level [61–63]. However, three or more component systems are a somewhat complex matter in respect to their physico-chemical properties as each part may interact with all the others alone and at once. Consequently, our focus was on binary systems formed by drug incorporation though the authors of this study are aware of the fact that several other compounds are of high interest regarding DES technology. To the best of our knowledge, the influence of commonly used drug molecules on the physico-chemical properties of matrix polymers, such as PLLA, against the background of DES coatings has not been systematically investigated. For this work, as one of the most widely used coating technique [64], especially in industrial application, drug loaded PLLA films were generated via airbrush spray-coating process.

In summary, our aim in the presented study was to analyze the effects of different drug candidates on the properties of the respective polymer/drug matrices from a biomedical engineering viewpoint. It addresses thermal and mechanical properties, long term stability, and phase behavior of PLLA/drug blends, which are parameters of crucial relevance to ensure shelf life and performance of stent coatings. In addition to the already comprehensive literature data concerning drug release behavior and biocompatibility, our results shall provide a complementary contribution towards an understanding of such drug coatings.

2. Materials and Methods

2.1. Chemicals

Chloroform and methanol were received from VWR international (Darmstadt, Germany) in technical grade quality.

HMW PLLA used was Resomer L 210 S, intrinsic viscosity in chloroform: 3.8 dL/g, M_W = 320 kDa (Evonik Industries AG, Essen, Germany). Drugs used were: Paclitaxel (Cfm Oskar Tropitzsch GmbH, Marktredwitz, Germany), sirolimus (Cfm Oskar Tropitzsch

GmbH, Marktredwitz, Germany), cyclosporine A (Synopharm GmbH & Co. KG, Glinde, Germany) and dexamethasone (Dr. Gerhard Mann Chem.-Pharm. Fabrik GmbH, Berlin, Germany).

All chemicals were used as received without further purification.

2.2. Preparation of Polymer Films via Spray Coating

Thin film specimens of PLLA with incorporated drugs were produced using airbrush spray coating process as was reported by our group before [35]. In brief, PLLA was dissolved in $CHCl_3$ and drug solution in MeOH (PTX, SIR, DEX) or $CHCl_3$ (CYCLO) was added. For each drug, a final ratio of 10 w/w%, 15 w/w% and 20 w/w% was adjusted with respect to the dissolved polymer. As reference, pure PLLA film was manufactured in the same manner without the addition of drugs.

Following to this, thin films of thicknesses of around 7 µm were generated using a custom-made airbrush device on rectangular glass slides as substrate (6.5 × 2.5 cm^2). Residual solvent from the process was removed from the coated glass slides under reduced pressure at 80 °C. A total amount of approximately 250 µg polymer film was formed and checked via weighing. Films were removed manually from the glass substrates using a scalpel to slightly lift the films, which led to easy detachment.

2.3. Raman Microscopy Imaging

Polymer films obtained via spray coating were investigated with regard to drug distrubution at the surface by means of Raman imaging. A WITec alpha 300 confocal Raman microscope (WITec GmbH, Ulm, Germany) with 10× magnification equipped with an input laser with a wavelength of ν = 532 nm was used. For Raman area scans, a 500 µm × 500 µm field with 50 dots per row and column was used, giving a resulting resolution of 10 μm^2. The area ratio of signals that are specific for the PLLA matrix ($\tilde{v}$ = 878 rel cm^{-1}) and the distinct drugs (PTX: $\tilde{v}$ = 1012 rel cm^{-1}, SIR: $\tilde{v}$ = 1642 rel cm^{-1}, DEX: $\tilde{v}$ = 1668 rel cm^{-1}) were chosen for visualizing drug distribution. The areas of distinct drug signals identified from preliminary measured reference spectra have been normalized to the area of the PLLA signal at $\tilde{v}$ = 883 rel cm^{-1}. The measurements have been performed for two separately manufactured drug containing PLLA films and the median of the quotients was formed. In the case of CYCLO incorporation, no distinct drug signal could be detected.

2.4. FTIR Measurements

FTIR-ATR-measurements were performed using a Bruker Vertex 70 IR-Spectrometer (Bruker, Leipzig, Germany) equipped with a DLaTGS-detector. Data were collected in the range of $\tilde{v}$ = 500 cm^{-1} to 4000 cm^{-1} with a resolution of $\tilde{v}$ = 4 cm^{-1} averaged over 100 scans in reflection mode using a Graseby Golden Gate Diamond ATR-unit. All spectra were subsequently baseline corrected and atmospheric compensation has been performed. Subsequently, the area of the CYCLO signal at $\tilde{v}$ = 1629 cm^{-1} has been compared to the area of PLLA signal at $\tilde{v}$ = 1749 cm^{-1}. The quotient formed from these areas in a similar manner as for Raman measurements can be found in Figure 1b.

2.5. SEM Imaging

Morphology of the polymer films was examined with scanning electron microscopy SEM QUANTA FEG 250 (FEI Company, Dreieich, Germany) operating in high vacuum and 10 kV, using an Everhart-Thornley secondary electron detector (ETD). The samples were fixed onto aluminum carriers using conductive carbon pads and Au sputter coated. The images were taken at magnification ×1000.

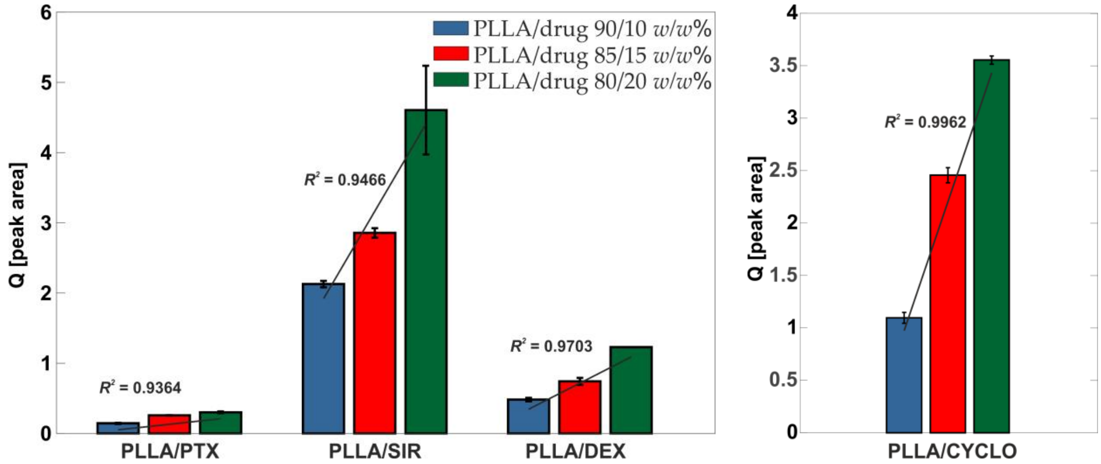

(**a**) (**b**)

Figure 1. (**a**) Quotients of drug signal found in Raman spectroscopy (PTX: $\widetilde{\upsilon}$ = 1012 rel cm^{-1}, SIR: $\widetilde{\upsilon}$ = 1642 rel cm^{-1}, DEX: $\widetilde{\upsilon}$ = 1668 rel cm^{-1}) compared to PLLA reference signal to ensure drug loading. (**b**) Quotient of the CYCLO signal at $\widetilde{\upsilon}$ = 1629 cm^{-1} from FT-IR spectroscopy compared to PLLA reference signal. Linear regression of the means has been performed and R^2 values are given.

2.6. Contact Angle Measurements

Contact angle measurements have been performed using a mobile surface analyzer MSA (Krüss GmbH, Hamburg, Germany) equipped with a double pressure dosing unit at ambient conditions with 2 µL drop volume and 1 s equilibration time. As test liquids, deionized water and diiodomethane were used to calculate free surface energy. Contact angles have been determined in triplicate for each drug loaded polymer film using separate cutouts. Contact angles were calculated by averaging the values for both sides of the drops. To avoid bending of the test samples and to ensure a plain shape, the PLLA films have been mounted on pyrolytic graphite planchets.

2.7. Thermal Analysis

The DSC 1 system (Mettler-Toledo, Greifensee, Switzerland) was used to determine the thermal properties of drug-loaded PLLA spray-coated films using the conventional calibration methods with highly pure standards. The specimens were heated up from 25 °C at a rate of 10 K/min operating under nitrogen at atmospheric pressure. The end temperature was between 210 °C and 280 °C, depending on the incorporated drug. The sample weights were in the range of 0.3–2.5 mg. Samples were analyzed with respect to glass transition (T_g), crystallization temperature (T_c), melting temperature (T_m), and degree of crystallinity of PLLA (χ). The heats of fusion ΔH and crystallization χ were quantitatively evaluated by means of Equation (1)

$$\chi = 100\% \cdot \left[\frac{\Delta H_m}{\Delta H_{m0}}\right] \cdot \frac{1}{W} \tag{1}$$

where ΔH_{m0} is the enthalpy value of a pure crystalline material, ΔH_m is the enthalpy corresponding to the fusion process and W the amount of each component in the polymer/drug system. The reference value taken for ΔH_{m0} of PLLA was χ_{100} = 93.7 J/g [65]. All results were averaged over n = 5 samples.

2.8. Mechanical Testsing

Tensile tests were carried out using the uniaxial tensile test instrument Zwicki ZN 2.5 (Zwick/Roell, Ulm, Germany). Samples were cut into dumbbell shape specimens with effective dimensions of 12 mm × 2 mm according to DIN EN ISO 527-2 1BB standards [66]. Sample thickness was measured using SEM QUANTA FEG 250 (FEI Company, Dreieich, Germany). It was determined using the reverse form of the dogbone sample. 10 mm samples directly neighboring the cutouts of the specimens for mechanical testing were mounted on the edge of the aluminum trays. The carrier was positioned vertically using a 90° adapter in the SEM to obtain a top view of the cutting edge. For each sample, at three distinct positions with n = 3, thickness values were determined.

Mechanical tests were conducted with a 10 N load cell and a crosshead speed of 25 mm/min. All tests were performed at room temperature (20 °C). The tensile force as a function of elongation was measured. Based on these data, the elastic modulus (E) was calculated in the linear elastic region. Furthermore, the tensile strength (σ_{max}) and elongation at break (ε_B) were determined for n = 5 samples. For statistical analysis, a twofold Nalimov's test has been performed and data were corrected for outliers.

2.9. Statistical Analysis

All data are given as mean ± standard deviation. For statistical analysis of contact angle, mechanical and DSC data, two tailed *t*-tests of the means versus PLLA reference have been performed. For statistical analysis, SigmaPlot software (V13.0, Systat Software, Inc., San Jose, CA, USA) has been used. Significances are given at a significance level of $p < 0.05$ and marked with an asterisk.

3. Results

3.1. Spectroscopical Analysis of Drug Loaded PLLA Films

Our first interest was whether drugs were homogeneous distributed into the PLLA films. Therefore, drug incorporation has been ensured by the use of Raman spectroscopy. The resulting quotient $Q = \left[\frac{A_{Drug}}{A_{PLLA}}\right]$ is given in Figure 1a. Raman spectra are given in the supporting information (Supplementary Figure S1).

From Raman data, a linear progression can be seen for all drugs leading to the assumption that no separation and precipitation from the solution during airbrush process occurred and that all drugs are distributed homogeneously in the polymer films. For CYCLO loaded PLLA films, no distinct Raman signal for the drug could be detected. To ensure the successful drug loading, FT-IR spectroscopy has been used. As for the drugs analyzed with Raman, linearity in the drug distribution was observed.

FTIR-ATR-measurements have been performed for all drug loaded PLLA films to investigate a potential polymer/drug interaction on a molecular level. Figure 2 shows IR spectra for 20 *w*/*w*% drug in PLLA, spectra for 10 *w*/*w*% and 15 *w*/*w*% can be found in the supporting information (Supplementary Figure S2). Characteristic IR bands of PLLA have been assigned according to [51] and are $\tilde{v}$ = 3001 cm^{-1} (CH stretch), $\tilde{v}$ = 1749 cm^{-1} (C=O stretch), $\tilde{v}$ = 1454 cm^{-1} (CH_3 bend), $\tilde{v}$ = 1359 cm^{-1} (C-H deformation), $\tilde{v}$ = 1180 cm^{-1} (C-O-C stretch), and $\tilde{v}$ = 1082 cm^{-1} (C-O-C stretch).

3.2. Influence of Drug Incorporation on the Surface Morphology and Drug Distribution

Changes in morphology due to the drug incorporation were investigated by means of macrophotography, scanning electron microscopy and Raman imaging. Image analysis of macro photography for drug containing PLLA films showed no significant changes compared to pure PLLA reference films such as phase separation or roughening. Macroscopic images are given in SI (Supplementary Figure S3). For a more detailed view, SEM imaging has been used to investigate the microscopic appearance of the drug loaded polymer films. At a magnification of 1000×, no such thing as microcrystals or other inhomogenities as well as changes in surface morphology could be observed for PTX and CYCLO. These drug containing films appeared smooth and comparable to the PLLA reference. The crater like shapes are most probably due to solvent evaporation. Regarding SIR and DEX, the surfaces show bumps in submicron range for all investigated concentrations, 10 *w*/*w*%, 15 *w*/*w*% and 20 *w*/*w*%. It must be noted that the side which was attached to the glass slid showed in all cases a plainer appearance. In Figure 3, exemplary SEM images for all PLLA/drug combinations at the highest drug concentration of 20 *w*/*w*% at 1000× magnification are shown. SEM images for 10 *w*/*w*% and 15 *w*/*w*% can be found in Supplementary Figure S4.

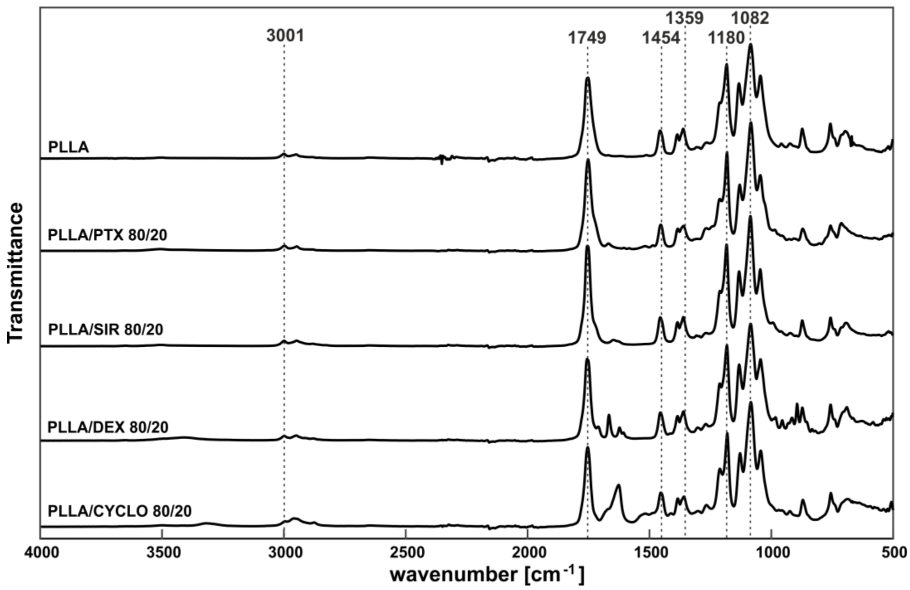

Figure 2. IR spectra of PLLA film and PLLA films with 20 *w*/*w*% incorporated drugs. IR bands of PLLA have been identified with reference to [51].

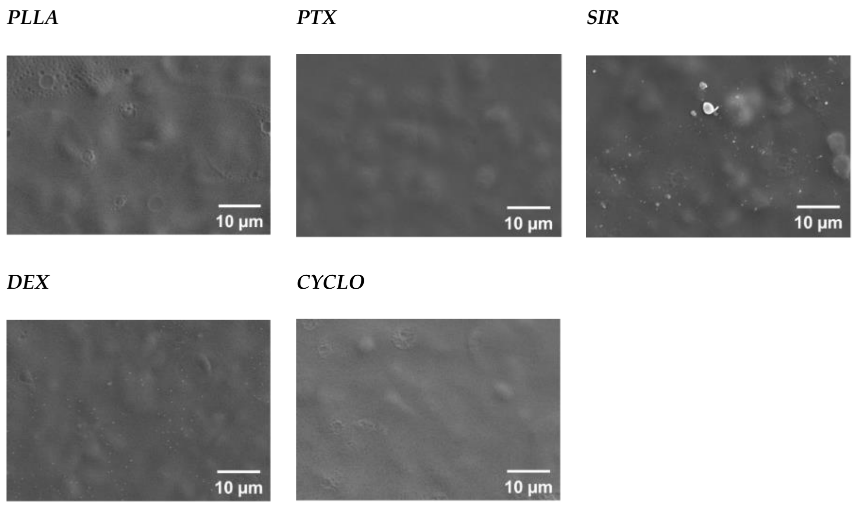

Figure 3. Exemplary SEM images for different drugs incorporated in PLLA samples (PLLA/drug 80/20 *w*/*w*%). Drugs used were paclitaxel (PTX), sirolimus (SIR), dexamethasone (DEX) and cislosporine (CYCLO).

As for Raman microscopy, distinct drug signals (PTX: $\widetilde{v}$= 1012 rel cm^{-1}, SIR: $\widetilde{v}$ = 1642 rel cm^{-1}, DEX: $\widetilde{v}$= 1668 rel cm^{-1}, Supplementary Figure S1) were mapped in respect to their intensity. As mentioned before, CYCLO gave no measurable Raman signal when blended with PLLA and could therefore not be analyzed via Raman mapping. All drugs showed homogeneous distribution even at highest concentration of 20 *w*/*w*%, see Figure 4. No such things as macroscopic crystals, agglomerates or drug enriched phases were observed. Raman mapping images for 10 *w*/*w*% and 15 *w*/*w*% can be found in Supplementary Figure S5.

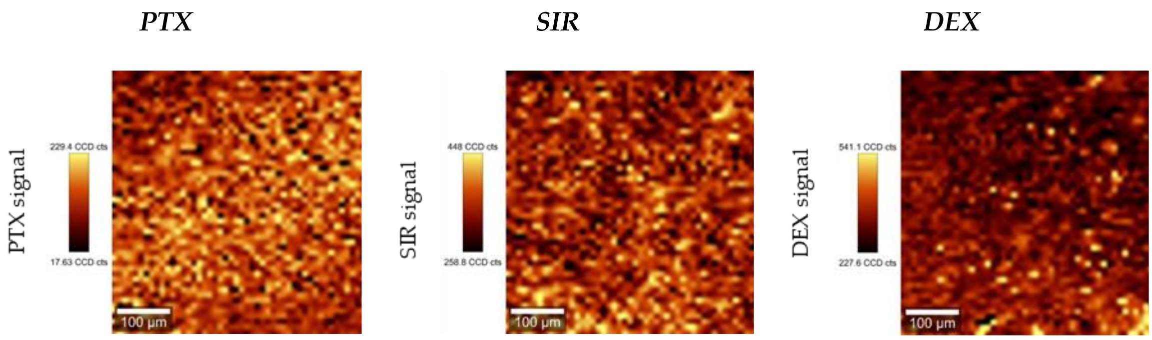

Figure 4. Exemplary Raman mapping images for different drugs incorporated in PLLA (PLLA/drug 20/80 *w*/*w*%). For CYCLO no distinct Raman signal could be detected.

3.3. Influence of Drug Incorporation on Surface Hydrophilicity

Figure 5 gives an overview on the contact angles for the polymer films addressed in this study. Exemplary images of the drops can be found in the Supplementary Figure S6. Compared to PLLA reference film, drug incorporation showed to have no effect on the surface wettability as all contact angles are in a range of 70–80°. Furthermore, surface free energy (SFE) calculated from contact angle data acquired from water and diiodomethane have been calculated. As can be seen, incorporation of the chosen drugs did not result in observable changes in SFE.

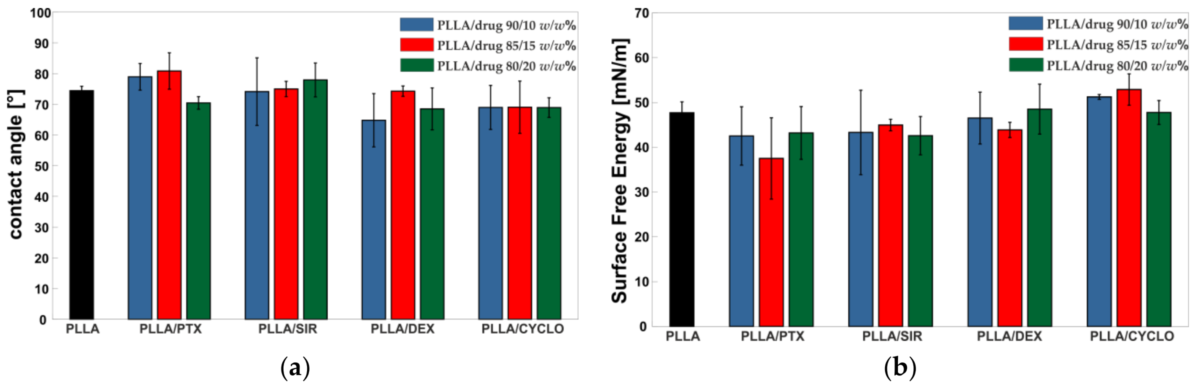

Figure 5. (**a**) Water contact angle and (**b**) surface free energy data for drug incorporated PLLA films (mean values for n = 3 with droplet angles taken each from both sides of the drops are shown). Statistical analysis (two-tailed *t*-test) did not show any significant differences ($p < 0.05$) of contact angle values and SFE values of drug incorporated PLLA films when compared to pure PLLA reference.

3.4. Influence of Drug Incorporation on the Thermal Properties—DSC

Figure 6 shows the first DSC heating curve of the spray coated films with the different drug ratios (90/10, 85/15, 80/20 *w*/*w*%) after thermal annealing. For reference, both the DSC curves of the pure polymer PLLA and the pure drug are included for each diagram.

The DSC heating curves of pure PLLA spray coated film exhibit a glass transition temperature at T_g = 72.8 °C. No exothermic peak, but an endothermic melting peak at 179 °C is observed, which is comparable to reported T_m data for HMW PLLA [67]. For 20 *w*/*w*% PTX, T_g of PLLA is shifted to lower temperatures, as shown in Table 3. Furthermore, an exothermic peak $T_{c,PLLA}$ is formed with increasing drug content, whose peak temperature is shifted to higher temperatures as the ratio increases (Figure 6a). The melting peak $T_{m,PLLA}$ is nearly identical at all concentrations. No other endothermic peak was identified that would be indicative of the presence of a pure PTX phase.

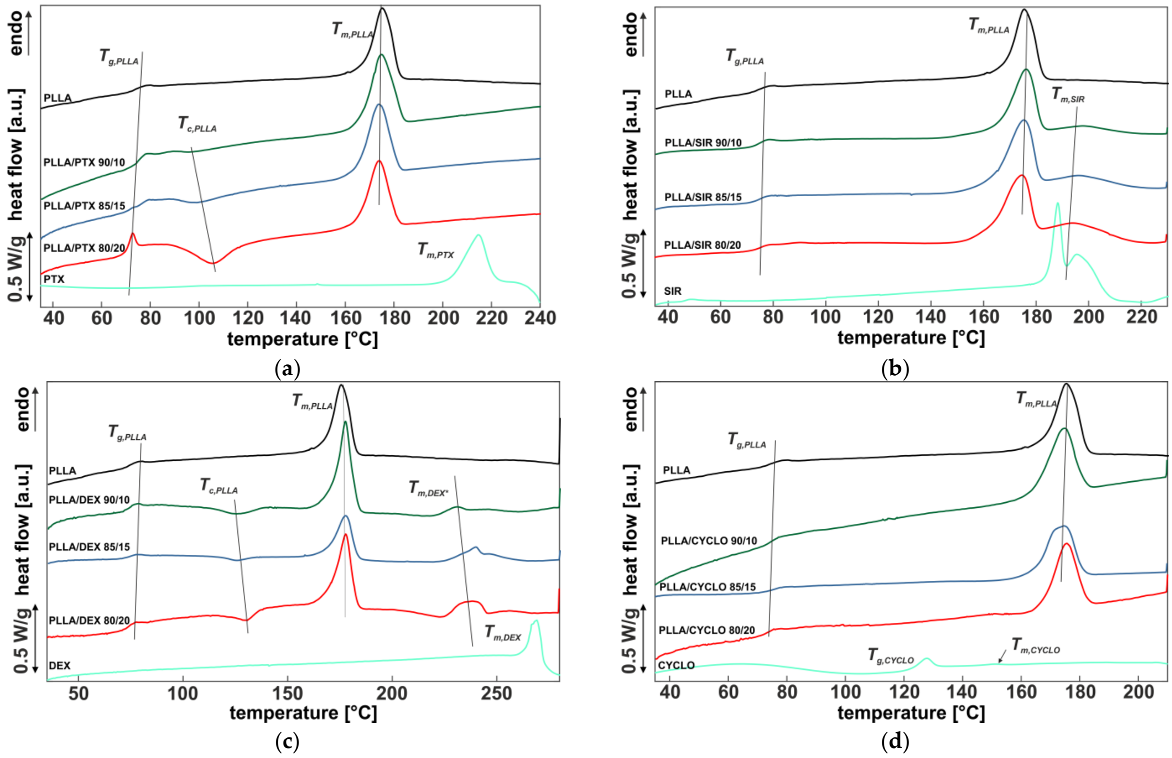

Figure 6. DSC thermograms of PLLA (black), drug (cyan) and PLLA/drug (**a**) PLLA/PTX, (**b**) PLLA/SIR, (**c**) PLLA/DEX and (**d**) PLLA/CYCLO) in different ratios (90/10, 85/15, 80/20 *w*/*w*%). The straight lines are guides for the eyes, only.

SIR incorporation into PLLA (Figure 6b) did not lead to distinct changes in $T_{g,PLLA}$ compared to pure PLLA. Even the endothermic melting peak $T_{m,PLLA}$ is kept constant. In addition, a further endothermic peak $T_{m,SIR}$ at 184 °C is observed, which can be related to the drug according to the reference measuring curve of the pure SIR material. There is no cold crystallization observed as in PTX.

PLLA/DEX DSC curves show no distinct shift in $T_{g,PLLA}$ (Table 3), but an exothermic peak $T_{c,PLLA}$ is formed with increasing drug content, whose peak temperature is shifted to higher temperatures as the drug content increases (Figure 6c). The PLLA melting peak $T_{m,PLLA}$ is almost identical at all concentrations. In addition, there is a further endothermic peak $T_{m,DEX}$ which can be identified from the measurement curve of the pure DEX material and which is shifted to higher temperatures and broadens as the drug ratio increases.

Thermograms of PLLA including CYCLO show no significant changes compared to pure PLLA (Figure 6d). As for that we conclude complete incorporation of the drug into the polymer matrix. However, as only little to no changes in $T_{g,PLLA}$ or $T_{m,PLLA}$ occur, low interaction of the polymer chains with the drug molecules can be assumed.

To evaluate the influence of drug incorporation on PLLA crystallinity, the percentage values as determined according to Equation (1) are plotted in Figure 7. The black bar refers to PLLA without drug content and with a value of χ = 37.8 ± 1.9 %, which is comparable with the literature for HMW PLLA [67]. With increasing PTX content, χ values of PLLA decreased from χ = 33 ± 7% down to χ = 11.3 ± 1.7%. In contrast, χ values of PLLA with SIR increased with increasing drug content. PLLA crystallinity including DEX or CYCLO show only little to no changes compared to pure PLLA. All χ values are given in Table 3.

Table 3. DSC results (glass transition (T_g), melting temperature (T_m) and degree of crystallinity (χ)) of PLLA/drug spray coated films in different ratios (90/10, 85/15, 80/20 *w*/*w*%) (n = 5 for each group). * in T_{m,DEX^*} indicates that shift in melting point occurs in comparison to pure drug.

PLLA/PTX	T_g (°C)	ΔH_{PLLA} (J/g)	χ (%)	$T_{m,PLLA}$ (°C)	ΔH_{PTX} (J/g)	$T_{m,PTX}$ (°C)
100/0	72.8 ± 0.5	35.4 ± 1.8	37.8 ± 1.9	177.08 ± 0.25	—	—
90/10	75.4 ± 0.4	31 ± 7	33 ± 7	174.72 ± 0.19	—	—
85/15	74.4 ± 2.6	26 ± 10	27 ± 10	173.84 ± 0.07	—	—
80/20	69.2 ± 0.8	10.6 ± 1.6	11.3 ± 1.7	173.78 ± 0.13	—	—
0/100	—	—	—	—	32.4 ± 1.2	213.48 ± 0.17
PLLA/SIR	T_g **(°C)**	ΔH_{PLLA} **(J/g)**	χ **(%)**	$T_{m,PLLA}$ **(°C)**	ΔH_{SIR} **(J/g)**	$T_{m,SIR}$ **(°C)**
100/0	72.8 ± 0.5	35.4 ± 1.8	37.8 ± 1.9	177.08 ± 0.25	—	—
90/10	73.45 ± 0.24	30 ± 5	32 ± 6	175.5 ± 0.5	43 ± 5	199.5 ± 0.6
85/15	74.9 ± 0.7	38 ± 8	41 ± 9	174.82 ± 0.28	45 ± 13	198.6 ± 0.6
80/20	73.9 ± 0.5	48.5 ± 2.9	52 ± 3	174.32 ± 0.07	49 ± 13	196.5 ± 0.5
0/100	—	—	—	—	64.9 ± 2.8	183.9 ± 0.5
PLLA/DEX	T_g **(°C)**	ΔH_{PLLA} **(J/g)**	χ **(%)**	$T_{m,PLLA}$ **(°C)**	ΔH_{DEX} **(J/g)**	T_{m,DEX^*} **(°C)**
100/0	72.8 ± 0.5	35.4 ± 1.8	37.8 ± 1.9	177.08 ± 0.25	—	—
90/10	74.3 ± 0.5	44.0 ± 2.4	46.9 ± 2.6	177.3 ± 0.3	1.9 ± 0.8	231.8 ± 1.5
85/15	71.7 ± 1.7	38 ± 6	40 ± 6	177.0 ± 0.5	19 ± 4	238.2 ± 0.9
80/20	74.9 ± 0.5	42 ± 10	45 ± 11	177.69 ± 0.15	8 ± 5	240.1 ± 1.4
0/100	—	—	—	—	15.2 ± 2.8	263.5 ± 0.8
PLLA/CYCLO	T_g **(°C)**	ΔH_{PLLA} **(J/g)**	χ **(%)**	$T_{m,PLLA}$ **(°C)**	ΔH_{CYCLO} **(J/g)**	$T_{m,CYCLO}$ **(°C)**
100/0	72.8 ± 0.5	35.4 ± 1.8	37.8 ± 1.9	177.08 ± 0.25	—	—
90/10	74.5 ± 0.7	43.1 ± 2.8	46 ± 3	174.51 ± 0.21	—	—
85/15	75.9 ± 2.0	40 ± 4	42 ± 4	174.61 ± 0.02	—	—
80/20	72.7 ± 2.4	36 ± 5	38 ± 6	173.7 ± 0.7	—	—
0/100	—	—	—	—	—	146.9 ± 0.7

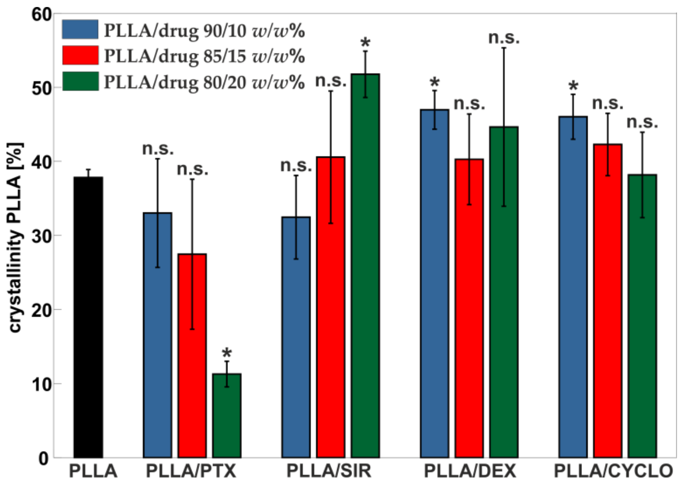

Figure 7. Crystallinity of PLLA in PLLA/drug spray coated films with different ratios (90/10, 85/15, 80/20 *w*/*w*%), determined from DSC measurements. Asterisks (*) mark significant differences of crystallinity data with $p < 0.05$ obtained by two-tailed *t*-test, each in comparison to PLLA reference. n.s. stands for not significant.

3.5. Coating Thickness Determination

For the calculation of mechanical parameters, adequately accurate thickness determination is necessary. A change in thickness accuracy of approximately ±1 µm would result in falsifying elastic modulus and tensile strength values of about 20 %. Consequently, as the films showed thicknesses in a range below 10 µm, thickness determination by the use of a dial indicator was not suitable.

To overcome this issue, film thickness has been determined using SEM imaging. Using a 90° adapter ensures precise sample characterization up to some few nanometers. However, measuring errors due to misalignment of the sample or manual setting of the scale bar have to be considered. As for that, a cutout close to the point of rupture of the strain samples has been threefold measured at three distinct points by SEM. A sample image for one of such measuring points is given in Figure 8a.

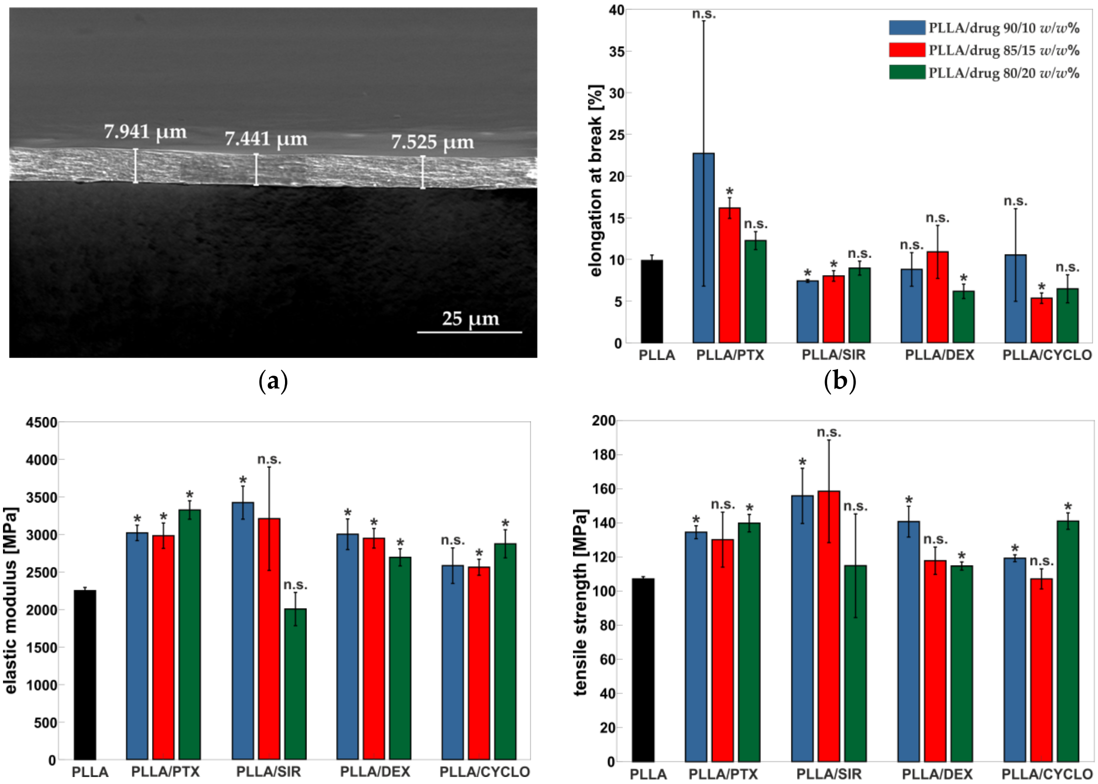

Figure 8. (**a**) Exemplary SEM image of PLLA reference film with determined thicknesses. (**b**–**d**) Mechanical properties ((**b**) elongation at break, (**c**) elastic modulus and (**d**) tensile strength), determined from uniaxial tensile tests of PLLA/drug spray coated films in different drug ratios (90/10, 85/15 and 80/20 *w*/*w*%). Asterisks (*) mark significant differences of the values with $p < 0.05$ obtained by two-tailed *t*-test, each in comparison to PLLA reference. n.s. stands for not significant.

3.6. Influence of Drug Incorporation on the Mechanical Properties

An overview on the mechanical parameters is given in Figure 8b–d. From tensile tests, elongation at break, elastic modulus and tensile strength have been calculated.

In general, drug incorporation results in an increase of elastic modulus up to 3420 ± 220 MPa for PLLA/SIR 90/10 compared to pure PLLA with a value of E = 2250 ± 40 MPa. Only SIR at 20/80 *w*/*w*% resulted in a decrease down to E = 2000 ± 220 MPa. Regarding the mechanical behavior, PTX leads to a high deviation for elongation at break values. SIR did not show to have any influence on the elongation at break. For DEX, a tendency to a decrease in elongation at break can be observed. Results for CYCLO also indicate a slight decrease in ε_B from 11 ± 6% (10 *w*/*w*%) to 6.4 ± 1.7% (20 *w*/*w*%) compared to PLLA at 9.9 ± 0.7%. All polymer/drug materials show higher tensile strength values up to 160 ± 30 MPa or comparable ones compared to pure PLLA with σ_{max} = 107.1 ± 1.3 MPa. Results of mechanical properties are given in Table 4 and the stress strain curves are given in Supplementary Figure S7.

Table 4. Mechanical properties (elastic modulus (E), tensile strength (σ_{max}), elongation at break (ε_B)), determined from uniaxial tensile tests of PLLA/drug spray coated films in different drug ratios (90/10, 85/15 and 80/20 *w*/*w*%).

PLLA/PTX	E (MPa)	σ_{max} (MPa)	ε_B (%)
100/0	2250 ± 40	107.1 ± 1.3	9.9 ± 0.7
90/10	3020 ± 100	134 ± 4	23 ± 16
85/15	2980 ± 170	130 ± 16	16.1 ± 1.2
80/20	3320 ± 120	140 ± 5	12.3 ± 1.1
PLLA/SIR	**E (MPa)**	**σ_{max} (MPa)**	**ε_B (%)**
100/0	2250 ± 40	107.1 ± 1.3	9.9 ± 0.7
90/10	3420 ± 220	156 ± 16	7.40 ± 0.17
85/15	3200 ± 700	160 ± 30	8.0 ± 0.7
80/20	2000 ± 220	115 ± 30	8.9 ± 0.8
PLLA/DEX	**E (MPa)**	**σ_{max} (MPa)**	**ε_B (%)**
100/0	2250 ± 40	107.1 ± 1.3	9.9 ± 0.7
90/10	3000 ± 200	141 ± 9	8.8 ± 2.0
85/15	2940 ± 130	118 ± 8	11 ± 3
80/20	2690 ± 110	115 ± 2.4	6.1 ± 0.9
PLLA/CYCLO	**E (MPa)**	**σ_{max} (MPa)**	**ε_B (%)**
100/0	2250 ± 40	107.1 ± 1.3	9.9 ± 0.7
90/10	2580 ± 240	119.2 ± 2.0	11 ± 6
85/15	2560 ± 110	107 ± 6	5.4 ± 0.7
80/20	2870 ± 190	141 ± 5	6.4 ± 1.7

4. Discussion

In this work, drug incorporated PLLA films were manufactured by spray-coating using PLLA/drug solutions, which is also the method of choice in industrial settings [64]. This technique allows the generation of homogeneous polymer coatings on complex structures, such as those represented by scaffolds for cardiovascular intervention in particular. Still, the removal of solvent residues remains crucial, as these, even in trace amounts, may show negative effects on biocompatibility as well as influence the mechanical and thermal properties of the coating. To investigate to what extend drugs influence the polymer matrix, rinsing protocols for solvent removal are unsuitable, as such treatments lead to washout of the drugs. For spray-coated thin films, however, thermal annealing above T_g under reduced pressure has shown to be sufficient to remove solvent residues, making rinsing steps unnecessary [35,68]. Nevertheless, thermal treatment may lead to further altering of the properties of the drug containing films, which must be taken into account.

Our initial interest was in macroscopic film morphology and drug distribution, whereas no macroscopic changes were observed. Raman and IR spectroscopy were used to prove the incorporation of drugs in the polymer films. For all drugs except for CYCLO, which was unmeasurable, Raman mapping showed a homogeneous distribution. Furthermore, contact angle and SFE measurements showed that drug incorporation did not result in significant changes even at a high concentration of 20 *w*/*w*%. This is interesting in a way such that the drugs addressed in this study exhibit very different logP values. Moreover, the observed phase separation and formation of microcrystals for DEX and SIR in accordance to DSC measurements appear to have no influence on surface wettability. This leads to the assumption that wettability of drug coating is not affected by drug addition, but remains comparable to the pure PLLA matrix.

The IR-spectra showed no distinct changes in IR bands but appear as overlapping spectra of PLLA and the incorporated drugs. As for that, we assume no chemical interaction of SIR, PTX, DEX, or CYCLO with the PLLA matrix as no shift in characteristic signals appears.

Regarding thermal analysis, the drugs showed a different behavior. CYCLO showed little to no influence on the polymer matrix and thus barely any effect on the thermal properties.

As for PTX, a slight shift of T_g of the polymer matrix was observed. In the literature, it has been reported that PTX is miscible with the amorphous domains of PLLA, in consequence softening the polymer matrix, leading to a decrease in T_g [69]. Furthermore, this also leads to the formation of an exothermic peak (T_c), which increases with increasing PTX amount, as the incorporated PTX decelerates polymer recrystallization [31,70]. Liggins and Burt explained it in a way that hydrogen bonding between PLLA and PTX lead to accumulation of PTX in the amorphous regions and therefore in a reduced rate of polymer chain diffusion and thus slowed crystallization [71]. In accordance to this, our results indicate a similar behavior for thin films accessible by spray coating. No PTX signal at around 217 °C was detected in the thermogram leading to the conclusion that PTX is completely blended into the polymer. However, the appearance of an exothermic peak at 104–107 °C for 20 *w*/*w*% PTX indicates that thermal annealing at 80 °C is not sufficient to achieve thermal equilibrium state and therefore may have an impact on long term properties in respect to biomedical application of such a drug containing matrix, e.g., shelf life.

For PLLA/SIR films, the presence of a SIR melting peak, up to 199.5 ± 0.6 °C, which is considerably higher than the T_m of the pure SIR component at 183.9 ± 0.5 °C, leads to the conclusion that SIR is not completely miscible with PLLA and phase separation occurs. This is underlined by means of the inhomogenities observed in SEM imaging. A similar observation has been made by Nukula for SIR in poly (butyl methacrylate)/poly(ethylene vinyl acetate) (PBMA/PEVA) [72]. They assumed from the broaden appearance of the SIR melting peak close to the melting peak of pure SIR in the thermogram that the drug is mainly encapsulated in an amorphous state with only little crystallinity. It is still unclear whether the SIR crystal formation is an effect due to immiscibility of PLLA or appeared when generating the test samples as SIR showed limited solubility in $CHCl_3$. To bypass this, the drug had been dissolved in MeOH, which has been added to the $CHCl_3$-polymer-solution. Precipitation may have been occurred at this point leading to micro crystals, though this has not been investigated in this study.

In the case of DEX incorporation, the shift of the endothermic peak $T_{m,DEX}$ from 231.8 ± 1.5 °C to 240.1 ± 1.4 °C indicates an interaction between DEX and PLLA. Consequently, a certain amount of DEX must have been incorporated into the PLLA matrix up to a threshold whereas phase separation occurs. Otherwise, we observed similar behavior as it has been reported for DEX containing PCL nanofibers by means of a drug melting signal [73]. As Martins et al. concluded, DEX precipitates from the polymer/drug solution during the manufacturing process in a similar way as for SIR. Also, the increased T_m of DEX leads to the conclusion that the drug exists in amorphous state in accumulated regions in the PLLA matrix. However, via Raman mapping, no DEX enriched areas could be detected. Both, for DEX and SIR, we assume that microcrystals have been formed which are below the resolution limit of the applied Raman mapping technique. As for area scans a 500 µm × 500 µm field with 50 dots per row and column was used, the resolution limit is ≥10 µm^2. As for SIR, SEM indicated the formation of submicron crystals when incorporating DEX in PLLA.

CYCLO resulted in a slight increase in crystallinity of PLLA. The absence of a distinct $T_{m,CYCLO}$ signal in comparison to the drug T_m for SIR or DEX showed complete blending of the drug with the polymer.

Altogether, our results point out complex phase transitioning processes during manufacturing. As a drug-polymer-solvent system is present, interaction of the three components in solution as well as during solvent evaporation and thus shifting of solubilities must been taken into account for manufacturing and application as it may alter crucial parameters such as drug release or mechanical resilience. Still, real time analysis of such processes remains challenging and technically sophisticated. Further research, e.g., by means of X-ray diffraction, may help to understand the drug PLLA interaction in combination with solvent influences.

Mechanical analysis of PLLA films containing PTX gave seemingly contradictory results regarding DSC analysis, especially crystallinity of the PLLA matrix. In this case, a decrease in crystallinity of approx. 13%, from 37.8 ± 1.9% down to 33 ± 7%, was observed which is accompanied by an approximate doubling of the elongation at break, from 9.9 ± 0.7% to 23 ± 16% yet an increase in the elastic modulus of up to 25%, from 2250 ± 40 MPa to 3020 ± 100 MPa was observed. The latter indicates a higher embrittlement. SIR incorporation leads to higher elastic modulus values of about 34%, from 2250 ± 40 MPa to 3420 ± 220 MPa, indicating a hardening effect. However, elastic modulus values decrease as drug content increases and approximate at 20 *w*/*w*% SIR the original PLLA value. DSC data show an increase of crystallinity of PLLA with increasing SIR amount. This, in addition to the formation of SIR crystallites, counteracts the elastic modulus increasing influence of SIR molecules interacting with the polymer chains. Therefore, we assume that SIR shows complex behavior in the polymer crystal lattice. The investigation of such interactions of PTX or SIR with PLLA may be of certain interest for future work in particular by means of crystal structure analysis, as the formation of multiple phases crucially alters properties highly relevant for biomedical applications such as drug release. In addition, such effects are in particular important regarding dilation behavior and drug carrying coating integrity after the exposure of mechanical stress as it appears at stent implantation.

DEX incorporation results in a tendency to lower elongation at break at high drug concentrations. Still, a decrease in elastic modulus of about 10%, from 3000 ± 200 MPa to 2690 ± 110 MPa, is observed. This may be due to the fact that on the one hand the drug interacts with the PLLA polymer chains on a molecular level, thus acting as plasticizer. However, on the other hand, the formation of aforementioned submicron crystals leads to the development of predetermined breaking points, therefore to a decrease in elongation at break of about 31%, from 8.8 ± 2.0% to 6.1 ± 0.9%. CYCLO shows with increasing drug ratio a reduction of elongation at break of ca. 40%, from 11 ± 6% to 6.4 ± 1.7% accompanied by an increase in elastic modulus and tensile strength of ca. 20%.

Regarding the mechanical analysis of PLLA/drug blends, it must be stated that handling of polymer films of a thickness of around 10 µm is challenging, as minimal defects or insufficient mounting in the testing device may drastically alter the results. However, the generation of thicker samples, e.g., by solvent casting process, may also be unsuitable as an increase in sample thickness leads to incomplete removal of residual solvent by evaporation. The remaining solvent may thus act as plasticizers, impairing the results on the drug influence. As for that, the literature and our DSC data for thin films obtained by spray-coating showed complete solvent removal after thermal annealing for which reason we decided to choose this manufacturing method for PLLA/drug films. Still, mechanical properties of such films, notably in the field of DES, are of particular interest. In the literature, some considerations about thermal analysis of drug incorporated polymers such as PLLA can be found. Yet, only limited data for mechanical investigations are available for reference. Consequently, further insight regarding the material properties of drug containing coatings is required.

5. Conclusions

Drug-eluting polymer coatings are an indispensable tool in biomedical device engineering, in particular for so-called combination products. Whereas drug release kinetics are clearly important and have been in the focus of extensive research, understanding the interaction of drugs with the drug-carrying polymer matrix is of great interest, especially in the field of drug-eluting stents.

In this study, PLLA/drug thin films have been investigated regarding the influence of the drug on thermal and mechanical properties of the polymer matrix. SIR, PTX, CYCLO and DEX were blended with HMW PLLA in ratios of 10, 15, and 20 *w*/*w*% with respect to the polymer. Our results showed that the selected drugs lead to an increase in tensile strength of the coating material. Regarding thermal properties, SIR and DEX showed PLLA/drug phase separation. PTX and DEX incorporation resulted in thermal destabilization of the polymer, which is evident by the formation of exothermic peaks in the DSC thermograms. High amounts of PTX lead to a strong decrease in crystallinity of PLLA. CYCLO showed complete blending with the PLLA matrix and did only little affect the polymer properties.

Our aim was to contribute to the understanding of the complex interaction between PLLA and API. Different drugs possess crucially different chemical properties and ways of interacting when blended with polymers, and thus, the influence on the polymer matrix cannot be easily predicted. Advances in current established DES technology to overcome limitations and side effects, such as the risk of late stent thrombosis, inflammation and in stent-restenosis, demand for novel polymer/drug coatings. The present data underline that this in turn requires target-oriented thermal treatment to ensure shelf life and mechanical resilience.

Supplementary Materials: The following are available online at https://www.mdpi.com/2073-4360/13/2/292/s1, Figure S1: Raman spectra of PLLA and PLLA with incorporated drugs at a ratio of drug/PLLA = 10/90 *w*/*w*%. Figure S2: IR spectra of PLLA and PLLA with incorporated cyclosporine A at a ratio of CYCLO/PLLA = 10/90 *w*/*w*%. Figure S3: Macrophotographical images of polymer film cutouts of PLLA and drug loaded PLLA films. Figure S4: SEM images of pure PLLA film drug and loaded PLLA films obtained via spray-coating. Figure S5: Raman mapping of PLLA with incorporated drugs at given drug/PLLA ratios. Mapping has been performed for the drug signal intensity according to the signal in the related Raman spectra. Figure S6: Representative contact angle images for PLLA reference and SIR/PLLA = 10/90 *w*/*w*%. Given are images of the droplets of deionized water for CA determination and images of MeI_2 droplets for SFE calculation. Figure S7: Stress-strain curves of drug loaded PLLA films obtained via spray-coating.

Author Contributions: Conceptualization: D.A. and S.O.; methodology: D.A.; mechanical testing and DSC analysis: D.A.; SEM imaging: V.S.; Raman spectroscopy and mapping: T.R.; IR spectroscopy: M.T.; polymer film generation: D.B.; writing—original draft preparation: D.A. and S.O.; writing—review and editing: all; project administration: K.-P.S. and N.G.; funding acquisition: K.-P.S. and N.G. All authors have read and agreed to the published version of the manuscript.

Funding: Financial support by the Federal Ministry of Education and Research (BMBF) within RESPONSE "Partnership for Innovation in Implant Technology" and by the European Social Fund (ESF) within the excellence research program of the state Mecklenburg-Vorpommern Card-ii-Omics is gratefully acknowledged.

Institutional Review Board Statement: Not applicable.

Informed Consent Statement: Not applicable.

Data Availability Statement: The data presented in this study are available upon request from the corresponding author.

Acknowledgments: The authors thank Katja Hahn and Caroline Dudda for their expert technical assistance.

Conflicts of Interest: The authors declare no conflict of interest.

References

1. Seidlitz, A. Drug-Eluting Stents. In *In vitro Drug Release Testing of Special Dosage Forms*, 1st ed.; Fotaki, N., Klein, S., Eds.; Wiley: Hoboken, NJ, USA, 2020; pp. 87–117. ISBN 9781118341476.
2. Torii, S.; Jinnouchi, H.; Sakamoto, A.; Kutyna, M.; Cornelissen, A.; Kuntz, S.; Guo, L.; Mori, H.; Harari, E.; Paek, K.H.; et al. Drug-eluting coronary stents: Insights from preclinical and pathology studies. *Nat. Rev. Cardiol.* **2020**, *17*, 37–51. [CrossRef] [PubMed]
3. Ali, R.M.; Abdul Kader, M.; Wan Ahmad, W.A.; Ong, T.K.; Liew, H.B.; Omar, A.-F.; Mahmood Zuhdi, A.S.; Nuruddin, A.A.; Schnorr, B.; Scheller, B. Treatment of Coronary Drug-Eluting Stent Restenosis by a Sirolimus- or Paclitaxel-Coated Balloon. *JACC Cardiovasc. Interv.* **2019**, *12*, 558–566. [CrossRef] [PubMed]
4. Schmidt, W.; Lanzer, P.; Behrens, P.; Brandt-Wunderlich, C.; Öner, A.; Ince, H.; Schmitz, K.-P.; Grabow, N. Direct comparison of coronary bare metal vs. drug-eluting stents: Same platform, different mechanics? *Eur. J. Med. Res.* **2018**, *23*, 2. [CrossRef] [PubMed]

5. Wu, J.J.; Way, J.A.H.; Kritharides, L.; Brieger, D. Polymer-free versus durable polymer drug-eluting stents in patients with coronary artery disease: A meta-analysis. *Ann. Med. Surg. (Lond.)* **2019**, *38*, 13–21. [CrossRef] [PubMed]
6. Von Birgelen, C.; Buiten, R.A. Superiority of biodegradable polymer sirolimus-eluting stents in STEMI. *Lancet* **2019**, *394*, 1208–1210. [CrossRef]
7. Grubman, D.; Saito, Y.; Lansky, A. The Firehawk stent: A review of a novel abluminal groove-filled biodegradable polymer sirolimus-eluting stent. *Argentina de Cardioangiología Intervencionista* **2019**, *10*, 73–77. [CrossRef]
8. Yoshioka, G.; Nishihira, K.; Asada, Y.; Node, K. In-stent restenosis following third-generation sirolimus-eluting stent implantation: First report analysed from imaging modalities and histopathological findings. *Eur. Heart J.* **2020**, *17*, 1707. [CrossRef]
9. Bünger, C.M.; Grabow, N.; Sternberg, K.; Kröger, C.; Ketner, L.; Schmitz, K.-P.; Kreutzer, H.J.; Ince, H.; Nienaber, C.A.; Klar, E.; et al. Sirolimus-eluting biodegradable poly-L-lactide stent for peripheral vascular application: A preliminary study in porcine carotid arteries. *J. Surg. Res.* **2007**, *139*, 77–82. [CrossRef]
10. Stone, G.W.; Ellis, S.G.; Cox, D.A.; Hermiller, J.; O'Shaughnessy, C.; Mann, J.T.; Turco, M.; Caputo, R.; Bergin, P.; Greenberg, J.; et al. A polymer-based, paclitaxel-eluting stent in patients with coronary artery disease. *N. Engl. J. Med.* **2004**, *350*, 221–231. [CrossRef]
11. Razavi, M.K.; Donohoe, D.; D'Agostino, R.B.; Jaff, M.R.; Adams, G. Adventitial Drug Delivery of Dexamethasone to Improve Primary Patency in the Treatment of Superficial Femoral and Popliteal Artery Disease: 12-Month Results from the DANCE Clinical Trial. *JACC Cardiovasc. Interv.* **2018**, *11*, 921–931. [CrossRef]
12. König, A.; Leibig, M.; Rieber, J.; Schiele, T.M.; Theisen, K.; Siebert, U.; Gothe, R.M.; Klauss, V. Randomized comparison of dexamethasone-eluting stents with bare metal stent implantation in patients with acute coronary syndrome: Serial angiographic and sonographic analysis. *Am. Heart J.* **2007**, *153*, 979.e1–979.e8. [CrossRef] [PubMed]
13. Sternberg, K.; Kramer, S.; Nischan, C.; Grabow, N.; Langer, T.; Hennighausen, G.; Schmitz, K.-P. In vitro study of drug-eluting stent coatings based on poly(L-lactide) incorporating cyclosporine A—drug release, polymer degradation and mechanical integrity. *J. Mater. Sci. Mater. Med.* **2007**, *18*, 1423–1432. [CrossRef] [PubMed]
14. Majewska, P.; Oledzka, E.; Sobczak, M. Overview of the latest developments in the field of drug-eluting stent technology. *Biomater. Sci.* **2020**, *8*, 544–551. [CrossRef]
15. Wessely, R. New drug-eluting stent concepts. *Nat. Rev. Cardiol.* **2010**, *7*, 194–203. [CrossRef] [PubMed]
16. Wessely, R.; Schömig, A.; Kastrati, A. Sirolimus and Paclitaxel on polymer-based drug-eluting stents: Similar but different. *J. Am. Coll. Cardiol.* **2006**, *47*, 708–714. [CrossRef]
17. Vos, N.S.; Fagel, N.D.; Amoroso, G.; Herrman, J.-P.R.; Patterson, M.S.; Piers, L.H.; van der Schaaf, R.J.; Slagboom, T.; Vink, M.A. Paclitaxel-Coated Balloon Angioplasty versus Drug-Eluting Stent in Acute Myocardial Infarction: The Revelation Randomized Trial. *JACC Cardiovasc. Interv.* **2019**, *12*, 1691–1699. [CrossRef]
18. Dash, A.K. The dark side of paclitaxel. *Oncol. Rev.* **2010**, *4*, 71–72. [CrossRef]
19. Strohbach, A.; Busch, R. Polymers for Cardiovascular Stent Coatings. *Int. J. Polym. Sci.* **2015**, *2015*, 1–11. [CrossRef]
20. Liu, X.; de Scheerder, I.; Desmet, W. Dexamethasone-eluting stent: An anti-inflammatory approach to inhibit coronary restenosis. *Expert Rev. Cardiovasc. Ther.* **2004**, *2*, 653–660. [CrossRef]
21. Prunotto, M.; Bacchetta, M.; Jayaraman, S.; Galloni, M.; van Eys, G.; Gabbiani, G.; Bochaton-Piallat, M.-L. Cytostatic drugs differentially affect phenotypic features of porcine coronary artery smooth muscle cell populations. *FEBS Lett.* **2007**, *581*, 5847–5851. [CrossRef]
22. Jonasson, L.; Holm, J.; Hansson, G.K. Cyclosporin A inhibits smooth muscle proliferation in the vascular response to injury. *Proc. Natl. Acad. Sci. USA* **1988**, *85*, 2303–2306. [CrossRef] [PubMed]
23. Verdoia, M.; Kedhi, E.; Suryapranata, H.; Galasso, G.; Dudek, D.; de Luca, G. Polymer-Free vs. Polymer-Coated Drug-Eluting Stents for the Treatment of Coronary Artery Disease: A Meta-Analysis of 16 Randomized Trials. *Cardiovasc. Revasc. Med.* **2020**, *21*, 745–753. [CrossRef] [PubMed]
24. Parker, T.; Davé, V.; Falotico, R. Polymers for drug eluting stents. *Curr. Pharm. Des.* **2010**, *16*, 3978–3988. [CrossRef] [PubMed]
25. Lee, D.-H.; La Torre Hernandez, J.M.D. The newest generation of drug-eluting stents and beyond. *Eur. Cardiol. Rev.* **2018**, *13*, 54. [CrossRef]
26. Mokhena, T.C.; Mochane, M.J.; Sadiku, E.R.; Agboola, O.; John, M.J. Opportunities for PLA and Its Blends in Various Applications. In *Green Biopolymers and Their Nanocomposites*, 1st ed.; Gnanasekaran, D., Ed.; Springer: Singapore, 2019; pp. 55–81. ISBN 978-981-13-8063-1.
27. Hu, T.; Yang, J.; Cui, K.; Rao, Q.; Yin, T.; Tan, L.; Zhang, Y.; Li, Z.; Wang, G. Controlled Slow-Release Drug-Eluting Stents for the Prevention of Coronary Restenosis: Recent Progress and Future Prospects. *ACS Appl. Mater. Interfaces* **2015**, 11695–11712. [CrossRef]
28. Nguyen, K.T.; Shaikh, N.; Wawro, D.; Zhang, S.; Schwade, N.D.; Eberhart, R.C.; Tang, L. Molecular responses of vascular smooth muscle cells to paclitaxel-eluting bioresorbable stent materials. *J. Biomed. Mater. Res. A* **2004**, *69*, 513–524. [CrossRef]
29. Can, E.; Udenir, G.; Kanneci, A.I.; Kose, G.; Bucak, S. Investigation of PLLA/PCL blends and paclitaxel release profiles. *AAPS PharmSciTech* **2011**, *12*, 1442–1453. [CrossRef]
30. Steele, T.W.J.; Huang, C.L.; Widjaja, E.; Boey, F.Y.C.; Loo, J.S.C.; Venkatraman, S.S. The effect of polyethylene glycol structure on paclitaxel drug release and mechanical properties of PLGA thin films. *Acta Biomater.* **2011**, *7*, 1973–1983. [CrossRef]

31. Hobzova, R.; Hampejsova, Z.; Cerna, T.; Hrabeta, J.; Venclikova, K.; Jedelska, J.; Bakowsky, U.; Bosakova, Z.; Lhotka, M.; Vaculin, S.; et al. Poly(d,l-lactide)/polyethylene glycol micro/nanofiber mats as paclitaxel-eluting carriers: Preparation and characterization of fibers, in vitro drug release, antiangiogenic activity and tumor recurrence prevention. *Mater. Sci. Eng. C Mater. Biol. Appl.* **2019**, *98*, 982–993. [CrossRef]
32. Wulf, K.; Teske, M.; Matschegewski, C.; Arbeiter, D.; Bajer, D.; Eickner, T.; Schmitz, K.-P.; Grabow, N. Novel approach for a PTX/VEGF dual drug delivery system in cardiovascular applications-an innovative bulk and surface drug immobilization. *Drug Deliv. Transl. Res.* **2018**, *8*, 719–728. [CrossRef]
33. Seidlitz, A.; Schick, W.; Reske, T.; Senz, V.; Grabow, N.; Petersen, S.; Nagel, S.; Weitschies, W. In vitro study of sirolimus release from a drug-eluting stent: Comparison of the release profiles obtained using different test setups. *Eur. J. Pharm. Biopharm.* **2015**, *93*, 328–338. [CrossRef] [PubMed]
34. Venkatraman, S.; Boey, F. Release profiles in drug-eluting stents: Issues and uncertainties. *J. Control Release* **2007**, *120*, 149–160. [CrossRef] [PubMed]
35. Petersen, S.; Hussner, J.; Reske, T.; Grabow, N.; Senz, V.; Begunk, R.; Arbeiter, D.; Kroemer, H.K.; Schmitz, K.-P.; Meyer zu Schwabedissen, H.E.; et al. In vitro study of dual drug-eluting stents with locally focused sirolimus and atorvastatin release. *J. Mater. Sci. Mater. Med.* **2013**, *24*, 2589–2600. [CrossRef] [PubMed]
36. Grabow, N.; Bünger, C.M.; Kischkel, S.; Timmermann, J.H.; Reske, T.; Martin, D.P.; Williams, S.F.; Schareck, W.; Sternberg, K.; Schmitz, K.-P. Development of a sirolimus-eluting poly (L-lactide)/poly(4-hydroxybutyrate) absorbable stent for peripheral vascular intervention. *Biomed. Tech. (Berl.)* **2013**, *58*, 429–437. [CrossRef] [PubMed]
37. Lincoff, A.M.; Furst, J.G.; Ellis, S.G.; Tuch, R.J.; Topol, E.J. Sustained Local Delivery of Dexamethasone by a Novel Intravascular Eluting Stent to Prevent Restenosis in the Porcine Coronary Injury Model. *J. Am. Coll. Cardiol.* **1997**, *29*, 808–816. [CrossRef]
38. Wissgott, C.; Schmidt, W.; Brandt, C.; Behrens, P.; Andresen, R. Preliminary Clinical Results and Mechanical Behavior of a New Double-Layer Carotid Stent. *J. Endovasc. Ther.* **2015**, *22*, 634–639. [CrossRef]
39. *Cardiovascular Implants—Endovascular Devices. Part 2—Vascular Stents*; DIN EN ISO 25539-2:2019-07; Beuth Verlag GmbH: Berlin, Germany, 2019.
40. Wu, D.; Zhang, Y.; Yuan, L.; Zhang, M.; Zhou, W. Viscoelastic interfacial properties of compatibilized poly(ε-caprolactone)/polylactide blend. *J. Polym. Sci. B Polym. Phys.* **2010**, *48*, 756–765. [CrossRef]
41. Hilianen-Vainio, M.; Varpomaa, P. Modification of poly(L-lactides) by blending: Mechanical and hydrolytic behavior. *Macromol. Chem. Phys.* **1995**, *197*, 1503–1523. [CrossRef]
42. López-Rodríguez, N.; López-Arraiza, A.; Meaurio, E.; Sarasua, J.R. Crystallization, morphology, and mechanical behavior of polylactide/poly(ε-caprolactone) blends. *Polym. Eng. Sci.* **2006**, *46*, 1299–1308. [CrossRef]
43. Arbeiter, D.; Eickner, T.; Oschatz, S.; Reske, T.; Specht, O.; Teske, M.; Senz, V.; Schmitz, K.-P.; Grabow, N. Physico chemical and phase separation characterization of high molecular PLLA blended with low molecular PCL obtained from solvent cast processes. *Mater. Res. Express* **2020**, *7*, 95302. [CrossRef]
44. Darie-Niţă, R.N.; Vasile, C.; Irimia, A.; Lipşa, R.; Râpă, M. Evaluation of some eco-friendly plasticizers for PLA films processing. *J. Appl. Polym. Sci.* **2016**, *133*. [CrossRef]
45. Farah, S.; Anderson, D.G.; Langer, R. Physical and mechanical properties of PLA, and their functions in widespread applications—A comprehensive review. *Adv. Drug Deliv. Rev.* **2016**, *107*, 367–392. [CrossRef] [PubMed]
46. Jacobsen, S.; Fritz, H.G. Plasticizing polylactide?the effect of different plasticizers on the mechanical properties. *Polym. Eng. Sci.* **1999**, *39*, 1303–1310. [CrossRef]
47. Baiardo, M.; Frisoni, G.; Scandola, M.; Rimelen, M.; Lips, D.; Ruffieux, K.; Wintermantel, E. Thermal and mechanical properties of plasticized poly(L-lactic acid). *J. Appl. Polym. Sci.* **2003**, *90*, 1731–1738. [CrossRef]
48. Ozkoc, G.; Kemaloglu, S. Morphology, biodegradability, mechanical, and thermal properties of nanocomposite films based on PLA and plasticized PLA. *J. Appl. Polym. Sci.* **2009**, *114*, 2481–2487. [CrossRef]
49. Ljungberg, N.; Wesslén, B. The effects of plasticizers on the dynamic mechanical and thermal properties of poly(lactic acid). *J. Appl. Polym. Sci.* **2002**, *86*, 1227–1234. [CrossRef]
50. Siepmann, F.; Le Brun, V.; Siepmann, J. Drugs acting as plasticizers in polymeric systems: A quantitative treatment. *J. Control Release* **2006**, *115*, 298–306. [CrossRef] [PubMed]
51. Nguyen, D.D.; Luo, L.-J.; Lai, J.-Y. Effects of shell thickness of hollow poly(lactic acid) nanoparticles on sustained drug delivery for pharmacological treatment of glaucoma. *Acta Biomater.* **2020**, 302–315. [CrossRef]
52. Lee, C.-H.; Li, Y.-J.; Huang, C.-C.; Lai, J.-Y. Poly(ε-caprolactone) nanocapsule carriers with sustained drug release: Single dose for long-term glaucoma treatment. *Nanoscale* **2017**, *9*, 11754–11764. [CrossRef]
53. Wulf, K.; Arbeiter, D.; Matschegewski, C.; Teske, M.; Huling, J.; Schmitz, K.-P.; Grabow, N.; Kohse, S. Smart releasing electrospun nanofibers—Poly-L-lactide fibers as dual drug delivery system for biomedical application. *Biomed. Mater.* **2020**. [CrossRef]
54. Kunze, C.; Freier, T.; Kramer, S.; Schmitz, K.-P. Anti-inflammatory prodrugs as plasticizers for biodegradable implant materials based on poly(3-hydroxybutyrate). *J. Mater. Sci. Mater. Med.* **2002**, *13*, 1051–1055. [CrossRef] [PubMed]
55. Savla, R.; Browne, J.; Plassat, V.; Wasan, K.M.; Wasan, E.K. Review and analysis of FDA approved drugs using lipid-based formulations. *Drug Dev. Ind. Pharm.* **2017**, *43*, 1743–1758. [CrossRef] [PubMed]
56. Hansch, C.; Leo, A.; Hoekman, D. Exploring QSAR: Hydrophobic, Electronic, and Steric Constants. *J. Med. Chem.* **1996**, *39*, 1189–1190. [CrossRef]

57. Lallemand, F.; Schmitt, M.; Bourges, J.-L.; Gurny, R.; Benita, S.; Garrigue, J.-S. Cyclosporine A delivery to the eye: A comprehensive review of academic and industrial efforts. *Eur. J. Pharm. Biopharm.* **2017**, *117*, 14–28. [CrossRef] [PubMed]
58. Ihlenfeldt, W.D.; Takahashi, Y.; Abe, H.; Sasaki, S. Computation and management of chemical properties in CACTVS: An extensible networked approach toward modularity and compatibility. *J. Chem. Inf. Model.* **1994**, *34*, 109–116. [CrossRef]
59. Tarini, M.; Cignoni, P.; Montani, C. Ambient occlusion and edge cueing to enhance real time molecular visualization. *IEEE Trans. Vis. Comput. Graph.* **2006**, *12*, 1237–1244. [CrossRef]
60. Finkelstein, A.; McClean, D.; Kar, S.; Takizawa, K.; Varghese, K.; Baek, N.; Park, K.; Fishbein, M.C.; Makkar, R.; Litvack, F.; et al. Local drug delivery via a coronary stent with programmable release pharmacokinetics. *Circulation* **2003**, *107*, 777–784. [CrossRef]
61. Mochizuki, A.; Niikawa, T.; Omura, I.; Yamashita, S. Controlled release of argatroban from PLA film—Effect of hydroxylesters as additives on enhancement of drug release. *J. Appl. Polym. Sci.* **2008**, *108*, 3353–3360. [CrossRef]
62. Shi, W.; Gu, C.; Jiang, H.; Zhang, M.; Lang, M. Effects of amphiphilic chitosan-g-poly(ε-caprolactone) polymer additives on paclitaxel release from drug eluting implants. *Mater. Sci. Eng. C Mater. Biol. Appl.* **2014**, *45*, 502–509. [CrossRef]
63. Kim, S.M.; Park, S.-B.; Bedair, T.M.; Kim, M.-H.; Park, B.J.; Joung, Y.K.; Han, D.K. The effect of solvents and hydrophilic additive on stable coating and controllable sirolimus release system for drug-eluting stent. *Mater. Sci. Eng. C Mater. Biol. Appl.* **2017**, *78*, 39–46. [CrossRef]
64. Livingston, M.; Tan, A. Coating Techniques and Release Kinetics of Drug-Eluting Stents. *J. Med. Devices* **2019**, *10*. [CrossRef] [PubMed]
65. Fischer, E.W.; Sterzel, H.J.; Wegner, G. Investigation of the structure of solution grown crystals of lactide copolymers by means of chemical reactions. *Kolloid-Z. Z. Polym.* **1973**, *251*, 980–990. [CrossRef]
66. International Standard Organisation. *Plastics-Determination of Tensile Properties*; International Standard Organisation: Geneva, Switzerland, 2012.
67. Migliaresi, C.; de Lollis, A.; Fambri, L.; Cohn, D. The effect of thermal history on the crystallinity of different molecular weight PLLA biodegradable polymers. *Clin. Mater.* **1991**, *8*, 111–118. [CrossRef]
68. Freier, T.; Kunze, C.; Schmitz, K.-P. Solvent removal from solution-cast films of biodegradable polymers. *J. Mate. Sci. Lett.* **2001**, *20*, 1929–1931. [CrossRef]
69. Liggins, R.T.; Burt, H.M. Paclitaxel loaded poly(L-lactic acid) (PLLA) microspheres. II. The effect of processing parameters on microsphere morphology and drug release kinetics. *Int. J. Pharm.* **2004**, *281*, 103–106. [CrossRef] [PubMed]
70. Mandelkern, L. The crystallization kinetics of polymer-diluent mixtures: The temperature coefficient of the process. *Polymer* **1964**, *5*, 637–648. [CrossRef]
71. Liggins, R.T.; Burt, H.M. Paclitaxel-loaded poly(L-lactic acid) microspheres 3: Blending low and high molecular weight polymers to control morphology and drug release. *Int. J. Pharm.* **2004**, *282*, 61–71. [CrossRef]
72. Nukala, R.K.; Boyapally, H.; Slipper, I.J.; Mendham, A.P.; Douroumis, D. The application of electrostatic dry powder deposition technology to coat drug-eluting stents. *Pharm. Res.* **2010**, *27*, 72–81. [CrossRef]
73. Martins, A.; Duarte, A.R.C.; Faria, S.; Marques, A.P.; Reis, R.L.; Neves, N.M. Osteogenic induction of hBMSCs by electrospun scaffolds with dexamethasone release functionality. *Biomaterials* **2010**, *31*, 5875–5885. [CrossRef]

Publikation 4

Biomed. Mater. (**2021**), *16(1)*, 015022.

Smart releasing electrospun nanofibers-poly: L.lactide fibers as dual drug delivery system for biomedical application.

Wulf K, **Arbeiter D**, Matschegewski C, Teske M, Huling J, Schmitz K-P, Grabow N, Kohse S.

Eingereicht: 15.09.2020, veröffentlicht: 11.12.2020

DOI: 10.1088/1748-605X/abbec8 (IF = 3,174)

Abstract: An ongoing challenge in drug delivery systems for a variety of medical applications, including cardiovascular diseases, is the delivery of multiple drugs to address numerous phases of a treatment or healing process. Therefore, an extended dual drug delivery system (DDDS) based on our previously reported cardiac DDDS was generated. Here we use the polymer poly(L-lactide) (PLLA) as drug carrier with the cytostatic drug Paclitaxel (PTX) and the endothelial cell proliferation enhancing growth factor, human vascular endothelial growth factor (VEGF), to overcome typical in-stent restenosis complications. We succeeded in using one solution to generate two separate DDDS via spray coating (film) and electrospinning (nonwoven) with the same content of PTX and the same post processing for VEGF immobilisation. Both processes are suitable as coating techniques for implants. The contact angle analysis revealed differences between films and nonwovens. Whereas, the morphological analysis demonstrated nearly no changes occurred after immobilisation of both drugs. Glass transition temperatures (T_g) and degree of crystallinity (χ) show only minor changes. The amount of immobilised VEGF on nonwovens was over 300 % higher compared to the films. Also, the nonwovens revealed a much faster and over three times higher PTX release over 70 d compared to the films. The almost equal physical properties of nonwovens and films allow the comparison of both DDDS independently of their fabrication process. Both films and nonwovens have significantly increased in vitro cell viability for human umbilical vein endothelial cells (EA.hy926) with dual loaded PTX and VEGF compared to PTX-only loaded samples.

IOP Publishing Biomed. Mater. 16 (2021) 015022 https://doi.org/10.1088/1748-605X/abbec8

Biomedical Materials

PAPER

RECEIVED
12 June 2020

REVISED
15 September 2020

ACCEPTED FOR PUBLICATION
6 October 2020

PUBLISHED
11 December 2020

Smart releasing electrospun nanofibers—poly: L.lactide fibers as dual drug delivery system for biomedical application

Katharina Wulf[1], **Daniela Arbeiter**[1], **Claudia Matschegewski**[2], **Michael Teske**[1], **Jennifer Huling**[1], **Klaus-Peter Schmitz**[1,2], **Niels Grabow**[1] **and Stefanie Kohse**[1]

[1] Institute for Biomedical Engineering, Rostock University Medical Center, Friedrich-Barnewitz-Straße 4, 18119 Rostock, Germany

[2] Institute for Implant Technology and Biomaterials e.V., Friedrich-Barnewitz-Straße 4, 18119 Rostock, Germany

E-mail: Katharina.wulf@uni-rostock.de

Keywords: PLLA, electrospinning, nanofibers, VEGF and PTX, endothelialisation, cancer therapies, multi-drug delivery systems

Supplementary material for this article is available online

Abstract

An ongoing challenge in drug delivery systems for a variety of medical applications, including cardiovascular diseases, is the delivery of multiple drugs to address numerous phases of a treatment or healing process. Therefore, an extended dual drug delivery system (DDDS) based on our previously reported cardiac DDDS was generated. Here we use the polymer poly(L-lactide) (PLLA) as drug carrier with the cytostatic drug Paclitaxel (PTX) and the endothelial cell proliferation enhancing growth factor, human vascular endothelial growth factor (VEGF), to overcome typical in-stent restenosis complications. We succeeded in using one solution to generate two separate DDDS via spray coating (film) and electrospinning (nonwoven) with the same content of PTX and the same post processing for VEGF immobilisation. Both processes are suitable as coating techniques for implants. The contact angle analysis revealed differences between films and nonwovens. Whereas, the morphological analysis demonstrated nearly no changes occurred after immobilisation of both drugs. Glass transition temperatures (T_g) and degree of crystallinity (χ) show only minor changes. The amount of immobilised VEGF on nonwovens was over 300% higher compared to the films. Also, the nonwovens revealed a much faster and over three times higher PTX release over 70 d compared to the films. The almost equal physical properties of nonwovens and films allow the comparison of both DDDS independently of their fabrication process. Both films and nonwovens have significantly increased *in vitro* cell viability for human umbilical vein endothelial cells (EA.hy926) with dual loaded PTX and VEGF compared to PTX-only loaded samples.

1. Introduction

Currently, the development of multi-drug delivery systems is attracting increasing interest due to their great potential as novel therapeutics for different medical applications, such as cardiology and oncology [1–7]. For complex diseases the combination of drugs has the benefit of targeting multiple therapeutic pathways, while reducing the risk of drug resistance and toxicity [8]. Cardiovascular diseases, for instance, require treatments that address multiple clinical needs. Bare metal stents are associated with complications like in-stent restenosis which can be addressed by the inclusion of cytotoxic or cytostatic drugs, such as paclitaxel (PTX).

However, PTX also interferes with the natural vascular healing processes by arresting re-endothelialisation of the stent surface. Consequently, new multi-drug delivery strategies often contain several active ingredients, such as PTX for the prevention of restenosis via inhibition of fibroblast growth paired with biomolecules, NO-releasing molecules, antibodies, proteins, peptides or growth factors meant to enhance re-endothelialisation. Existing strategies include bilayered PLGA nanoparticles containing VEGF plasmids and PTX [9, 10]. Additionally, Zhang *et al* described a stent covered with dual drug-loaded polylactic acid (PLA) electrospun fibers containing PTX-loaded mesoporous silica nanoparticles and surface coated with VEGF [11]. However, these example strategies still have limitations related to the undefined clinical risks associated with *in vivo* delivery of plasmids and the use of nanoparticles [12]. In recent years, electrospun polymeric nanofibers have proven to be an interesting strategy for drug delivery systems and can overcome these risks. The high surface to volume ratio of nonwovens can be ideal for maximising surface conjugation and improving encapsulated drug release [13]. Furthermore, in contrast to nanofibers, nanoparticles cannot create independent, implantable structures. These must always be embedded or immobilized and the danger of overcoming the blood-brain barrier cannot be excluded. We believe that electrospinning is particularly well suited to dual drug delivery because it is an ideal platform for both surface modifications and diffusion based drug release. Additionally, the biomimetic fiber structure of electrospun materials can lead to better cell attachment [14–16]. Modification of implant surfaces by means of spray coating has been previously applied in numerous cases [17–19].

Dual drug encapsulation can introduce challenges due to subsequent changes in mechanical properties of the drug loaded polymer, potential drug interactions and limited individual control of each drug's release profile. In contrast to the aforementioned dual drug delivery system (DDDS), our proposed strategy aims to simplify fabrication by directly immobilizing PTX and VEGF in a single polymer system. We have focused on combining different drug loading methods to individually tailor the delivery of each drug. In 2018, we described the development of an innovative polymer-based DDDS which successfully combined bulk incorporated PTX, released based on diffusion, and a surface immobilisation of VEGF, release via hydrolysis. We demonstrated that independent release of VEGF and Fluorescein diacetate (FDAc), used as a model of PTX, can be achieved in combination with multiple single polymer systems [20].

Dual drug systems are often designed to combat complex, multifaceted clinical problems that can require the combination of dissimilar drug delivery strategies. The novelty of the new design in this study is the inclusion of both the transient diffusion-based release of PTX and stable surface-conjugated VEGF. Furthermore, we aim to create a novel DDDS suitable for coating applications and capable of reducing restenosis and encouraging long-term re-endothelialisation established by combining PTX and the angiogenic protein VEGF [9, 21].

In detail, we modified our previous method by investigating the loading, release and bioactivity of both PTX and VEGF in a poly lactic acid (PLLA) polymer system. Moreover, we aimed to demonstrate the wide applicability and versatility of this novel DDDS by fabricating thin PLLA film (fPLLA) and PLLA nanofiber forms (nfPLLA) by using similar solutions. PLLA is a well-studied, biocompatible, applications [22]. Oxygen plasma was used to activate the polymer surface for stable VEGF surface immobilisation, instead of chemical linkages susceptible to hydrolysis. Clinical observation of long-term healing after implant placement indicates that the re-endothelialisation process can continue for months. For this reason we wanted to extend the bioavailability of VEGF for as long as possible via stable covalent surface conjugation [23]. In this work we could adapted the methods to be compatible with electrospinning and spraycoating to directly compare the properties of thin film coatings and electrospun nanofibers independently of the fabrication method. We demonstrated successful dual drug loading in film and nanofiber forms, revealing that nanofibers have superior VEGF surface loading and PTX release characteristics.

The dual delivery of PTX and VEGF in the manner outlined here could be critical in addressing existing clinical limitations in multi-drug delivery, and the framework of this method could also be widely applicable to other medical device coatings and drug combinations (figure 1).

2. Materials and methods

2.1. Materials

The polymers Resomer L 210 S (poly(L-lactide), PLLA, intrinsic viscosity in chloroform: 3.8 dL g^{-1}, was received from Evonik Industries AG (Darmstadt, Germany)). The crosslinkers (1-ethyl-3-(3-dimethylamino) propyl carbodiimide, hydrochloride/N-hydroxysuccinimide (EDC/NHS) and human vascular endothelial growth factor (VEGF) were purchased from Fisher Scientific GmbH (Schwerte, Germany) and tebu-bio GmbH (Offenbach, Germany). The drug Paclitaxel (PTX) was received from Cfm Oskar Tropitzsch GmbH (Marktredwitz, Germany). The Smart-Block solution was purchased from Candor Bioscience GmbH (Wangen, Germany).

2.2. Sample preparation

2.2.1. Film preparation

Polymer films were processed according to our previously established method [20]. Thus, 0.27 g of PLLA was diluted in 100 ml of chloroform. When creating drug-loaded polymers films, 14.9 wt% relative to polymer weight was added to the polymer solution. Films were deposited on glass slides (Ø = 6 mm) using a self-made spray coating set-up. The slides were spray coated for 1500 s at a pressure of 0.3 bar with a distance of 35 mm between the nozzle and slide. After spraying, polymer films (fPLLA) were dried at 80 °C under vacuum. The slides were weighted before and after spray coating and the spray coating process was continued until 250 μg of

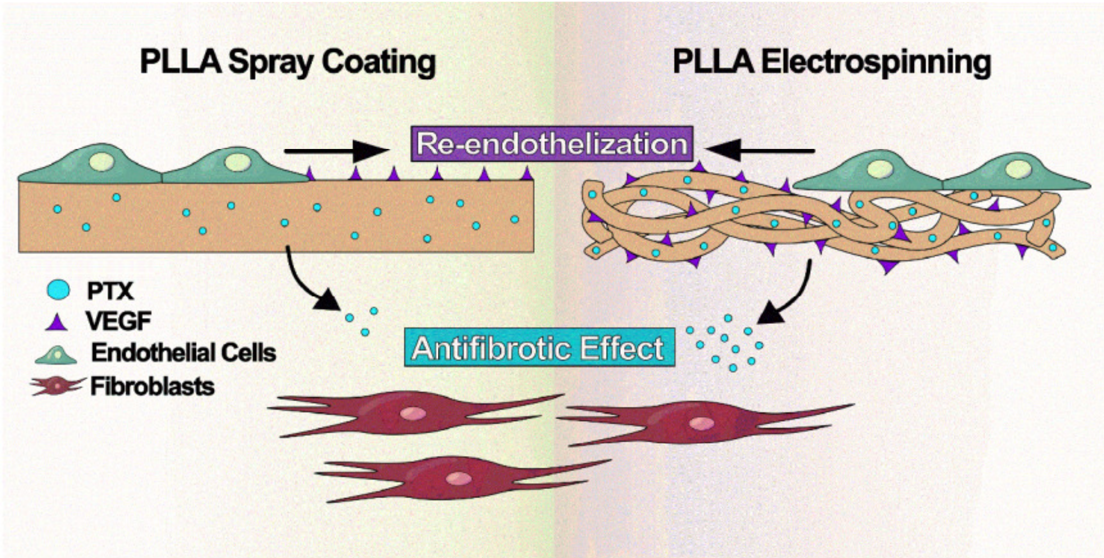

Figure 1. Schematic description of the sprayed and electrospun coatings developed in this investigation. Both coatings release PTX to reduce fibrosis and are surface conjugated with VEGF to encourage re-endothelization. However, electrospun fibers maximized drug loading and release properties.

2.2.2. Nonwoven preparation

Preparation of nonwoven samples was done by electrospinning using a protocol previously developed in our lab [24]. Clear and homogenous polymer solution was obtained by dissolving 5% (w/w) of the polymer in a choroform and tetrafluoroethanol (1:4 v/v). Polymer solution was loaded with 14.9% (w/w) PTX with respect to polymer weight. The described spinning process was performed for 1 ½ hours to reach a workable layer thickness. For quality assurance of the produced nonwoven structures, SEM images were used to observe fiber structure in different areas of the nonwoven.

2.3. Surface characterisation

2.3.1. SEM

Morphology of the polymer films and nonwoven samples was examined with scanning electron microscopy (SEM) QUANTA FEG 250 (FEI Company, Frankfurt, Germany) with an accelerating voltage of 10 kV and a spotsize of 3.0. All samples were fixed onto aluminum trays with conductive tape and sputter coated with gold. The images were taken at magnification x500.

2.3.2. Water contact angle

A Contact Angle System (OCA 20, Dataphysics Instruments GmbH, Filderstadt, Germany) was used for analysing surface modifications by contact angle measurements of ultra-pure water sessile drops (5 μl, 1 μl/s). Presented mean values (MV) and standard deviations (SD) were calculated from $n = 10$ samples.

2.3.3. Differential scanning calorimetry (DSC)

The thermal behaviour of the polymer films were specimens were heated from −30 °C up to 270 °C in a DSC 1 system (Mettler-Toledo, Schwerzenbach, Switzerland) at a rate of 10 °C/min operating at nitrogen atmospheric pressure. The samples were analysed with respect to glass transition (T_g), melting temperature (T_m), and degree of crystallinity (χ). The heats of fusion and crystallisation were quantitatively evaluated by determining the endothermic and exothermic peak areas, which were compared with the melting peak area of totally crystalline PLLA ($\chi_{100} = 93{,}7\ \mathrm{J\ g^{-1}}$) [26]. All results were averaged over at least $n = 5$ samples.

2.3.4. Attenuated total reflection Fourier transform infrared spectroscopy (ATR-FTIR)

A Vertex 70 infrared-spectrometer (Bruker, Ettlingen, germany) was used for FTIR-ATR measurements of fPLLA and nfPLLA with and without PTX. Spectra were measured between 4000 cm^{-1} and 500 cm^{-1} with 32 scans. Spectra were baseline corrected, smoothed and vector normalized between 1900 cm^{-1} and 600 cm^{-1} using Bruker OPUS software.

2.4. VEGF immobilisation

2.4.1. Plasma activation

Polymer films and nonwoven samples were activated as previously described in Rudolph *et al* [5]. Briefly, plasma activation was performed at 0.3 mbar for 30 s min with a plasma etching (PE) electrode and 40 W generator output in an oxygen (O_2) radio frequency (RF) plasma (frequency 13.56 MHz, Diener electronic GmbH & Co. KG, Ebhausen, Germany).

2.4.2. Covalent coupling

The VEGF biofunctionalisation of the activated carbodiimide hydrochloride)/N-hydroxysuccinimide (EDC/NHS) as a crosslinker system was realised as follows: The modified PLLA samples (Ø = 6 mm) were added to a 150 mM/100 mM EDC/NHS solution, diluted in 2-(N-morpholino)ethanesulfonic acid buffer (MES, 50 mM, pH 5,0), for 1 h at room temperature (RT). After modification with EDC/NHS, samples were rinsed in PBS once and then rinsed twice in deionized water. Samples were then soaked at RT in 1 μg ml^{-1} VEGF in PBS for 1 h. Samples were rinsed at least three times with PBS and water and then dried overnight under vacuum. The supernatant washing solutions were analysed via indirect ELISA in order to detect the soluble VEGF amount. VEGF-coupled samples were stored at 4 °C until use.

2.4.3. Quantification of VEGF loading

The VEGF loading for the PLLA films and PLLA nanofibers was determined via an indirect ELISA. Therefore, the VEGF soaking solutions were analysed after the surface coupling in order to determine the remaining VEGF amount in solution. Also, the supernatant washing solutions were analysed via indirect ELISA to determine if any VEGF detached during washing. The difference between before and after the coupling process corresponds to the VEGF surface loading of the samples. ELISA was performed using a Sandwich ELISA Kit (human VEGF ELISA Kit RayBio®, Hölzel Diagnostika, Köln, Germany) and was carried out according to the manufacturer's instructions. Antibody detection was done via a horseradish peroxidase and 3,3′,5,5′-tetramethylbenzidine reaction. The reaction was measured based on absorbance at 450 nm using a plate reader (FLUOstar Optima, BMG LABTECH, Ortenberg, Germany). $N = 5$ samples were measured for each group.

2.5. In vitro drug release

2.5.1. PTX release

The *in vitro* PTX release studies were carried out under sink conditions. Each polymer sample (Ø = 9 mm) was left in the dark on a shaker at 37 °C immersed in 1 ml Dulbecco's Phosphate buffered saline (DPBS) with additional 0.06% Tween 20 between defined withdrawal time-periods. At the specific time, the elution medium is completely removed, replaced with 1 ml fresh DPBS and analysed via HPLC according to [27]. The chromatography was performed under isocratic conditions with a mobile phase consisting of acetonitrile/PBS solution 0.005 M pH 3.5 (50/50 v/v). The flow rate was set to 1.0 ml min^{-1}. UV detection was conducted at a wavelength of 230 nm. MV and SD were calculated from $n = 5$ samples. In order to compare the release, the released amounts were converted into (100%) in the samples. The total PTX amount in the samples ranged from 140–153 μg.

2.6. Biocompatiblity studies

2.6.1. Cell viability assay

The biocompatibility studies of the PTX- and VEGF-surface functionalised PLLA samples were done using a protocol previously developed in our lab [20]. Prior to use, all polymer samples were disinfected with ethanol. EA.hy926 cells were then seeded on the disinfected PLLA samples with a density of 4×10^4 cells cm^{-2} in DMEM with 10% FCS and incubated for 46 h at 37 °C and 5% CO_2. Cells were then incubated in a solution of 10% CellQuanti-Blue in DMEM for 2 h. The fluorescence of the media was measured (λemission = 590 nm, λexcitation = 544 nm) with a FLUOstar OPTIMA plate reader. $N = 6$ biological replicates were measured for each group. To emphasize the effects of PTX and VEGF, data were presented with pure polymer cell viability defined as 100% viability.

2.6.2. Statistical analysis

All statistical analyse was done using either SPSS 15.0 or GraphPad Prism 5.0 (La Jolla, CA, USA) software. The statistical significance between means for contact angles and drug release rates was assessed with a Wilcoxon-test. The results of the cell viability assays were compared with 1-way ANOVA analysis. Asterics indicate significances ($^*p < 0.05$, $^{**}p < 0.01$, $^{***}p < 0.001$).

3. Results

3.1. Surface morphology

All investigated polymer surfaces were characterised via SEM, contact angle measurements, FTIR and DSC.

The PLLA surface morphology for fPLLA and nfPLLA seemed unaffected by the incorporation of PTX (figure 2) and by the O_2 plasma activation (supplementary materials; figures S1, S2 (https://stacks.iop.org/BMM/15/015022/mmedia)) and the VEGF (data not shown) coupling process. Even the diameter of the PLLA nanofiber remained similar with addition of PTX.

These results are also supported by the contact angle measurements. The PTX incorporation showed only minor effects on the contact angle. However, the contact angles for both systems are significantly decreased after the modification via plasma, indicating a more hydrophilic polymer surface (figure 3).

3.2. FTIR-ATR measurements

FTIR-spectra for nfPLLA and fPLLA with and without PTX are presented in figure 4. According to Renuga Devi *et. al.* Signal 1 at 1716 cm^{-1} corresponds

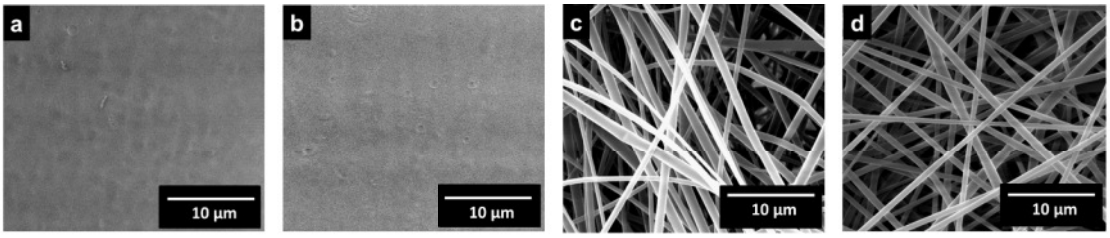

Figure 2. Representative SEM micrographs of fPLLA incorporated with (a) 0 %; (b) 14.9% PTX and nfPLLA incorporated with (c) 0%; (d) 14.9% PTX.

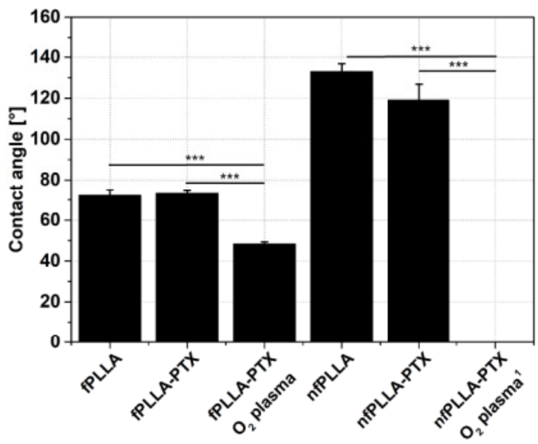

Figure 3. Average contact angle of water ΘW + SD of unmodified and O_2 plasma modified PLLA slides (fPLLA) and PLLA nanofiber (nfPLLA) surfaces measured via sessile drops method (5 μl drop volume; 10 samples), [1]detected contact angle was below 10°; Statistical data were analysed using SPSS 15.0 by Wilcoxon-test, (*** $p < 0.001$ significantly different between untreated or PTX-loaded and O_2 plasma modified polymer system).

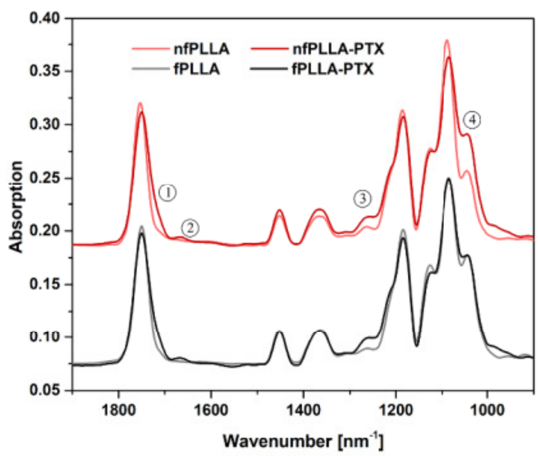

Figure 4. Attenuated total reflection fourier transform infrared spectroscopy (ATR-FTIR) spectra of nfPLLA, nfPLLA-PTX, fPLLA and fPLLA-PTX in the range of 900–1900 cm^{-1}; corresponding signals to PTX;signal 1 C = O stretching, signal 2 C–C stretching, signal 3 C–N stretching and signal 4 C–O stretching.

C–C stretching, signal 3 at 1263 cm^{-1} to C–N stretching and signal 4 at 1058 cm^{-1} to the C–O stretching

Table 1. Glass transition temperature T_g (°C) and degree of crystallinity χ (%) ± standard deviation (SD) of PLLA films and nanofibers using differential scanning calorimetry.

	T_g [°C ± SD]	Degree of crystallinity (χ) [% ± SD]
PTX (pure)	/	/
fPLLA	68.6 ± 2.2	35.6 ± 1.4
fPLLA O_2 plasma	71.8 ± 0.2	34.6 ± 2.7
fPLLA-PTX	71.7 ± 0.2	33.3 ± 0.5
fPLLA-PTX O_2 plasma	72.3 ± 1.0	32.9 ± 1.8
nfPLLA	71.2 ± 0.4	42.3 ± 1.3
nfPLLA O_2 plasma	71.0 ± 0.2	41.0 ± 1.0
nfPLLA-PTX	74.5 ± 0.6	39.6 ± 3.6
nfPLLA-PTX O_2 plasma	73.4 ± 1.4	37.3 ± 2.3

as nfPLLA-PTX and fPLLA-PTX reveal the same IR-spectra and therefore no chemical difference in the composition were visible.

3.3. Thermal properties

DSC measurements were performed for PTX (pure), non-modified PLLA films and nanofibers, O_2 plasma activated systems and the PTX immobilised PLLA samples. All DSC curves are presented in supplementary materials. For all samples, T_g and the degree of crystallinity were determined (table 1). For pure PTX, solved in chloroform during the preparation, no T_g or crystallinity could be measured (figure S3). The T_g of PLLA films is slightly increased from 68.6 ± 2.2 °C to 71.7 ± 0.2 °C and for PLLA nanofibers from 71.2 ± 0.4 °C to 74.5 ± 0.6 °C with addition of PTX (figures S4 and S5). The T_g for the investigated systems are nearly unaffected by the O_2 plasma treatment, which we already described in former publication (figures S4 and S5) [20]. The degree of crystallinity is negligibly decreased with the addition of PTX for the PLLA films and nanofibers.

3.4. PTX release

The *in vitro* PTX release from the PLLA-based samples (with and without VEGF) is shown in figure 5. In order to compare the release, the released amounts were converted into percentages and refer to the total amount of PTX (100%) in the samples. The total PTX amount in the samples ranged from 140–

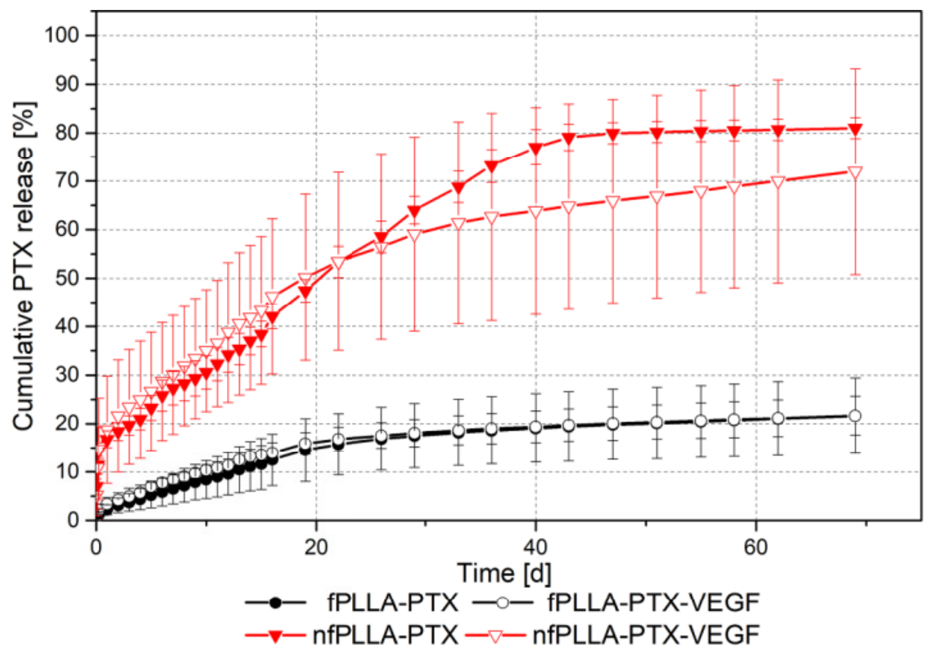

Figure 5. Cumulative *in vitro* release of incorporated PTX on PLLA films (fPLLA, black dots) or PLLA nanofibers (nfPLLA, red triangles) with and without VEGF modification in DPBS medium under agitation and at 37 °C (Ø = 9 mm; PTX:PLLA ratio 14.9:85.1 wt%, each with $n = 5$). Statistical data were analysed using SPSS 15.0 by Wilcoxon-test, ($^{***}p < 0.001$, significant different between the PLLA films and PLLA nanofibers).

influence the *in vitro* PTX release slightly. The PTX release profiles with and without VEGF follow the same long-term release. After 69 d only 20% of PTX was released into the medium. In contrast, the PTX release from the PLLA nanofibers system showed an accelerated release compared to the fPLLA. Within the first 20 d around 50% PTX is already released. At later time points, less PTX was released from the nfPLLA-PTX-VEGF samples with around 72% of the total PTX release after 69 d, compared to around 81% in the same time frame from the nfPLLA-PTX samples.

3.5. Quantification of VEGF coupling

The PLLA films and fibers were activated by O_2 plasma to generate hydroxyl groups on the polymer surface. These hydroxyl groups acted as sites for the zero length crosslinker EDC/NHS to covalently surface-couple VEGF. Table 2 shows the absolute VEGF loading in fPLLA and nfPLLA samples measured via an indirect ELISA. The reaction solutions and the washing solutions were analysed and the values combined.

The detected VEGF amounts were similar for the PTX loaded films. PLLA nanofibers had a much higher VEGF loading than the films. Surprisingly, the VEGF loading is significantly increased with addition of PTX for the nfPLLA.

Table 2. VEGF content on PLLA films and PLLA nanofibers immobilised by coupling with EDC/NHS as crosslinker ($n = 5$). $^{***}p < 0.001$; significant difference between the fPLLA-VEGF and nfPLLA-PTX-VEGF).

	Absolute VEGF amount [ng/mm^2 ± SD]
fPLLA-VEGF	0.018 ± 0.003
fPLLA-PTX-VEGF	0.016 ± 0.004
nfPLLA-VEGF	5.99 ± 0.87
nfPLLA-PTX-VEGF***	8.97 ± 0.75

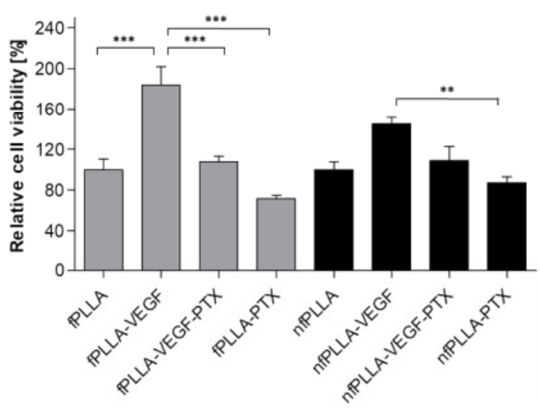

Figure 6. Relative cell viability of human endothelial EA.hy926 cells after 48 h on VEGF- and PTX-functionalised films (f) and nanofibrous (nf) PLLA surfaces normalised to untreated fPLLA and nfPLLA, respectively. (mean + SEM, $n = 6$, $^{***}p < 0.001$, $^{*}p < 0.05$).

3.6. Biocompatibility and biofunctionality of PTX and VEGF-functionalised PLLA

Cell viability of human endothelial EA.hy926 cells

PTX- and VEGF-surface modification is shown in figure 6. Relative cell viability was normalised to functional effect of PTX and VEGF on endothelial cell viability. For both PLLA surfaces similar effects of VEGF and PTX-functionalisation on EA.hy926 viability could be observed. In detail, cell viability was significantly increased on fPLLA-VEGF (184.0%) as well as on nfPLLA-VEGF (145.2%) when compared to the unmodified fPLLA and nfPLLA samples, respectively. Similarly, cells grown on the VEGF-PTX dual-functionalised surfaces, fPLLA-VEGF-PTX and nfPLLA-VEGF-PTX, exhibited 107.7% and 122.1% viability, respectively. This is a slightly higher viability in comparison to unmodified fPLLA and nfPLLA samples but a lower cell viability compared to those grown on only VEGF-treated surfaces. PTX surface functionalisation significantly diminished cell viability of human endothelial EA.hy926 cells on both PLLA surfaces with 71.7% for fPLLA and 93.9% for nfPLLA. In general, the effect of surface functionalisation with VEGF and PTX was similarly detectable on smooth and nanofibrous PLLA while being more pronounced on fPLLA than on nfPLLA.

4. Discussion

Combining multiple therapeutic substances in order to address several problems simultaneously has become an attractive option in the treatment of diseases, tissue regeneration and cancer therapies. For instance, the challenge of designing a DDDS which can simultaneously inhibit cell proliferation and promote re-endothelialisation has not yet been solved. The bulk incorporation of drugs, such as PTX or VEGF, in a polymeric drug delivery system was already successfully described, but it is becoming increasingly clear that a single drug cannot address the complexities of vascular healing [29–33]. In 2018, we presented an alternative strategy to create bulk PTX (modelled by FDAc) loaded polymeric systems, which were surface coated with VEGF with minor changes to PTX incorporation and release. This system resulted in independent diffusion diffusion-controlled release of PTX and chemically-controlled release of VEGF and represented the development of a novel DDDS design [17]. In contrast to the publication described earlier, PLLA, a well-established polymer for biomedical applications, was used as the coating polymer and different coating methods were examined. For this purpose, polymer spraying and electrospinning processes methods were developed using the same polymer solution. Whereby the release curves could be compared and similar properties (thermal and crystallinity) of the film and non-woven were achieved. Furthermore, FDAc was replaced with the chemotherapy agent PTX so that the actual bulk loading effects on polymer characteristics, VEGF loading and bioactivity could be evalu-

the coating process, while VEGF incorporation was achieved via surface acitvation process.

The PLLA polymer surfaces were activated by O_2 plasma to generate hydroxyl groups. These hydroxyl groups acted as sites for the zero length crosslinker EDC to covalently surface-couple VEGF. The method used to quantify VEGF before and after coupling cannot differentiate between adsorptively and covalently immobilized VEGF. However, Guex *et al* showed that EDC/NHS conjugated VEGF has similar effects on endothelial cell proliferation when compared to free VEGF in the media [34]. Previous work has shown that VEGF retains its beneficial effects on endothelial cells even when covalently bound to a surface [29]. Thus, it can be assumed that coating surfaces with covalently immobilised and adsorbed VEGF will enhance re-endothelialisation primarily by immobilized VEGF.

We also believe that incorporating a long term, stable, bioactive source of VEGF is well suited for polymer coatings. Evaluations of implants in clinical application suggest that the re-endothelialisation process can continue for months after implant placement, underscoring the need for an extended VEGF presence [30].

The selected parameters for VEGF coupling were chosen so that only neglitible morphological changes occurred for fPLLA and nfPLLA but the highest possible amount of functional groups were generated. This is confirmed by the SEM images as well as the contact angle measurements. Here it can be seen that the surface of the nonwovens becomes significantly more hydrophilic after the O_2 plasma treatment. No contact angle could be detected after plasma treatment for nfPLLA.

Also, the thermal properties of the PLLA based samples were changed negligible after the O_2 plasma activation compared to the non-activated form. This has also been confirmed by the results of the DSC measurements.

Although the surface activation seems to have minor influence on the bulk properties of the polymer, different amounts of VEGF were detected on the sample surfaces. The higher VEGF loading by an order of magnitude in nfPLLA compared to the fPLLA is most likely due to the larger surface area and the resulting increased target area for the formation of functional groups. The VEGF loading for the fPLLA is similar for the fPLLA-PTX. Surprisingly, the VEGF loading is increased with addition of PTX for the nfPLLA. A possible cause can be that the surface became rougher due to the plasma activation and an increase in surface area is the result. As a result, a higher interaction between the surface and the VEGF or crosslinker can occur. This can be more obvious for the nanofibers due to the extisting higher surface to volume ratio.

Even if the PTX incorporation partially influenseems to have a negligible influence on the PTX release for fPLLA and nfPLLA, which is highly beneficial.

In contrast to the nfPLLA it seems that the PLLA films did not exhibits a burst release. Furthermore, a much higher total PTX amount of about 75% was released for the nanofibers compared to 20% from the films within the 70 d. This is most probably caused by the higher surface area, and the better permeability and the significantly better wettability by the medium of nfPLLA. Furthermore, we can assume also a molecular weight degradation over a time of 70 d [31] and the reduction of molecular weight resulting in higher crystallinity and lower release [32]. Most PTX is located within the bulk of fPLLA and only small amounts are located near the surface. Previous studies have shown that drugs are only partially released from PLLA coatings by diffusion. Degradation of PLLA must occur in order to enable further release of PTX incorporated in the film [33].

For both, fPLLA and nfPLLA coatings, functionalisation with VEGF without the addition of PTX had the expected outcome of increasing cell viability. Although the effect was significant only for fPLLA, nfPLLA also showed an increase in cell viability of almost 50%. Thus, the effect of VEGF seems to improve cell viability only slightly with increasing VEGF amount in nfPLLA. Miyagi *et al* reported no significant differences in the number of endothelial cells for porous chitosan scaffolds with high and low VEGF loading [35]. As expected, the cytotoxic drug PTX on its own had a negative effect on cell viability in both coatings. fPLLA and nfPLLA systems have remarkably different PTX release with profiles. Nevertheless, in both systems a sufficiently toxic concentration of the cytotoxic ingredient PTX was probably released in the cell culture media despite the low water solubility of PTX [36]. However, the inhibitory effect of PTX was significantly diminished when combined with surface VEGF modification. The viability returns to levels similar to the pure polymer, demonstrating the significance of VEGF to the system and therefore underlining the benefit of the presented DDDS. This effect is also supported by work in Yang *et al* demonstrating that VEGF plasmid/PTX-co-eluting stents better supported both, normal re-endothelialisation and reduced in-stent restenosis compared to commercial DES [10].

The increased drug loading and release of PTX and VEGF support by electrospun nanofibers are very promising for our presented DDDS. In addition to having ideal functional characteristics, electrospinning is extremely versatile and adaptable for various medical applications.

Electrospinning can also be used to directly coat biomedical devices as a way to modify existing technologies such as bone implants, esophageal stents

fibers the ideal carrier for poorly water-soluble or low-bioavailability pharmaceutical components like PTX [40].

Nanofibers as drug carriers can be formed into stand-alone, implantable sheets used for localized drug delivery for tissue engineering scaffolds, drug release systems, wound dressings, cancer treatments and other applications [41].

5. Conclusion

For fPLLA and nfPLLA, nearly identical physical properties in crystallinity and T_g were observed. Therefore, when comparing film and nonwoven samples and their advantages as DDDS, differences in performance are due to the different biofabrication methods. As expected, the nonwoven nfPLLA has a much higher amount of immobilized VEGF than the film fPLLA. Interestingly, the incorporation of PTX further increases the amount of VEGF immobilized on nfPLLA, while no such influence is observable for fPLLA. Also, the release of incorporated PTX from nfPLLA is 3 times higher than the release from fPLLA, with over 70% released after 70 d. The changes in vitality of the EA.hys926 endothelial cells are the same for both fPLLA and nfPLLA. PTX-loaded material is cytotoxic, VEGF-loaded material enhances cell vitality and PTX-VEGF dual-loaded material overcomes the cytotoxic effect of PTX for the tested endothelial cells.

Thus, our nfPLLA and fPLLA systems are highly promising as a novel DDDS to address some current critical limitations of DDDS for cardiovascular diseases. Both PTX and VEGF modified systems seem suitable and have high differences in drug release over 2 month. Their application can be chosen to suit to the desired drug release needs. Our DDDS is designed to both inhibit the proliferation of fibroblasts (non cell specific PTX) and encourage re-endothelialisation by the endothelial specific growth factor VEGF. Moreover, the basic principle of this method could also be widely applicable to other medical device coatings and drug combinations.

Acknowledgments

The authors thank Andrea Rohde, Paul Queisler, Dalibor Bajer, Babette Hummel, Martina Nerger, Gabriele Karsten, Valeria Khaimov and Caroline Dudda for their expert technical assistance.

The authors declare no conflict of interest.

ORCID iDs

Katharina Wulf https://orcid.org/0000-0002-9891-5174
Daniela Arbeiter https://orcid.org/0000-0002-

References

[1] Yang Z, Yang Y, Xiong K, Li X, Qi P, Tu Q, Jing F, Weng Y, Wang J and Huang N 2015 *Biomaterials* **63** 80–92

[2] Lin Q, Ding X, Qiu F, Song X, Fu G and Ji J 2010 *Biomaterials* **31** 4017–25

[3] Aoki J *et al* 2005 *J. Am. Coll. Cardiol.* **45** 1574–9

[4] Choi W S, Joung Y K, Lee Y, Bae J W, Park H K, Park Y H, Park J-C and Park K D 2016 *ACS Appl. Mater. Interfaces* **8** 4336–46

[5] Rudolph A, Teske M, Illner S, Kiefel V, Sternberg K, Grabow N, Wree A and Hovakimyan M 2015 *PloS One* **10** e0142075

[6] Tu Q, Zhao X, Liu S, Li X, Zhang Q, Yu H, Xiong K, Huang N and Yang Z 2020 *Appl. Mater. Today* **19** 100546

[7] Feng Q *et al* 2014 *Biomaterials* **35** 5028–38

[8] Parhi P, Mohanty C and Sahoo S K 2012 *Drug Discovery Today* **17** 1044–52

[9] Zhu X *et al* 2017 *ACS Appl. Mater. Interfaces* **9** 27522–32

[10] Yang J *et al* 2013 *Biomaterials* **34** 1635–43

[11] Zhang Y, Wang J, Xiao J, Fang T, Hu N, Li M, Deng L, Cheng Y, Zhu Y and Cui W 2019 *Acta Biomater.* **94** 295–305

[12] Rawal M, Singh A and Amiji M M 2019 *Pharm. Res.* **36** 153

[13] Gao S, Tang G, Hua D, Xiong R, Han J, Jiang S, Zhang Q and Huang C 2019 *J. Mater. Chem.* B **7** 709–29

[14] Pant B, Park M and Park S-J 2019 *Pharmaceutics* **11** 305

[15] Herrero-Herrero M, Gómez-Tejedor J A and Vallés-Lluch A 2018 *Eur. Polym. J.* **99** 445–55

[16] Ismail H M, Zamani S, Elrayess M A, Kafienah W and Younes H M 2018 *Polymers* **10** 455

[17] Pan C J, Tang J J, Weng Y J, Wang J and Huang N 2007 *J. Mater. Sci., Mater. Med.* **18** 2193–8

[18] Siewert S *et al* 2017 *Biomed. Microdevices* **19** 78

[19] Shanshan C, Lili T, Yingxue T, Bingchun Z and Ke Y 2013 *Mater. Sci. Eng. C, Mater. Biol. Appl.* **33** 1476–80

[20] Wulf K, Teske M, Matschegewski C, Arbeiter D, Bajer D, Eickner T, Schmitz K-P and Grabow N 2018 *Drug Deliv. Transl. Res.* **8** 719–28

[21] Bachmann B O, Luetjen-Drecoll E, Bock F, Wiegand S J, Hos D, Dana R, Kruse F E and Cursiefen C 2009 *Br. J. Ophthalmol.* **93** 1075–80

[22] Simamora P and Chern W 2006 *J. Drugs Dermatol.* **5** 436–40

[23] Nasuno T, Tokura M, Kageyama M, Toyoda S, Sakuma M, Komatsu T, Taguchi I, Abe S and Inoue T 2016 *Heart Vessels* **31** 985–9

[24] Kohse S, Arbeiter D, Reske T, Stiehm M, Schmitz K-P and Grabow N 2018 *Curr. Directions Biomed. Eng.* **4** 89–92

[25] Arbeiter D, Kohse S, Eickner T, Grabow N and Schmitz K-P 2018 *Curr. Directions Biomed. Eng.* **4** 493–6

[26] Fischer E W, Sterzel H J and Wegner G 1973 *Kolloid-Z.u.Z.Polymere* **251** 980–90

[27] Seidlitz A, Kotzan N, Nagel S, Reske T, Grabow N, Harder C, Petersen S, Sternberg K and Weitschies W 2013 *PloS One* **8** e83992

[28] Renuga Devi T S and Gayathri S 2010 *Int. J. Pharm. Sci. Rev. Res.* **2** 106–10

[29] Shen Y H, Shoichet M S and Radisic M 2008 *Acta Biomater.* **4** 477–89

[30] Joner M, Finn A V, Farb A, Mont E K, Kolodgie F D, Ladich E, Kutys R, Skorija K, Gold H K and Virmani R 2006 *J. Am. Coll. Cardiol.* **48** 193–202

[31] Liu S, Wu G, Chen X, Zhang X, Yu J, Liu M, Zhang Y and Wang P 2019 *Polymers* **11** 1015

[32] Hrib J, Sirc J, Hobzova R, Hampejsova Z, Bosakova Z, Munzarova M and Michalek J 2015 *Beilstein J. Nanotechnol.* **6** 1939–45

[33] Zilberman M 2005 *Acta Biomater.* **1** 615–24

[34] Guex A G, Hegemann D, Giraud M N, Tevaearai H T, Popa A M, Rossi R M and Fortunato G 2014 *Colloids Surf.* B **123** 724–33

[35] Miyagi Y, Chiu L L Y, Cimini M, Weisel R D, Radisic M and Li R-K 2011 *Biomaterials* **32** 1280–90

[36] Danhier F, Vroman B, Lecouturier N, Crokart N, Pourcelle V, Freichels H, Jérôme C, Marchand-Brynaert J, Feron O and Préat V 2009 *J. Control. Release* **140** 166–73

[37] Ashbaugh A G *et al* 2016 *Proc. Natl Acad. Sci. USA* **113** E6919–E6928

[38] Zhu Y, Hu C, Li B, Yang H, Cheng Y and Cui W 2013 *Acta Biomater.* **9** 8328–36

[39] Tefft B J, Uthamaraj S, Harburn J J, Hlinomaz O, Lerman A, Dragomir-Daescu D and Sandhu G S 2017 *J. Magn. Magn. Mater.* **427** 100–4

[40] Torres-Martinez E J, Cornejo Bravo J M, Serrano Medina A, Pérez González G L and Villarreal Gómez L J 2018 *Curr. Drug Deliv.* **15** 1360–74

[41] Han D, Sasaki M, Yoshino H, Kofuji S, Sasaki A T and Steckl A J 2017 *J. Drug Deliv. Sci. Technol.* **40** 45–50